frontiers | Research Topics

Rising stars in nutrition and food science technology: Development and utilization of active ingredients in food

Edited by
Chanchan Sun, Wenjie Sui and Bin Liang

Published in
Frontiers in Nutrition

FRONTIERS EBOOK COPYRIGHT STATEMENT

The copyright in the text of individual articles in this ebook is the property of their respective authors or their respective institutions or funders. The copyright in graphics and images within each article may be subject to copyright of other parties. In both cases this is subject to a license granted to Frontiers.

The compilation of articles constituting this ebook is the property of Frontiers.

Each article within this ebook, and the ebook itself, are published under the most recent version of the Creative Commons CC-BY licence. The version current at the date of publication of this ebook is CC-BY 4.0. If the CC-BY licence is updated, the licence granted by Frontiers is automatically updated to the new version.

When exercising any right under the CC-BY licence, Frontiers must be attributed as the original publisher of the article or ebook, as applicable.

Authors have the responsibility of ensuring that any graphics or other materials which are the property of others may be included in the CC-BY licence, but this should be checked before relying on the CC-BY licence to reproduce those materials. Any copyright notices relating to those materials must be complied with.

Copyright and source acknowledgement notices may not be removed and must be displayed in any copy, derivative work or partial copy which includes the elements in question.

All copyright, and all rights therein, are protected by national and international copyright laws. The above represents a summary only. For further information please read Frontiers' Conditions for Website Use and Copyright Statement, and the applicable CC-BY licence.

ISSN 1664-8714
ISBN 978-2-83252-085-7
DOI 10.3389/978-2-83252-085-7

About Frontiers

Frontiers is more than just an open access publisher of scholarly articles: it is a pioneering approach to the world of academia, radically improving the way scholarly research is managed. The grand vision of Frontiers is a world where all people have an equal opportunity to seek, share and generate knowledge. Frontiers provides immediate and permanent online open access to all its publications, but this alone is not enough to realize our grand goals.

Frontiers journal series

The Frontiers journal series is a multi-tier and interdisciplinary set of open-access, online journals, promising a paradigm shift from the current review, selection and dissemination processes in academic publishing. All Frontiers journals are driven by researchers for researchers; therefore, they constitute a service to the scholarly community. At the same time, the *Frontiers journal series* operates on a revolutionary invention, the tiered publishing system, initially addressing specific communities of scholars, and gradually climbing up to broader public understanding, thus serving the interests of the lay society, too.

Dedication to quality

Each Frontiers article is a landmark of the highest quality, thanks to genuinely collaborative interactions between authors and review editors, who include some of the world's best academicians. Research must be certified by peers before entering a stream of knowledge that may eventually reach the public - and shape society; therefore, Frontiers only applies the most rigorous and unbiased reviews. Frontiers revolutionizes research publishing by freely delivering the most outstanding research, evaluated with no bias from both the academic and social point of view. By applying the most advanced information technologies, Frontiers is catapulting scholarly publishing into a new generation.

What are Frontiers Research Topics?

Frontiers Research Topics are very popular trademarks of the *Frontiers journals series*: they are collections of at least ten articles, all centered on a particular subject. With their unique mix of varied contributions from Original Research to Review Articles, Frontiers Research Topics unify the most influential researchers, the latest key findings and historical advances in a hot research area.

Find out more on how to host your own Frontiers Research Topic or contribute to one as an author by contacting the Frontiers editorial office: frontiersin.org/about/contact

Rising stars in nutrition and food science technology: Development and utilization of active ingredients in food

Topic editors

Chanchan Sun — Yantai University, China

Wenjie Sui — Tianjin University of Science and Technology, China

Bin Liang — Ludong University, China

Citation

Sun, C., Sui, W., Liang, B., eds. (2023). *Rising stars in nutrition and food science technology: Development and utilization of active ingredients in food*. Lausanne: Frontiers Media SA. doi: 10.3389/978-2-83252-085-7

Table of contents

05 Editorial: Rising stars in nutrition and food science technology: Development and utilization of active ingredients in food
Chanchan Sun, Bin Liang and Wenjie Sui

07 Effects of drying strategies on sporulation and titer of microbial ecological agents with *Bacillus subtilis*
Chonglei Li, Kai Zhao, Litong Ma, Ji Zhao and Zhi-Min Zhao

18 Yeast mannoproteins are expected to be a novel potential functional food for attenuation of obesity and modulation of gut microbiota
Xiang Li, Junsong Wu, Yijun Kang, Dan Chen, Guijie Chen, Xiaoxiong Zeng and Jialian Wang

33 Structural characteristics of polysaccharide from *Zingiber striolatum* and its effects on gut microbiota composition in obese mice
Wei Jiang, Ying Hu and Zhenyuan Zhu

49 Extraction and immunomodulatory activity of the polysaccharide obtained from *Craterellus cornucopioides*
Caixuan Zhang, Ying Shu, Yang Li and Mingzhu Guo

62 Isolation, identification, and characterization of corn-derived antioxidant peptides from corn fermented milk by *Limosilactobacillus fermentum*
Jue Xu, Yingyan Chen, Xiankang Fan, Zihang Shi, Mingzhen Liu, Xiaoqun Zeng, Zhen Wu and Daodong Pan

74 Phytochemistry, health benefits, and food applications of sea buckthorn (*Hippophae rhamnoides* L.): A comprehensive review
Zhen Wang, Fenglan Zhao, Panpan Wei, Xiaoyun Chai, Guige Hou and Qingguo Meng

94 A new iron supplement: The chelate of pig skin collagen peptide and Fe^{2+} can treat iron-deficiency anemia by modulating intestinal flora
Shan Jiang, Weichao Dong, Zhen Zhang, Jing Xu, Haoran Li, Jiayu Zhang, Long Dai and Shaoping Wang

109 Steam explosion pretreatment enhancing enzymatic digestibility of overground tubers of tiger nut (*Cyperus esculentus* L.)
Zhi-Min Zhao, Wenqing Yu, Caitong Huang, Huiting Xue, Juan Li, Dejian Zhang and Guanhua Li

118 Identification and virtual screening of novel anti-inflammatory peptides from broccoli fermented by *Lactobacillus strains*
Yao Li, Xinchang Gao, Daodong Pan, Zhu Liu, Chaogeng Xiao, Yongzhao Xiong, Lihui Du, Zhendong Cai, Wenjing Lu, Yali Dang and Xiuzhi Zhu

134 Red-fleshed apple flavonoid extract alleviates CCl_4-induced liver injury in mice
Yizhou Chen, Yanbo Wang, Shenghui Jiang, Jihua Xu, Bin Wang, Xiaohong Sun and Yugang Zhang

149 Antioxidant activity and interactions between whey protein and polysaccharides from different parts of *Houttuynia cordata*
Xiaocui Liu, Jin Tian, Zhiran Zhou, Yinzhen Pan and Zhongqiao Li

frontiers | Frontiers in Nutrition

TYPE Editorial
PUBLISHED 21 March 2023
DOI 10.3389/fnut.2023.1177158

Check for updates

OPEN ACCESS

EDITED AND REVIEWED BY
Elena Ibañez,
Institute of Food Science Research (CSIC), Spain

*CORRESPONDENCE
Chanchan Sun
✉ sunchan88@126.com

SPECIALTY SECTION
This article was submitted to Nutrition and Food Science Technology, a section of the journal Frontiers in Nutrition

RECEIVED 01 March 2023
ACCEPTED 09 March 2023
PUBLISHED 21 March 2023

CITATION
Sun C, Liang B and Sui W (2023) Editorial: Rising stars in nutrition and food science technology: Development and utilization of active ingredients in food. *Front. Nutr.* 10:1177158. doi: 10.3389/fnut.2023.1177158

COPYRIGHT
© 2023 Sun, Liang and Sui. This is an open-access article distributed under the terms of the Creative Commons Attribution License (CC BY). The use, distribution or reproduction in other forums is permitted, provided the original author(s) and the copyright owner(s) are credited and that the original publication in this journal is cited, in accordance with accepted academic practice. No use, distribution or reproduction is permitted which does not comply with these terms.

Editorial: Rising stars in nutrition and food science technology: Development and utilization of active ingredients in food

Chanchan Sun[1]*, Bin Liang[2] and Wenjie Sui[3]

[1]College of Life Sciences, Yantai University, Yantai, Shandong, China, [2]School of Food Engineering, Ludong University, Yantai, Shandong, China, [3]State Key Laboratory of Food Nutrition and Safety, Tianjin University of Science and Technology, Tianjin, China

KEYWORDS

protein, peptide, polysaccharide, flavonoid, high-tech manufacturing technology

Editorial on the Research Topic
Rising stars in nutrition and food science technology: Development and utilization of active ingredients in food

In recent years, people's demand for food is undergoing a transition from quantity to quality and gradually to nutrition. The nutrition of food is not only of great significance to the normal progress of human metabolism, but also plays a key role in the healthy growth, such as defense of viruses and prevention of diseases. The nutritional index of food is the main object of concern in the field of food manufacturing.

In the process of food manufacturing, the nutritional characteristics are mainly controlled by the content of relevant components (nutritional fortifiers, food additives, etc.) and the rational food structure design. Moreover, other challenges associated deal with nutritious foods manufacturing technology and equipment involved. First of all, there is a lack of development in technologies for achieving nutrients with high activity and high absorption rate. Secondly, in terms of equipment, there are still problems related to poor production continuity, large amount of waste water and energy consumption, and poor product quality. The existence of these technical and equipment problems has seriously restricted the healthy development of the food industry and cannot meet people's needs for nutrition.

The papers included in this topic have conducted in-depth research on the regulatory mechanism of active ingredients in food and high-tech manufacturing technology on the nutritional characteristics of food, and have achieved systematic research results. Li Y. et al., Jiang S. et al., Xu et al., and Li X. et al. respectively fermented broccoli by *Lactobacillus strains*, hydrolyzed pig skin collagen with protease, fermented corn milk with probiotics and extracted yeast mannoproteins from *Saccharomyces cerevisiae* to obtain broccoli peptides, pig skin collagen peptides, corn-derived antioxidant peptides and yeast mannoproteins. The study of Li Y. et al. confirmed that broccoli peptides exert anti-inflammatory activity by inhibiting the secretion of inflammatory factors by inflammatory cells. The results of Jiang S. et al. elucidate the interactions between gut bacteria and related cytokines and reveal the mechanisms underlying the anti-Iron deficiency anemia effect of pig skin collagen peptides ferrous chelates. Xu et al. found that IGGIGTVPVGR and LTTVTPGSR isolated and extracted from fermented milk have antioxidant capacity. The findings of Li X. et al. evealed that the prevention of obesity by yeast mannoproteins is highly linked to the promotion of *Parabacteroides distasonis* and inhibition of *Lactobacillus*.

Jiang W. et al., Liu et al., and Zhang et al. respectively established BALB/c mice model, high-fat diet mice model, and anti-oxidation model *in vitro* to confirm the immunomodulatory activity of the polysaccharide obtained from *Craterellus cornucopioides* (Zhang et al.), the advantage in alleviating high-fat diet induced obesity of *Zingiber striolatum* polysaccharides (Jiang W. et al.), and the antioxidant activity of *Houttuynia cordata* polysaccharides (Liu et al.).

Chen et al. found that red-fleshed apple flavonoid extract ameliorated CCl4-induced liver damage by modulating the abundance and composition of intestinal microorganisms in mice. Wang et al. reviewed the nutritional active components of sea buckthorn, such as vitamins, carotenoids, polyphenols, fatty acids, and phytosterols, and their health benefits, such as antioxidant, anticancer, anti-hyperlipidemic, anti-obesity, anti-inflammatory, antimicrobial, antiviral, dermatological, neuroprotective, and hepatoprotective activities. And they revealed the potential of sea buckthorn to be developed into functional foods or dietary supplements for the prevention and treatment of certain chronic diseases (Wang et al.).

Li C. et al. and Zhao et al. respectly investigated effects of drying strategies and steam explosion pretreatment on sporulation and titer of microbial ecological agents with *Bacillus subtilis* and enzymatic digestibility of overground tubers of tiger nut (*Cyperus esculentus* L.). Li C. et al. found that 80°C-hot air drying is an effective drying strategy for promoting sporulation, which improves the titer of microbial ecological agents with *B. subtilis*. The investigation of Zhao et al. revealed that steam explosion pretreatment promoted saccharification of the overground tubers of tiger nut, which paves the way for value-added valorization of the tiger nut plants.

In conclusion, the above research works provide theoretical support for the development and utilization of active ingredients such as protein/polypeptide, polysaccharide and flavonoid in food. This can play a role in improving the quality of both traditional food products and the processing technology, and guiding the investigation of new foods.

Author contributions

CS drafted the manuscript. BL and WS provided critical review and insight and revised the final version of the editorial. All authors contributed to the article and approved the submitted version.

Acknowledgments

The editors of this topic would like to thank all authors and reviewers for their contributions to the present collection.

Conflict of interest

The authors declare that the research was conducted in the absence of any commercial or financial relationships that could be construed as a potential conflict of interest.

Publisher's note

All claims expressed in this article are solely those of the authors and do not necessarily represent those of their affiliated organizations, or those of the publisher, the editors and the reviewers. Any product that may be evaluated in this article, or claim that may be made by its manufacturer, is not guaranteed or endorsed by the publisher.

frontiers | Frontiers in Nutrition

TYPE Original Research
PUBLISHED 27 September 2022
DOI 10.3389/fnut.2022.1025248

Check for updates

OPEN ACCESS

EDITED BY
Wenjie Sui,
Tianjin University of Science and Technology, China

REVIEWED BY
Wei Jiang,
Technical University of Denmark, Denmark
Xueping Song,
Guangxi University, China

*CORRESPONDENCE
Zhi-Min Zhao
zmzhao@imu.edu.cn

†These authors have contributed equally to this work and share first authorship

SPECIALTY SECTION
This article was submitted to Nutrition and Food Science Technology, a section of the journal Frontiers in Nutrition

RECEIVED 22 August 2022
ACCEPTED 06 September 2022
PUBLISHED 27 September 2022

CITATION
Li C, Zhao K, Ma L, Zhao J and Zhao Z-M (2022) Effects of drying strategies on sporulation and titer of microbial ecological agents with *Bacillus subtilis*. *Front. Nutr.* 9:1025248. doi: 10.3389/fnut.2022.1025248

COPYRIGHT
© 2022 Li, Zhao, Ma, Zhao and Zhao. This is an open-access article distributed under the terms of the Creative Commons Attribution License (CC BY). The use, distribution or reproduction in other forums is permitted, provided the original author(s) and the copyright owner(s) are credited and that the original publication in this journal is cited, in accordance with accepted academic practice. No use, distribution or reproduction is permitted which does not comply with these terms.

Effects of drying strategies on sporulation and titer of microbial ecological agents with *Bacillus subtilis*

Chonglei Li[1,2†], Kai Zhao[1,2†], Litong Ma[3], Ji Zhao[1] and Zhi-Min Zhao[1,2*]

[1]Inner Mongolia Key Laboratory of Environmental Pollution Control and Wastes Reuse, School of Ecology and Environment, Inner Mongolia University, Hohhot, China, [2]Key Laboratory of Ecology and Resource Use of the Mongolian Plateau (Ministry of Education), Inner Mongolia University, Hohhot, China, [3]Inner Mongolia Engineering Research Center of Comprehensive Utilization of Bio-coal Chemical Industry, School of Chemistry and Chemical Engineering, Inner Mongolia University of Science and Technology, Baotou, China

Drying operation is beneficial to the preservation and transportation of microbial ecological agents. In this study, drying kinetics and water distribution variations in solid biomass medium during hot air drying (HAD) and vacuum freeze drying (VFD) were systematically investigated. Meanwhile, the effects of different drying strategies on the sporulation of *Bacillus subtilis* and the titer of microbial ecological agents were compared. The results showed that both HAD and VFD induced rapid water removal from the solid biomass medium. VFD retained bound water and maintained the porous structure of the solid medium. Both HAD and VFD induced sporulation. The expression level of sporulation-regulatory genes *spo0A*, *sigF*, and *sigE* followed the order 80°C-HAD > 60°C-HAD > VFD. The spore number in the medium after 80°C-HAD drying for 6 h was 0.72×10^{10}/g dry medium, which was 9.1 and 12.5% larger than that of the medium with 60°C-HAD and VFD, respectively. Therefore, 80°C-HAD is an effective drying strategy for promoting sporulation, which improves the titer of microbial ecological agents with *B. subtilis*.

KEYWORDS

microbial ecological agents, *Bacillus subtilis*, sporulation, hot air drying, vacuum freeze drying, low-field nuclear magnetic resonance

Introduction

The indiscriminate use of antibiotics leads to the occurrence of antibiotic resistance genes (ARGs) and antibiotic-resistant bacteria (ARB) from environments (1, 2). *Bacillus subtilis* microbial ecological agents are environmentally friendly alternatives to antibiotics, which can be utilized as feed additives for preventing disease and promoting animal growth (3–5). The preparation process of microbial ecological agents consists of strain breeding, fermentation, and drying processes, among which the drying process aims to reduce water content (WC) in the solid substrate and enhance the stability of probiotics products for preservation and transportation (6, 7). Hot air

drying (HAD) is widely used for the production of dehydrated food and solid medium. Vacuum freeze-drying (VFD) method sublimates water at subfreezing temperatures. It is the preferred drying method for biomaterials because most biomaterials are vulnerable to heat (8). However, there was rare information about the effects of HAD and VFD on the sporulation and titer of *B. subtilis* microbial ecological agents.

Low-field nuclear magnetic resonance (LF-NMR) has been regarded as a powerful tool to analyze the water states and distribution in the solid medium due to its fast analysis speed, good sensitivity, and non-invasiveness (9, 10). Using the LF-NMR technique, Li et al. (11) identified three different proton fractions (T_{2b}, T_{21}, and T_{22}) with various mobilities in the glutinous rice during solid-state fermentation (SSF). Recently, the LF-NMR technique has exhibited an excellent ability to explore the water dynamics during the drying process for solid substrates (12). Bacteria spore number is a key indicator to evaluate the quality of microbial ecological agents (13). By forming spores, bacteria cells can survive in severe environments (e.g., acid and mechanical force) and reawaken when favorable conditions return (14). Spores of *B. subtilis* are resistant to environmental stress, which includes heat in the drying process (15). The sporulation process begins with the activation of the master transcriptional gene *spo0A*, which leads to the sequential activation of the *sigF* gene in the forespore and the *sigE* gene in the parent cell (16). Therefore, the expression of *spo0A*, *sigF*, and *sigE* genes can indicate the sporulation process of *B. subtilis* with different drying strategies.

This study aimed to compare the effects of different drying strategies on the sporulation of *B. subtilis* and improved the titer of microbial ecological agents. The key metrics, such as water dynamics, molecular genetic expressions, viable cell, and spore number variations, were systematically evaluated and compared. These together could help to reveal the relationship between water distribution and sporulation during different drying processes, which could further benefit the production of microbial ecological agents of *B. subtilis*.

Materials and methods

Solid-state fermentation

Bacillus subtilis 10732 was purchased from the China Center of Industrial Culture Collection (CICC). The strain was stored in Luria-Bertani (LB) medium slant at 4°C. *B. subtilis* 10732 was precultivated in 100 ml of a liquid medium that contained 1% (w/w) yeast extract, 4% (w/w) glucose, 1% (w/w) peptone, 1% (w/w) $CaCO_3$, and 0.05% (w/w) $MgSO_4$ at 37°C and was shaken at 150 rpm for 24 h.

The solid medium consisted of 3.0 g of soybean meal, 30 g wheat bran, 0.75 g glucose, 1.5 g $CaCO_3$, 30 ml of 1.25% (w/w) $(NH_4)_2SO_4$, 0.05% (w/w) $MnSO_4$, 2.5% (w/w) KH_2PO_4 inorganic salt solution, and 9.6 ml of deionized water. The medium was put into 250 ml Erlenmeyer flasks and sterilized at 121°C for 20 min. Afterward, the medium was cooled at room temperature and then inoculated by adding 12 ml of seed solution. The fermentation was conducted in an incubator at 37°C for 72 h.

Drying experiment

After fermentation, the solid medium was subjected to different drying treatments. The solid biomass medium was dehydrated until reaching constant weight. The temperatures of HAD were set at 60 and 80°C. The process of VFD included two steps: freezing and drying. All water in the solid medium was frozen in the first freezing step at −80°C for 1 h. The drying step was set at −45°C and 10 Pa to remove water in a vacuum environment until the medium reached a constant weight (8, 17).

Water content and drying rate (DR) are two important indicators to reveal the drying performance (12, 18). During the drying process, the mass of the solid medium was weighed, and the WCs (dry basis, $g{\cdot}g^{-1}$) were calculated using Equation (1):

$$WC_t = (m_t - m_e)/m_e \quad (1)$$

where WC_t is the WC ($g{\cdot}g^{-1}$) at the time t, m_t is the mass (g) of the solid medium at t h, and m_e is the final dry mass (g) of the solid medium. DR ($g{\cdot}g^{-1}{\cdot}h^{-1}$) was calculated according to Equation (2):

$$DR = (WC_t - WC_{t+\Delta t})/\Delta_t \quad (2)$$

where WC_t and $WC_{t+\Delta t}$ are the WC at t and $t + \Delta t$, respectively. The samples were taken at intervals of 1 h for WC and DR analyses.

LF-NMR measurements

Low-field nuclear magnetic resonance was applied to analyze water states and dynamics in a solid medium on a MesoMR23-060H-I Analyst Analyzing and Imaging System (Niumag Co., Ltd., Shanghai, China). In total, 2.60 g of solid medium samples were obtained from the central part of the substrates. The samples were placed into 25 mm NMR glass tubes first and then inserted into the NMR probe for detection. The T_{2i} relaxation times were measured using Carr-Purcell-Meiboom-Gill (CPMG) sequence with a τ-value of 100 μs. A total of 3,000 echoes were collected as 16 scan repetitions, and the repetition time between two successive scans was 2.5 s. The relaxation time measurements were performed at 32°C. Data

analysis was performed with the NMR Analyzing System version 1.0 (Niumag Co., Ltd., Shanghai, China). Relaxation time T_{2i} and its corresponding water proportion M_{2i} were presented.

Measurement of viable cell and spore number

Approximately 3 g of the solid medium was mixed with sterile water (1:20, w/v) in a 250 ml Erlenmeyer flask and shaken at 150 rpm for 30 min at 37°C. In total, 100 μl of the supernatant was carefully sampled and serially diluted (10^6-fold). Afterward, the cell count was determined by the spread plate method on LB plates. After incubation at 37°C for 24 h, the viable cell number was counted and expressed as colony-forming units (CFUs). Similarly, 5.0 ml of the mixture after shaking at 150 rpm for 30 min at 37°C in the determination of viable cell number was sampled and cultured at 80°C for 15 min. Afterward, 100 μl of the mixture was serially diluted (10^6-fold) and spread on LB plates. After incubation at 37°C for 24 h, the spore number was determined.

Quantitative polymerase chain reaction (qPCR) analysis of *spo0A*, *sigF*, and *sigE* gene expressions

Approximately 1 g of the solid medium was sampled and mixed with sterile water (1:20, w/v) in a 50 ml sterile test tube and shaken at 150 rpm for 5 min. Afterward, the mixture was centrifuged at 8,000 rpm for 10 min, and the precipitate was separated and stored at −80°C. Total RNA of *B. subtilis* was extracted using Cetyltrimethylammonium Bromide (CTAB) method (19). Before reverse transcription, the purity of the total RNA was tested by measuring OD260 and OD280 with a Nano Photometer P-Class P360 Ultraviolet Spectrophotometer. In total, 10 μl of total RNA was used as a template and was reverse transcribed to cDNA using PrimeScript RT Regent Kit (Takara Company) with a final volume of 20 μl. Moreover, the mixture was incubated at 37°C for 15 min and then at 85°C for 5 min to inactivate the enzyme. The primers for qPCR were synthesized by Sangon Biotech (Shanghai, China). The qPCR procedure was 30 s at 95°C followed by 35 cycles of 30 s at 95°C, 45 s at the annealing temperature of 35°C, and 45 s at 72°C, with a melt curve increasing from 65 to 95°C at increments of 0.5°C. The sample dried for 0 h was selected as the calibration sample for the gene expressions of *spo0A*, *sigF*, and *sigE*. The relative quantification of gene transcription was analyzed using the $2^{-\Delta\Delta Ct}$ method (20).

Statistical analysis

Statistical analysis was performed by using SPSS version 21.0. Differences between the means were evaluated by the one-way ANOVA and the independent samples *t*-tests.

Results and discussion

Changes of WC and DR during different drying processes

Water content and DR are two important indicators to evaluate the drying process of a solid medium. Effects of different drying strategies on WC and DR were investigated (Figure 1). The WC of all media was decreased during the drying processes. The solid medium reached constant weight after 4 h drying with 80°C-HAD, while the time needed to reach constant weight with VFD and 60°C-HAD was 5 and 6 h, respectively. The higher the drying temperature, the faster the WC of the solid medium declined (12). Figure 1B shows that DR of 80°C-HAD and VFD increased from 0 to 1 h and then decreased gradually to the end of the drying process. The maximum DR values of 80°C-HAD and VFD were 0.60 and 0.72 $g{\cdot}g^{-1}{\cdot}h^{-1}$, respectively. The highest DR of 60°C-HAD was 0.45 $g{\cdot}g^{-1}{\cdot}h^{-1}$, which appeared during the period of 1–2 h. Sun et al. (18) reported that there were three stages during microwave freeze-drying for raspberry: the speed-up drying stage (I), the speed-down drying stage (II), and the low-speed drying stage (III), respectively. In line with the previous study, the drying process of solid biomass medium with HAD and VFD in this study could also be divided into three periods: (I) the speed-up drying period (0–1 h for 80°C-HAD and VFD and 0–2 h for 60°C-HAD); (II) the speed-down drying period (1–4 h for 80°C-HAD and VFD and 2–4 h for 60°C-HAD); and (III) the low-speed drying stage (4–8 h for 60°C-HAD, 80°C-HAD, and VFD). In the drying period I, the solid biomass medium presented higher WC and stronger heat absorption ability as compared to periods II and III, which caused the rapid water removal (7). With the extension of drying, the WC and heat absorption capacity of the medium were decreased. Meanwhile, the change in the internal structure of the solid medium also inhibited the water distribution (18), which was responsible for the DR decrease.

Comparison of water state variations of solid media during different drying processes

Low-field nuclear magnetic resonance can be used to evaluate water states in the substrate, which are significantly related to the microstructure of the solid medium (21). In this study, water dynamics and relaxation times of T_{2i} fractions

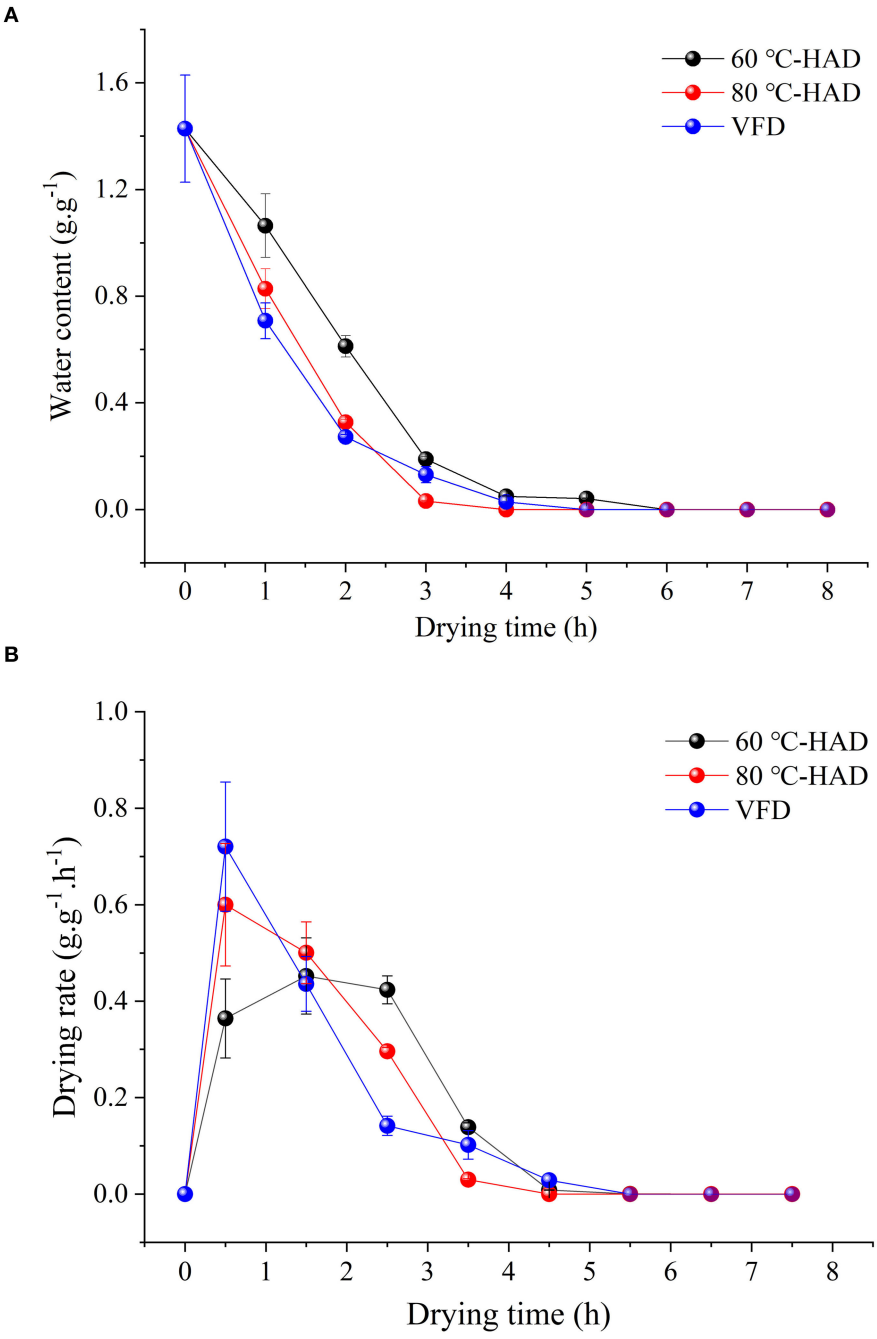

FIGURE 1
Changes in water content **(A)** and drying rate **(B)** during different drying processes.

were investigated to elucidate the microstructure changes of solid medium treated by different drying strategies. Figure 2 shows that three kinds of proton fractions are found in the solid medium after fermentation (curve at 0 h). The different fractions represent three different states of water, namely, (1) bound water, T_{2b} associated with hydroxyl and/or carboxyl hydrophilic groups (22); (2) capillary water, T_{21} attributed to the water molecules in pores of solid media (23); and (3) lumen water, T_{22} ascribed to water molecules in the cavities of the three-dimensional network in solid media (11). M_{2b}, M_{21}, and

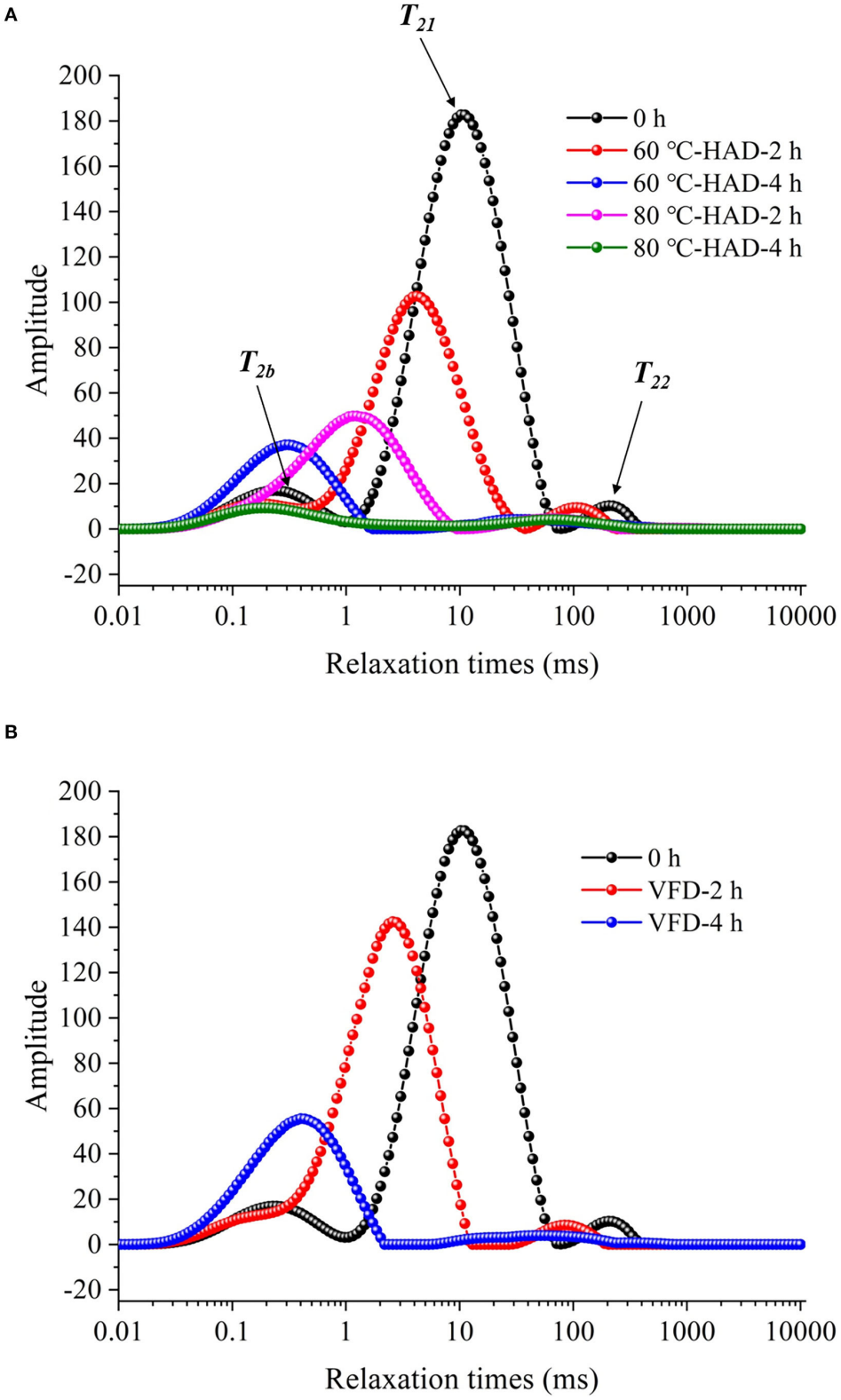

FIGURE 2
Development curves in relaxation time of solid medium with different drying strategies. **(A)** Hot air drying (HAD). 60°C-HAD-2 h: hot air drying at 60°C for 2 h; 60°C-HAD-4 h: hot air drying at 60°C for 4 h; 80°C-HAD-2 h: hot air drying at 80°C for 2 h; and 80°C-HAD-4 h: hot air drying at 80°C for 4 h. **(B)** Vacuum freeze-drying (VFD). VFD-2 h: vacuum freeze-drying for 2 h; VFD-4 h: vacuum freeze-drying for 4 h.

TABLE 1 Relaxation times (T_{2i}) and water proportion (M_{2i}) of the solid biomass medium during drying processes.

T_{2i} and M_{2i} / Drying condition	T_{2b}(ms)	T_{21}(ms)	T_{22}(ms)	M_{2b} (Peak area/a.u.)	M_{21} (Peak area/a.u.)	M_{22} (Peak area/a.u.)	$\sum M_{2i}$ (Peak area/a.u.)
0 h	0.25	11.10	240.94	408	4630	125	5163
60°C-HAD-2 h	0.16	4.20	107.19	250	2701	65	3016
60°C-HAD-4 h	0.29	34.49 ($T_{21}T_{22}M$)		1023	140 ($M_{21}M_{22}M$)		1163
80°C-HAD-2 h	1.15	65.93 ($T_{21}T_{22}M$)		1617	107 ($M_{21}M_{22}M$)		1724
80°C-HAD-4 h	0.21	65.93 ($T_{21}T_{22}M$)		313	115 ($M_{21}M_{22}M$)		428
VFD-2 h	2.58 ($T_{2b}T_{21}M$)	84.07		3842 ($M_{2b}M_{21}M$)	116		3958
VFD-4 h	0.40	51.71 ($T_{21}T_{22}M$)		1601	132 ($M_{21}M_{22}M$)		1733

$T_{21}T_{22}M$: T_{21} and T_{22} merged; $T_{2b}T_{21}M$: T_{2b} and T_{21} merged; $M_{21}M_{22}M$: M_{21} and M_{22} merged; $M_{2b}M_{21}M$: M_{2b} and M_{21} merged; $\sum M_{2i}$ is the sum of M_{2b}, M_{21}, and M_{22}.

M_{22} were the corresponding water proportion, respectively. Table 1 shows that the T_{2b}, T_{21}, and T_{22} relaxation times and M_{2b}, M_{21}, and M_{22} water proportions are decreased during 60°C-HAD for 2 h, which indicates the reduction of water fluidity and a decrease of WC. T_{21} capillary water and T_{22} lumen water were the relatively free water in solid biomass medium, which can be removed first in the drying process. However, T_{2b} bound water was associated with hydroxyl and/or carboxyl hydrophilic groups, which was relatively difficult to remove. It should be noted that T_{21} and T_{22} peaks were merged into 1 weak peak at 60°C-HAD-4 h, 80°C-HAD-2 h, 80°C-HAD-4 h, and VFD-4 h conditions. T_{2b} and T_{21} peaks were merged into 1 weak peak at VFD-2 h. It was speculated that drying treatments can break the barriers between different water fractions, thereby leading to the merging of T_{21} and T_{22} and T_{2b} and T_{21} peaks. Tang et al. (24) also reported that water fractions can only be distinguished where microstructural barriers exist because they can hinder the inter-compartment water diffusion, which was consistent with the present results.

The $\sum M_{2i}$ of the solid medium at 80°C-HAD-2 h decreased by 42.8% than that at 60°C-HAD-2 h, while the $\sum M_{2i}$ at 80°C-HAD-4 h decreased by 63.2% than that at 60°C-HAD-4 h. These results indicated that the higher drying temperature during HAD could accelerate the water release from the medium. The proportion of M_{2b} to $\sum M_{2i}$ at VFD-4 h was 92.4%, which was higher than that of 60°C-HAD and 80°C-HAD at the same drying time. VFD is a process in which water is crystallized at a low temperature and thereafter sublimated from the solid state directly into the vapor phase (25). The capillary water and lumen water were frozen as ice crystals and sublimated, but the bound water was retained with VFD. In summary, both HAD and VFD decreased the water fraction amplitudes and altered the water fraction distributions within a solid biomass medium. These different water states within the media should influence the sporulation process of *B. subtilis*.

Expression of sporulation-regulatory genes during different drying processes

The expression of *spo0A*, *sigF*, and *sigE* genes associated with sporulation during the drying processes was systematically investigated. Figure 3A shows that the expression of the *spo0A* gene exhibited an increasing tendency with the extension of drying time. Since the *spo0A* gene is the major regulator for the initiation of sporulation (26, 27), the increasing expression of *spo0A* illustrated the enhanced sporulation process with the HAD and VFD drying strategies. After drying for 6 h, the expression of the *spo0A* gene in 80°C-HAD reached 2.8, which was higher than that of 60°C-HAD (1.8) and VFD (1.8). It suggested that the 80°C-HAD drying strategy can facilitate the sporulation process more significantly.

As seen in Figures 3B,C, the expression of *sigF* and *sigE* genes in 80°C-HAD is increased by 206 and 249% from 0 to 6 h drying time, respectively. The expression of *sigF* and *sigE* genes in 60°C-HAD was increased by 70 and 120% from 0 to 6 h drying time, respectively. The expression of *sigF* and *sigE* genes in VFD increased by 10 and 100% from 0 to 6 h drying time, respectively. These results showed that the *sigF* and *sigE* genes exhibited increasing tendencies with the extension of drying time, which were similar to the *spo0A* gene expression variation. The expression levels of *sigF* and *sigE* gene at 80°C-HAD after 6 h drying were 1.76 and 1.57 times of those at 60°C-HAD. Fimlaid et al. (28) reported that the *sigF* and *sigE* genes are expressed in a *spo0A*-dependent manner. The higher the drying temperature, the more intense the sporulation process. Activation of the master transcriptional gene *spo0A* leads to the sequential activation of *sigF* and *sigE* genes, which can activate compartment-specific transcriptional programs that drive sporulation through its morphological stages (16). Both HAD and VFD induced sporulation. The expressions of *spo0A*, *sigF*, and *sigE* genes during drying followed the order 80°C-HAD > 60°C-HAD > VFD. These results indicated that high temperature in HAD facilitated sporulation-regulatory gene

10.3389/fnut.2022.1025248

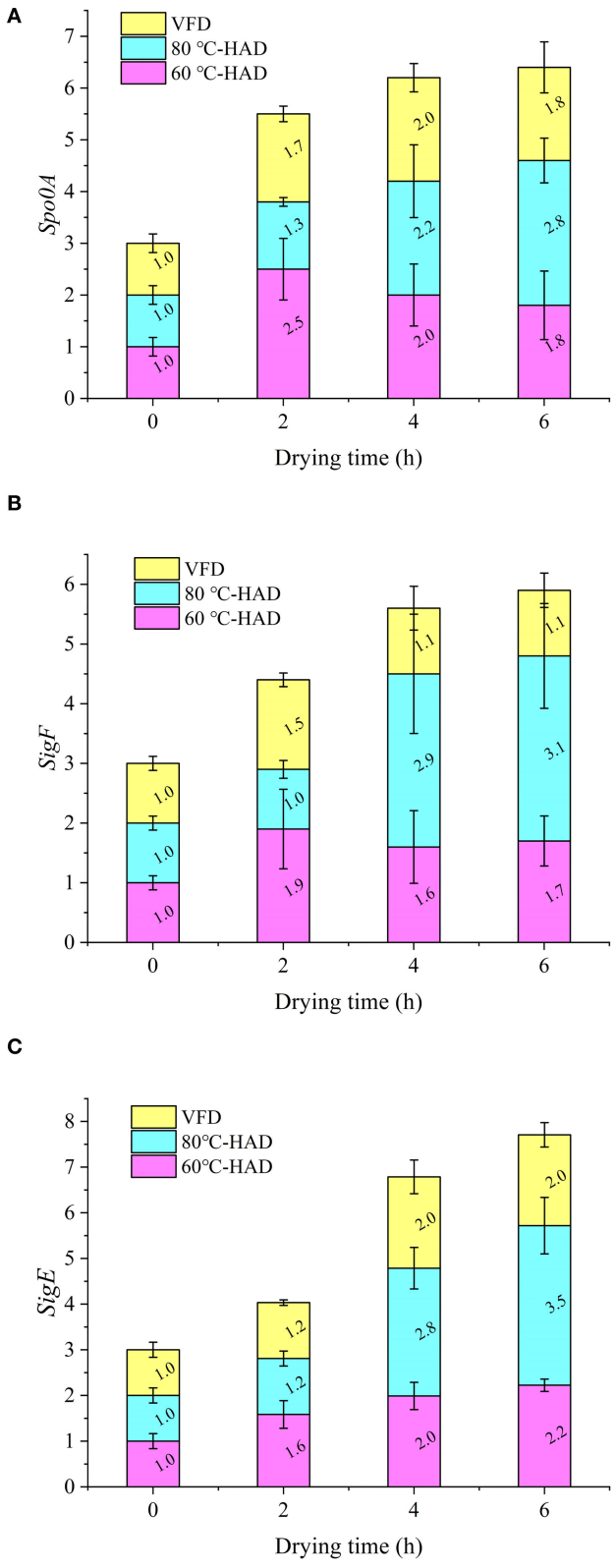

FIGURE 3
Expressions of *spo0A* **(A)**, *sigF* **(B)**, and *sigE* **(C)** genes during different drying processes.

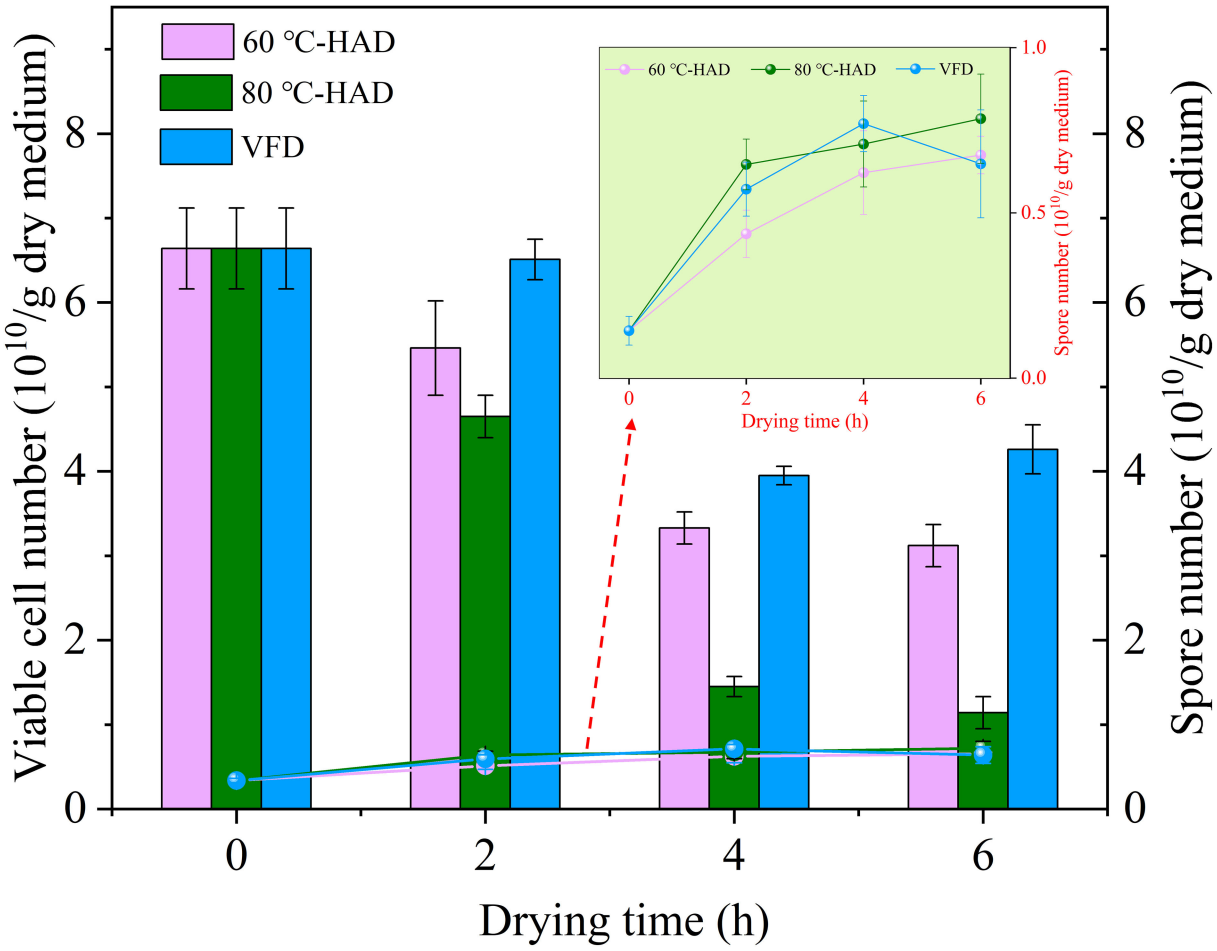

FIGURE 4
Comparison of viable cell and spore numbers during different drying processes.

expression, which was more likely to promote sporulation of *B. subtilis*.

Viable cell and spore number changes during different drying processes

The number of viable cells and spores can be used to evaluate the quality of microbial ecological agents, food additives, etc. (13, 29, 30). Figure 4 shows the variation of viable cell and spore numbers in media with different drying strategies. The viable cell number exhibited decreasing tendencies, while the spore number showed increasing trends with the extension of drying time in all media. It should be noted that the viable cell number decreased fast while the spore number increased rapidly from 0 to 4 h in 80°C-HAD, 60°C-HAD, and VFD processes. The possible reason for this phenomenon was that WC decreased fast during this drying period. Influenced by the rapid removal of water, the viable cell formed spores to resist harsh environments.

With the extension of drying time, the viable cell number of 80°C-HAD was always lower than that of 60°C-HAD, while the spore number of 80°C-HAD was always higher than that of 60°C-HAD. Especially, the viable cell numbers of 80°C-HAD at 4 and 6 h drying time were 1.45×10^{10} and 1.14×10^{10}/g dry medium, respectively, which were lower than that of 60°C-HAD at 4 h (3.33×10^{10}/g dry medium) and 6 h (3.12×10^{10}/g dry medium). Moreover, the 80°C-HAD strategy caused a more rapid water decrease in the solid medium than 60°C-HAD, resulting in a more hydropenic environment. This severe condition induced more viable cell death or transformation to spores under 80°C-HAD. Previous studies reported that air drying caused physical alterations (e.g., shrinkage), which decreased the porosity of the microscopic structure of substrate materials (31–33). Similarly, HAD in the present study also led to the shrinkable structure of solid biomass medium with the

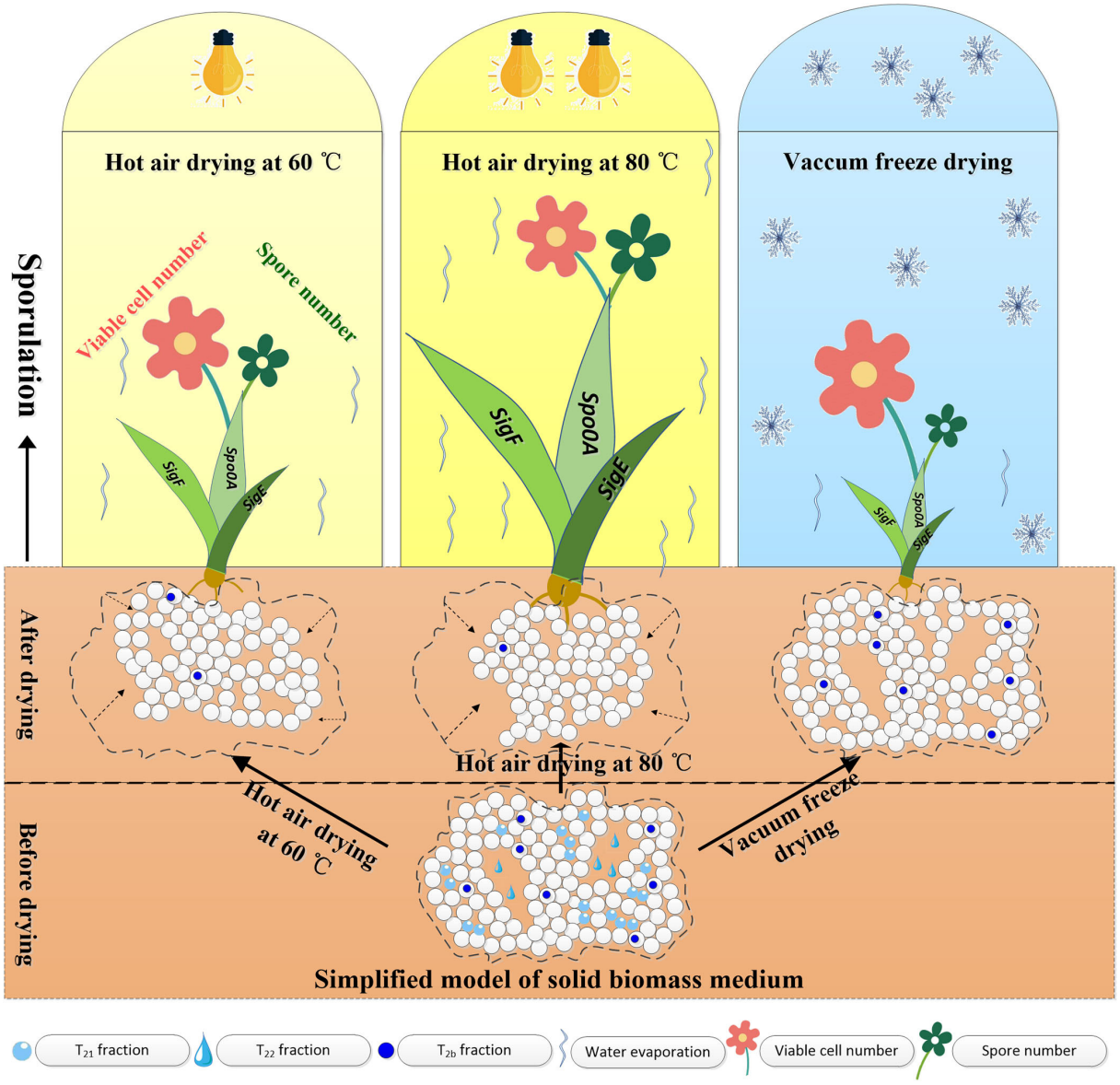

FIGURE 5
Proposed model for water state variations, microstructural changes of solid media, and *B. subtilis* sporulation during different drying processes.

extension of drying. The inferior porosity of the solid biomass medium was harmful to the growth of vegetative cells, which enhanced sporulation. The spore number of 80°C-HAD was 0.72×10^{10}/g dry medium after 6 h of drying, which was 9.1 and 12.5% larger than that of 60°C-HAD and VFD, respectively. The spore number of 80°C-HAD, 60°C-HAD, and VFD was increased by 115, 95, and 90%, respectively, during 0–6 h drying processes. Therefore, it can be concluded that the drying processes in the present study promoted sporulation. It should also be noted that the viable cell number of VFD showed a slight increase while the spore number decreased slightly during drying for 4–6 h. This phenomenon was contrary to the general trend of viable cell and spore numbers but can be explained by the specific sublimation drying process of VFD. By drying in the frozen state, the free water fractions within the solid medium were presented as ice crystals. Then, these water fractions were sublimated continuously with the extension of drying time (25). As a result, the pores and cavities were vacated in the final period of drying, providing a porous medium and effective contact space for spore germination during 4–6 h drying time. Overall, VFD can maintain the porous structure of a solid medium, but HAD, especially 80°C-HAD, presented the vigorous sporulation process, which improved the titer of microbial ecological agents with *B. subtilis*.

Based on the above experimental results, a comprehensive model was proposed to elucidate the water state variations, microstructural changes of solid media, and *B. subtilis* sporulation during different drying processes. As seen in Figure 5, HAD leads to the shrinkage of pores and cavities in solid media, but VFD retains bound water and maintains the porous structure. Both HAD and VFD induced sporulation. The expression levels of *spo0A*, *sigF*, and *sigE* genes with 80°C-HAD were the highest as compared to 60°C-HAD and VFD, resulting in the largest spore number in medium with 80°C-HAD. The proposed model clearly elucidated the water states and microstructure changes within solid biomass media, which provided a better understanding of the effects of drying strategies on the sporulation of *B. subtilis*.

Conclusion

Effects of different drying strategies on the sporulation of *B. subtilis* were revealed. Both HAD and VFD induced rapid water removal from solid biomass medium and facilitated sporulation. The expression level of sporulation-regulatory genes followed the order 80°C-HAD > 60°C-HAD > VFD. Accordingly, the spore number with 80°C-HAD was increased by 9.1 and 12.5% than that of 60°C-HAD and VFD, respectively. Therefore, 80°C-HAD is an effective drying strategy for promoting sporulation, which improves the titer of *B. subtilis* microbial ecological agents effectively.

Data availability statement

The original contributions presented in the study are included in the article/supplementary material, further inquiries can be directed to the corresponding author/s.

Author contributions

Conceptualization: Z-MZ. Formal analysis: CL, KZ, and Z-MZ. Funding acquisition: Z-MZ and LM. Investigation: KZ, CL, and Z-MZ. Project administration: Z-MZ and JZ. Writing—original draft: CL and KZ. Writing—review and editing. CL, KZ, LM, JZ, and Z-MZ. All authors contributed to the article and approved the submitted version.

Funding

This work was supported by the National Natural Science Foundation of China (Grant Numbers 21706136 and 21766025) and the Natural Science Foundation of Inner Mongolia (Grant Number 2019MS02026).

Conflict of interest

The authors declare that the research was conducted in the absence of any commercial or financial relationships that could be construed as a potential conflict of interest.

Publisher's note

All claims expressed in this article are solely those of the authors and do not necessarily represent those of their affiliated organizations, or those of the publisher, the editors and the reviewers. Any product that may be evaluated in this article, or claim that may be made by its manufacturer, is not guaranteed or endorsed by the publisher.

References

1. Guan AM, Qi WX, Peng Q, Zhou JM, Bai YH, Qu JH. Environmental heterogeneity determines the response patterns of microbially mediated N-reduction processes to sulfamethoxazole in river sediments. *J Hazard Mater.* (2021) 11:126730. doi: 10.1016/j.jhazmat.2021.126730

2. Barrios RE, Khuntia HK, Bartelt-Hunt SL, Gilley JE, Schmidt AM, Snow DD Li X. Fate and transport of antibiotics and antibiotic resistance genes in runoff and soil as affected by the timing of swine manure slurry application. *Sci Total Environ.* (2020) 712:136505. doi: 10.1016/j.scitotenv.2020.136505

3. Pan X, Cai YL, Kong LL, Xiao CP, Zhu QD, Song ZG. Probiotic effects of *Bacillus licheniformis* DSM5749 on growth performance and intestinal microecological balance of laying hens. *Front Nutr.* (2022) 9:868093. doi: 10.3389/fnut.2022.868093

4. Kaspar F, Neubauer P, Gimpel M. Bioactive secondary metabolites from *Bacillus subtilis*: a comprehensive review. *J Nat Prod.* (2019) 82:7. doi: 10.1021/acs.jnatprod.9b00110

5. Gao DY, Sun XB, Liu MQ, Liu YN, Zhang HE, Shi XL, et al. Characterization of thermostable and chimeric enzymes via isopeptide bond-mediated molecular cyclization. *J Agr Food Chem.* (2019) 67:6837–46. doi: 10.1021/acs.jafc.9b01459

6. Chen H, Chen SW, Li CN, Shu GW. Response surface optimization of lyoprotectant for *lactobacillus bulgaricus* during vacuum freeze-drying. *Prep Biochem Biotech.* (2015) 45:463–75. doi: 10.1080/10826068.2014.923451

7. Ambros S, Mayer R, Schumann B, Kulozik U. Microwave-freeze drying of lactic acid bacteria: Influence of process parameters on drying behavior and viability. *Innov Food Sci Emerg.* (2018) 48:90–8. doi: 10.1016/j.ifset.2018.05.020

8. Byun SY, Kang JS, Chang YS. Analysis of primary drying of poly-γ-glutamic acid during vacuum freeze drying. *J Mech Sci Technol.* (2020) 34:4323–32. doi: 10.1007/s12206-020-0922-9

9. Kirtil E, Oztop MH. ^{1}H nuclear magnetic resonance relaxometry and magnetic resonance imaging and applications in food science and processing. *Food Eng Rev.* (2015) 8:1–22. doi: 10.1007/s12393-015-9118-y

10. Kirtil E, Cikrikci S, Mccarthy MJ, Oztop MH. Recent advances in time domain NMR & MRI sensors and their food applications. *Curr Opin Food Sci.* (2017) 17:9–15. doi: 10.1016/j.cofs.2017.07.005

11. Li T, Tu C, Rui X, Gao Y, Li W, Wang K, et al. Study of water dynamics in the soaking, steaming, and solid-state fermentation of glutinous rice by

LF-NMR: a novel monitoring approach. *J Agr Food Chem.* (2015) 63:3261–70. doi: 10.1021/acs.jafc.5b00769

12. Cheng SS, Li RR, Yang HM, Wang SQ, Tan MQ. Water status and distribution in shiitake mushroom and the effects of drying on water dynamics assessed by LF-NMR and MRI. *Dry Technol.* (2020) 38:1001–10. doi: 10.1080/07373937.2019.1625364

13. Veen B, Xie H, Esveld E, Abee T, Mastwijk H, Groot MN. Inactivation of chemical and heat-resistant spores of *Bacillus* and *Geobacillus* by nitrogen cold atmospheric plasma evokes distinct changes in morphology and integrity of spores. *Food Microbiol.* (2015) 45:26–33. doi: 10.1016/j.fm.2014.03.018

14. Setlow P, Johnson EA. Spores and their significance. *Food Microbiol Fundam Front*. (2019) 23–63. doi: 10.1128/9781555819972.ch2

15. Zhao ZM, Xi JT, Xu JF, Ma LT, Zhao J. Enhancement of *Bacillus subtilis* growth and sporulation by two-stage solid-state fermentation strategy. *Processes.* (2019) 7:644. doi: 10.3390/pr7100644

16. Tan IS, Ramamurthi KS. Spore formation in *Bacillus subtilis*. *Env Microbiol Rep*. (2014) 6:212–25. doi: 10.1111/1758-2229.12130

17. Patel SM, Doen T, Pikal MJ. Determination of end point of primary drying in freeze-drying process control. *AAPS PharmSciTech.* (2010) 11:73–84. doi: 10.1208/s12249-009-9362-7

18. Sun Y, Zhang M, Mujumdar AS Yu D. Pulse-spouted microwave freeze drying of raspberry: control of moisture using ANN model aided by LF-NMR. *J Food Eng.* (2021) 292:110354. doi: 10.1016/j.jfoodeng.2020.110354

19. Farrag M, Abri S, Leipzig ND. pH-dependent RNA isolation from cells encapsulated in chitosan-based biomaterials. *Int J Biol Macromol.* (2020) 146:422–30. doi: 10.1016/j.ijbiomac.2019.12.263

20. Hong Y, Zhou Z, Yu LZ, Jiang KY, Xia JM Mi YL, Zhang CQ Li J. *Lactobacillus salivarius* and *lactobacillus agilis* feeding regulates intestinal stem cells activity by modulating crypt niche in hens. *Appl Microbiol Biot.* (2021) 105:8823–35. doi: 10.1007/s00253-021-11606-2

21. Liu ZH, Chen HZ. Biomass-water interaction and its correlations with enzymatic hydrolysis of steam-exploded corn stover. *ACS Sustain Chem Eng.* (2016) 4:1274–85. doi: 10.1021/acssuschemeng.5b01303

22. Li T, Rui X, Li W, Chen XH, Jiang M, Dong MS. Water distribution in tofu and application of *T[[sb]]2[[/s]]* relaxation measurements in determination of Tofu's water-holding capacity. *J Agr Food Chem.* (2014) 62:8594–601. doi: 10.1021/jf503427m

23. Felby C, Thygesen LG, Kristensen JB, Jrgensen H, Elder T. Cellulose-water interactions during enzymatic hydrolysis as studied by time domain NMR. *Cellulose.* (2008) 15:703–10. doi: 10.1007/s10570-008-9222-8

24. Tang HR, Godward J, Hills B. The distribution of water in native starch granules—a multinuclear NMR study. *Carbohyd Polym.* (2000) 43:375–87. doi: 10.1016/S0144-8617(00)00183-1

25. Liu Y, Zhao Y, Feng X. Exergy analysis for a freeze-drying process. *Appl Thermal Eng.* (2008) 28:675–90. doi: 10.1016/j.applthermaleng.2007.06.004

26. Molle V, Fujita M, Jensen ST, Eichenberger P, Losick R. The spo0A regulon of *bacillus subtilis*. *Mol Microbiol.* (2004) 50:1683–701. doi: 10.1046/j.1365-2958.2003.03818.x

27. Fujita M, Gonzalez-Pastor JE, Losick R. High- and low-threshold genes in the Spo0A regulon of *Bacillus subtilis*. *J Bacteriol.* (2005) 187:1357–68. doi: 10.1128/JB.187.4.1357-1368.2005

28. Fimlaid KA, Shen A. Diverse mechanisms regulate sporulation sigma factor activity in the firmicutes. *Curr Opin Microbiol.* (2015) 24:88–95. doi: 10.1016/j.mib.2015.01.006

29. Velmourougane K, Prasanna R, Saxena AK. Agriculturally important microbial biofilms: Present status and future prospects. *J Basic Microbiol.* (2017) 57:548–73. doi: 10.1002/jobm.201700046

30. Mohsin MZ, Omer R, Huang J, Mohsin A, Zhuang Y. Advances in engineered *Bacillus subtilis* biofilms and spores, and their applications in bioremediation, biocatalysis, and biomaterials. *Syn Syst Biotechno.* (2021) 6:180–91. doi: 10.1016/j.synbio.2021.07.002

31. Ratti C. Hot air and freeze-drying of high-value foods: a review. *J Food Eng.* (2001) 49:311–9. doi: 10.1016/S0260-8774(00)00228-4

32. Witrowa-Rajchert D, Lewicki PP. Rehydration properties of dried plant tissues. *Int J Food Sci Technol.* (2006) 41:1040–6. doi: 10.1111/j.1365-2621.2006.01164.x

33. Ciurzyńska A, Lenart A. Freeze-drying-application in food processing and biotechnology–a review. *Pol J Food Nutr Sci.* (2011) 61:3. doi: 10.2478/v10222-011-0017-5

frontiers | Frontiers in Nutrition

TYPE Original Research
PUBLISHED 14 October 2022
DOI 10.3389/fnut.2022.1019344

Check for updates

OPEN ACCESS

EDITED BY
Bin Liang,
Ludong University, China

REVIEWED BY
Yan Jin,
Tianjin University of Science and Technology, China
Simin Feng,
Zhejiang University of Technology, China
Hongshun Yang,
National University of Singapore, Singapore

*CORRESPONDENCE
Guijie Chen
guijiechen@njau.edu.cn
Xiaoxiong Zeng
zengxx@njau.edu.cn

SPECIALTY SECTION
This article was submitted to Nutrition and Food Science Technology, a section of the journal Frontiers in Nutrition

RECEIVED 15 August 2022
ACCEPTED 21 September 2022
PUBLISHED 14 October 2022

CITATION
Li X, Wu J, Kang Y, Chen D, Chen G, Zeng X and Wang J (2022) Yeast mannoproteins are expected to be a novel potential functional food for attenuation of obesity and modulation of gut microbiota. *Front. Nutr.* 9:1019344. doi: 10.3389/fnut.2022.1019344

COPYRIGHT
© 2022 Li, Wu, Kang, Chen, Chen, Zeng and Wang. This is an open-access article distributed under the terms of the Creative Commons Attribution License (CC BY). The use, distribution or reproduction in other forums is permitted, provided the original author(s) and the copyright owner(s) are credited and that the original publication in this journal is cited, in accordance with accepted academic practice. No use, distribution or reproduction is permitted which does not comply with these terms.

Yeast mannoproteins are expected to be a novel potential functional food for attenuation of obesity and modulation of gut microbiota

Xiang Li[1], Junsong Wu[2], Yijun Kang[1], Dan Chen[3], Guijie Chen[3]*, Xiaoxiong Zeng[3]* and Jialian Wang[1]

[1]School of Marine and Biological Engineering, Yancheng Teachers' University, Yancheng, China, [2]Department of Basic Medical Science, Jiangsu Vocational College of Medicine, Yancheng, China, [3]College of Food Science and Technology, Nanjing Agricultural University, Nanjing, China

The yeast mannoproteins (MPs), a major component of yeast cell walls with large exploration potentiality, have been attracting increasing attention due to their beneficial effects. However, the information about the anti-obesogenic activity of MPs is still limited. Thus, the effects of MPs on the high-fat diet (HFD)-induced obesity and dysbiosis of gut microbiota were investigated in this work. The results showed that MPs could significantly attenuate the HFD-induced higher body weight, fat accumulation, liver steatosis, and damage. Simultaneously, the inflammation in HFD-induced mice was also ameliorated by MPs. The pyrosequencing analysis showed that intervention by MPs could lead to an obvious change in the structure of gut microbiota. Furthermore, the prevention of obesity by MPs is highly linked to the promotion of *Parabacteroides distasonis* (increased from 0.39 ± 0.12% to 2.10 ± 0.20%) and inhibition of *Lactobacillus* (decreased from 19.99 ± 3.94% to 2.68 ± 0.77%). Moreover, the increased level of acetate (increased from 3.28 ± 0.22 mmol/g to 7.84 ± 0.96 mmol/g) and activation of G protein-coupled receptors (GPRs) by MPs may also contribute to the prevention of obesity. Thus, our preliminary findings revealed that MPs from yeast could be explored as potential prebiotics to modulate the gut microbiota and prevent HFD-induced obesity.

KEYWORDS

yeast, mannoproteins, obesity, gut microbiota, *Parabacteroides distasonis*, *Lactobacillus*

Introduction

Obesity, recognized as a disease with serious morbidity and increased mortality, has dramatically spread throughout the developed and developing countries due to a shift to diets, including addictive and/or high-calorie foods and lack of exercise (1, 2). In the past four decades, the prevalence of obesity and overweight has nearly tripled

worldwide, which has become a growing public health challenge of the twenty-first century (3). Furthermore, obesity may lead to an increased risk of other obesity-related metabolic disorders, such as non-alcoholic fatty liver disease (NAFLD), type 2 diabetes (T2DM), and cardiovascular diseases (CDs) (4, 5). Obesity is a chronic and progressive process with multi-factorial factors and complex interactions, including physiological, sociopolitical, behavioral, and environmental factors (3, 6). Although the molecular mechanism for obesity is still not fully understood, obesity essentially represents a long-term positive imbalance between energy intake and energy expenditure, thereby increasing body fat (7). Pharmaceutical drugs, such as orlistat, could prevent, and treat obesity, however, its adverse effects, including acute kidney injury, subacute liver failure, and gastrointestinal adverse effects, block its further application (8). Thus, a potential novel therapeutic strategy for the prevention and treatment of obesity is still highly needed.

In recent decades, the effect of the gut microbiota on obesity has attracted much attention due to its key role in calorie harvest, energy homeostasis, and regulation of fat storage (9, 10). Recently and more strikingly, the experiments using germ-free mice and fecal microbiota transplantation have demonstrated the causality between the gut microbiota and the development of obesity (11, 12). More specifically, some key beneficial gut microbiota responsible for the prevention of obesity, such as *Akkermansia muciniphila* (13), *Parabacteroides distasonis* (14), and *Dysosmobacter welbionis* (15), and pathogenic bacteria which could promote obesity, such as *Erysipelatoclostridium Ramosum* (16) and *Enterobacter cloacae* B29 (17), have been identified, separated, and verified at the species level. The gut microbiota is expected to be a novel therapeutic target for the prevention and treatment of obesity. Thus, a series of microbiota-targeted diets are presented and evaluated with the growing public awareness of the gut microbiota (18, 19). Thereinto, dietary polysaccharides, which served as potential prebiotics, have recently emerged with the growing public awareness of their probiotic effect on gut microbiota (20).

Yeast is an important food resource used for fermentation in the food industry, and a large amount of yeast by-products is available every year (21). The yeast cell wall is mainly composed of β-glucan (60%) and mannoproteins (MPs, 40%), making them a potential source for providing functional ingredients (22). Nowadays, yeast by-products are mainly processed into animal feed or used to produce β-glucan (22, 23). β-Glucan from yeast has been widely investigated, whereas MPs from yeast attract much less attention. MPs are highly glycosylated proteins with molecular weights ranging from 20 to 200 kDa, containing 80–90% of carbohydrates and 5–20% of protein, and the potential structure of MPs has been reported in previous work (22, 24, 25). In recent years, the MPs have attracted more and more attention due to their alleged health-promoting functions, such as stimulation of angiogenesis, immunoactivities, and antineoplastic activities (25–27). However, the effects of MPs on obesity and gut microbiota are still unknown. Thus, the aim of the present work was to evaluate the potential anti-obesogenic effect of MPs on a high-fat diet (HFD)-induced obesity. Furthermore, the role of gut microbiota in the prevention of obesity by MPs was also investigated.

Materials and methods

Materials

The MPs from *Saccharomyces cerevisiae* were kindly provided by Angel Nutritech Co., Ltd. (China). The MPs were prepared according to the previous work with some modifications (25, 26). Briefly, after being sieved and purified, the slurry of *S. cerevisiae* cells was mixed with 3% sodium chloride, and the solution was incubated at 55°C for 24 h with agitation at 120 rpm/min. The residual autolyzed cells were obtained by centrifugation at 5,000 g for 10 min, and the MPs were extracted by water at 121°C for 4 h. The supernatant was collected and mixed with a triple volume of absolute alcohol. After keeping at 4°C for one night, the precipitated MPs were collected and deproteinized using the trichloroacetic acid method. The obtained solution was further mixed with a triple volume of absolute alcohol. The precipitate was collected, dissolved in distilled water, and further separated by Sepharose CL-4B to obtain the purified MPs. The contents of carbohydrates and protein were 86.3 ± 2.37% and 14.6 ± 1.45%, respectively. The molecular weight of MPs was 78 kD. The mice diets, including D12450J with 10 kcal% fat and D12492 with 60 kcal% fat, were purchased from Research Diets, Inc. (New Brunswick, NJ, USA).

Mice and diets

Six-week-old C57BL/6 male mice (n = 24, Shanghai SLAC Laboratory Animal Co., Ltd., Shanghai, China) were bred in the Animal Center of Nanjing Agricultural University (SYXK < Jiangsu > 2011-0037). All animal experimental protocols in this work were approved by the Institutional Animal Ethics Committee of the Experimental Animal Center of Nanjing Agricultural University. The mice were housed in specific pathogen-free (SPF) animal rooms under a 12-h dark-light cycle with *ad libitum* access to food and water. After an accommodation period of 1 week, mice were randomly divided into three groups (n = 8 per group), and fed for 10 weeks with a normal-chow diet (D12450J, coded as ND group), HFD (D12492, coded as HFD group), and HFD plus daily yeast MPs with a dosage of 400 mg/kg of body weight (coded as HFD-MP). The dosage of MPs in this work was chosen according to the previous work (23). Mice were supplemented daily with 0.2 mL of water in the ND and HFD groups and 0.2 mL of MPs

solution (400 mg of MP was dissolved in 10 mL of sterilized water) in the HFD-MP group by intragastric gavage. The body weight and food intake were assessed on a weekly basis. After overnight fasting, mice were anesthetized using carbon dioxide and then euthanized by cardiac puncture at the end of 10 weeks. The blood was drawn in tubes containing EDTA and centrifuged at 4,000 g to obtain plasma. The adipose tissue and liver were obtained and weighed. A part of the epididymis fat and liver samples were fixed with a 4% of paraformaldehyde solution. After embedding in paraffin, the epididymis fat and liver samples were sectioned and stained with hematoxylin and eosin (H&E stain). Then, the slices were observed under a light microscope.

Biochemical analysis

The plasma levels of triglycerides (TGs), low-density lipoprotein cholesterol (LDL-C), total cholesterol (TC), fasting plasma glucose, and alanine transaminase (ALT) were detected by a commercial kit according to the manufacturer's instructions. The plasma interleukin-1β (IL-1β), IL-10, IL-6, and tumor necrosis factor-alpha (TNF-α) levels were evaluated by commercial ELISA kits from Neobioscience Biological Technology Co., Ltd. (Shenzhen, China).

Gut microbiota analysis by 16S rRNA gene sequencing

The genomic DNA was extracted from the feces of the mice using the QiAamp DNA Stool Mini Kit (no. 51504, Qiagen, Germany). The V3-V4 region was amplified from purified DNA with the primers 341F (CCTACGGGNGGCWGCAG) and 805R (GACTACHVGGGTATCTAATCC). Sequencing was performed at an Illumina MiSeq platform by DeepBiome Co., Ltd. (Jinan, China) based on the manufacturer's guidelines to obtain the raw fastq files. The quality filtering of data was carried out using Trimmomatic (version 0.36). The paired reads were merged by USEARCH (version 11.2.64)[1] using the default parameters. The zero-radius operational taxonomic unit (ZOTU) was obtained using USEARCH. The bioinformatic analysis was performed by a previously reported method (28).

Short-chain fatty acid analyses

The levels of short-chain fatty acids (SCFAs) in mice cecal contents, including acetic, propionic, and n-butyric, were analyzed by gas chromatography (GC, 6890 N, Agilent) equipped with flame ionization detector (FID) and HP-INNOWAX capillary column (30 m × 0.25 mm × 0.25 μm, Agilent) using 2-ethylbutyric acid as internal standard (29). Briefly, the distilled water was added to cecal contents at a ratio of 1:5 (w/v). After centrifugation, the samples were mixed with internal standard solution (0.3 mg/mL of 2-ethylbutyric acid prepared in 0.2 mol/L of HCl solution) in equal volumes to obtain the solutions for GC analysis. The conditions of GC analysis were described in the previous work (29).

Ribonucleic acid extraction and quantification of gene expression

The total ribonucleic acid (RNA) in liver tissue was extracted by TaKaRa MiniBEST Universal RNA Extraction Kit (TaKaRa Bio. Inc., Beijing, China). The RNA was diluted and reverse-transcribed to cDNA by PrimeScript RT Master Mix (TaKaRa) after quantifying by using NanoDrop 2000 Spectrophotometer (Thermo Fisher Scientific Inc., Waltham, MA, USA). Then, the cDNA was used for RT-qPCR analysis using SYBR Green Master Mix on a QuantStudio 6 Flex (Thermo Fisher Scientific Inc.). The glyceraldehyde-3-phosphate dehydrogenase (GAPDH) was used as a housekeeping gene, and the mRNA expression was calculated using the $2^{-\Delta\Delta Ct}$ method. The specific primers used are summarized in **Supplementary Table 1**.

Statistical analysis

The outliers in this work were checked by GraphPad Prism 9.3.1 based on the Grubbs test (San Diego, CA, USA). The data were presented as mean ± SEM. The normality of all data was checked by SPSS 22 software (IBM) according to Shapiro–Wilk test. If the data for multiple-group comparisons had normal distribution, the statistical significance was performed by SPSS 22 software (IBM) using the one-way ANOVA procedure followed by the Tukey test; otherwise, the statistical significance was calculated using the Mann–Whitney test. The relationship between the parameters of obesity and gut microbiota was analyzed by Spearman's correlation analysis using SPSS 22 software using the data of all samples in ND, HFD, and HFD-MP groups (24 samples). All results were considered statistically significant at $p < 0.05$.

Results

Mannoproteins treatment ameliorated obesity and liver steatosis in high-fat diet-induced obese mice

As shown in **Figure 1**, HFD significantly resulted in the obesity of mice by increasing the body weight, promoting the accumulation of white adipose tissue, and inducing hepatic lipid

1 http://drive5.com

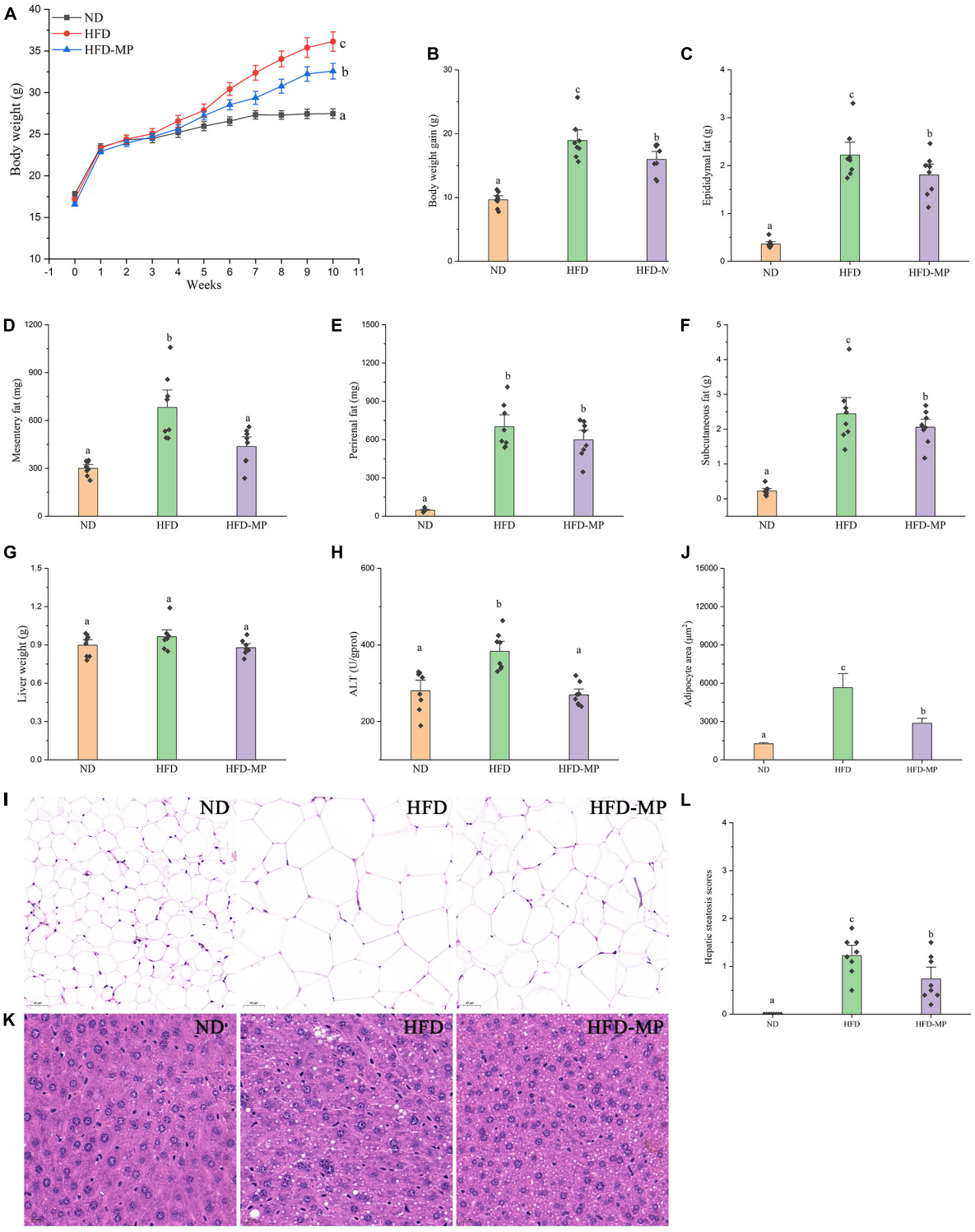

FIGURE 1
Impact of HFD and MP intervention on body features of mice. **(A)** Body weight, **(B)** body weight gain, weights of **(C)** epididymal, **(D)** mesentery, **(E)** perirenal, **(F)** subcutaneous fat pads, **(G)** liver weight, **(H)** plasma alanine transaminase (ALT) level, epididymal adipocyte sections after H&E staining **(I)**, quantification of adipocyte area by ImageJ software **(J)**, liver **(K)** sections after H&E staining, and hepatic steatosis scores **(L)**. The data are represented as the mean ± SEM. Statistical differences were carried out by one-way ANOVA followed by Turkey's test, $p < 0.05$ indicates significant differences.

accumulation and steatosis. MP treatment could significantly decrease body weight gain from the sixth week until the end of this work. Compared with the HFD group, the MP-treated mice showed reduced body weight, and accumulation of epididymal, mesentery, and subcutaneous fat tissues (Figures 1A–F). Furthermore, MP intervention could significantly ameliorate the steatosis and damage to the liver. as indicated by decreased levels of ALT in plasma (Figure 1H) and H&E staining of liver tissue (Figures 1K,L). It was observed that HFD could induce extensive liver injury, increased fatty vesicles, and inflammatory cell infiltration, which was significantly reversed by MP intervention. However, MPs showed a limited effect on the accumulation of perirenal fat (Figure 1E) and liver weight (Figure 1G). As shown in Supplementary Figure 1, the food intake and energy intake of the HFD-MP group showed no significant difference from that of the HFD group. Thus, the attenuation of obesity by MP treatment was not due to the reduction in food consumption.

Mannoproteins treatment improved hyperlipidemia, decreased plasma glucose, and ameliorated systemic inflammation in high-fat diet-induced obese mice

High-fat diet could significantly increase the level of glucose in plasma, which was reduced after administration of MPs (Figure 2A). HFD usually leads to hyperlipidemia, and thereby increases the potential risk for metabolism-related diseases. Thus, the plasma levels of TC, TG, and LDL-C were also evaluated, and the results showed that high concentrations of TC, TG, and LDL-C induced by HFD were largely reduced by treatment with MPs (Figures 2B–D). Thereinto, the levels of TG and LDL-C in the HFD-MP group showed no significant difference from those in the ND group ($p > 0.05$), suggesting the superior action of MPs for the prevention of hyperlipidemia.

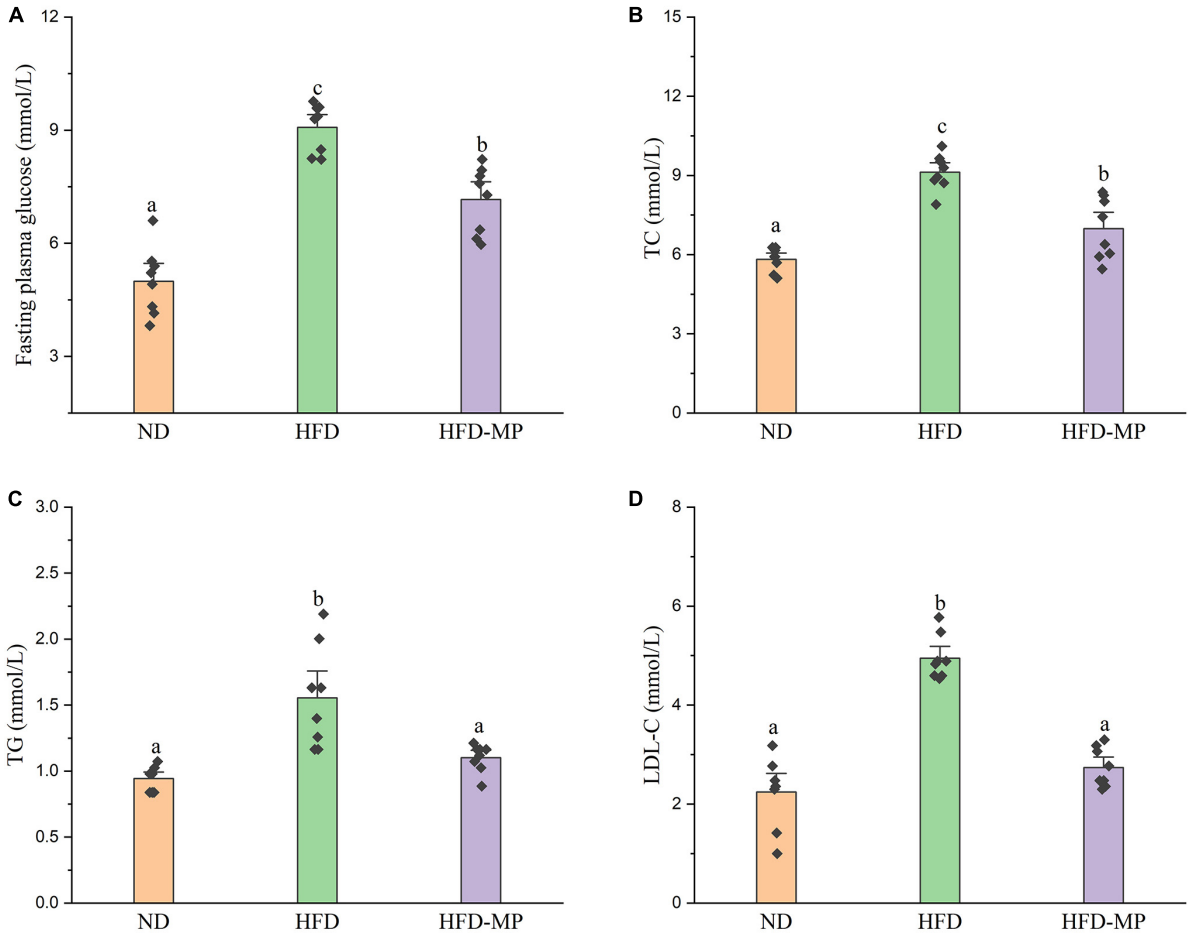

FIGURE 2
MP intervention reduced HFD-induced high levels of **(A)** fasting plasma glucose, **(B)** TC, **(C)** TG, and **(D)** LDL-C in plasma. The data are represented as the mean ± SEM. Statistical differences were carried out by one-way ANOVA followed by Turkey's test, $p < 0.05$ indicates significant differences.

Obesity is closely related to chronic low-grade inflammation (30). The pro-inflammatory cytokines in plasma, including TNF-α, IL-1β, IL-6, and IL-10, were detected to evaluate the anti-inflammation effect of MPs in HFD-induced obese mice (**Figure 3**). It was found that HFD could significantly increase the plasma levels of IL-1β and IL-6, but showed a limited effect on the content of TNF-α and IL-10. MP treatment could reverse the level of IL-6, which showed no significant difference from that in the ND group. However, MP intervention could not change the levels of TNF-α, IL-1β, and IL-10. Furthermore, the effect of MPs on the relative mRNA expression levels of TNF-α, IL-1β, and IL-6 in the liver was investigated (**Supplementary Figure 2**). It was found that HFD could increase the relative mRNA expression levels of TNF-α, IL-1β, and IL-6, whereas MP treatment could significantly downregulate the mRNA expression levels of TNF-α, IL-1β, and IL-6 ($p < 0.05$).

Mannoproteins attenuated high-fat diet-induced dysbiosis of gut microbiota

An increasing number of studies have demonstrated that gut microbiota is related to the etiology of obesity and obesity-related complications (31). Thus, it was hypothesized that the gut microbiota was a potential target responsible for the prevention of obesity by MPs. In the present work, the high-throughput sequencing technology was used to systematically analyze the changes in gut microbiota after supplementation with MPs. The Chao1, Richness, Simpson, and Shannon indexes were calculated to quantify the alpha-diversity of gut microbiota, as shown in **Supplementary Figure 3**. HFD could significantly reduce the Chao1 and Richness indexes. Furthermore, Simpson and Shannon indexes in the HFD group also showed increased or decreased trends compared with those in the ND group

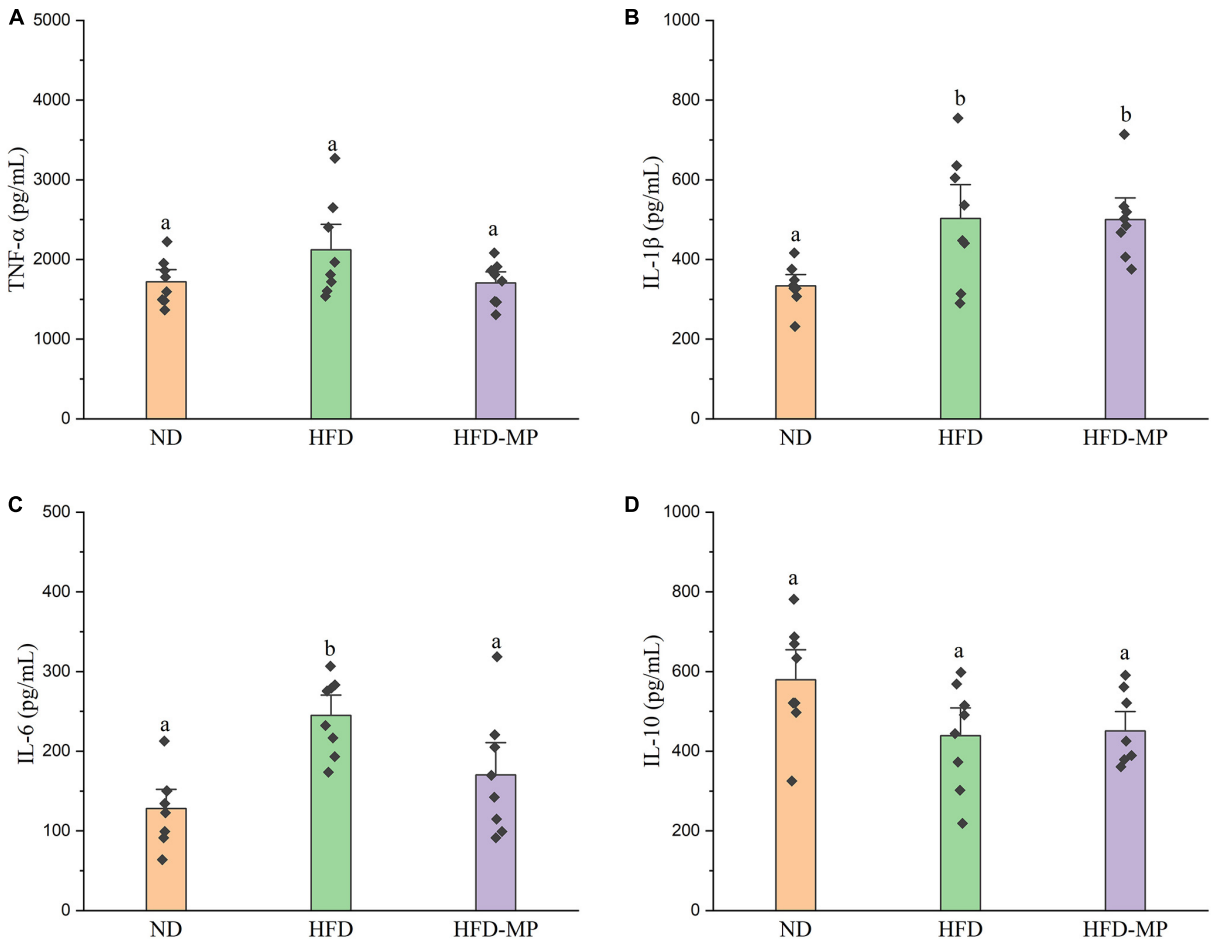

FIGURE 3
MP intervention attenuated HFD-induced chronic inflammation, including **(A)** TNF-α, **(B)** IL-1β, **(C)** IL-6, and **(D)** IL-10. The data are represented as the mean ± SEM. Statistical differences were carried out by one-way ANOVA followed by Tukey's test, $p < 0.05$ indicates significant differences.

with no significant difference. As expected, MPs could reverse these changes of alpha-diversity induced by HFD, by increasing the Chao1, Richness, and Shannon indexes, and decreasing the Simpson index.

Diet plays an important role in shaping the structure and composition of gut microbiota (32). Principal coordinate analysis (PCoA) was first carried out to visualize the differences in the structure of gut microbiota after HFD and MP treatments. It was found that ND and HFD groups could be clearly distinguished on the basis of the results of PCoA (**Figure 4A**). Compared with the HFD group, significant separation was also observed after MP treatment, suggesting that MP intervention could change the HFD-treated structure of gut microbiota. Furthermore, principal component analysis (PCA) and hierarchical cluster analysis largely agreed with the result of PCoA (**Figures 4B,C**). Interestingly, based on the PC1 (41.43%) value in the result of PCA, MPs could lead to a significant shift in the gut microbiota from the HFD group toward the ND group. Thus, MPs significantly modulated the HFD-induced dysbiosis of gut microbiota back to health status. At the phylum level, the gut microbiota of ND, HFD, and HFD-MP groups was all mainly composed of Firmicutes and Bacteroidetes (**Figure 5A**), which was consistent with the previous works (33, 34). Differently, HFD could significantly increase the relative abundance of Firmicutes and decrease the level of Bacteroidetes compared with the ND group, thereby significantly enhancing the ratio of Firmicutes to Bacteroidetes (**Figures 5B–D**). MPs could reverse this change induced by HFD treatment, by increasing the relative abundance of Bacteroidetes and decreasing the level of Firmicutes. Furthermore, the ratio of Firmicutes to Bacteroidetes in the HFD-MP group showed no significant difference compared to that observed in the ND group.

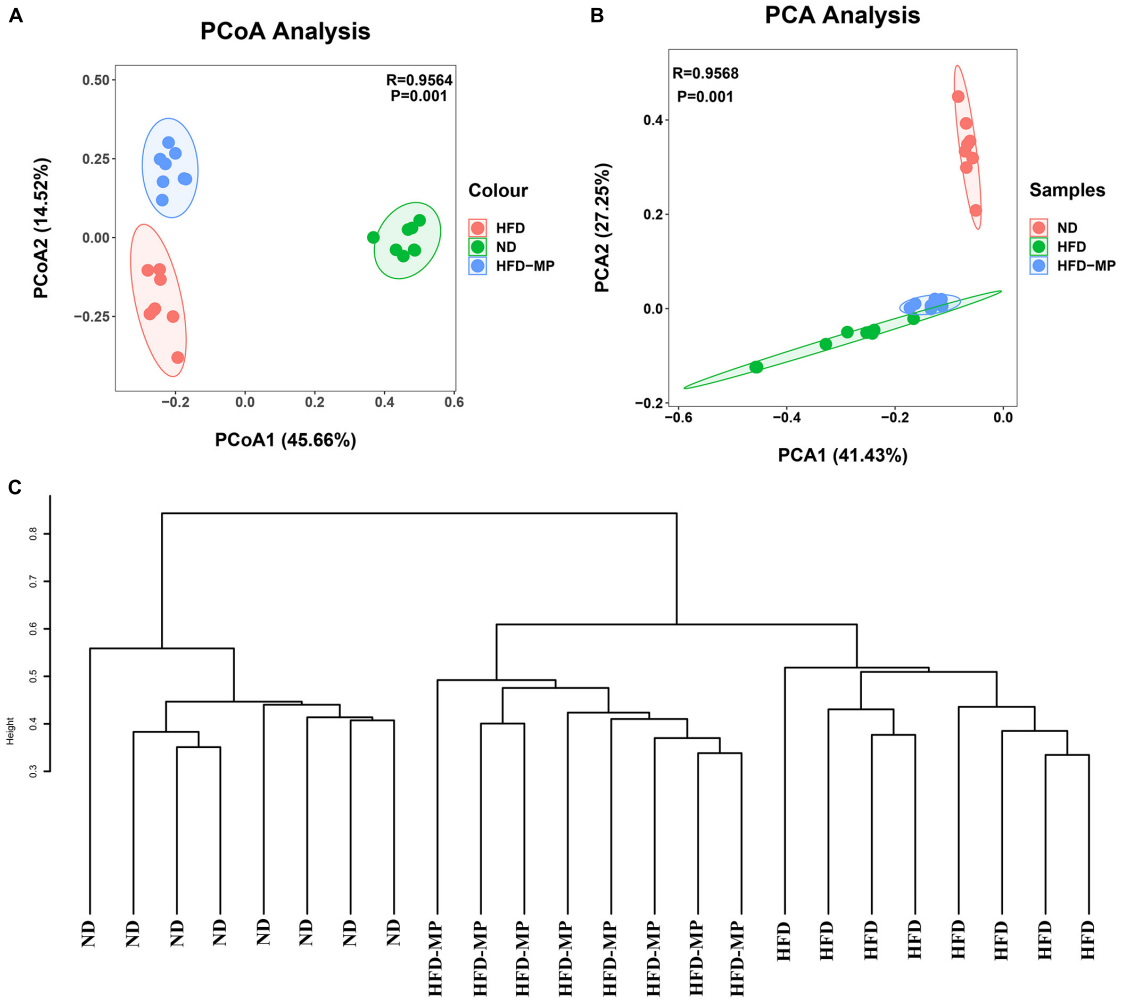

FIGURE 4
MPs attenuated HFD-induced dysbiosis of gut microbiota evaluated by beta-diversity analyses, including **(A)** PCoA, **(B)** PCA, and **(C)** hierarchical cluster analysis.

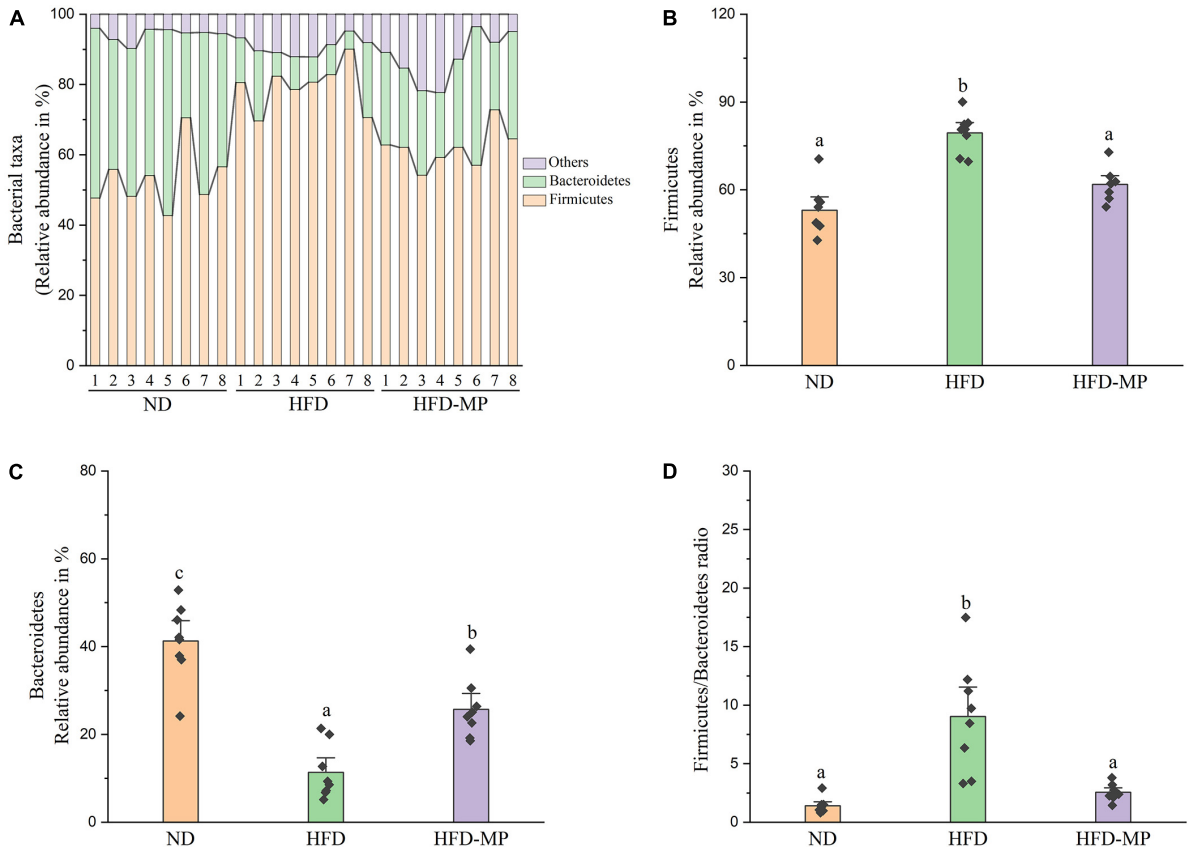

FIGURE 5
MPs modulate the HFD-disrupted gut microbiota composition at the phylum level. **(A)** Bacterial taxonomic profiling and relative abundances of **(B)** Firmicutes, **(C)** Bacteroidetes, and **(D)** the ratio of Firmicutes to Bacteroidetes. The data are represented as the mean ± SEM. Statistical differences were carried out by one-way ANOVA followed by Tukey's test, $p < 0.05$ indicates significant differences.

The gut microbiota at the family level was comparatively analyzed in this work (Figure 6). The result showed that HFD treatment could decrease the relative abundance of Porphyromonadaceae and increase the levels of Lactobacillaceae, Ruminococcaceae, Rikenellaceae, and Desulfovibrionaceae. Compared with the HFD group, MP intervention could significantly increase the relative abundance of Bacteroidaceae, Ruminococcaceae, and Rikenellaceae, and decrease the level of Lactobacillaceae. The gut microbiota at the genus level was also analyzed, as shown in Table 1. Most strikingly, the relative abundance of *Lactobacillus* was increased from 3.94 ± 1.30% to 19.99 ± 3.94% after HFD treatment, which was then decreased to 2.68 ± 0.77% by MP intervention. Likewise, HFD resulted in a significant decrease in the level of *Parabacteroides*, which was reversed by MP treatment. Thus, the modulated effect of MPs on the relative abundance of *Lactobacillus* and *Parabacteroides* may play an important role in the prevention of HFD-induced obesity. Furthermore, MPs could also increase the relative abundance of *Alistipes*, *Bacteroides*, and *Mucispirillum* compared with that in the ND and HFD groups. Then, the relationship between the changed gut microbiota at the genus level by MP and phenotypical changes in obesity was analyzed by Spearman correlation, as shown in Supplementary Figure 4. It was found that *Parabacteroides* and *Alistipes* showed a significant correlation with obesity.

The different gut microbiota at the same genus level may show different responses after treatment with MPs, thus the gut microbiota at the ZOTU level was analyzed to further excavate the key gut microbiota contributing to the prevention of obesity. The ZOTUs with a relative abundance of more than 0.1% were used to proceed with further analysis. As shown in Figure 7, HFD and MPs could significantly change 62 ZOTUs compared with the ND group. HFD could lead to 41 changed ZOTUs, including increasing 23 ZOTUs and decreasing 18 ZOTUs. Thereinto, nine ZOTUs were found to be significantly reversed by MP intervention. Then, the relationship between the relative abundance of these reversed ZOTUs and phenotypical changes of obesity was analyzed by Spearman correlation (Figure 8), and the result showed that seven ZOTUs were positively corrected with obesity, and two ZOTUs were negatively associated with obesity. Thereinto, two ZOTUs (ZOTU2 and ZOTU14)

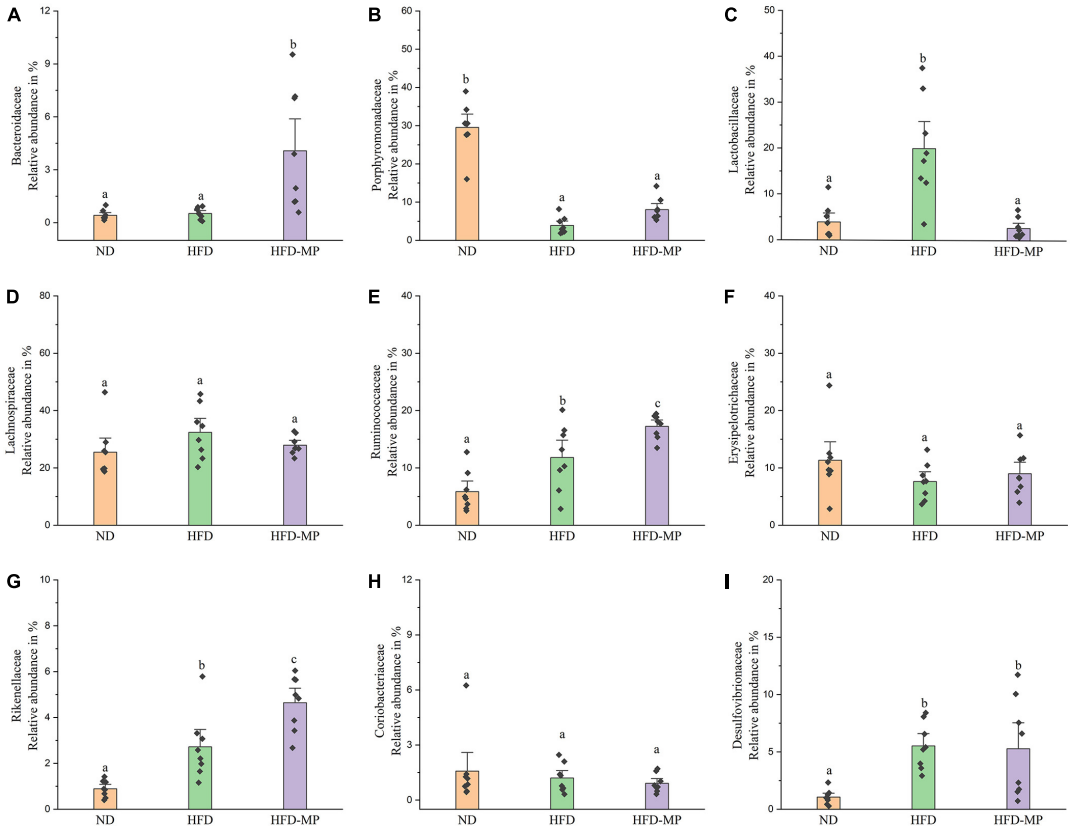

FIGURE 6
The comparative analysis of nine main families of the gut microbiota, including **(A)** Bacteroidaceae, **(B)** Porphyromonadaceae, **(C)** Lactobacillaceae, **(D)** Lachnospiraceae, **(E)** Ruminococcaceae, **(F)** Erysipelotrichaceae, **(G)** Rikenellaceae, **(H)** Coriobacteriaceae, and **(I)** Desulfovibrionaceae. The data are represented as the mean ± SEM. Statistical differences were carried out by one-way ANOVA followed by Tukey's test, $p < 0.05$ indicates significant differences.

belonging to *Lactobacillus* and two ZOTUs (ZOTU43 and ZOTU108) belonging to *Parabacteroides distasonis* may play a key role in the prevention of obesity.

Mannoproteins increased the content of acetic acid in high-fat diet-fed mice

The SCFAs are the main metabolites produced by the fermentation of polysaccharides by gut microbiota, which are speculated to play an important role in the biological activities of polysaccharides (35). Thereinto, acetic acid, propionic acid, and butyric acid are the most abundant SCFAs in the human body and colon, whereas other SCFAs, such as formate, valerate, and caproate, are minor end products in the colon (36). Thus, the levels of acetate, propionate, and butyrate were measured in different groups, and the result showed that HFD significantly reduced the levels of acetate, propionate, and butyrate in the cecal contents of mice (**Supplementary Figure 5**). The MP intervention could lead to a significant increase in the level of acetic acid from 3.28 ± 0.22 mmol/g to 7.84 ± 0.96 mmol/g; however, MPs showed a limited effect on the content of propionic acid and butyric acid. Furthermore, the effect of MPs on the mRNA expression of G protein-coupled receptors (GPRs), including GPR43 and GPR41, in the liver was investigated to further verify the key role of SCFAs in the attenuation of obesity (**Supplementary Figure 6**). The result showed that HFD treatment significantly reduced the mRNA expression of GPR41 and GPR43, whereas MP intervention could upregulate the expression of GPR41 and GPR43.

Discussion

Obesity has become a leading public health problem with pandemic proportions and can further increase the rates of complications, such as cardiovascular disease and type 2 diabetes (T2D) (37). An increasing number of studies have demonstrated that gut microbiota populations are sensitive to genetic, environmental, and diet influences, and hence can directly or indirectly affect the energy balance and energy stores (12). Thus, the gut microbiota is expected

TABLE 1 Comparative analysis of the gut microbiota between the groups at the genus level.

	ND	HFD	HFD-MP
Lactobacillus	3.94 ± 1.30a	19.99 ± 3.94b	2.68 ± 0.77a
Barnesiella	12.65 ± 1.37b	0.00 ± 0.00a	0.00 ± 0.00a
Desulfovibrio	0.99 ± 0.22a	5.51 ± 0.72b	5.21 ± 1.51b
Alistipes	0.89 ± 0.13a	2.62 ± 0.52b	4.59 ± 0.43c
Turicibacter	7.72 ± 1.12b	0.00 ± 0.00a	0.00 ± 0.00a
Clostridium_XlVa	2.97 ± 0.79a	1.85 ± 0.43a	2.57 ± 0.24a
Lactococcus	0.00 ± 0.00a	4.09 ± 1.55b	1.22 ± 0.22ab
Bacteroides	0.42 ± 0.10a	0.52 ± 0.11a	4.07 ± 1.21b
Parabacteroides	2.28 ± 0.43b	0.39 ± 0.12a	2.10 ± 0.20b
Helicobacter	0.66 ± 0.28a	0.62 ± 0.19a	2.25 ± 0.75a
Mucispirillum	0.40 ± 0.15a	0.82 ± 0.37ab	2.14 ± 0.64b
Oscillibacter	0.80 ± 0.23a	0.94 ± 0.21ab	1.56 ± 0.13b
Roseburia	0.00 ± 0.00a	1.49 ± 0.51b	1.07 ± 0.39ab
Romboutsia	0.02 ± 0.01a	1.29 ± 0.3b	0.38 ± 0.21a
Clostridium_XlVb	0.25 ± 0.05a	0.57 ± 0.09ab	0.81 ± 0.13b
Enterorhabdus	0.78 ± 0.36a	0.19 ± 0.06a	0.16 ± 0.04a
Bifidobacterium	0.87 ± 0.22b	0.25 ± 0.07a	0.00 ± 0.00a
Prevotella	1.10 ± 0.26b	0.00 ± 0.00a	0.00 ± 0.00a
Acetatifactor	0.07 ± 0.03a	0.29 ± 0.11ab	0.35 ± 0.06b
Clostridium_sensu_stricto	0.60 ± 0.15b	0.00 ± 0.00a	0.06 ± 0.02a
Clostridium_IV	0.32 ± 0.05b	0.16 ± 0.05a	0.14 ± 0.03a
Clostridium_XVIII	0.03 ± 0.01a	0.2 ± 0.06ab	0.34 ± 0.09b
Odoribacter	0.10 ± 0.05a	0.38 ± 0.19a	0.07 ± 0.05a
Olsenella	0.17 ± 0.09ab	0.03 ± 0.01a	0.27 ± 0.07b
Akkermansia	0.40 ± 0.24a	0.00 ± 0.00a	0.00 ± 0.00a
Ruminococcus	0.37 ± 0.08b	0.00 ± 0.00a	0.00 ± 0.00a
Streptococcus	0.01 ± 0.00a	0.29 ± 0.10b	0.07 ± 0.02a
Parasutterella	0.27 ± 0.06b	0.00 ± 0.00a	0.00 ± 0.00a
Anaerotruncus	0.01 ± 0.00a	0.13 ± 0.06a	0.12 ± 0.04a
Others	60.91 ± 1.74	57.41 ± 3.27	67.75 ± 2.29

The data are represented as the mean ± SEM. Statistical differences were carried out by one-way ANOVA followed by Tukey's test, $p < 0.05$ indicates significant differences. The different letters indicate significant differences between the groups ($p < 0.05$).

as a promising target for the prevention and treatment of obesity (38). Polysaccharides, serving as a superior prebiotic, could modulate the gut microbiota by selectively stimulating the growth of beneficial bacteria and inhibiting the harmful microbiota, thereby improving host health (39). Furthermore, polysaccharides could also modulate the metabolism of probiotics (40). MP is one of the most important components of yeast cell walls. The previous work has shown that MPs could stimulate angiogenesis (27) and had immunoactivities and antineoplastic activities (26). However, the effects of MPs on obesity and gut microbiota are still unknown. Here, the HFD-induced obesity mice model was used to investigate the potential anti-obesogenic effect of MPs. Over 10 weeks of treatment, HFD could significantly induce obesity in the mice model. As expected, MPs significantly prevented HFD-induced body weight gain, fat accumulation, and liver steatosis. Furthermore, the levels of glucose, TC, TG, and LDL-C in plasma were also ameliorated by the treatment with MP. Thus, the results in the present work demonstrated that MP intervention could reduce obesity and metabolic disorders in HFD-fed mice. However, it would be more convincing if the dose setting or positive control was involved in this work.

It has been reported that HFD could damage the gut integrity and lead to a leaky gut, and the endotoxin lipopolysaccharide (LPS) released from Gram-negative bacteria in the gut enter the bloodstream, thereby leading to metabolic inflammation in obese mice (30). Thus, HFD-induced obesity is usually associated with chronic, low-grade inflammation. In the present work, IL-1β, and IL-6 levels were significantly enhanced after HFD treatment, and MPs could significantly reduce the level of IL-6, which showed no significant difference from those in the ND group. The decrease in the pro-inflammatory cytokines by the dietary polysaccharides contributing to the prevention of metabolic diseases has been widely reported. For example, an insoluble polysaccharide from the sclerotium of *Poria cocos* could reduce the plasmatic TNF-α in ob/ob mice (41). Likewise, the polysaccharides isolated from *Hirsutella sinensis* decreased the serum levels of the pro-inflammatory cytokines IL-1β and TNF-α in the HFD-fed mice (42). Thus, the improvement of metabolic disorders by MPs might be related to the suppression of chronic inflammation.

The accumulating evidence has demonstrated that dietary habit, especially a HFD, could lead to dysbiosis of gut microbiota, which might thereby lead to some pathologic conditions of obesity and obesity-related complications. Recently, some foods or food additives, such as processed foods (43), dietary emulsifiers (44), and artificial sweeteners (45), could promote metabolic diseases by disordering the gut microbiota. Alpha-diversity, including Chao1, Richness, Simpson, and Shannon indexes, could reflect the diversity and richness of bacteria (46). In this work, HFD could significantly affect the structure and composition of gut microbiota, which is evidenced by decreasing alpha-diversity and changing beta-diversity indexes. The reports in animal and clinical studies showed that decreased alpha-diversity and richness values were observed in obese subjects and animals (28, 47, 48). MP treatment could not only increase the alpha-diversity, including Chao1, Richness, Simpson, and Shannon indexes, but could also change the structure of gut microbiota from the HFD group toward the ND group based on beta-diversity.

The result at the phylum level indicated that the gut microbiota was dominated by Firmicutes and Bacteroidetes. The ratio of Firmicutes to Bacteroidetes has been reported to relate to metabolic diseases, and high levels of Firmicutes and low levels of Bacteroidetes were observed in obese humans and animals (49–51). Thus, the decrease in the ratio of Firmicutes to Bacteroidetes may contribute to the prevention of obesity

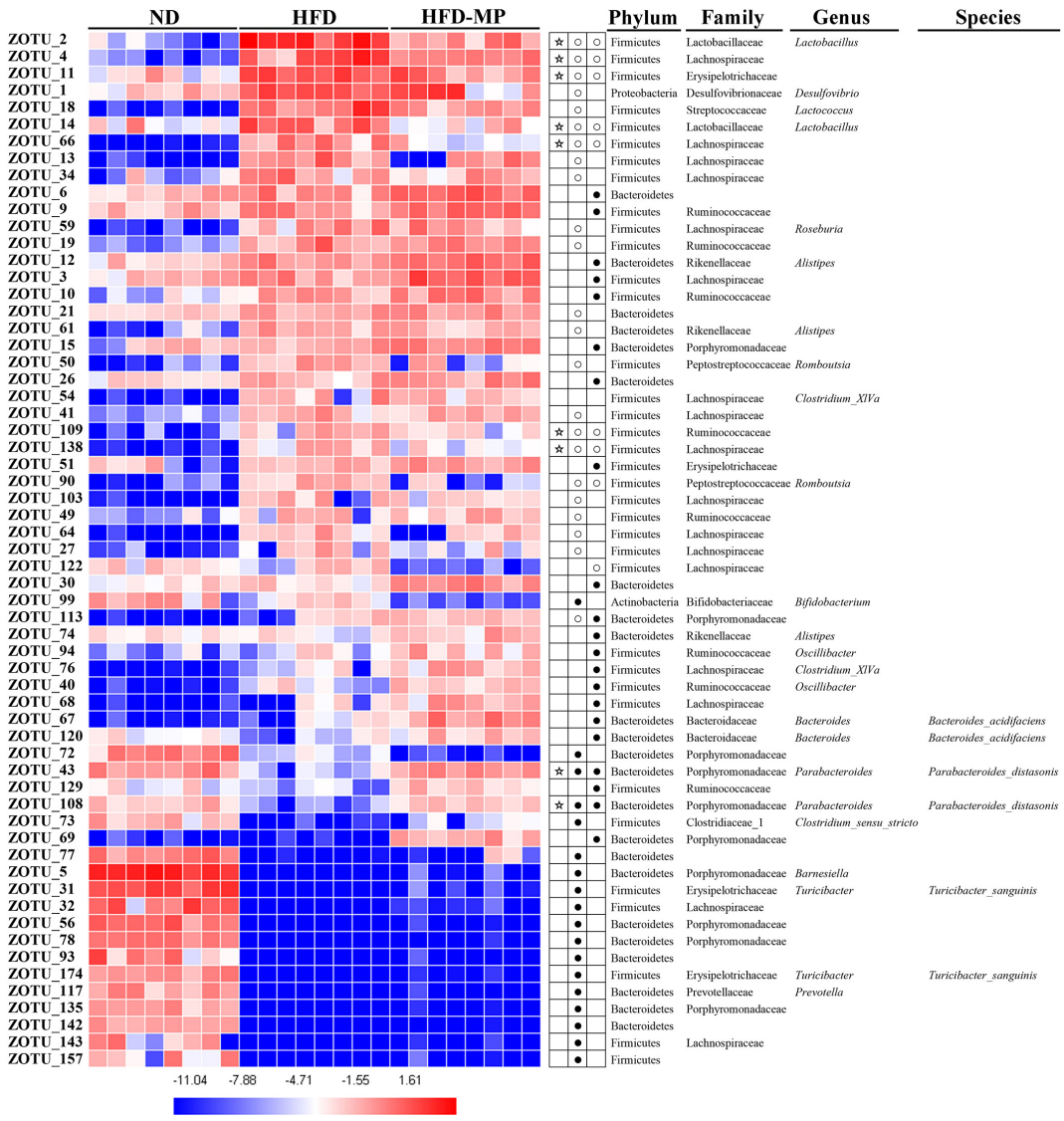

FIGURE 7
Gut microbiota composition was altered by HFD or MP intervention at the ZOTUs levels. Heatmap shows the relative abundance of 62 ZOTUs (ln transformed). The dots (●) and circles (○) showed the more or less relative abundances of ZOTUs in ND or MPs groups compared with the HFD group. The star (☆) represented ZOTUs changed by HFD but were reversed after treatment with MPs. Statistical differences were carried out by one-way ANOVA followed by Tukey's test, $p < 0.05$ indicates significant differences.

and metabolic diseases. A decrease in the ratio of Firmicutes to Bacteroidetes by anti-obesogenic candidates was widely reported (52, 53). In this work, a similar trend toward a decreased ratio of Firmicutes to Bacteroidetes was obtained after MP treatment, which may contribute to the prevention of obesity by MPs. At the family level, the MPs induced increased levels of Bacteroidaceae, Ruminococcaceae, and Rikenellaceae. Therefore, the relative abundance of Bacteroidaceae has been reported to negatively link to obesity (54, 55). Furthermore, the level of Bacteroidaceae is determined by SCFA-producing bacteria (56), which could be regarded as a positive outcome predictor of individual weight loss (57). Lactobacillaceae was usually considered as beneficial bacteria in the gut for the prevention of obesity (58, 59). On the other hand, some reports showed that Lactobacillaceae has a positive relationship with obesity (60, 61). The different bacteria in the same family may play different roles in the metabolic phenotype of obesity, thus the gut microbiota was also analyzed at the genus or ZOTU levels.

It was found that *Lactobacillus,* belonging to Lactobacillaceae, and *Parabacteroides,* belonging to Porphyromonadaceae, were significantly reversed by MP treatment. Furthermore, *Alistipes* (belonging to Rikenellaceae) which was increased by MPs showed a significant correlation

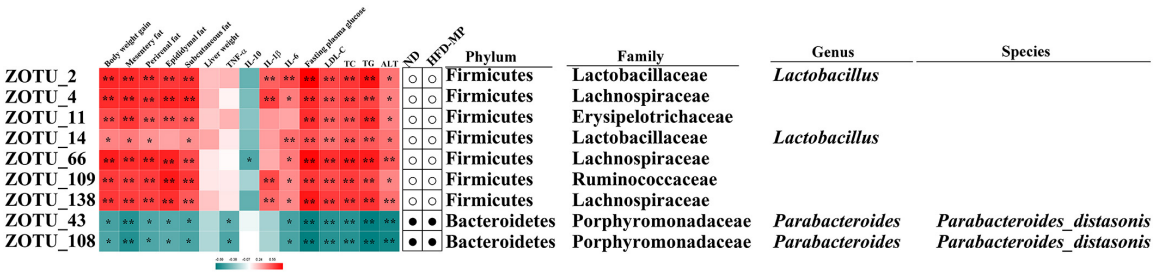

FIGURE 8
Nine ZOTUs reversed by MP intervention were significantly correlated with features of obesity. The heatmap shows the *R*-value of Spearman's correlation between the relative abundance of ZOTUs and features of obesity. The dots (correlation between the more or less relative abundance of ZOTUs in the ND or MP groups compared with the HFD group. * and **Show the significant associations ($p < 0.05$ and $p < 0.01$, respectively) based on Spearman's correlation analysis.

with obesity. To further identify species-level phylotypes or specific bacterial taxa contributing to the prevention of obesity by MPs, the gut microbiota was analyzed at the ZOTU level. *Lactobacillus* (ZOTU2 and ZOTU14), which was positively corrected with obesity, and *P. distasonis* (ZOTU43 and ZOTU108), which showed negative relation to obesity, were significantly reversed after MP intervention. *P. distasonis*, regarded as one of the 18 core members in the human gut microbiota, plays an important role in human health (62). The lower level of *P. distasonis* has been observed in patients and animals with metabolic diseases (63, 64). Furthermore, the alleviation of obesity and obesity-related dysfunctions by *P. distasonis* has been reported, which was due to the generation of succinate and secondary bile acids in the gut (14). Moreover, the other health-promoting functions of *P. distasonis*, such as blocking colon tumor formation (65) and alleviating colitis (66), have also been widely reported. Thus, *P. distasonis* has been regarded as potential probiotic for improving our health (67). The previous work showed that polysaccharides, such as inulin, could promote the proliferation of *P. distasonis* and thereby improve human health (68). In this work, the MPs could also increase the level of *P. distasonis* in HFD-induced obese mice contributing to the prevention of obesity. *Lactobacillus* showed a particularly interesting role in this work. It is well known that lots of species in the genus *Lactobacillus* are probiotic bacteria (69, 70), which can reduce the risk of metabolic diseases. On the other hand, a report showed that some species belonging to *Lactobacillus,* such as *Lactobacillus reuteri,* were positively associated with obesity, while others were related to normal weight (71). Recently, a systematic review of randomized controlled clinical trials summarized the effect of *Lactobacillus* on obesity, and it was found that the beneficial or detrimental effects of *Lactobacillus* on obesity are strain-dependent (72). Thus, the prevention of obesity by MPs might be related to the inhibition of *Lactobacillus*. Unfortunately, the species for *Lactobacillus* in this work could not be identified by sequencing, which should be further investigated.

SCFAs, the key metabolites produced by gut microbiota, play an important role in improving colonic and systemic health (35), which could help to explain why and how the changes in gut microbiota contribute to human health and diseases (73). A growing amount of evidence suggests that SCFAs could enter into the bloodstream, and thereby affect the tissues and organs beyond the gut (74). Therefore, the specific species, diversity, and absolute amount of gut microbiota play a key role in the production of SCFAs (75). The diet intervention could alter either the bacterial species or the bacterial biosynthetic enzymes, thereby leading to alterations in microbial SCFA production (76). A potential strategy based on the modulation of gut microbiota by prebiotics has been presented to stimulate the production of SCFAs, thereby preventing diseases and improving human health (77, 78). Thus, we suspected that the SCFAs would be changed due to the modulation of gut microbiota by MP, which thereby contributes to the prevention of obesity. In this work, MPs could increase the level of acetate decreased by HFD treatment, whereas they showed limited effects on the contents of propionate and butyrate. Furthermore, the mRNA expression of GPR41 and GPR43 in the liver was significantly upregulated by MPs, suggesting that SCFAs played a key role in the prevention of obesity by MPs. A lot of reports have shown that acetate administration could reduce body weight, decrease hepatic fat accumulation, and improve insulin sensitivity in HFD-fed mice (79, 80). Likewise, SCFA intervention studies in humans also further demonstrated that consumption of acetate could significantly reduce the body weight of patients with obesity (81). SCFAs could activate GPR41 and GPR43 to improve immune responses, and the activation of GPR41/43 could further modulate the levels of pro-inflammatory factors. It has been reported that polysaccharides-derived SCFAs could significantly reduce the level of pro-inflammatory factors, such as LPS in the blood. Furthermore,SCFA might also directly reverse LPS-induced inflammation (75, 82). In addition, acetate can significantly regulate the levels

of DNA methylation at the host miR-378a promoter, which also contribute to the improvement of obesity and glucose intolerance (83). It has been reported that Parabacteroides could utilize polysaccharides with its glycoside hydrolase, and further produced acetate to affect host health (84, 85). It is expected to be a potential strategy to increase the level of acetate by prebiotics, thereby preventing and treating obesity. Thus, the increased level of acetate by MPs may also contribute to the prevention of obesity in this work. In addition to SCFAs, the other metabolites were not measured in the present study, which could be further investigated by metabolomics in our next work (86).

Conclusion

In conclusion, the HFD-induced obese mice model was used to investigate the potential anti-obesogenic effect of MPs and its potential mechanism. The result showed that MPs significantly attenuated HFD-induced obesity. MPs could not only increase the alpha-diversity of gut microbiota, but also change the structure of gut microbiota from the HFD group to the ND group. Furthermore, harmful *Lactobacillus* and probiotic *P. distasonis* may be potential key gut microbiota responsible for the prevention of obesity by MPs. This preliminary research showed promise for the efficacy of MPs in the prevention of HFD-induced obesity, thus MPs were expected to serve as a functional food for the improvement of human health.

Data availability statement

The original contributions presented in this study are publicly available. This data can be found here: Genome Sequence Archive in the BIG Data Center Chinese Academy of Sciences (https://ngdc.cncb.ac.cn/gsa/) with BioProject number of PRJCA009982 under accession codes of CRA007210.

Ethics statement

All animal experiment protocols were approved by the Institutional Animal Ethics Committee of Experimental Animal Center of Nanjing Agricultural University.

Author contributions

XL, JSW, JLW, GC, and XZ contributed to the conception and design of the study. YK organized the database. DC performed the statistical analysis. XL wrote the first draft of the manuscript. GC and XZ wrote sections of the manuscript. All authors contributed to manuscript revision, read, and approved the submitted version.

Funding

This study was supported by the Angel Nutritech Nutrition Fund (AF2019002), the Research on Open project of Jiangsu Key Laboratory for Bioresources of Saline Soils (JKLBS2020014), and the Priority Academic Program Development of Jiangsu Higher Education Institutions.

Conflict of interest

The authors declare that the research was conducted in the absence of any commercial or financial relationships that could be construed as a potential conflict of interest.

Publisher's note

All claims expressed in this article are solely those of the authors and do not necessarily represent those of their affiliated organizations, or those of the publisher, the editors and the reviewers. Any product that may be evaluated in this article, or claim that may be made by its manufacturer, is not guaranteed or endorsed by the publisher.

Supplementary material

The Supplementary Material for this article can be found online at: https://www.frontiersin.org/articles/10.3389/fnut.2022.1019344/full#supplementary-material

References

1. Lingvay I, Sumithran P, Cohen RV, le Roux CW. Obesity management as a primary treatment goal for type 2 diabetes: time to reframe the conversation. *Lancet*. (2022) 399:394–405. doi: 10.1016/S0140-6736(21)01919-X

2. SantaCruz-Calvo S, Bharath L, Pugh G, SantaCruz-Calvo L, Lenin RR, Lutshumba J, et al. Adaptive immune cells shape obesity-associated type 2 diabetes mellitus and less prominent comorbidities. *Nat Rev Endocrinol*. (2022) 18:23–42. doi: 10.1038/s41574-021-00575-1

3. Malik VS, Hu FB. The role of sugar-sweetened beverages in the global epidemics of obesity and chronic diseases. *Nat Rev Endocrinol*. (2022) 18:205–18. doi: 10.1038/s41574-021-00627-6

4. Xu Z, Jiang W, Huang W, Lin Y, Chan FKL, Ng SC. Gut microbiota in patients with obesity and metabolic disorders - a systematic review. *Genes Nutr.* (2022) 17:2. doi: 10.1186/s12263-021-00703-6

5. Shi Q, Wang Y, Hao Q, Vandvik PO, Guyatt G, Li J, et al. Pharmacotherapy for adults with overweight and obesity: a systematic review and network meta-analysis of randomised controlled trials. *Lancet.* (2022) 399:259–69. doi: 10.1016/S0140-6736(21)01640-8

6. Xu X, Zhao C, Li B, Tang G, Shang A, Gan R, et al. Effects and mechanisms of tea on obesity. *Crit Rev Food Sci.* (2021):1–18. Online ahead of print. doi: 10.1080/10408398.2021.1992748

7. Gérard P. Gut microbiota and obesity. *Cell Mol Life Sci.* (2016) 73:147–62. doi: 10.1007/s00018-015-2061-5

8. Martel J, Ojcius DM, Chang C, Lin C, Lu C, Ko Y, et al. Anti-obesogenic and antidiabetic effects of plants and mushrooms. *Nat Rev Endocrinol.* (2017) 13:149–60. doi: 10.1038/nrendo.2016.142

9. de Clercq NC, Groen AK, Romijn JA, Nieuwdorp M. Gut microbiota in obesity and undernutrition. *Adv Nutr.* (2016) 7:1080–9. doi: 10.3945/an.116.012914

10. Lynch SV, Pedersen O. The human intestinal microbiome in health and disease. *N Engl J Med.* (2016) 375:2369–79. doi: 10.1056/NEJMra1600266

11. Zhao L. The gut microbiota and obesity: from correlation to causality. *Nat Rev Microbiol.* (2013) 11:639–47. doi: 10.1038/nrmicro3089

12. Rosenbaum M, Knight R, Leibel RL. The gut microbiota in human energy homeostasis and obesity. *Trends Endocrinol Metab.* (2015) 26:493–501. doi: 10.1016/j.tem.2015.07.002

13. Yoon HS, Cho CH, Yun MS, Jang SJ, You HJ, Kim J, et al. Akkermansia muciniphila secretes a glucagon-like peptide-1-inducing protein that improves glucose homeostasis and ameliorates metabolic disease in mice. *Nat Microbiol.* (2021) 6:563–73. doi: 10.1038/s41564-021-00880-5

14. Wang K, Liao M, Zhou N, Bao L, Ma K, Zheng Z, et al. *Parabacteroides distasonis* alleviates obesity and metabolic dysfunctions via production of succinate and secondary bile acids. *Cell Rep.* (2019) 26:222–35. doi: 10.1016/j.celrep.2018.12.028

15. Le Roy T, Moens De Hase E, Van Hul M, Paquot A, Pelicaen R, Régnier M, et al. Dysosmobacter welbionis is a newly isolated human commensal bacterium preventing diet-induced obesity and metabolic disorders in mice. *Gut.* (2022) 71:534–43. doi: 10.1136/gutjnl-2020-323778

16. Woting A, Pfeiffer N, Loh G, Klaus S, Blaut M. *Clostridium ramosum* promotes high-fat diet-induced obesity in gnotobiotic mouse models. *mBio.* (2014) 5:e01530–14. doi: 10.1128/mBio.01530-14

17. Fei N, Bruneau A, Zhang X, Wang R, Wang J, Rabot S, et al. Endotoxin producers overgrowing in human gut microbiota as the causative agents for nonalcoholic fatty liver disease. *mBio.* (2020) 11:e03263–19. doi: 10.1128/mBio.03263-19

18. Gentile CL, Weir TL. The gut microbiota at the intersection of diet and human health. *Science.* (2018) 362:776–80. doi: 10.1126/science.aau5812

19. Gimeno RE, Briere DA, Seeley RJ. Leveraging the gut to treat metabolic disease. *Cell Metab.* (2020) 31:679–98. doi: 10.1016/j.cmet.2020.02.014

20. Makki K, Deehan EC, Walter J, Bäckhed F. The impact of dietary fiber on gut microbiota in host health and disease. *Cell Host Microbe.* (2018) 23:705–15. doi: 10.1016/j.chom.2018.05.012

21. Li J, Karboune S. Characterization of the composition and the techno-functional properties of mannoproteins from *Saccharomyces cerevisiae* yeast cell walls. *Food Chem.* (2019) 297:124867. doi: 10.1016/j.foodchem.2019.05.141

22. Li J, Karboune S, Sedman J, Ismail A. Characterization of the structural properties of mannoproteins isolated from selected yeast-based products upon the enzymatic treatment. *LWT Food Sci Technol.* (2020) 131:109596. doi: 10.1016/j.lwt.2020.109596

23. Chen G, Chen D, Zhou W, Peng Y, Chen C, Shen W, et al. Improvement of metabolic syndrome in high-fat diet-induced mice by yeast β-Glucan is linked to inhibited proliferation of *Lactobacillus* and *Lactococcus* in gut microbiota. *J Agric Food Chem.* (2021) 69:7581–92. doi: 10.1021/acs.jafc.1c00866

24. Wu J, Guan Y, Zhong Q. Yeast mannoproteins improve thermal stability of anthocyanins at pH 7.0. *Food Chem.* (2015) 172:121–8. doi: 10.1016/j.foodchem.2014.09.059

25. Liu H, Liu L, Hui H, Wang Q. Structural characterization and antineoplastic activity of *Saccharomyces cerevisiae* mannoprotein. *Int J Food Prop.* (2015) 18:359–71. doi: 10.1080/10942912.2013.819364

26. Liu H, Wang Q, He Y. Immunoactivities and antineoplastic activities of *Saccharomyces cerevisiae* mannoprotein. *Carbohyd Polym.* (2011) 83:1690–5. doi: 10.1016/j.carbpol.2010.10.026

27. Yoon BH, Lee SM, Chang H, Ha CH. Mannoproteins from *Saccharomyces cerevisiae* stimulate angiogenesis by promoting the akt-eNOS signaling pathway in endothelial cells. *Biochem Bioph Res Commun.* (2019) 519:767–72. doi: 10.1016/j.bbrc.2019.09.069

28. Chen G, Xie M, Wan P, Chen D, Dai Z, Ye H, et al. Fuzhuan brick tea polysaccharides attenuate metabolic syndrome in High-Fat diet induced mice in association with modulation in the gut microbiota. *J Agric Food Chem.* (2018) 66:2783–95. doi: 10.1021/acs.jafc.8b00296

29. Chen G, Xie M, Wan P, Chen D, Ye H, Chen L, et al. Digestion under saliva, simulated gastric and small intestinal conditions and fermentation in vitro by human intestinal microbiota of polysaccharides from Fuzhuan brick tea. *Food Chem.* (2018) 244:331–9. doi: 10.1016/j.foodchem.2017.10.074

30. Chang C, Lin C, Lu C, Martel J, Ko Y, Ojcius DM, et al. *Ganoderma lucidum* reduces obesity in mice by modulating the composition of the gut microbiota. *Nat Commun.* (2015) 6:7489. doi: 10.1038/ncomms8489

31. Canfora EE, Meex RCR, Venema K, Blaak EE. Gut microbial metabolites in obesity, NAFLD and T2DM. *Nat Rev Endocrinol.* (2019) 15:261–73. doi: 10.1038/s41574-019-0156-z

32. Choi BSY, Daniel N, Houde VP, Ouellette A, Marcotte B, Varin TV, et al. Feeding diversified protein sources exacerbates hepatic insulin resistance via increased gut microbial branched-chain fatty acids and mTORC1 signaling in obese mice. *Nat Commun.* (2021) 12:3377. doi: 10.1038/s41467-021-23782-w

33. Chen G, Xie M, Dai Z, Wan P, Ye H, Zeng X, et al. Kudingcha and fuzhuan brick tea prevent obesity and modulate gut microbiota in High-Fat diet fed mice. *Mol Nutr Food Res.* (2018) 62:1700485. doi: 10.1002/mnfr.201700485

34. Zhang X, Chen J, Yi K, Peng L, Xie J, Gou X, et al. Phlorizin ameliorates obesity-associated endotoxemia and insulin resistance in high-fat diet-fed mice by targeting the gut microbiota and intestinal barrier integrity. *Gut Microbes.* (2020) 12:1842990. doi: 10.1080/19490976.2020.1842990

35. Koh A, De Vadder F, Kovatcheva-Datchary P, Bäckhed F. From dietary fiber to host physiology: short-chain fatty acids as key bacterial metabolites. *Cell.* (2016) 165:1332–45. doi: 10.1016/j.cell.2016.05.041

36. Dalile B, Van Oudenhove L, Vervliet B, Verbeke K. The role of short-chain fatty acids in microbiota–gut–brain communication. *Nat Rev Gastroenterol Hepat.* (2019) 16:461–78. doi: 10.1038/s41575-019-0157-3

37. López-Almela I, Romaní-Pérez M, Bullich-Vilarrubias C, Benítez-Páez A, Gómez Del Pulgar EM, Francés R, et al. *Bacteroides uniformis* combined with fiber amplifies metabolic and immune benefits in obese mice. *Gut Microbes.* (2021) 13:1865706. doi: 10.1080/19490976.2020.1865706

38. Clemente JC, Ursell LK, Parfrey LW, Knight R. The impact of the gut microbiota on human health: an integrative view. *Cell.* (2012) 148:1258–70. doi: 10.1016/j.cell.2012.01.035

39. Verspreet J, Damen B, Broekaert WF, Verbeke K, Delcour JA, Courtin CM. A critical look at prebiotics within the dietary fiber concept. *Annu Rev Food Sci Technol.* (2016) 7:167–90. doi: 10.1146/annurev-food-081315-032749

40. Le Y, Yang H. Xanthan gum modified fish gelatin and binary culture modulates the metabolism of probiotics in fermented milk mainly via amino acid metabolism pathways. *Food Res. Int.* (2022) 161:111844. doi: 10.1016/j.foodres.2022.111844

41. Sun S, Wang K, Ma K, Bao L, Liu H. An insoluble polysaccharide from the sclerotium of *Poria cocos* improves hyperglycemia, hyperlipidemia and hepatic steatosis in ob/ob mice via modulation of gut microbiota. *Chin J Nat Med.* (2019) 17:3–14. doi: 10.1016/S1875-5364(19)30003-2

42. Wu T, Lin C, Chang C, Lin T, Martel J, Ko Y, et al. Gut commensal *Parabacteroides goldsteinii* plays a predominant role in the anti-obesity effects of polysaccharides isolated from *Hirsutella sinensis*. *Gut.* (2019) 68:248–62. doi: 10.1136/gutjnl-2017-315458

43. Snelson M, Tan SM, Clarke RE, de Pasquale C, Thallas-Bonke V, Nguyen T, et al. Processed foods drive intestinal barrier permeability and microvascular diseases. *Sci Adv.* (2021) 7: eabe4841. doi: 10.1126/sciadv.abe4841

44. Chassaing B, Koren O, Goodrich JK, Poole AC, Srinivasan S, Ley RE, et al. Dietary emulsifiers impact the mouse gut microbiota promoting colitis and metabolic syndrome. *Nature.* (2015) 519:92–6. doi: 10.1038/nature14232

45. Suez J, Korem T, Zeevi D, Zilberman-Schapira G, Thaiss CA, Maza O, et al. Artificial sweeteners induce glucose intolerance by altering the gut microbiota. *Nature.* (2014) 514:181–6. doi: 10.1038/nature13793

46. Zhao X, Chen L, Wongmaneepratip W, He Y, Zhao L, Yang H. Effect of vacuum impregnated fish gelatin and grape seed extract on moisture state, microbiota composition, and quality of chilled seabass fillets. *Food Chem.* (2021) 354:129581. doi: 10.1016/j.foodchem.2021.129581

47. Zhernakova A, Kurilshikov A, Bonder MJ, Tigchelaar EF, Schirmer M, Vatanen T, et al. Population-based metagenomics analysis reveals markers for gut

microbiome composition and diversity. *Science.* (2016) 352:565–9. doi: 10.1126/science.aad3369

48. Sommer F, Bäckhed F. The gut microbiota - masters of host development and physiology. *Nat Rev Microbiol.* (2013) 11:227–38. doi: 10.1038/nrmicro2974

49. Turnbaugh PJ, Bäckhed F, Fulton L, Gordon JI. Diet-Induced obesity is linked to marked but reversible alterations in the mouse distal gut microbiome. *Cell Host Microbe.* (2008) 3:213–23. doi: 10.1016/j.chom.2008.02.015

50. Zeng S, Li S, Xiao P, Cai Y, Chu C, Chen B, et al. Citrus polymethoxyflavones attenuate metabolic syndrome by regulating gut microbiome and amino acid metabolism. *Sci Adv.* (2020) 6:eaax6208. doi: 10.1126/sciadv.aax6208

51. Rom O, Liu Y, Liu Z, Zhao Y, Wu J, Ghrayeb A, et al. Glycine-based treatment ameliorates NAFLD by modulating fatty acid oxidation, glutathione synthesis, and the gut microbiome. *Sci Transl Med.* (2020) 12:eaaz2841. doi: 10.1126/scitranslmed.aaz2841

52. Hong Y, Sheng L, Zhong J, Tao X, Zhu W, Ma J, et al. *Desulfovibrio vulgaris*, a potent acetic acid-producing bacterium, attenuates nonalcoholic fatty liver disease in mice. *Gut Microbes.* (2021) 13:1930874. doi: 10.1080/19490976.2021.1930874

53. Guo J, Han X, Tan H, Huang W, You Y, Zhan J. Blueberry extract improves obesity through regulation of the gut microbiota and bile acids via pathways involving FXR and TGR5. *iScience.* (2019) 19:676–90. doi: 10.1016/j.isci.2019.08.020

54. Wang Z, Lam K, Hu J, Ge S, Zhou A, Zheng B, et al. Chlorogenic acid alleviates obesity and modulates gut microbiota in high-fat-fed mice. *Food Sci Nutr.* (2019) 7:579–88. doi: 10.1002/fsn3.868

55. Zhang C, Wu W, Li X, Xin X, Liu D. Daily supplementation with fresh angelica keiskei juice alleviates High-Fat Diet-Induced obesity in mice by modulating gut microbiota composition. *Mol Nutr Food Res.* (2019) 63:1900248. doi: 10.1002/mnfr.201900248

56. Wu J, Liu Y, Dou Z, Wu T, Liu R, Sui W, et al. Black garlic melanoidins prevent obesity, reduce serum LPS levels and modulate the gut microbiota composition in high-fat diet-induced obese C57BL/6J mice. *Food Funct.* (2020) 11:9585–98. doi: 10.1039/D0FO02379E

57. Zhang S, Wu P, Tian Y, Liu B, Huang L, Liu Z, et al. Gut microbiota serves a predictable outcome of short-term low-carbohydrate diet (LCD) intervention for patients with obesity. *Microbiol Spectr.* (2021) 9:e0022321. doi: 10.1128/Spectrum.00223-21

58. Saeb A, Grundmann SM, Gessner DK, Schuchardt S, Most E, Wen G, et al. Feeding of cuticles from Tenebrio molitor larvae modulates the gut microbiota and attenuates hepatic steatosis in obese Zucker rats. *Food Funct.* (2022) 13:1421–36. doi: 10.1039/D1FO03920B

59. Ojo BA, O'Hara C, Wu L, El-Rassi GD, Ritchey JW, Chowanadisai W, et al. Wheat germ supplementation increases lactobacillaceae and promotes an anti-inflammatory gut milieu in C57BL/6 mice fed a High-Fat, High-Sucrose diet. *J Nutr.* (2019) 149:1107–15. doi: 10.1093/jn/nxz061

60. Ye J, Zhao Y, Chen X, Zhou H, Yang Y, Zhang X, et al. Pu-erh tea ameliorates obesity and modulates gut microbiota in high fat diet fed mice. *Food Res Int.* (2021) 144:110360. doi: 10.1016/j.foodres.2021.110360

61. Zeng H, Larson KJ, Cheng W, Bukowski MR, Safratowich BD, Liu Z, et al. Advanced liver steatosis accompanies an increase in hepatic inflammation, colonic, secondary bile acids and Lactobacillaceae/Lachnospiraceae bacteria in C57BL/6 mice fed a high-fat diet. *J Nutr Biochem.* (2020) 78:108336. doi: 10.1016/j.jnutbio.2019.108336

62. Falony G, Joossens M, Vieira-Silva S, Wang J, Darzi Y, Faust K, et al. Population-level analysis of gut microbiome variation. *Science.* (2016) 352:560–4. doi: 10.1126/science.aad3503

63. Yang J, Wei H, Zhou Y, Szeto C, Li C, Lin Y, et al. High-Fat diet promotes colorectal tumorigenesis through modulating gut microbiota and metabolites. *Gastroenterology.* (2022) 162:135–49. doi: 10.1053/j.gastro.2021.08.041

64. Del Chierico F, Nobili V, Vernocchi P, Russo A, De Stefanis C, Gnani D, et al. Gut microbiota profiling of pediatric nonalcoholic fatty liver disease and obese patients unveiled by an integrated meta-omics-based approach. *Hepatology.* (2017) 65:451–64. doi: 10.1002/hep.28572

65. Koh GY, Kane A, Lee K, Xu Q, Wu X, Roper J, et al. *Parabacteroides distasonis* attenuates toll-like receptor 4 signaling and Akt activation and blocks colon tumor formation in high-fat diet-fed azoxymethane-treated mice. *Int J Cancer.* (2018) 143:1797–805. doi: 10.1002/ijc.31559

66. Cuffaro B, Assohoun ALW, Boutillier D, Súkeníková L, Desramaut J, Boudebbouze S, et al. In vitro characterization of gut Microbiota-Derived commensal strains: selection of *Parabacteroides distasonis* strains alleviating TNBS-Induced colitis in mice. *Cells.* (2020) 9:2104. doi: 10.3390/cells9092104

67. Ezeji JC, Sarikonda DK, Hopperton A, Erkkila HL, Cohen DE, Martinez SP, et al. *Parabacteroides distasonis*: intriguing aerotolerant gut anaerobe with emerging antimicrobial resistance and pathogenic and probiotic roles in human health. *Gut Microbes.* (2021) 13:1922241. doi: 10.1080/19490976.2021.1922241

68. Kiewiet MBG, Elderman ME, El Aidy S, Burgerhof JGM, Visser H, Vaughan EE, et al. Flexibility of gut microbiota in ageing individuals during dietary fiber Long-Chain inulin intake. *Mol Nutr Food Res.* (2021) 65:2000390. doi: 10.1002/mnfr.202000390

69. Wang M, Zhang B, Hu J, Nie S, Xiong T, Xie M. Intervention of five strains of *Lactobacillus* on obesity in mice induced by high-fat diet. *J Funct Foods.* (2020) 72:104078. doi: 10.1016/j.jff.2020.104078

70. Long X, Zeng X, Tan F, Yi R, Pan Y, Zhou X, et al. *Lactobacillus plantarum* KFY04 prevents obesity in mice through the PPAR pathway and alleviates oxidative damage and inflammation. *Food Funct.* (2020) 11:5460–72. doi: 10.1039/D0FO00519C

71. Million M, Maraninchi M, Henry M, Armougom F, Richet H, Carrieri P, et al. Obesity-associated gut microbiota is enriched in *Lactobacillus reuteri* and depleted in *Bifidobacterium animalis* and *Methanobrevibacter smithii*. *Int J Obes.* (2012) 36:817–25. doi: 10.1038/ijo.2011.153

72. Crovesy L, Ostrowski M, Ferreira DMTP, Rosado EL, Soares-Mota M. Effect of *Lactobacillus* on body weight and body fat in overweight subjects: a systematic review of randomized controlled clinical trials. *Int J Obes.* (2017) 41:1607–14. doi: 10.1038/ijo.2017.161

73. van der Hee B, Wells JM. Microbial regulation of host physiology by short-chain fatty acids. *Trends Microbiol.* (2021) 29:700–12. doi: 10.1016/j.tim.2021.02.001

74. Sanders ME, Merenstein DJ, Reid G, Gibson GR, Rastall RA. Probiotics and prebiotics in intestinal health and disease: from biology to the clinic. *Nat. Rev. Gastroenterol. Hepatol.* (2019) 16:605–16. doi: 10.1038/s41575-019-0173-3

75. Canfora EE, Jocken JW, Blaak EE. Short-chain fatty acids in control of body weight and insulin sensitivity. *Nat. Rev. Endocrinol.* (2015) 11:577–91. doi: 10.1038/nrendo.2015.128

76. Zhang LS, Davies SS. Microbial metabolism of dietary components to bioactive metabolites: opportunities for new therapeutic interventions. *Genome Med.* (2016) 8:46. doi: 10.1186/s13073-016-0296-x

77. Lavelle A, Sokol H. Gut microbiota-derived metabolites as key actors in inflammatory bowel disease. *Nat. Rev. Gastroenterol. Hepatol.* (2020) 17:223–37. doi: 10.1038/s41575-019-0258-z

78. Sonnenburg ED, Sonnenburg JL. Starving our microbial self: the deleterious consequences of a diet deficient in microbiota-accessible carbohydrates. *Cell Metab.* (2014) 20:779–86. doi: 10.1016/j.cmet.2014.07.003

79. den Besten G, Bleeker A, Gerding A, van Eunen K, Havinga R, van Dijk TH, et al. Short-Chain fatty acids protect against High-Fat diet–induced obesity via a PPARγ-Dependent switch from lipogenesis to fat oxidation. *Diabetes.* (2015) 64:2398–408. doi: 10.2337/db14-1213

80. Kondo T, Kishi M, Fushimi T, Kaga T. Acetic acid upregulates the expression of genes for fatty acid oxidation enzymes in liver to suppress body fat accumulation. *J Agric Food Chem.* (2009) 57:5982–6. doi: 10.1021/jf900470c

81. Kondo T, Kishi M, Fushimi T, Ugajin S, Kaga T. Vinegar intake reduces body weight, body fat mass, and serum triglyceride levels in obese japanese subjects. *Biosci Biotechnol Biochem.* (2009) 73:1837–43. doi: 10.1271/bbb.90231

82. Fernández J, Redondo-Blanco S, Gutiérrez-del-Río I, Miguélez EM, Villar CJ, Lombo F. Colon microbiota fermentation of dietary prebiotics towards short-chain fatty acids and their roles as anti-inflammatory and antitumour agents: a review. *J Funct Foods.* (2016) 25:511–22. doi: 10.1016/j.jff.2016.06.032

83. Du J, Zhang P, Luo J, Shen L, Zhang S, Gu H, et al. Dietary betaine prevents obesity through gut microbiota-drived microRNA-378a family. *Gut Microbes.* (2021) 13:1862612. doi: 10.1080/19490976.2020.1862612

84. Liu Z, Zhang Y, Ai C, Wen C, Dong X, Sun X, et al. Gut microbiota response to sulfated sea cucumber polysaccharides in a differential manner using an in vitro fermentation model. *Food Res Int.* (2021) 148:110562. doi: 10.1016/j.foodres.2021.110562

85. Lei Y, Tang L, Liu S, Hu S, Wu L, Liu Y, et al. *Parabacteroides* produces acetate to alleviate heparanase-exacerbated acute pancreatitis through reducing neutrophil infiltration. *Microbiome.* (2021) 9:115. doi: 10.1186/s40168-021-01065-2

86. Li S, Tian Y, Jiang P, Lin Y, Liu X, Yang H. Recent advances in the application of metabolomics for food safety control and food quality analyses. *Crit Rev Food Sci Nutr.* (2021) 61:1448–69. doi: 10.1080/10408398.2020.1761287

frontiers | Frontiers in Nutrition

TYPE Original Research
PUBLISHED 26 October 2022
DOI 10.3389/fnut.2022.1012030

Check for updates

OPEN ACCESS

EDITED BY
Chanchan Sun,
Yantai University, China

REVIEWED BY
Yaxin Sang,
Hebei Agricultural University, China
Qian Li,
Tianjin Agricultural University, China
Tingting Cui,
Qilu University of Technology, China
Jiangxin Wang,
Shenzhen University, China

*CORRESPONDENCE
Zhenyuan Zhu
zhyuanzhu@tust.edu.cn

SPECIALTY SECTION
This article was submitted to Nutrition and Food Science Technology, a section of the journal Frontiers in Nutrition

RECEIVED 05 August 2022
ACCEPTED 10 October 2022
PUBLISHED 26 October 2022

CITATION
Jiang W, Hu Y and Zhu Z (2022) Structural characteristics of polysaccharide from *Zingiber striolatum* and its effects on gut microbiota composition in obese mice.
Front. Nutr. 9:1012030.
doi: 10.3389/fnut.2022.1012030

COPYRIGHT
© 2022 Jiang, Hu and Zhu. This is an open-access article distributed under the terms of the Creative Commons Attribution License (CC BY). The use, distribution or reproduction in other forums is permitted, provided the original author(s) and the copyright owner(s) are credited and that the original publication in this journal is cited, in accordance with accepted academic practice. No use, distribution or reproduction is permitted which does not comply with these terms.

Structural characteristics of polysaccharide from *Zingiber striolatum* and its effects on gut microbiota composition in obese mice

Wei Jiang[1,2,3], Ying Hu[4] and Zhenyuan Zhu[1,2]*

[1]Key Laboratory of Food Nutrition and Safety, Ministry of Education, Tianjin Key Laboratory of Food Nutrition and Safety, Tianjin University of Science and Technology, Tianjin, China, [2]College of Food Science and Engineering, Tianjin University of Science and Technology, Tianjin, China, [3]Department of Health Management, Zunyi Medical and Pharmaceutical College, Guizhou, China, [4]School of Public Health, Zunyi Medical University, Guizhou, China

To investigate a polysaccharide from *Zingiber striolatum* favorably modulates gut microbiota in mice fed a high-fat diet. *Z. striolatum* was utilized to extract the crude polysaccharide CZSP, which was subsequently refined using DEAE-52 cellulose and Sephadex G-150 to yield the novel polysaccharide *Zingiber strioatum* pure polysaccharide-1 (ZSPP-1). ZSPP-1 was an acidic heteroglycan made up of galactose, mannose, glucose, xylose, arabinose, glucuronic acid, and galacturonic acid with an average molecular weight of 1.57×10^6 Da. The structure of ZSPP-1 was investigated by FT-IR, methylation and NMR analysis, and the results denoted that the linkage structure types include T-Man*p*-linked, β-Xyl*p*-(1,2)-linked, β-Gal*p*-(1,4)-linked, α-Glc*p*A-(1,6)-linked, β-Ara*p*-(1,4)-linked, α-Glc*p*-(1,3,4,6)-linked, α-Glc*p*-(1,2)-linked, and β-T-Xyl*p*-linked, in which β-Gal*p*-(1,4)-linked and α-Gal*p*A-(1,4)-linked might be the main linkage. The results of the intervention experiments showed that ZSPP-1 changed the intestinal flora structure of the Firmicutes and Bacteroidetes in obese mice, and promoted the growth of beneficial bacteria such as *Akkermansia*, *Lactobacillus*, and *Bacteroides* in the intestine. It also restored the imbalanced flora structure due to high-fat diet to normal. It also restored the imbalanced flora structure due to high-fat diet to normal. *Z. striolatum* polysaccharides presented a considerable advantage in alleviating high-fat diet induced obesity, which indicates that it can be further exploited as a natural functional food resource.

KEYWORDS

***Zingiber strioatum*, polysaccharide, chemical structure, gut microbiota, obesity**

Introduction

Intestinal microbes are crucial for digestion and absorption of food; However, research indicates that intestinal microbial imbalance is intimately linked to obesity and related chronic metabolic illnesses (1). Since Fredrik Bäckhed et al. (2) initially postulated in the correlation between obesity and gut microbiota (i.e., It is confirmed that gut microbiota, as an environmental factor, regulates the accumulation of fat in the host). Zou et al. (3) transplanted the intestinal flora of obese and lean mice into new host mice; the results demonstrated that the new host mice had identical fat and lean phenotypes as the donor. Therefore, the tight association between obesity and intestinal microflora has drew the attention of an increasing number of researchers. Firmicutes/Bacteroidetes (F/B value) in the composition of intestinal microflora is a typical biomarker of intestinal microflora imbalance; the decrease or increase of F/B value indicates the remission of obesity or fat accumulation (4). Intestinal flora serves as a biological barrier to protect the body from hazardous toxins (such as endotoxin, harmful bacteria, etc.). Once intestinal flora is out of equilibrium, the gut wall becomes more permeable, allowing hazardous substances to invade the body. Obesity usually is accompanied by inflammation, and the increase of lipopolysaccharide in blood aggravates the inflammatory response (5). Obesity and the associated metabolic syndrome could be alleviated by probiotic supplementation (6). Consequently, the restoration of gut microbiota balance is regarded as a crucial intervention target for the prevention and treatment of obesity and related chronic metabolic illnesses (7).

Intestinal microbes are highly capable of digesting polysaccharides and can interact with intestinal epithelial cells, hence influencing energy intake and obesity (8). Plant polysaccharides are natural products extracted from plants; although the absorption efficiency of plant polysaccharides in the mammalian gastrointestinal tract is very low, studies have exhibited that the majority of them have a wide range of pharmacological effects, particularly the regulation of glycolipid and energy metabolism, which is often believed to be closely related to the regulation of gut microbiota (9).

Zingiber striolatum (*Zingiber striolatum Diels*) is a perennial herb belonging to *Zingiberaceae* which has certain special biological activities and can be used as a potential plant polysaccharide resource for the regulation of gut microbiota *Z. striolatum* is frequently utilized for vegetable consumption or traditional Chinese medicine (i.e., It is principally for the treatment of diseases including constipation, diabetes, hypertension, hyperlipidemia and inflammation). As a member of plant polysaccharides, the polysaccharide from *Z. striolatum* also has a variety of physical and chemical properties. However, little is known regarding the precise chemical structure and effect on glycolipid metabolism *in vivo* of the polysaccharides purified from *Z. striolatum*.

In this study, a novel acidic polysaccharide termed ZSPP-1 was purified from *Z. striolatum*. SEM imagery, molecular mass, physicochemical characterization, monosaccharide composition, Fourier transform infrared spectrometer (FT-IR) spectrogram, methylation, and 1D-NMR and 2D-NMR analyses were performed to characterize ZSPP-1. In the meantime, the effect of ZSPP-1 on the gut microbiota of obese mice was also investigated, which could provide theoretical reference for the clinical application and development of the polysaccharide.

Materials and methods

Materials and chemical reagents

Fresh *Z. striolatum* were harvested in Qixingguan County, Bijie City, Guizhou Province, China. All chemicals and solvents utilized in the study were analytical reagent grades. 20–22 g male SPF C57BL/6J mice, 6–8 weeks old, production license number: SCXK (Beijing, 2019-0010) were supplied by Sibeifu Biotechnology Co., Ltd. (Beijing, China). Complying with the pertinent legislation and the Guide for the Care and Use of Laboratory Animals, animal welfare and experimental procedures were conducted [Ministry of Science and Technology of China, (10)]. The license number of the experimental unit is SYXK (Tianjin) 2018-0001. None of the experimentation involved human subjects.

Extraction of crude polysaccharide of *Zingiber striolatum*

Zingiber striolatum were rinsed in water to remove soil from their surface, then drained and air-dried. Afterward, *Z. striolatum* were cut into pieces, dried and crushed into powder (100 mesh). The powder was then rehydrated 20 times with water, thoroughly mixed, extracted for 2 h in an 80°C water bath, and filtered with a brinell funnel to secure filtrate. Next, the filter residues were extracted twice and all filtrates were combined. Filtrates were concentrated at 60°C under reduced pressure, then precipitated overnight at 4°C with four times the volume of 95% ethanol. The precipitates were collected after centrifugation at 4,000 r·min^{-1} for 10 min. The precipitate is dissolved in an adequate volume of distilled water, placed in the cone separation funnel, thoroughly mixed with 1/4 volume of sevage reagent, and allowed to stand for 4 h. After stratification, the mixed layer of sevage and protein in the cone separation funnel's intermediate and lower layers is removed and the process is repeated numerous times. Evaporate and concentrate the crude protein-free polysaccharide solution to evaporate the remaining sevage reagent in the polysaccharide solution. Last but not least, there is a large amount of pigment in *Z. striolatum*, 1/2 volume of AB-8 macroporous adsorption resins are added

to the concentrated solution and placed in a shaking table for 160 rpm overnight, in order to remove the pigment from the polysaccharide. The crude polysaccharide of *Z. striolatum* (CZSP) was eventually obtained after the polysaccharide was placed in a 100 kDa dialysis bag, dialyzed with flowing water and distilled water for 48 h respectively, and then vacuum freeze-dried.

Purification of crude polysaccharide of *Zingiber striolatum*

Crude polysaccharide of *Z. striolatum* was applied to a DEAE Cellulose-52 column and stepwise elution with distilled water (0.1, 0.3, and 0.5 M NaCl) at a flow rate of 1.2 mL/min was then conducted to produce four fractions (ZSP-1, ZSP-2, and ZSP-3). The principal fraction (ZSP-1) was subsequently desalted by filtration through membranes with a molecular mass of 3,500 Da. CZSP-1 was preserved following freeze-drying under vacuum. Then 10 mg of ZSP-1 was redissolved in 1 mL of deionized water and filtered through a 0.45 m membrane. Sephadex G-150 was utilized for separation, while distilled water was employed for elution. Before elution, it was allowed to stand and balance for 10 min, the elution flow rate was 0.16 mL/min, and 1.3 mL of eluent is gathered from each collecting tube. At 490 nm, the sugar content of the eluent was measured employing the phenol sulfuric acid methodology. To acquire *Z. striolatum* pure polysaccharide, also known as ZSPP-1, the elution curve was drawn, the major peak eluent was collected, the identical components were combined, and lyophilization was used.

Characterization of ZSPP-1

Scanning electron microscopy analysis

With an SU1510 electron microscope, SEM image of lyophilized ZSPP-1 were observed (Hitachi, Japan). Prior to measurements, the specimens' surfaces were coated with a thin gold film to optimize conductivity.

Homogeneity and molecular mass determination

Homogeneity and molecular mass of ZSPP-1 were determined employing high performance liquid chromatography with an Agilent 1200 HPLC system outfitted with a TSK-GEL G4000PWxl column and a refractive index detector (RID). Sample (10 μL) solution (1 mg/mL) was injected in each run, with ultrapure water as the mobile phase at a flow rate of 0.6 mL/min (30°C). The molecular mass of ZSPP-1 was evaluated by comparing with the retention times based on the standard curve of a succession of molecular mass standards (10, 40, 70, 500, and 2,000 kDa) (11).

Physicochemical characterization determination

The total carbohydrate content was measured by the phenol sulfuric acid methodology using D-glucose as the benchmark. At 490 nm, the absorbance was observed, and the glucose standard curve was constructed (12). With galacturonic acid as the reference, the content of uronic acid was evaluated by sulfuric acid carbazole methodology, the absorbance was detected at 525 nm, and the galacturonic acid standard curve was constructed (13). The protein content was assessed using the Coomassie brilliant blue G-250 method, with bovine serum protein serving as the standard, and the absorbance was measured at 595 nm. Furthermore, the protein content of *Z. striolatum* polysaccharide was validated by the UV absorption spectrum recorded between 190 and 400 nm using a spectrophotometer.

Monosaccharide composition determination

The monosaccharide composition of ZSPP-1 was evaluated using gas chromatography-mass spectrometer (GC-MS) with some modifications (14). Add 1.5 mL of a 2 mol/L TFA solution to a ZSPP-1 sample (10 mg) and hydrolyze it in an oil bath heated to 110°C for 3 h. After hydrolysis was complete, dry with nitrogen and add 1 ml of distilled water to generate ZSPP-1 hydrolysis solution. ZSPP-1 hydrolysis solution was mixed with 0.5 mol/L sodium carbonate solution (reacting in a 30°C water bath for 30 min), 0.5 mL 4% sodium borohydride solution (reacting in a 30°C water bath for 1.5 h) was then added, and 25% acetic acid solution is dropped until no bubbles emerge. The reaction solution was eluted with distilled water after passing through the cation exchange column Dowex-50w8-200 (type H+). Following collecting the eluent, evaporate the sample under reduced pressure at 80°C until it is completely dry. The dry residue added 1 mL of pyridine and n-propylamine, respectively (sealed and dried with nitrogen after reacting at 55°C for 30 min), and added 2 mL of pyridine and acetic anhydride, respectively (reacted overnight at 25°C, dried with nitrogen). The residue is diluted in 1 mL of carbon dichloride, extracted with water for 2–3 times to eliminate impurities, and the organic solvent layer is filtered through a 0.22 μm membrane for GC-MS analysis.

Fourier transform infrared spectrometer analyses

The structure of ZSPP-1 was investigated by FT-IR employing a Vector 22 FT-IR (Bruker, Germany) operated in the region of 400–4,000 cm^{-1}. The infrared spectra were gathered at resolution of 2 cm^{-1} with 16 scans. ZSPP-1 were separately ground with KBr powder and compressed into pellets for FT-IR measurement. Briefly, the samples (1 mg) and KBr (150 mg) were precisely weighed and compressed into pellets, and the data was collected with the FT-IR.

Methylation analysis

The methylation experimental method was referenced and slightly modified (15). Before methylation, acidic polysaccharide uronic acid should be decreased. Initially, 5 mg of ZSPP-1 was dissolved in 5 mL water. Afterward, 5 mg of carbodiimide was added to the ZSPP-1 acidic polysaccharide solution, and the pH was adjusted to 4.75 using 0.1 M hydrochloric acid (stirring evenly). Then, 5 mL of sodium boron deuterate solution (while stirring constantly at pH = 7.0 for 0.5 h) was added to the solution and the pH was adjusted to 4.0 using 2 M hydrochloric acid. The reaction solution was dialyzed overnight with 3,500 Da at 25°C. The Reduced sample was dried and set it aside. The sample was added 2 mL mixed solution of acetic acid and methanol (v/v = 1/9), dried with nitrogen and repeated for four times. Finally, the sample was added a few drops of methanol and dried the solution with nitrogen to eliminate any residual boric acid.

The dry neutral ZSPP-1 was dissolved in 2 mL dimethyl sulfoxide (DMSO with an anhydration with 3A molecular sieves). Under nitrogen protection, 25 mg NaH was added to the solution (reacted in ultrasonic and darkened settings at 18–20°C for 30 min). Then, 1 mL of iodomethane was added to the solution, and the reaction was maintained at the same conditions for 1 h. Repeat these methylation operations more than five times, and add 0.5 mL of water to terminate the reaction. The methylation sample was extracted using carbon dichloride and dried with nitrogen. The methylation sample was then evaluated using FT-IR.

The methylation sample was hydrolyzed with 2 mL trifluoroacetic acid (2 mol/L) at 110°C for 3 h. The hydrolyzate was dried with nitrogen and added 25 mg sodium boron deuterate with 2 mL deionized water (reacted at 25°C for 2 h). The solution was pH-adjusted to 5.0 with ethylic acid and then nitrogen-dried. The dried sample was co-distilled with 3 mL of methanol and 0.1 mL of acetic acid five times in order to decompose the sodium boron deuterate (no ethylic acid at last two times). Next, ZSPP-1 polysaccharide derivatives need to be prepared. Reduced methylated sample were dissolved in 2 mL of acetic anhydride (reacted at 100°C for 1 h) and dried with nitrogen. Following that, the residue was co-distilled to dry with 3 mL methanol (three times) and dissolved with 1 mL dichloromethane for GC-MS analysis.

NMR spectroscopy analyses

The 1D (1H, 13C) and 2D (HSQC) NMR spectra were investigated by a Bruker AVANCE III HD 600 MHz spectrometer (Brucker, Germany). Each sample (50 mg) was dissolved in D_2O (0.5 mL) at 25°C, and the data was analyzed employing Bruker Topspin-NMR software.

Animal experiment design

Sixty mice (6 weeks old) were classified into six groups. All mice were quarantined at the Tianjin University of Science and Technology Experimental Animal Center before being placed in the experimental chamber at a temperature (21–24°C), humidity (50–60%), and a 12 h light/dark cycle. The C57BL/6J mice were fed normally for a week. Then, nine mice were chosen at random to constitute the normal group (NG), which continued to receive basal fodder.

In comparison to the average weight of the NG group, the average weight of mice fed a high-fat diet for roughly 9 weeks was significantly greater than that of the NG group. When mice with a weight of over 20% were identified as obese mice, denoting that the obesity model was successfully constructed. The NG group continued to be fed basal fodder. The obese mice with successful modeling were randomly divided into five subgroups: the model group (MG) was fed with HFD and given the same amount of distilled water as ZSPP-1 every day; The low-dose group (LZG), medium-dose group (MZG), and high-dose group (HZG) were fed with HFD and given ZSPP-1 polysaccharide of 100, 200, and 400 mg/kg for at least 7 weeks, respectively; The 100 mg/kg Orlistat was utilized to gavage mice as positive control group (CG). The body weight of mice in each treatment group was recorded every week.

Fecal sample collection

Before the mice were sacrificed, the anal region was cleaned with medical alcohol, the tail was fixed, and the lower abdomen was stimulated with cotton swabs to induce defecation. When mice defecated, sterilized EP tubes were used to collect the feces. Following the collection of around eight feces from each mouse, the EP tubes were placed in the −80°C refrigerator for sequencing of gut microbiota.

Intestinal flora analysis

DNA extraction and PCR amplification

Microbial community genomic DNA was extracted from mice feces samples using the E.Z.N.A.® soil DNA Kit (Omega Bio-tek, Norcross, GA, USA) according to manufacturer's instructions. The DNA extract was checked on 1% agarose gel, and DNA concentration and purity were investigated with NanoDrop 2000 UV-vis spectrophotometer (Thermo Scientific, Wilmington, DE, USA). The hypervariable region V3–V4 of the bacterial 16S rRNA gene were amplified with primer pairs 338F (5′-ACTCCTACGGGAGGCAGCAG-3′) and 806R (5′-GGACTACHVGGGTWTCTAAT-3′) by an ABI GeneAmp® 9700 PCR thermocycler (ABI, Los Angeles, CA, USA). The PCR amplification of 16S rRNA gene was implemented as follows: initial denaturation at 95°C for 3 min, followed by 27 cycles of denaturing at 95°C for 30 s, annealing at 55°C for 30 s and extension at 72°C for 45 s, and single extension at 72°C for 10 min, and end at 4°C. The PCR mixtures contain 5 × TransStart FastPfu buffer 4 μL, 2.5 mM dNTPs 2 μL, forward primer (5 μM) 0.8 μL, reverse primer (5 μM) 0.8 μL, TransStart FastPfu DNA Polymerase 0.4 μL, template DNA 10 ng, and finally ddH_2O up to 20 μL. PCR reactions were

conducted in triplicate. The PCR product was extracted from a 2% agarose gel, purified utilizing the AxyPrep DNA Gel Extraction Kit (Axygen Biosciences, Union City, CA, USA) in accordance with the manufacturer's instructions, and quantified by Quantus^{TM} Fluorometer (Promega, USA).

Illumina MiSeq sequencing

Purified amplicons were pooled in equimolar and paired-end sequenced on an NovaSeq PE250 platform in accordance with the standard protocols by Majorbio Bio-Pharm Technology Co., Ltd. (Shanghai, China).

Processing of sequencing data

The raw 16S rRNA gene sequencing reads were demultiplexed, filtered for quality by fastp version 0.20.0 (16) and merged by FLASH version 1.2.7. Using UPARSE version 7.1, operational taxonomic units (OTUs) with a similarity cutoff of 97% were clustered, and chimeric sequences were spotted and eliminated. RDP Classifier version 2.2 was used to examine the taxonomy of each OTU representative sequence (17) against the 16S rRNA database using confidence threshold of 0.7.

Upload the data to the repository

The original sequencing data is uploaded to the official NCBI website. Link to: https://submit.ncbi.nlm.nih.gov/subs/. Registration No.: PRJNA871034.

Statistical analysis

The data were expressed as mean ± standard deviation (SD), where the mean data was calculated using Excel, 2010. SPSS 22 software was employed for one-way ANOVA and Duncan test for significance analysis, and the P-value < 0.05 was determined to be statistically significant.

Results and discussion

The SEM images and physicochemical compositions of ZSPP-1

The separation and purification flow chart of CZSP illustrated in **Figure 1**. CZSP is separated into three parts on DEAE-cellouse-52 column (**Figure 2**). As shown in the figure, ZSP-1 is higher in absorbance compared with ZSP-2 and ZSP-3. It can also be stated that ZSP-1 produced a better yield. In this study, only ZSP-1 that has been purified by Sephadex G-150 will be examined; the other two components will be used in other studies. The ZSPP-1 was obtained as depicted in **Supplementary Figure 1**. The percentages of total sugar, uronic acid, and protein in ZSPP-1 were approximately 90.6%, 12.31%, and undetectable, respectively. UV absorption spectrum further revealed that ZSPP-1 lacked

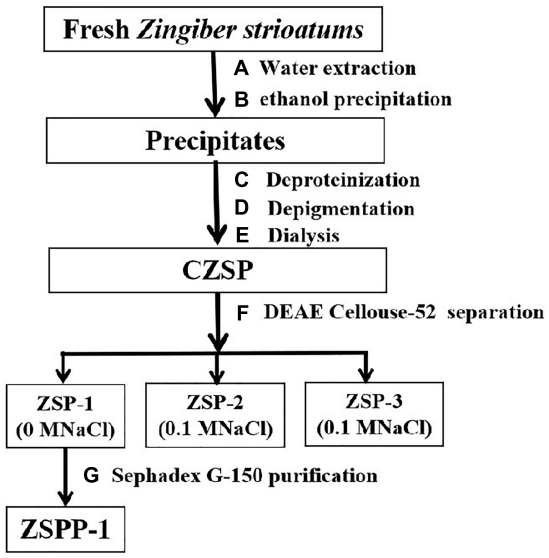

FIGURE 1
The procedure of ZSPP-1 extraction and purification.

absorption peaks at 260 and 280 nm (**Supplementary Figure 2**), demonstrating the absence of protein and nucleic acid (**Table 1**). As presented in **Supplementary Figure 3**, ZSPP-1 shows an aggregated flake structure, stacked together with each other, small fragment structure and scattered distribution, and there are more gaps between fragments from the appearance and morphology.

Homogeneity and molecular mass

The homogeneity was validated by elution, obtaining a single symmetrical peak at 8.37 min using high performance gel permeation chromatography (**Supplementary Figure 4**). Following are the calibration equations for carbohydrates with varying molecular weights: $\log M = -0.2798x + 8.5389$ ($R^2 = 0.9964$), M and x are the molecular weight and retention time of ZSPP-1, respectively; The molecular weight of ZSPP-1 is estimated to be 1.57×10^6 Da (**Table 1**).

Monosaccharide composition

According to GC-MS analysis, the monosaccharide composition of ZSPP-1 is illustrated in **Table 1**. The monosaccharide species were investigated in ZSPP-1 (seven types), indicating the structural complexity of ZSPP-1. As shown in **Table 1**, the ZSPP-1 was predominantly composed of galactose (36.8%), mannose (22.8%), and glucose (20.7%) in association with a small number of xylose (9.8%), arabinose (4.3%), glucuronic acid (2.9%), galacturonic acid (2.7%) units.

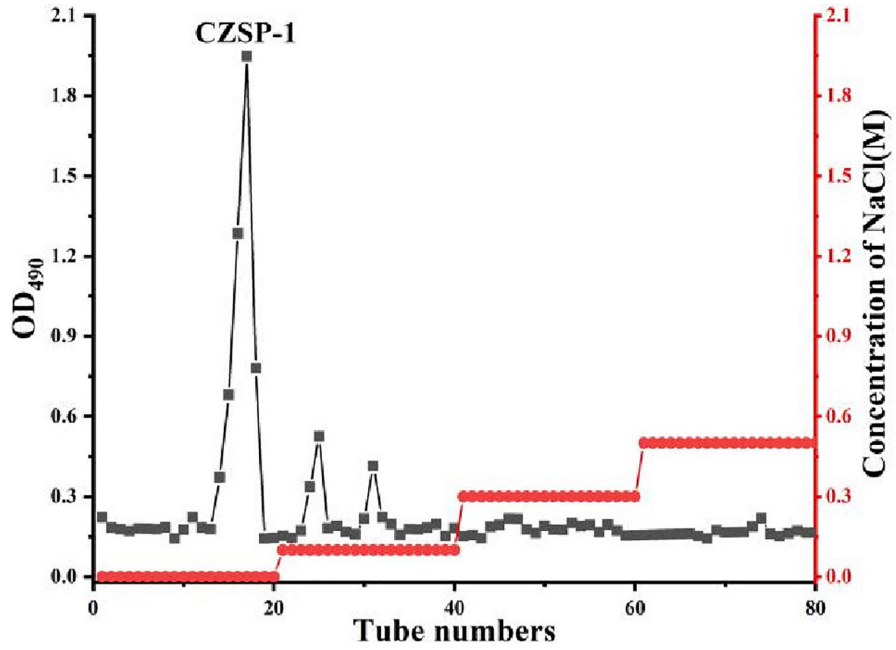

FIGURE 2
Elution profile of CZSP-1 on DEAE-cellulose-52 column.

Fourier transform infrared spectrometer analysis

Figure 3 shows that ZSPP-1's infrared spectrum exhibited a typical polysaccharide characteristic band, a broad band in the range of 3,000–3,750 cm^{-1}, and a strong absorption peak at 3,404.92 cm^{-1}, which is the -OH stretching vibration signal peak (18); The weak absorption peak at 2,924.51 cm^{-1} was the C-H stretching vibration signal peak (19); The above two peaks were typical hydroxyl and alkyl groups of polysaccharides, denoting that the sample is polysaccharide (20). Moreover, infrared analysis showed that there was a weak absorption peak near 1,730 cm^{-1}, and 1,733.43 cm^{-1} was the -COOH stretching vibration signal peak, indicating that the purified polysaccharide ZSPP-1 contained uronic acid (21). A strong absorption peak emerges at 1,609.37 cm^{-1}, which is the stretching vibration of C = O, signifying the presence of -CHO; 1,420.42 cm^{-1} was the C-H variable angle vibration signal peak, and the above two peaks are also the infrared characteristic absorption peaks of polysaccharides. The band at approximately 1,000–1,200 cm^{-1} presents the existence of C-O-C and C-O-H bonds. The peaks at 1,105.66, 1,073.64, and 1,030.05 cm^{-1} are three signal peaks resulting from the stretching vibration of C-O bond and C-C bond in the sugar ring, which proves that ZSPP-1 contains pyran monosaccharide (22); The bands of 896.25 and 833.01 cm^{-1} proved that the pure polysaccharide ZSPP-1 existed simultaneously α- and β-glycosidic bond of configuration (23).

Methylation analysis

To assess the chemical structure of glycosidic bonds in polysaccharides, methylation analysis is commonly employed. In this study, the methylation results were analyzed using the PMAA spectral standard database (complex carbohydrate research center, University of Georgia). Supplementary Figure 5 depicts the comparison of FT-IR spectra before and after ZSPP-1 methylation. Using methylation analysis, the glycosidic linkage and molar ratios of sugar residues in ZSPP-1 were determined. As shown in Table 2, the ZSPP-1 PMAA derivatives were measured to be 2,3,4,6-Me4-Man*p*, 2,3,5-Me3-Xyl*p*, 3,5-Me2-Xyl*p*, 2,3,6-Me3-Gal*p*, 2,3,4-Me3-Glc*p*, 2,3-Me2-Ara*p*, 2-Me-Glc*p*, and 3,4,6-Me3-Glc*p* with the molar of 21.5: 3.4: 5.66: 33.9: 11.1: 3.8: 6.74: 3.07. As shown by the monosaccharide composition of ZSPP-1, the total galactose content was the predominant fraction in ZSPP-1. Furthermore, the content of galactose and glucose increased after uronic acid reduction, signifying the content of galactose and glucose increased after methylation (24). This result suggested that ZSPP-1 mainly contained seven linkages: Man*p*-(1→, →2)-Xyl*p*-(1→, →4)-Gal*p*-(1→, →6)-Glc*p*-(1→, →4)-Ara*p*-(1→, →3,4,6)-Glc*p*-(1→, →2)-Glc*p*-(1→, and Xyl*p*-(1→ respectively, in which →4)-Gal*p*/Gal*p*A-(1→ might be the main linkage of ZSPP-1.

10.3389/fnut.2022.1012030

TABLE 1 Chemical composition of ZSPP-1.

Parameters	Sugar content (%)	Uronic acid content (%)	Protein content (%)	Molecular weight (Da)	Sugar component (mol%)						
					Rha	Ara	Xyl	Man	Glc	Gal	GlcA	GalA
ZSPP-1	90.6 ± 3.6	12.31 ± 4.2	–	1.57×10^6	–	4.3	9.8	22.8	20.7	36.8	2.9	2.7

NMR analysis

The structural features of ZSPP-1 were further identified by ^{1}H, ^{13}C, HSQC NMR spectral analysis at 600 MHz were investigated (**Figures 4A–D**). The entire assignment shifts of the ^{1}H and ^{13}C for ZSPP-1 were identified with reference to the previous literatures and then illustrated.

The chemical shifts in ^{1}H NMR spectrum (**Figure 4B**) and HSQC spectra (**Figures 4C,D**) presented eight signals in the anomeric region at δ 4.69, δ 5.25, δ4.52, δ 5.14, δ 5.19, δ 5.82, δ 4.75, and δ 4.59 ppm. These eight anomeric protons were assigned to nine distinct glycosidic bond types. The chemical shifts in ^{13}C NMR and HSQC spectra, these eight anomeric carbon signals appeared at δ 103.67, δ 109.18, δ 102.7, δ 98.80, δ 92.00, δ 106.91, δ 100.75, and δ 96.54 ppm, and all carbon chemical shifts were assigned to eight different types of glycosidic bonds. The eight detected sugar moieties were labeled as a, b, c, d, e, f, and h.

By combining the results of methylation analysis and literature data (25), the corresponding chemical shift at δ 106.91 ppm in the ^{13}C NMR and HSQC spectra could be identified as β→4)-Ara*p*-(1→. Particularly, the ^{13}C NMR signal at δ 175.27 and δ 176.02 ppm should be assigned to the carboxyl group of Glc*p*A and Gal*p*A, which indicated that ZSPP-1 was a novel acidic polysaccharide (26). The signals of ^{13}C at δ 98.80 and δ 92.00 ppm assigned from the HSQC were inferred α→4)-Gal*p*A-(1→ and α→6)-Glc*p*A-(1→. As reported in the literature (27), when δ > 101 ppm, the signals belonged to the (1→2,3,4,6)-linked Gal and the (1→6,1→3,6)-linked Man. Therefore, the signals δ 102.7 and δ 103.67 ppm were inferred as β→4)-Gal*p*-(1→ and Man*p*-(1→ According to relevant references (28), the anomeric carbon signal peak of glucose residues were dispersed between δ 92 and δ 103 ppm (29). Therefore, the signal δ 92.00 and δ 100.75 ppm were inferred as α→3,4,6)-Glc*p*-(1→ and α→2)-Glc*p*-(1→. However, due to NMR signal peak of xylose residues were rarely reported in the literature, the corresponding chemical shifted at δ 109.18 ppm in ^{13}C NMR and HSQC spectra could be inferred as xylose residues. This outcome requires additional discussion and clarity.

ZSPP-1 administration altered the structure of the gut microbiota

To determine if ZSPP-1 can regulate or restore the imbalance of gut microbiota in obese mice, HFD mice were fed a ZSPP-1-supplemented diet for approximately 8 weeks, and their gut microbiota was studied.

As illustrated in the Venn diagram of OTU (**Supplementary Figure 6**), a total of 4,371 OTUs were obtained. In this study, the number of OTUs in NG, MG, LZG, MZG, HZG, and CG groups were 813, 747, 693, 725, 804, and 589, respectively. The

10.3389/fnut.2022.1012030

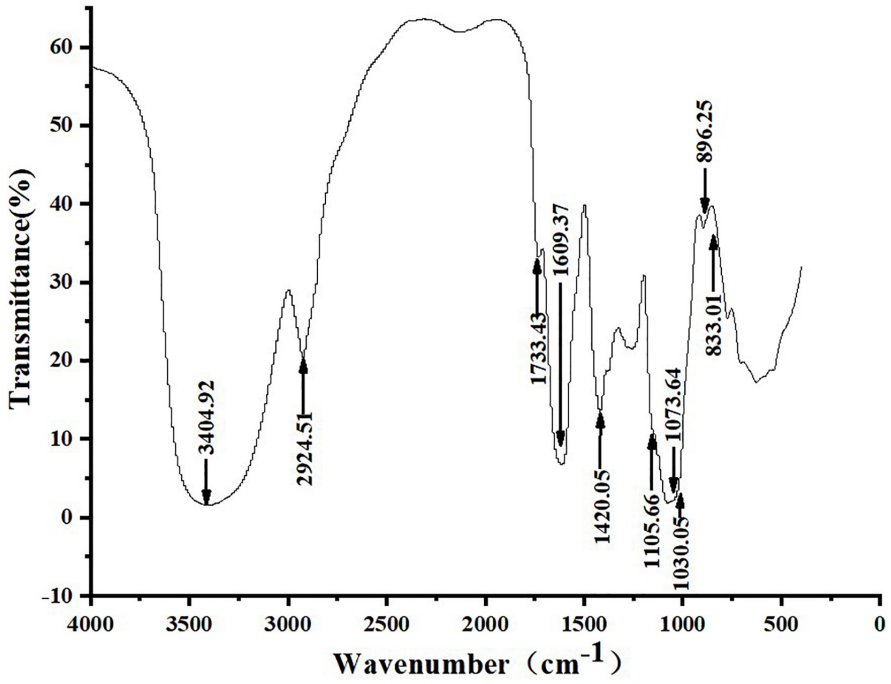

FIGURE 3
Fourier transform infrared spectrometer (FT-IR) spectrum of ZSPP-1.

TABLE 2 Methylation analysis data for ZSPP-1.

Retention time	Methylated sugars	Mass fragments (m/z)	Molar ratio	Type of linkages
29.409	2,3,4,6-Me4-Man*p*	43, 59, 71, 87, 101, 113, 129, 145, 157, 162, 205	21.5	Man*p*-(1→
29.641	2,3,5-Me3-Xyl*p*	43, 59, 73, 87, 101, 115, 129, 146, 157	3.4	Xyl*p*-(1→
32.022	3,5-Me2-Xyl*p*	43, 59, 74, 85, 99, 118, 130, 142, 160, 173,	5.66	→2)-Xyl*p*-(1→
32.254	2,3,6-Me3-Gal*p*	43, 59, 71, 87, 99, 118, 131, 142, 157, 173, 203	33.9	→4)-Gal*p*/Gal*p*A-(1→
33.184	2,3,4-Me3-Glc*p*	43, 59, 71, 87, 99, 118, 129, 143, 159, 173, 189	11.1	→6)-Glc*p*-(1→
33.610	2,3-Me2-Ara*p*	43, 59, 71, 87, 101, 118, 129, 142, 162, 173	3.8	→4)-Ara*p*-(1→
34.616	2-Me-Glc*p*	34, 59, 87, 97, 118, 139, 160, 171, 202, 231	6.74	→3,4,6)-Glc*p*-(1→
35.275	3,4,6-Me3-Glc*p*	34, 59, 74, 87, 113, 129, 160, 190, 234	3.07	→2)-Glc*p*-(1→

composition similarity and overlap of OTUs among different treatment groups were studied. It was figured out that each group shared 471 OTUs. Meanwhile, 342, 276, 222, 254, 333, and 118 OTUs were unique to NG, MG, LZG, MZG, HZG, and CG groups, respectively. The increase in OTU abundance does not necessarily indicate a return to normal intestinal flora (30). As can be seen, however, the addition of ZSPP-1 altered the quantity of intestinal flora in HFD mice, and the abundance boosted with increasing dose.

The analysis of the intestinal microbiota composition at the phylum level (**Figure 5**) exhibited that the gut microbiota of each treatment group consisted primarily of Bacteroidetes, Firmicutes, Desulfobacterota, Patescibacteria and Campylobacter. It is reported that the ratio of F/B value in intestinal microorganisms of obese mice will increase significantly (31). Compared with NG group, the F/B rate of MG group increased significantly; Besides, the F/B rate of LZG, MZG, HZG, and CG groups presented a downward trend compared with the NG group. Orlistat intake decreased the diversity and richness of intestinal microorganisms. Compared with the MG group, the proportions of Firmicutes and Bacteroidetes were further decreased by orlistat treatment, which reduced the abundance of obesity-associated bacteria Lachnospira.

These results are consistent with the findings of Ke et al. (32). Literature reports also confirmed that prebiotics can increase the relative abundance of Bacteroidetes and reduce the relative abundance of Firmicutes in the host intestine, so as to inhibit obesity (33). In this study, it was discovered that the relative abundance of Desulfobacterota and Campylobacter increased

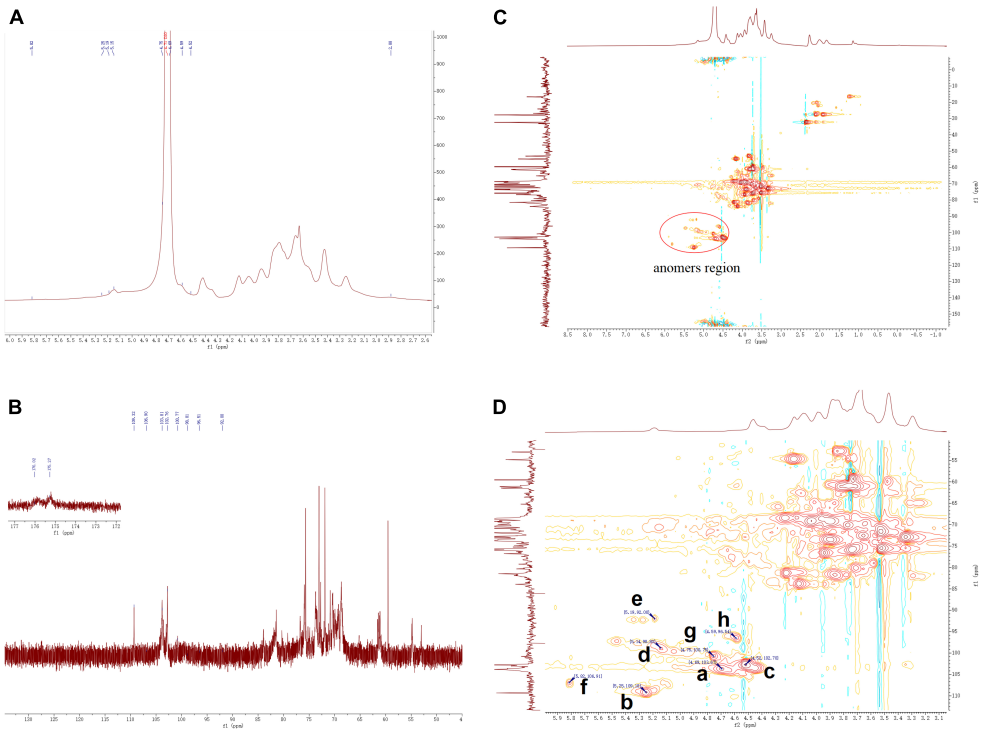

FIGURE 4
(A) The 1H NMR, **(B)** 13C NMR, and **(C,D)** HSQC spectra of ZSPP-1.

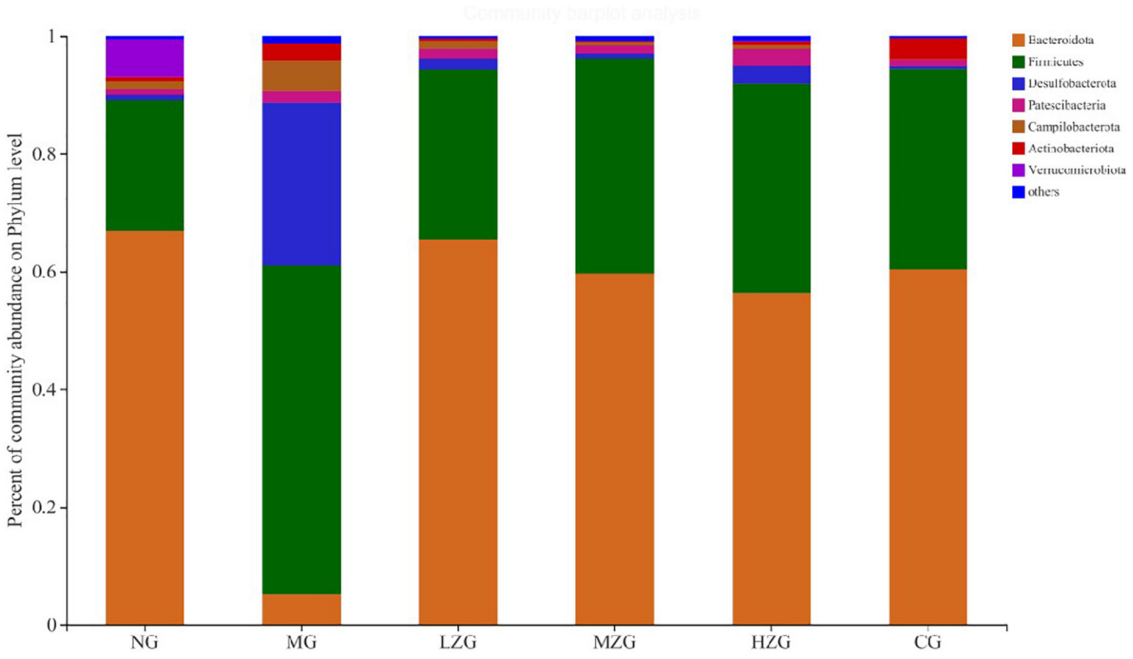

FIGURE 5
Gut microbial composition of different samples at the phylum level. The abscissa is the sample name, the ordinate is the proportion of the species in the sample, the columns with different colors represent different species, and the length of the columns represents the proportion of the species.

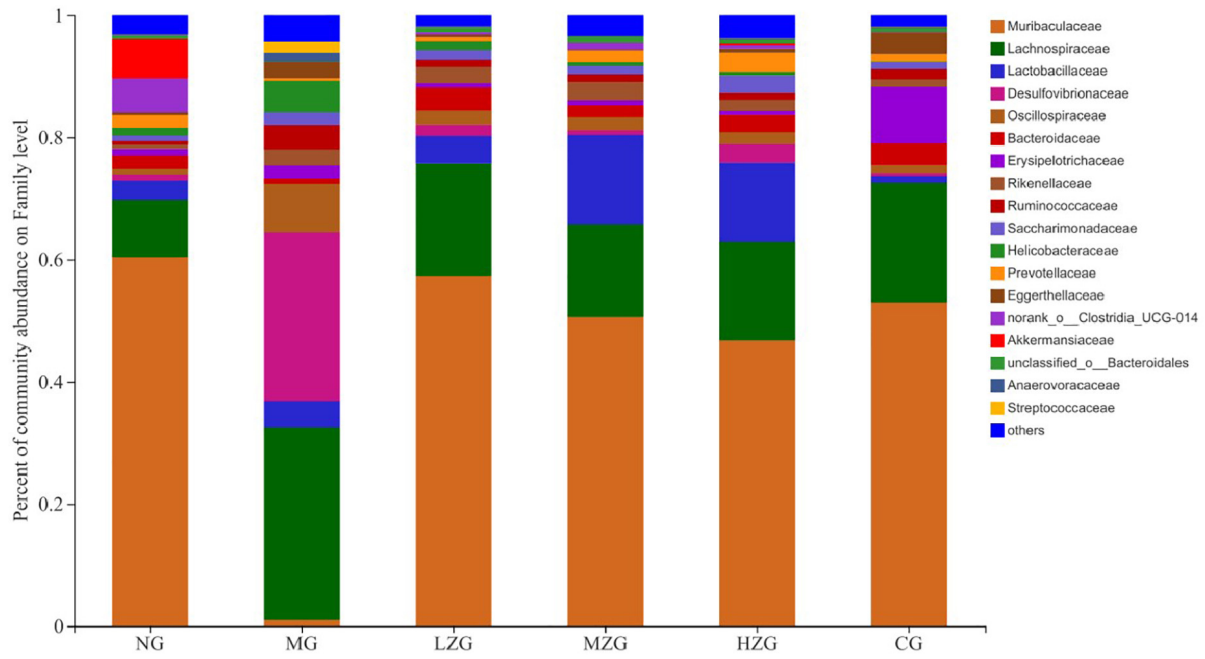

FIGURE 6
Gut microbial composition of different samples at the family level. The abscissa is the sample name, the ordinate is the proportion of the species in the sample, the columns with different colors represent different species, and the length of the columns represents the proportion of the species.

in the MG group, but decreased in the ZSPP-1 and positive medication treatment groups in comparison to the NG group.

At the family level, *Muribaculaceae*, *Lachnospiraceae*, *Lactobacillus*, *Desulfovibrionaceae*, *Oscillospiraceae*, *Bacteroidaceae*, *Rikenellaceae*, and *Ruminococcaceae* were the main components of gut microbiota as shown in **Figure 6**. According to relevant literature reports, *Muribaculaceae*, *Bacteroidaceae*, and *Rikenellaceae* are mucin monosaccharide feeders. Many intestinal pathogens can utilize mucin monosaccharide as an essential nutrient in the intestine and compete with pathogens for these nutrients in order to maintain a healthy intestinal ecosystem (34). In this study, except for MG group, the relative abundance of *Muribaculaceae* and *Bacteroidaceae* in NG, LZG, MZG, HZG, and CG groups increased significantly, demonstrating that mucin monosaccharide seekers may form a competitive relationship with intestinal harmful bacteria. In addition, *Ruminococcaceae* is a potential diagnostic indicator of obesity and flora imbalance generated by HFD, whereas *Lachnospiraceae* is thought to be associated with liver inflammation (35). In this study, it was investigated that the abundance of *Lachnospiraceae* and *Ruminococcaceae* increased significantly in MG group, but decreased in ZSPP-1 and positive drug treatment group, which verified the view that mucin monosaccharide seekers formulated competitive correlation with intestinal harmful bacteria. LPS has been proven to be closely associated with the occurrence and development of chronic inflammation and metabolic disorders (36); *Desulfovibrionaceae* is a category of sulfate reducing bacteria, which can convert sulfate into hydrogen sulfide and also can destroy the integrity of intestinal barrier. Furthermore, *Desulfovibrionaceae* belongs to Gram-negative bacteria containing LPS. The results displayed that after ZSPP-1 intervention, the abundance of *Desulfovibrionaceae* decreased significantly in obese mice. The glucan components that make up ZSPP-1 [e.g., →6)-Glc*p*-(1→, →3,4,6)-Glc*p*-(1→, and →2)-Glc*p*-(1→] are expected to form prebiotics through the fermentation of intestinal flora, which possess a role in decreasing inflammatory cells and inflammatory mediators. By modulating the immune response in liver tissue, Neyrinck et al. (37) revealed that using fermentable laminarin glucan can protect rats from LPS-induced hepatotoxicity. Meanwhile, Li et al. (38) characterized the structure of Tuber sinense polysaccharide (TPS) and found that TPS has → 4)-D-Glc*p*-(1→, →4,6)-D-Glc*p*-(1→, and D-Glc*p*-(1→ residue; TPS and β-lactoglobulin binds to form a conjugate can increase some probiotics including *Lactobacillaceae*, inhibit harmful inflammatory reaction, and avoid intestinal flora disorder. This also confirmed that glucan-containing ZSPP-1 may increase the number of *Lactobacillaceae* in the intestines of obese mice. *Lactobacillaceae* is an essential probiotic for preventing and treating metabolic disorders such as obesity and diabetes mellitus (39, 40); *Prevotellaceae* is considered related to the synthesis of short chain fatty acids (SCFAs). In addition, the lack of SCFAs weakened its protective effect on intestinal

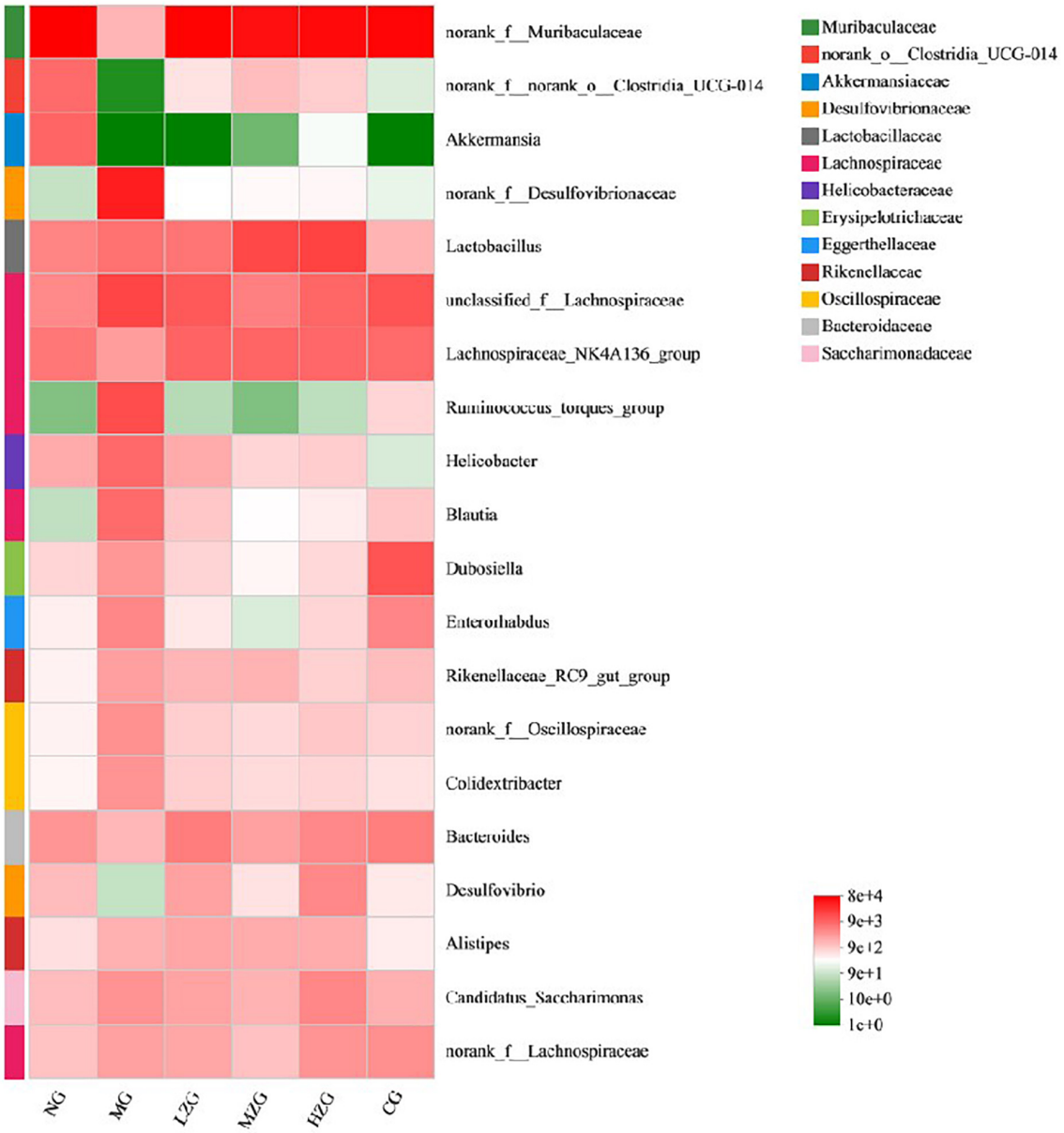

FIGURE 7
Heat map of gut microbial composition at the genus level. The abscissa is the group name, and the ordinate is the species name. The abundance changes of different species in the sample are displayed through the color gradient of the color block. The right side of the figure is the value represented by the color gradient.

mucosal barrier, which may render the increase of intestinal endotoxin level (41, 42); In this study, ZSPP-1 intervention could significantly enhance the abundance of *Lactobacillus* and *Prevotellaceae* in the intestinal microbial composition of obese mice. In conclusion, these findings demonstrate that ZSPP-1 positively regulates the imbalance of gut microbiota induced by obesity.

Results as shown in **Figure 7**, at the genus level, the relative abundance of harmful bacteria (such as *Desulfovibrionaceae*, *Lachnospiraceae*, *Ruminococcus*, *Helicobacter*, *Oscillospiraceae* etc.) decreased significantly and the relative abundance of beneficial bacteria (such as *Akkermansia*, *Lactobacillus*, *Bacteroides*) increased significantly in LZG, MZG, HZG and CG groups compared with MG group. It was reported that *Desulfovibrionaceae*, *Lachnospiraceae*, *Ruminococcus*, *Helicobacter*, and *Oscillospiraceae* can render chronic inflammatory and metabolic illnesses (43). It has also been reported that squid ink polysaccharide (Sugar component: Fuc, GlcA, and GalN in a molar ratio of 1:1:1) decreases the abundance of harmful bacteria (such as *Ruminococcus*,

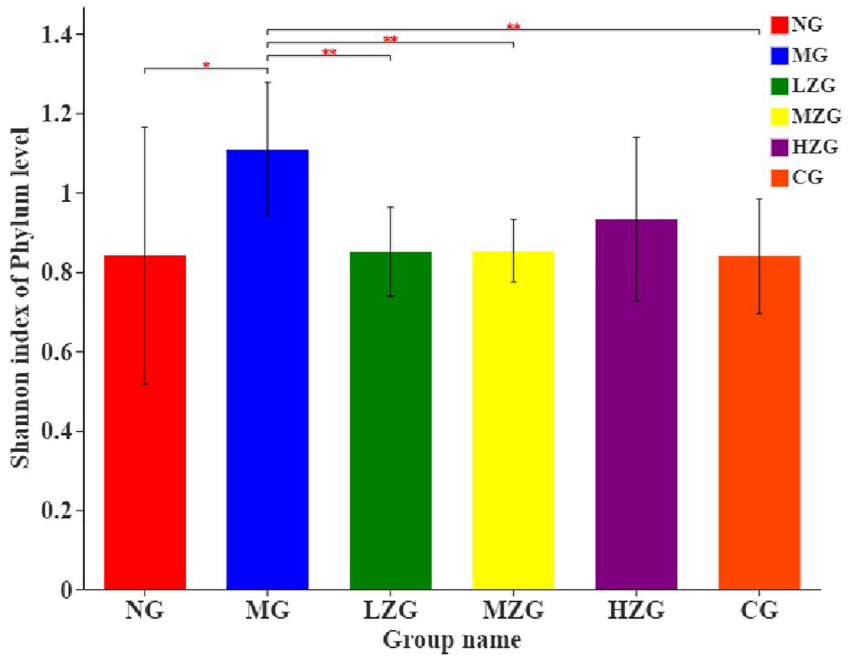

FIGURE 8
Alpha diversity analysis of the gut microbiota. The abscissa is the name of the group, and the ordinate is the average value of the index of each group. This figure shows the significant differences between the selected two groups of samples, and marks the two groups with significant differences. "*" means $P < 0.05$, "**" means $P < 0.01$.

Bilophila, *Oscillospira*, *Dorea*, *Mucispirillum*, etc.) which destroy the mucus layer on the colon surface and induce inflammatory diseases in the early stage (44). This suggests that ZSPP-1, comprised of seven monosaccharides GlcA, GalA, Ara, Xyl, Glc, Man, and Gal in a precise molar ratio of 1:1:1.5:3.6:7.6:8.4:13.6, may be the primary factor in reducing the number of hazardous bacteria. On the contrary, *Akkermansia*, *Lactobacillus*, and *Bacteroides* et al. can improve tissue inflammation resulted from obesity and boost host intestinal health (45). Polysaccharide molecular weight and monosaccharide composition have a crucial influence in the regulation of intestinal flora. Zhou et al. (46) assumed that ginseng polysaccharide (with molecular weight ranging from 1.00 to 1,308.98 kDa) made up of six monosaccharides (i.e., mannose, rhamnose, glucose, galactose, arabinose, and fucose) and one type of uronic acid (i.e., galacturonic acid) could restore the disturbed overall intestinal microbiota, especially promoting the growth of two main *Lactobacillus* and *Bacteroides*. Shang et al. (47) demonstrated that fucoidan, mostly consisting of fucose, glucuronic acid, and galactose, could ameliorate the metabolic syndrome brought on by HFD and increase the amount of *Akkermansia* bacteria in the intestinal microbiota of mice. Interestingly, this study discovered that the specific polysaccharide molecular weight (1,570 kDa) and monosaccharide composition of ZSPP-1 are similar to those reported in the literature, which may also be the key factor for ZSPP-1 to promote the growth of benign microorganisms conducive to the health of the host (e.g., *Akkermansia*, *Lactobacillus*, and *Bacteroides* et al.).

ZSPP-1 administration recovered the original structure of intestinal microbiota

The visual circle diagram reflected the distribution proportion of dominant species in each group, as illustrated in **Supplementary Figure 7**. The proportion of Firmicutes and Bacteroidetes in the MG group has been grossly misadjusted in comparison to the NG group. The outcomes were comparable to those reported by Clarke et al. (4). Nonetheless, it can also be seen from **Supplementary Figures 7B,C** that the F/B value in the ZSPP-1 treatment group is no longer significant, demonstrating that Firmicutes and Bacteroidetes gradually returned to the normal level under the intervention of ZSPP-1.

Shannon index was applied to consider the richness and evenness of a community (48, 49). Through the assessment of alpha diversity abundance information of Shannon index at the phylum level in conjunction with the statistical *T*-test method, a significant difference between the two groups was identified (**Figure 8**). The results demonstrated that the MG group differed significantly from the LZG, MZG, CG, and NG groups; However, there was no significant difference between the ZSPP-1 treatment group and the NG group, stating that

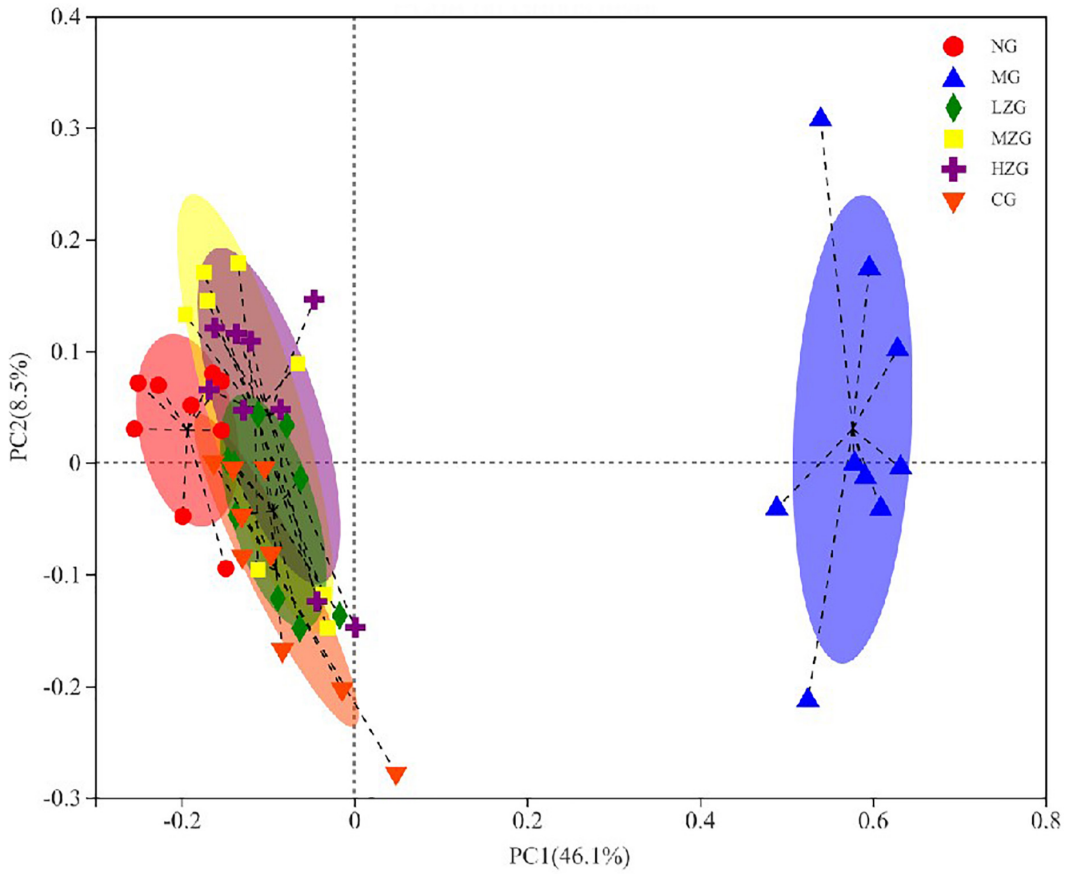

FIGURE 9
Beta diversity analysis of the gut microbiota (i.e., principal coordinates analysis). Points with different colors or shapes represent samples in different groups. The closer the two sample points are, the more similar the species composition of the two samples is.

ZSPP-1 treatment of mice with an imbalanced gut microbiota restored the original bacterial structure.

Principal coordinates analysis (PCoA) is used to analyze the composition of different samples. Through studying the differences and distances of samples, the Multi group difference data were reflected on the two-dimensional coordinate map. In other words, the smaller the distance on the coordinate axis, the more similar the composition of the two samples, so it is possible to determine if the composition of the samples under identical conditions is similar. As exhibited in **Figure 9**, the intestinal microorganisms of NG group, CG group, and ZSPP-1 treated group mice differed significantly from those of MG group mice; The flora in LZG group and NG group had a more similar composition, yet such similarity did not rise as the ZSPP-1 intervention dose was increased. This suggests that ZSPP-1 restored the structure of gut microbiota without regard to dose. In addition, PCoA analysis demonstrated that the flora structure of the MZG and HZG groups was not strictly consistent with that of the NG group. It demonstrated that the adding of medium and high doses of ZSPP-1 not only restored the intestinal flora, but posed a novel regulatory effect on the intestinal flora's composition.

Overall, in this study, through the changes of flora after different doses of ZSPP-1 intervention, it shows that ZSPP-1 regulates the structure of gut microbiota, improves the inflammation caused by obesity, and promotes intestinal health. Generally, the modulation of intestinal flora by polysaccharides is generally influenced by numerous factors. First, the chemical structure of polysaccharides is the foundation for the regulation of intestinal flora. By fermenting polysaccharides, intestinal flora may produce prebiotics, which can not only govern the structure of intestinal flora but also alter the host's metabolism to achieve lipid-lowering and weight loss. The effects of polysaccharide molecular weight, composition, glycosidic bond type, substituent group, and spatial structure on intestinal flora and obesity have received limited investigation. The team of Sadia Kanwal and Yi Xin found *Dictyophora indusiata* mushroom polysaccharide with the main functional components of Glu (59.84%), Man (23.55%), and Gal (12.95%); Dip can reduce inflammatory response and alleviate HFD induced obesity by regulating intestinal integrity and intestinal

microbial community (50–52). Therefore, there is justification to suppose that the effect of ZSPP-1 on the composition of intestinal flora in obese mice is mostly attributable to its unique functional components (36.8% galactose, 22.8% mannose, and 20% glucose).

Conclusion

A diet high in sugar and fat can alter the structure of gut microbiota, resulting in obesity and chronic metabolic illnesses; nevertheless, plant polysaccharides can modulate gut microbiota. In this study, a polysaccharide was separated from *Z. striolatum*. Using various methodologies and instruments, the chemical structure of ZSPP-1 was determined. It was discovered that ZSPP-1 altered the structure of the gut microbiota of obese mice, stimulated the growth of intestinal beneficial bacteria, and assisted in restoring the imbalanced flora structure to its normal form. The aforementioned outcomes suggest that ZSPP-1 may be a potential drug for addressing HFD-induced obesity, which necessitates extensive research. Meanwhile, the analysis of chemical structure and the investigation of intestinal regulatory function provide a theoretical foundation for the discovery of the structure-function relationship, as well as the utilization and advancement of *Z. striolatum*.

Data availability statement

The datasets presented in this study can be found in online repositories. The names of the repository/repositories and accession number(s) can be found below: https://submit.ncbi.nlm.nih.gov/subs/, accession number: PRJNA871034.

Ethics statement

The animal study was reviewed and approved by Tianjin University of Science and Technology Experimental Animal Center.

Author contributions

WJ: writing–original draft-lead and writing–review and editing-lead. YH: investigation-supporting, validation-supporting, and visualization-supporting. ZZ: writing–original draft-supporting and writing–review and editing-supporting. All authors contributed to the article and approved the submitted version.

Funding

This work was financially supported by the project program of Key Laboratory of Food Nutrition and Safety, Ministry of Education, Tianjin Key Laboratory of Food Nutrition and Safety, China (No. JYB202004) and Zunyi Science and Technology Plan Project (No. HZ2021226).

Conflict of interest

The authors declare that the research was conducted in the absence of any commercial or financial relationships that could be construed as a potential conflict of interest.

Publisher's note

All claims expressed in this article are solely those of the authors and do not necessarily represent those of their affiliated organizations, or those of the publisher, the editors and the reviewers. Any product that may be evaluated in this article, or claim that may be made by its manufacturer, is not guaranteed or endorsed by the publisher.

Supplementary material

The Supplementary Material for this article can be found online at: https://www.frontiersin.org/articles/10.3389/fnut.2022.1012030/full#supplementary-material

References

1. Angelakis E, Merhej V, Raoult D. Related actions of probiotics and antibiotics on gut microbiota and weight modification. *Lancet Infect Dis.* (2013) 13:889–99. doi: 10.1016/S1473-3099(13)70179-8

2. Bäckhed F, Ding H, Wang T, Hooper LV, Koh GY, Nagy A, et al. The gut microbiota as an environmental factor that regulates fat storage. *Proc Natl Acad Sci USA.* (2004) 101:15717–23. doi: 10.1073/pnas.0407076101

3. Zou J, Chassaing B, Singh V, Pellizzon M, Ricci M, Fythe MD, et al. Fiber-mediated nourishment of gut microbiota protects against diet-induced obesity by restoring il-22-mediated colonic health. *Cell Host Microbe.* (2018) 23:41–53.e4. doi: 10.1016/j.chom.2017.11.003

4. Clarke SF, Murphy EF, Nilaweera K, Ross PR, Shanahan F, O'Toole PW, et al. The gut microbiota and its relationship to diet and obesity: new insights. *Gut Microbes.* (2012) 3:186–202. doi: 10.4161/gmic.20168

5. Schroeder BO, Backhed F. Signals from the gut microbiota to distant organs in physiology and disease. *Nat Med.* (2016) 22:1079–89. doi: 10.1038/nm.4185

6. Liang D, Zhang L, Chen H, Zhang H, Hu H, Dai X. Potato resistant starch inhibits diet-induced obesity by modifying the composition of intestinal microbiota and their metabolites in obese mice. *Int J Biol Macromol.* (2021) 180:458–69. doi: 10.1016/j.ijbiomac.2021.02.209

7. Turnbaugh PJ, Ley RE, Mahowald MA, Magrini V, Mardis ER, Gordon JI. An obesity-associated gut microbiome with increased capacity for energy harvest. *Nature.* (2006) 444:1027–31. doi: 10.1038/nature05414

8. Maruvada P, Leone V, Kaplan LM, Chang EB. The human microbiome and obesity: moving beyond associations. *Cell Host Microbe.* (2017) 22:589–99. doi: 10.1016/j.chom.2017.10.005

9. Conlon MA, Topping DL. Dietary polysaccharides and polyphenols can promote health by influencing gut microbiota populations. *Food Funct.* (2016) 7:1730. doi: 10.1039/C6FO90009G

10. Ministry of Science and Technology of China. *Notice on Issuing the Guiding Opinions on Treating Experimental Animals Properly (GKFC Zi [2006] No. 398).* Beijing: Science and Technology Information of Animal Husbandry and Veterinary Medicine, (2006). p. 35–36.

11. Sun H, Zhu Z, Tang Y, Ren Y, Song Q, Tang Y, et al. Structural characterization and antitumor activity of a novel Se-polysaccharide from selenium-enriched *Cordyceps gunnii*. *Food Funct.* (2018) 9:2744–54. doi: 10.1039/C8FO00027A

12. Song Y, Zhu M, Hao H, Deng J, Li M, Sun Y, et al. Structure characterization of a novel polysaccharide from Chinese wild fruits (*Passiflora foetida*) and its immune-enhancing activity. *Int J Biol Macromol.* (2019) 136:324–31. doi: 10.1016/j.ijbiomac.2019.06.090

13. Tang Y, Zhu ZY, Liu Y, Sun H, Song QY, Zhang Y. The chemical structure and anti-aging bioactivity of an acid polysaccharide obtained from rose buds. *Food Funct.* (2018) 9:2300–12. doi: 10.1039/C8FO00206A

14. Pan LC, Sun YY, Zhang XL, Zhu ZY, Liu CY, Sun HQ, et al. Structure, antioxidant property and protection on PC12 of a polysaccharide isolated and screened from *Abelmoschus esculentus* L.Moench (okra). *Nat Prod Res.* (2022) 36:1441–7. doi: 10.1080/14786419.2021.1887867

15. Liu CY, Sun YY, Jia YQ, Geng XQ, Pan LC, Jiang W, et al. Effect of steam explosion pretreatment on the structure and bioactivity of *Ampelopsis grossedentata* polysaccharides. *Int J Biol Macromol.* (2021) 185:194–205. doi: 10.1016/j.ijbiomac.2021.06.002

16. Chen S, Zhou Y, Chen Y, Gu J. fastp: an ultra-fast all-in-one FASTQ preprocessor. *Bioinformatics.* (2018) 34:884–90. doi: 10.1093/bioinformatics/bty560

17. Wang Q, Garrity GM, Tiedje JM, Cole JR. Naive bayesian classifier for rapid assignment of rRNA sequences into the new bacterial taxonomy. *Appl Environ Microbiol.* (2007) 73:5261–7. doi: 10.1128/AEM.00062-07

18. Liang Z, Yi Y, Guo Y, Wang R, Hu Q, Xiong X. Chemical characterization and antitumor activities of polysaccharide extracted from *Ganoderma lucidum*. *Int J Mol Sci.* (2014) 15:9103–16. doi: 10.3390/ijms15059103

19. Yang B, Wu Q, Song X, Yang Q, Kan J. Physicochemical properties and bioactive function of Japanese grape (*Hovenia dulcis*) pomace insoluble dietary fibre modified by ball milling and complex enzyme treatment. *Int J Food Sci Technol.* (2019) 54:2363–73. doi: 10.1111/ijfs.14134

20. Chen G, Chen K, Zhang R, Chen X, Hu P, Kan J. Polysaccharides from bamboo shoots processing by-products: new insight into extraction and characterization. *Food Chem.* (2018) 245:1113–23. doi: 10.1016/j.foodchem.2017.11.059

21. Su Y, Li L. Structural characterization and antioxidant activity of polysaccharide from four auriculariales. *Carbohydr Polym.* (2020) 229:115407. doi: 10.1016/j.carbpol.2019.115407

22. Gao J, Zhang T, Jin ZY, Xu XM, Wang JH, Zha XQ, et al. Structural characterisation, physicochemical properties and antioxidant activity of polysaccharide from *Lilium lancifolium* Thunb. *Food Chem.* (2015) 169:430–8. doi: 10.1016/j.foodchem.2014.08.016

23. Jing Y, Huang L, Lv W, Tong H, Song L, Hu X, et al. Structural characterization of a novel polysaccharide from pulp tissues of *Litchi chinensis* and its immunomodulatory activity. *J Agric Food Chem.* (2014) 62:902–11. doi: 10.1021/jf404752c

24. Ru Y, Chen X, Wang J, Guo L, Lin Z, Peng X, et al. Structural characterization, hypoglycemic effects and mechanism of a novel polysaccharide from *Tetrastigma hemsleyanum* Diels et Gilg. *Int J Biol Macromol.* (2019) 123:775–83. doi: 10.1016/j.ijbiomac.2018.11.085

25. Qin J, Wang HY, Zhuang D, Meng FC, Zhang X, Huang H, et al. Structural characterization and immunoregulatory activity of two polysaccharides from the rhizomes of *Atractylodes lancea* (Thunb.) DC. *Int J Biol Macromol.* (2019) 136:341–51. doi: 10.1016/j.ijbiomac.2019.06.088

26. Li F, Wei Y, Liang L, Huang L, Yu G, Li Q. A novel low-molecular-mass pumpkin polysaccharide: structural characterization, antioxidant activity, and hypoglycemic potential. *Carbohydr Polym.* (2021) 251:117090. doi: 10.1016/j.carbpol.2020.117090

27. Liang X, Gao Y, Fei W, Zou Y, He M, Yin L, et al. Chemical characterization and antioxidant activities of polysaccharides isolated from the stems of *Parthenocissus tricuspidata*. *Int J Biol Macromol.* (2018) 119:70–8. doi: 10.1016/j.ijbiomac.2018.07.131

28. Mandal EK, Maity K, Maity S, Gantait SK, Behera B, Maiti TK, et al. Chemical analysis of an immunostimulating (1–>4)-, (1–>6)-branched glucan from an edible mushroom, *Calocybe indica*. *Carbohydr Res.* (2012) 347:172–7. doi: 10.1016/j.carres.2011.10.040

29. Wang L, Chen C, Zhang B, Huang Q, Fu X, Li C. Structural characterization of a novel acidic polysaccharide from *Rosa roxburghii* Tratt fruit and its alpha-glucosidase inhibitory activity. *Food Funct.* (2018) 9:3974–85. doi: 10.1039/C8FO00561C

30. Nguyen SG, Kim J, Guevarra RB, Lee JH, Kim E, Kim SI, et al. Laminarin favorably modulates gut microbiota in mice fed a high-fat diet. *Food Funct.* (2016) 7:4193–201. doi: 10.1039/C6FO00929H

31. Chang CJ, Lin CS, Lu CC, Martel J, Ko YF, Ojcius DM, et al. *Ganoderma lucidum* reduces obesity in mice by modulating the composition of the gut microbiota. *Nat Commun.* (2015) 6:7489. doi: 10.1038/ncomms8489

32. Ke J, An Y, Cao B, Lang J, Wu N, Zhao D. Orlistat-induced gut microbiota modification in obese mice. *Evid Based Complement Alternat Med.* (2020) 2020:9818349. doi: 10.1155/2020/9818349

33. Yan Y, Peng Y, Tang J, Mi J, Lu L, Li X, et al. Effects of anthocyanins from the fruit of *Lycium ruthenicum* Murray on intestinal microbiota. *J Funct Foods.* (2018) 48:533–41. doi: 10.1016/j.jff.2018.07.053

34. Pereira FC, Wasmund K, Cobankovic I, Jehmlich N, Herbold CW, Lee KS, et al. Rational design of a microbial consortium of mucosal sugar utilizers reduces *Clostridioides* difficile colonization. *Nat Commun.* (2020) 11:5104. doi: 10.1038/s41467-020-18928-1

35. Zeng H, Larson KJ, Cheng WH, Bukowski MR, Safratowich BD, Liu Z, et al. Advanced liver steatosis accompanies an increase in hepatic inflammation, colonic, secondary bile acids and Lactobacillaceae/Lachnospiraceae bacteria in C57BL/6 mice fed a high-fat diet. *J Nutr Biochem.* (2020) 78:108336. doi: 10.1016/j.jnutbio.2019.108336

36. Fei N, Zhao L. An opportunistic pathogen isolated from the gut of an obese human causes obesity in germfree mice. *ISME J.* (2013) 7:880–4. doi: 10.1038/ismej.2012.153

37. Neyrinck AM, Mouson A, Delzenne NM. Dietary supplementation with laminarin, a fermentable marine beta (1-3) glucan, protects against hepatotoxicity induced by LPS in rat by modulating immune response in the hepatic tissue. *Int Immunopharmacol.* (2007) 7:1497–506. doi: 10.1016/j.intimp.2007.06.011

38. Li M, Zhang X, Zhang Y, Shao X, Liu H, Guo L, et al. Study on the characterization of polysaccharide from *Tuber sinense* and its desensitization effect to β-lactoglobulin in vivo. *J Funct Foods.* (2022) 91:105028. doi: 10.1016/j.jff.2022.105028

39. Huang WC, Wei CC, Huang CC, Chen WL, Huang HY. The beneficial effects of *Lactobacillus plantarum* PS128 on high-intensity, exercise-induced oxidative stress, inflammation, and performance in triathletes. *Nutrients.* (2019) 11:353. doi: 10.3390/nu11020353

40. Schepper JD, Collins FL, Rios-Arce ND, Raehtz S, Schaefer L, Gardinier JD, et al. Probiotic *Lactobacillus reuteri* prevents postantibiotic bone loss by reducing intestinal dysbiosis and preventing barrier disruption. *J Bone Miner Res.* (2019) 34:681–98. doi: 10.1002/jbmr.3635

41. Zhu L, Baker RD, Baker SS. Gut microbiome and nonalcoholic fatty liver diseases. *Pediatr Res.* (2015) 77:245–51. doi: 10.1038/pr.2014.157

42. Shen F, Zheng R-D, Sun X-Q, Ding W-J, Wang X-Y, Fan J-G. Gut microbiota dysbiosis in patients with non-alcoholic fatty liver disease. *Hepatobiliary Pancreat Dis Int.* (2017) 16:375–81. doi: 10.1016/S1499-3872(17)60019-5

43. Cui M, Zhang M, Wu J, Han P, Lv M, Dong L, et al. Marine polysaccharides from *Gelidium pacificum* Okamura and *Cereus sinensis* reveal prebiotic functions. *Int J Biol Macromol.* (2020) 164:4381–90. doi: 10.1016/j.ijbiomac.2020.08.255

44. Lu S, Zuo T, Zhang N, Shi H, Liu F, Wu J, et al. High throughput sequencing analysis reveals amelioration of intestinal dysbiosis by squid ink polysaccharide. *J Funct Foods.* (2016) 20:506–15. doi: 10.1016/j.jff.2015.11.017

45. Du H, Zhao A, Wang Q, Yang X, Ren D. Supplementation of inulin with various degree of polymerization ameliorates liver injury and gut microbiota dysbiosis in high fat-fed obese mice. *J Agric Food Chem.* (2020) 68:779–87. doi: 10.1021/acs.jafc.9b06571

46. Zhou SS, Xu J, Zhu H, Wu J, Xu JD, Yan R, et al. Gut microbiota-involved mechanisms in enhancing systemic exposure of ginsenosides by coexisting polysaccharides in ginseng decoction. *Sci Rep.* (2016) 6:22474. doi: 10.1038/srep22474

47. Shang Q, Song G, Zhang M, Shi J, Xu C, Hao J, et al. Dietary fucoidan improves metabolic syndrome in association with increased *Akkermansia* population in the gut microbiota of high-fat diet-fed mice. *J Funct Foods.* (2017) 28:138–46. doi: 10.1016/j.jff.2016.11.002

48. Yuan Y, Zhou J, Zheng Y, Xu Z, Li Y, Zhou S, et al. Beneficial effects of polysaccharide-rich extracts from *Apocynum venetum* leaves on hypoglycemic and gut microbiota in type 2 diabetic mice. *Biomed Pharmacother.* (2020) 127:110182. doi: 10.1016/j.biopha.2020.110182

49. Sarkar P, Malik S, Laha S, Das S, Bunk S, Ray JG, et al. Dysbiosis of oral microbiota during oral squamous cell carcinoma development. *Front Oncol.* (2021) 11:614448. doi: 10.3389/fonc.2021.614448

50. Kanwal S, Aliya S, Xin Y. Anti-obesity effect of *Dictyophora indusiata* mushroom polysaccharide (DIP) in high fat diet-induced obesity via regulating inflammatory cascades and intestinal microbiome. *Front Endocrinol (Lausanne).* (2020) 11:558874. doi: 10.3389/fendo.2020.558874

51. Kanwal S, Joseph TP, Aliya S, Song S, Saleem MZ, Nisar MA, et al. Attenuation of DSS induced colitis by *Dictyophora indusiata* polysaccharide (DIP) via modulation of gut microbiota and inflammatory related signaling pathways. *J Funct Foods.* (2020) 64:103641. doi: 10.1016/j.jff.2019.103641

52. Kanwal S, Joseph TP, Owusu L, Xiaomeng R, Meiqi L, Yi X, et al. from *Dictyophora indusiata* promotes recovery from antibiotic-driven intestinal dysbiosis and improves gut epithelial barrier function in a mouse model. *Nutrients.* (2018) 10:1003. doi: 10.3390/nu10081003

frontiers | Frontiers in Nutrition

TYPE Original Research
PUBLISHED 08 November 2022
DOI 10.3389/fnut.2022.1017431

Check for updates

OPEN ACCESS

EDITED BY
Chanchan Sun,
Yantai University, China

REVIEWED BY
Fei Liu,
Université de Strasbourg, France
Liyuan Yun,
Tianjin Agricultural University, China

*CORRESPONDENCE
Mingzhu Guo
gmz523225334@hebau.edu.cn

SPECIALTY SECTION
This article was submitted to Nutrition and Food Science Technology, a section of the journal Frontiers in Nutrition

RECEIVED 12 August 2022
ACCEPTED 21 October 2022
PUBLISHED 08 November 2022

CITATION
Zhang C, Shu Y, Li Y and Guo M (2022) Extraction and immunomodulatory activity of the polysaccharide obtained from *Craterellus cornucopioides*. *Front. Nutr.* 9:1017431. doi: 10.3389/fnut.2022.1017431

COPYRIGHT
© 2022 Zhang, Shu, Li and Guo. This is an open-access article distributed under the terms of the Creative Commons Attribution License (CC BY). The use, distribution or reproduction in other forums is permitted, provided the original author(s) and the copyright owner(s) are credited and that the original publication in this journal is cited, in accordance with accepted academic practice. No use, distribution or reproduction is permitted which does not comply with these terms.

Extraction and immunomodulatory activity of the polysaccharide obtained from *Craterellus cornucopioides*

Caixuan Zhang, Ying Shu, Yang Li and Mingzhu Guo*

College of Food Science and Technology, Hebei Agricultural University, Baoding, China

In this study, we investigated the structural features of the polysaccharide obtained from *Craterellus cornucopioides* (CCP2) by high-performance liquid chromatography, Fourier transform infrared spectroscopy and ion chromatography. The results showed that CCP2 was a catenarian pyranose that principally comprised of mannose, galactose, glucose, and xylose in the ratio of 1.86: 1.57: 1.00: 1.14, with a molecular weight of 8.28×10^4 Da. Moreover, the immunoregulation effect of CCP2 was evaluated both *in vitro* and *in vivo*. It displayed a remarkable immunological activity and activation in RAW264.7 cells by enhancing the phagocytosis of macrophages in a dose-dependent manner without showing cytotoxicity at the concentrations of 10–200 μg/mL *in vitro*. Additionally, Histopathological analysis indicated the protective function of CCP2 against immunosuppression induced by cyclophosphamide (Cy). Meanwhile, the intake of CCP2 had better immunoregulatory activity for immunosuppression BALB/c mice model. After prevention by CCP2, the spleen and thymus weight indexes of BALB/c mice model were significantly increased. The RT-qPCR and Western Blot results provided comprehensive evidence that the CCP2 could activate macrophages by enhancing the production of cytokines (IL-2, IL-6, and IL-8) and upregulating the protein expression of cell membrane receptor TLR4 and its downstream protein kinase (TRAF6, TRIF, and NF-κB p65) production of immunosuppressive mice through TLR4-NFκB p65 pathway. The results demonstrated that CCP2 could be a potential prebiotic and might provide meaningful information for further research on the immune mechanism.

KEYWORDS

***Craterellus cornucopioides*, polysaccharide, structural characterization, immunoregulation, pathway**

Introduction

The immune system comprises a heterogeneous population of cells that are relatively quiescent in a steady-state, however, they respond to inflammation, infection, and other perturbations (1). In clinic settings, patients with compromised immunity may be particularly vulnerable to normal and opportunistic infections (2). The innate immune system comprises innate dendritic cells, natural killers cells (NK), macrophages, mast cells (MCs) and NKT cells as primary defense entity (3, 4) and protects against invading pathogens in non-specific way (4, 5). One of the most important non-specific immune actions is phagocytosis, which is performed by macrophages (6). Macrophages are involved in antiviral, anti-tumor activities, hypersensitivity reactions, autoimmune diseases, and immune regulation in adaptive and innate immune responses *via* the production of cytokines (such as interferon γ), interleukin-6 (IL-6), interleukin-10 (IL-10), and tumor necrosis factor α (TNF-α) (7). After regulating the activation and inhibition of receptors, the immune system activates the pathogen associated pattern-recognition receptors (PRRs) (8–10).

Polysaccharides, as metabolic products of plants, animals, and microorganisms, have attracted considerable attention due to their therapeutic effects, and are considered the immunological molecules of the innate immune system (11). It enhances the ability of macrophages to resist external stress and survive under various conditions by promoting the integrity and stability of the outer membrane (12). Several studies have been conducted to investigate the pharmacological activities and active components of edible and medicinal plants (13–16). It showed that fungal polysaccharides are efficacious in the treatment of diabetes, hypolipidemia, oxidative stress, and obesity, as well as in the activation of innate immune cells and stimulation of cytokines secretions (17, 18).

Yu, et al. (19) demonstrated that the porphyra-derived oligosaccharides possessed antigen-specific immune responses by regulating the levels of IgG1, IgG2a, and OVA-specific IgE, and producing IL-2, IFN-γ, IL-4, and IL17 in ovalbumin (OVA)-sensitized mice. Wusiman, et al. (20) verified that the Lagenaria siceraria (Molina) standl polysaccharide and sulfated modified LSP50 could induce long-lasting and high hemagglutination (HI) titers, antigen-specific lgG-NDV antibody, splenic lymphocyte proliferation, high immune organ index, which could be served as a novel and effective vaccine adjuvant in chicken to induce specific immune responses against infections and diseases.

Therefore, the activations of macrophages induced by fungal polysaccharides are essential for the innate immune system.

Craterellus cornucopioides is wild, edible fungus, that is widely distributed around the world (China, Japan, Korea, North America, and Europe). In our previous studies (21–23), a natural immune heteroglycan (average molecular weight of 1.97×10^6 Da) with the potential to activate RAW264.7 macrophages were obtained from *C. cornucopioides* (CCP) *in vitro*. This heteroglycan showed potent immunomodulatory properties and reversed immunosuppression by enhancing the development of the immune system and the activation of peritoneal macrophage phagocytosis *via* regulation of the TLR4-NFκB pathway in peritoneal macrophages of immunosuppressed mice, which shows excellent prospects for the commercial development of functional foods and medicines (21–24).

Similarly, polysaccharides obtained from *C. cornucopioides* (CCP2) also have strong immunoregulatory potential in the extrinsic pathway. However, to date, a comprehensive understanding of the immunomodulatory activity of CCP2 *in vitro* and its structural characteristics have not been reported. The structural and bioactivity diversities of CCP2 remain unclear. Generally, the comprehensive utilization of agricultural products has significant economic and social environmental benefits, and has thus gained growing interests in the development of agricultural products.

On this basis, the structure information and immunomodulatory activity of CCP2 were investigated by FTIR, and in terms of monosaccharide composition. The proliferation, phagocytosis, and morphology of RAW264.7 cells were applied to understand the relationship between structural properties and biological activities, which further expands the application and advantages of *C. cornucopioides*.

Materials and methods

Materials and reagents

The fruiting body of *C. cornucopioides* was collected at the Junzi mountain of Shizong in Yunnan Province, P.R. Different monosaccharide standards (L-rhamnose, D -glucose, D-mannose, D-galactose, D-arabinose, and D-xylose) and DEAE-52 column (1.6 cm × 100 cm) were provided by Solarbio Biological Technology Company (BJ, CHN). Neutral red and 3-(4,5-Dimethylthiazol-2-yl)-2,5-diphenyl-tetrazolium bromide (MTT) were provided by Sigma Company (St Louis, MO, USA). Phosphate buffered saline, dimethyl sulfoxide (DMSO), Dulbecco's Modified Eagle Medium (DMEM), and fetal bovine serum (FBS) were purchased from Gibco BRL (NY, USA). All the other reagents were of analytical grade.

Extraction and purification of CCP2

The *C. cornucopioides* powder was extracted with distilled water at 85°C for 2.5 h (twice) after degreasing with acetone. The water extract was concentrated and deproteinized using the sevag reagent [Chloroform: n-butanol = 4:1 (V:V), 30 min,

10 times]. Finally, three volumes of ethanol were added to precipitate the crude polysaccharide (CCCP), which were collected after centrifugation at 3,000 rpm at 25°C for 10 min and freeze-dried under −80°C after redissolving in water. The yield was calculated using formula 1 as follows:

$$\text{CCCP yield\%} \quad \frac{WCCCP\times\ 100}{W\text{sample}} \tag{1}$$

Where W_{CCCP} and W_{sample} are the weights of CCCP and *C. cornucopioides* powder, respectively.

CCCP (80 mg) was dissolved in distilled water (2 mL), purified by the DEAE-A52 column (1.6 cm × 100 cm), and eluted at the flow rate of 0.6 mL/min. The eluent contained a macromolecule that was discovered by HPLC and named *C. cornucopioides* polysaccharide (CCP2).

Molecular weight of CCP2

The Mw of CCP2 was determined by high-performance gel permeation chromatography (Agilent-1200) with a Shodex OHpak gel SB-805HQ column (8.0 mm × 300 mm, 35°C) and a refractive index detector (30°C). The sample solution (20 μL, 5 mg/mL) was injected into the apparatus. Deionized water was used as the flowing phase at the flow rate of 0.6 mL/min. The standard curve was established using the T-series Dextran (T-2000, T-500, T-70, T-40, T-20, and T-10) (25, 26).

Determination of monosaccharide composition of CCP2

The ICS2500 chromatography system (Thermo) with the high-performance anion chromatography column Carbo Pac PA20 (150 mm × 3 mm) and a dual pulse current sensor was used to determine the monosaccharide composition of CCP2 (NaOH at 2.00 and 10.00 mM was used as the eluent, the flow rate was 0.45 mL/min, and the temperature was set at 30°C). In total, 5.00 mg of CCP2 was hydrolyzed with 2 M Trifluoroacetic Acid (TFA, 5 mL) for 3 h at 120°C. Followed, the samples were diluted with ionized water according to the gradient. One milliliter CCP2 solution was injected into the apparatus. D-mannose, D-xylose, D-arabinose, L-rhamnose, D-galactose, and D-glucose were derivatized as standards.

FT-IR analysis

The experimental methods were referred to the literature reports (27). Briefly, 1.00 mg of CCP2 and 150 mg of KBr were mixed evenly and pressed into flake. Pure KBr flake was used as the blank background, and then the polysaccharide sample was analyzed on an Fourier Transform Infrared Spectroscopy (FT-IR) spectrophotometer with a resolution of 4 cm^{-1} (range: 4000 –400 cm^{-1}) (VECTOR 22, Bruker, Germany).

Cell culture

The RAW264.7 cells were cultured in DMEM supplemented with 10% (v/v) FBS streptomycin (100 units/mL), and penicillin (100 units/mL) at 37°C, and 5% CO_2 in a humidified atmosphere. Cells were passaged every 48 h for reserve.

Cell phagocytosis assays

The experimental method was according to the literature reports (28). For the neutral red uptake assay, the cell suspension (5×10^4 cell/mL) of the macrophages was added into 96-well plates at 37°C. After 4 h incubation, the supernates were removed and treated with different concentrations of CCP2 (0, 10, 25, 50, 100, 200, and 400 μg/mL) for 24, 36, and 48 h, respectively, and 100 μL of neutral red solutions were added and incubated for another 2 h. After staining, the cells were rinsed twice by Hank's solution. Afterward, the cells were lysed with a lysis buffer [ethanol and 0.01% acetic acid at the ratio of 1:1 (100 μL per well) and detected at 540 nm].

General observation

During the experiment, all BALB/c mice were carefully monitored daily for signs of disease, the body weight and water intake of mice were recorded daily. The feeding environment was as follows: temperature: 22 ± 0.5°C, humidity: 50 ± 5%, light–dark cycle: 12:12 h. The mental state, stool consistency, diarrhea and rectal bleeding were observed and recorded. The mice were fasted for 24 h after gavage and sacrificed on the 17th day.

Histopathological observation

The experimental methods were referred to the literature reports (29).

Establishment of cy-induced immunosuppressive BALB/c mice model and treatments

Protective effects of CCP2 on immunosuppression mice were evaluated using a cyclophosphamide (Cy)-induced immunocompromised model recommended by China Food and Drug Administration (CFDA Publication No. 107, revised 2012). Briefly, 50 mice were randomly assigned into 5 groups

(n = 10) according to the double-blind experiment after a week of adaptive feeding, including normal control group (NCG, 0.9% NaCl), immunocompromised model group (Cy-induced, CyMG), and three CCP2 as preventive treatment groups [CCP2 + Cy (L, M, H)]: 100, 200, and 400 mg kg^{-1} day^{-1}. The details were as follows:

(1) NCG: Mice were intragastric administration once daily with 0.9% normal saline (0.2 mL) for 17 consecutive days, and intraperitoneally injected administration with normal saline (0.1 mL day^{-1}) at 10th day for 3 days.

(2) CyG: Mice were intragastric administration once daily with 0.9% normal saline (0.2 mL) for 17 consecutive days and intraperitoneally injected administration with Cy (0.1 mL day^{-1}, Mw 261.09 Da) at 10th day for 3 days.

(3) [CCP2 + Cy (L, M, H)]: Mice were intragastric administration with once daily with CCP2 at the doses of 100, 200, and 400 mg kg^{-1} day^{-1}, respectively, for 17 consecutive days and intragastric administration with Cy at 10th day for 3 days.

On the 18th day after the various treatments, the BALB/c mice in each group were killed through the cervical dislocation method. The spleen and thymus were dissected and weighed.

The organ index was calculated as follows:

$$\text{Spleen index (mg per 10g)} \quad \frac{\text{spleen weight (mg)}}{\text{body weight (g)}} \times 10 \quad (2)$$

$$\text{Thymus index (mg per 10g)} \quad \frac{\text{thymus weight (mg)}}{\text{body weight (g)}} \times 10 \quad (3)$$

Western blot analysis

The experiment was conducted according to the method reported by Price et al. (30). Specifically, the total protein of peritoneal macrophage of BALB/c mice was extracted using radio immunoprecipitation assay lysis buffer according to the instruction of manufacture. After incubation of macrophages in 6-well plates (1×10^5 cells/mL) for 36 h, the macrophages were used for the protein extraction. All the primary antibodies were diluted with PBS for 1000 times (Cell Signaling Technology, Danvers, MA, USA).

In brief, cell lysates were subjected to 10% SDS-PAGE and transferred to nitrocellulose NC membranes, and then incubated overnight at 4°C with anti-TLR4, anti-TRIF, anti-TRAF6, anti-P-NF-kB p65, and anti-GAPHD monoclonal antibodies after a 1 h blocking on (5% (w/v) non-fat milk. The membranes were subsequently washed with Tris Buffered Saline Tween (TBST) and incubated for 1 h at room temperature with corresponding secondary anti-bodies. Immunoreactive bands were detected using enhanced chemiluminescence (ECL) kit (Millipore Co., Billerica, MA, USA), GAPHD was used as internal control.

Quantitative reverse transcription-polymerase chain reaction analysis

Quantitative reverse transcription Polymerase Chain Reaction (RT-qPCR) was conducted using SYBR RT-qPCR kit and Mx3000P^{TM} RT-qPCR system (Stratagene, USA) in triplicate for each sample reaction according to previous report (31) to determine the mRNA expression of cytokines IL-2, IL-6, IL-8, and TNF-α. The total RNAs of peritoneal macrophage of BALB/c mice was extracted using Trizol reagent (Solarbio, Beijing, China) according to the instruction of manufacture and to synthesize cDNA by PrimeScript RT kit (Takara Biological Engineering Company, Dalian, China). The designed specific primers (Sangon Biotechnology company, Shanghai, China) were list in **Table 1**.

Data analysis

In this study, all statistical analyses were performed using SPSS 20.0 software (SPSS, Inc., IL, USA). Data were expressed as mean ± standard error (SE). One-way analysis of variance (ANOVA) and T-tests were used to test for statistical significance. P-values less than 0.05 were considered statistically significant.

Results and discussions

Extraction, purification and purity of CCP2

100 mg of CCCP was dissolved in distilled water (2 mL), purified by DEAE-A52 column (1.6 cm × 100 cm) and sequentially eluted with distilled water and 0.3 M NaCl at a flow rate of 0.6 mL/min. The eluant contained a macromolecule discovered by HPLC and named CCP1, which contained three fractions with similar polarity (**Figure 1A**). Further, the SephadexG-100 column (1.6 cm × 100 cm) was used to obtain CCP2. The single symmetrical peak (**Figure 1B**) at 15.592 min in HPLC indicates high purity. The UV absorption spectrum of thiirane revealed no obvious absorption peaks between 260 and 280 nm after full-wave scanning indicated little protein of CCP2. The average Mw of CCP2 was determined with a universal calibration curve using Dextran as a standard (32). Based on the calibration, the Mw of CCP2 was 8.28×10^4 Da.

The monosaccharide compositions and FTIR spectrum analysis of CCP2

The retention time of monosaccharide standard (**Figure 2A**) and CCP2 after degrading by TFA acid (**Figure 2B**) were shown

TABLE 1 Primers sequence of polymerase chain reaction (RT-qPCR).

Target gene	Forward primer	Reverse primer	Product size (bp)
IL-2	atgaacttggacctctgcgg	atgtgttgtcagagcccttt	129
IL-6	gatgaagggctgcttccaac	gcttctccacagccacaatg	128
TNF-α	ctgaacttcggggtgatcgg	tgctcctccacttggtggtt	157
IL-8	atgacttccaagctggccgtg	ttatgaattctcagccctcttca	302
GAPHD	agatccctccaaaatcaagtgg	ggcagagatgatgacccttttt	220

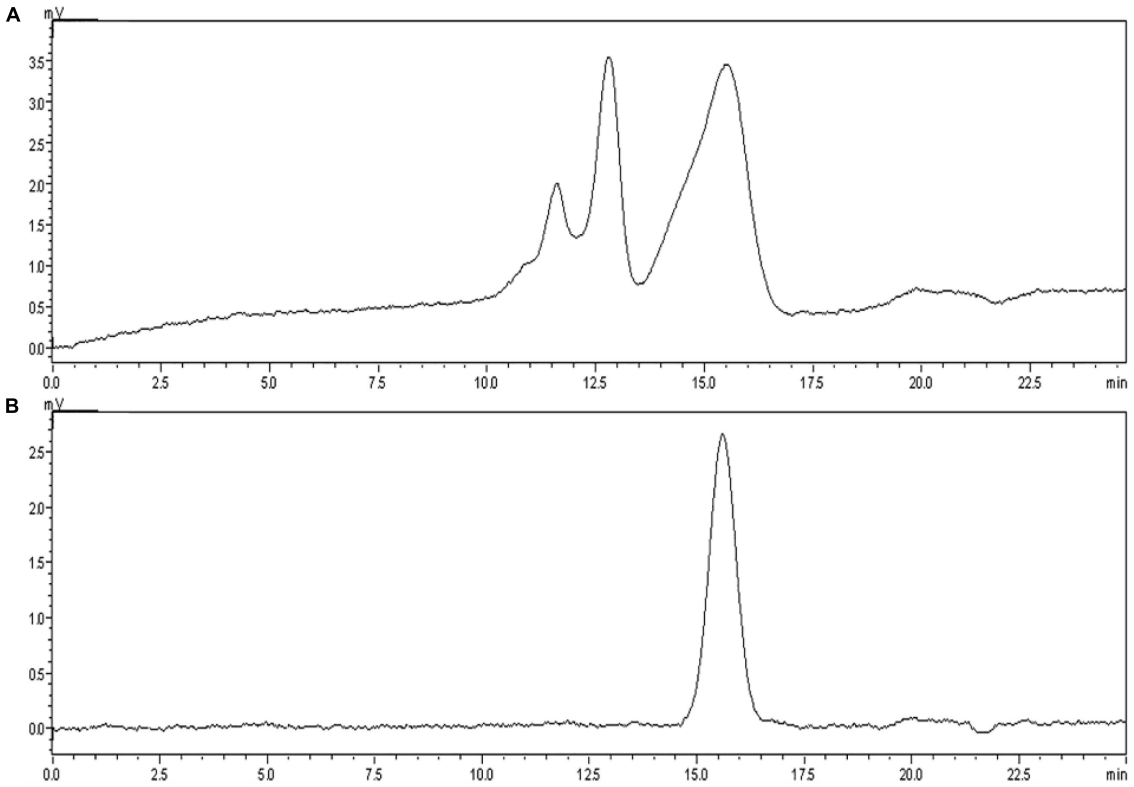

FIGURE 1
Weight average distribution of **(A)** CCP1 (crude polysaccharides eluted with 0.3 M NaCl) and **(B)** CCP2 (purified polysaccharides extracted from *C. cornucopioides*).

in the Figure 2 and Table 2. After comparing the remain time and area between standard and CCP2, the results indicated that the CCP2 composed of D-Mannose, D-Galactose, D-Glucose, and D-Xylose with the molar ratio of 1.86: 1.57: 1.00:1.14, showing mannose might be the backbone of the CCP2 chain (33).

The absorption band of CCP2 was performed (range: 4000–400 cm^{-1}). The band at 3405.22 cm^{-1} and 2920.21–2851.35 cm^{-1} were ascribed to the -OH and C-H stretching vibrations, respectively (21). The characteristic absorption peak of crystal water bending vibration was observed at 1637.15 cm^{-1} and the band at 1412.15 cm^{-1} was ascribed to -CH_2 deformation absorption (34). Bands around 1246.78 cm^{-1} reflected the deformation vibration the of C-H bond. Similarly, bands between 1042.27–1073.74 cm^{-1} reflected the C-O-C stretching in the pyranose ring. The absorption characteristic peak at 919.10 cm^{-1} indicated β-type glycosidic bond. The peaks at 1131.31 cm^{-1}, 1073.74 cm^{-1}, and 1042.27 cm^{-1} indicated the existence of pyranoid ring structure (12).

Effects of CCP2 on immunoregulation *in vitro*

CCP2 promoted phagocytosis activation of peritoneal macrophages

Recently, polysaccharides have been proven to participate in cell immune defense, proliferation, and differentiation (35).

A

Peak No.	Component Name	Retention Time	Area nC*min	Height nC	Amount	Relative Amount %
1	Rha	9.51	12.077	41.721	n.a.	n.a.
2	Ara	9.80	19.440	53.636	n.a.	n.a.
3	Gal	12.45	25.143	52.801	n.a.	n.a.
4	Glc	14.41	36.050	62.108	n.a.	n.a.
5	Xyl	17.15	31.524	49.259	n.a.	n.a.
6	Man	18.29	19.437	30.100	n.a.	n.a.
7	Glca	25.66	7.265	64.076	n.a.	n.a.
8	GalA	26.25	13.510	60.527	n.a.	n.a.

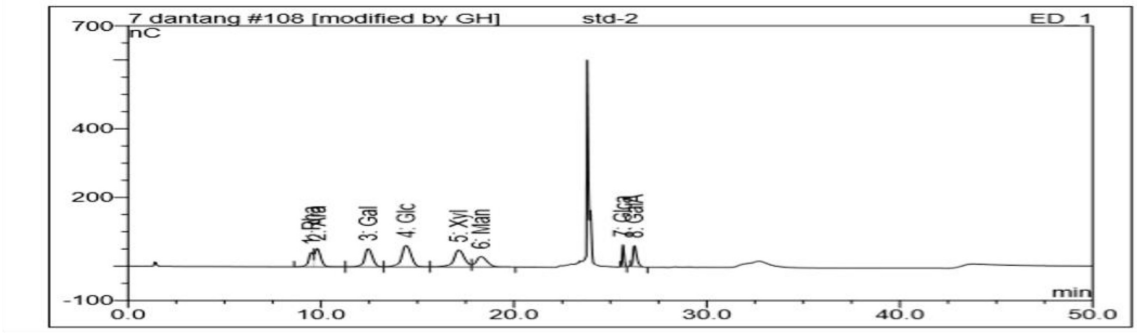

B

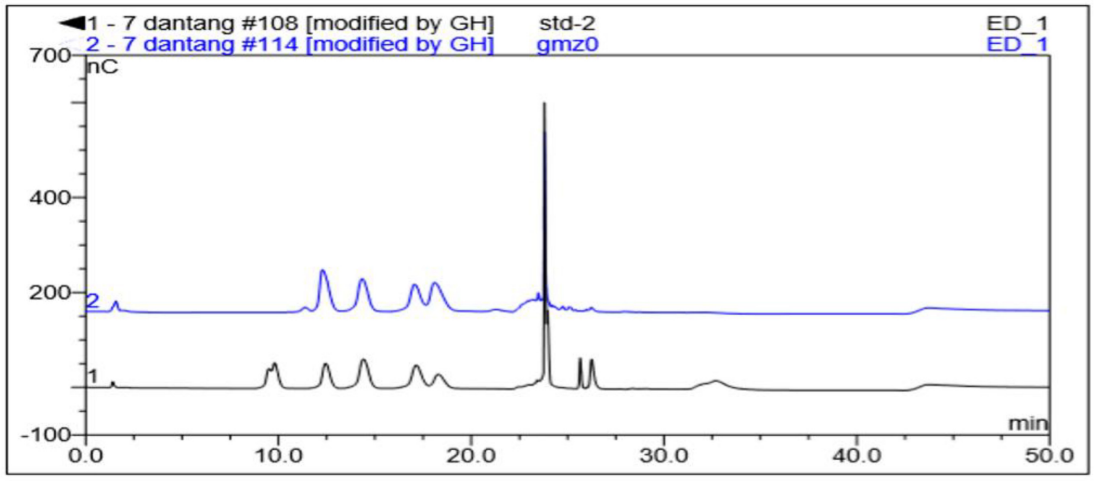

C

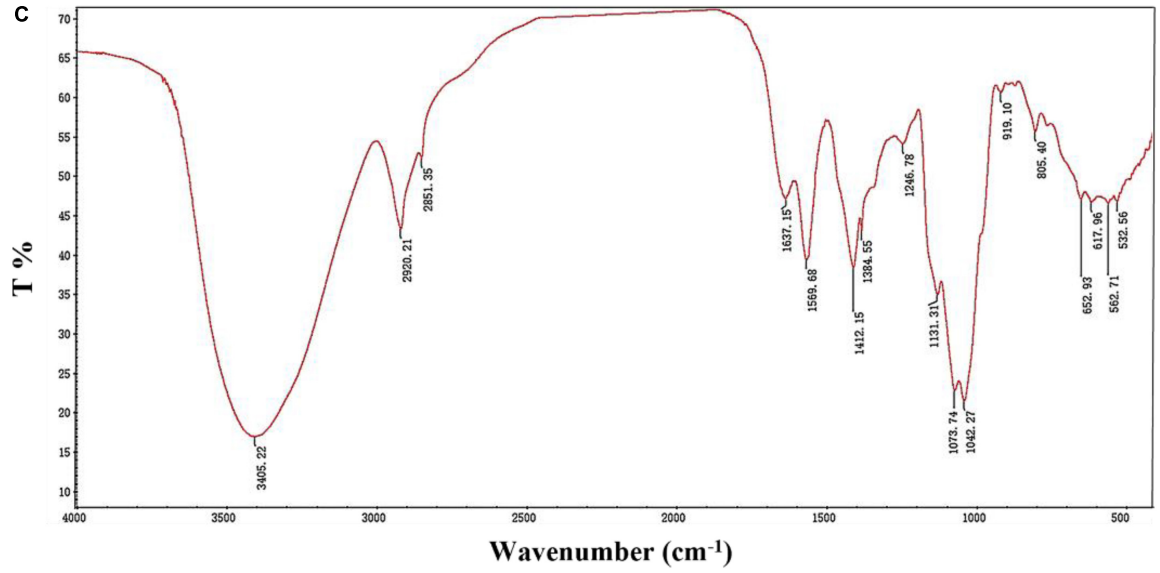

FIGURE 2
Monosaccharide composition [**(A)** Standards, **(B)** CCP2 (Blue line)] and the FTIR spectrum **(C)** of CCP2.

TABLE 2 Monosaccharide composition of CCP2.

Component	Area (standard nC*min)	Area (CCP2 nC*min)	Molecular Weight (g/mol)	Molar ratio
Xyl	31.524	37.3365	150.13	1.14
Man	19.437	46.8032	180.16	1.86
Glc	36.050	44.0274	180.16	1.00
Gal	25.143	50.6455	180.16	1.57

nC*min is the unit of area provided by the gas chromatography (Figure 2A).

Several polysaccharides were used as immunotherapeutic agents in the treatment of cancer and were clinically applied in combination with chemotherapy. Phagocytosis is the most important index to evaluate the activation and function of macrophages (36–38). In this study, the neutral red uptake assay was used to evaluate the phagocytosis of macrophages *in vitro*.

Relative cell phagocytosis of macrophages in the presence of CCP2 was significantly increased in a dose-dependent manner (10–200 μg/mL) than that of the control group ($P < 0.01$), reached maximum value at 100 μg/mL (Figure 3). Meanwhile, CCP2 significantly enhanced the phagocytosis of macrophages in a time-dependent (24, 36, and 48 h) and reached maximum at 36 h. Generally, the phagocytosis of RAW264.7 was significantly increased, attaining a maximum value at 36 h and 100 μg/mL of CCP2 ($P < 0.01$). The above results indicated that CCP2 holded a strong potential to stimulate macrophages, which was the key participant in innate and adaptive immunity. Compared with previous reports, CCP2 showed stronger effect on the activation of the phagocytosis of macrophages (22, 34, 39).

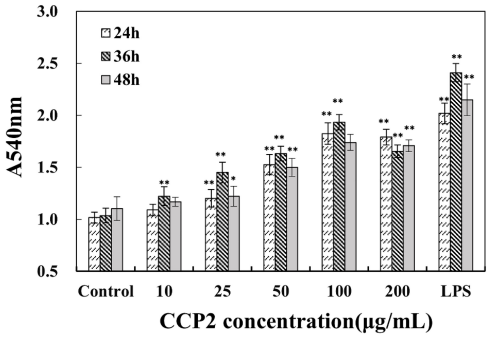

FIGURE 3
Effects of CCP2 on the phagocytic activity of macrophages. Cells were treated with CCP2 at various concentrations (10, 25, 50, 100, 200, and 400 μg/mL) for 24, 36, and 48 h, respectively. The control group was incubated with DMEM. *$p < 0.05$ and **$p < 0.01$ were significant when compared to the Control group. Data were expressed as means ± SD.

Effects of CCP2 on immunoregulation *in vivo*

The effect of CCP on thymus and spleen index of immunocompromised mice

The spleen and thymus index of various treatment groups were dissected and weighed accurately on the 17th day. The relative thymus index and spleen index of CyG group decreased significantly (6.94 ± 0.51 vs. 16.27 ± 0.89 mg/10 g, 20.11 ± 1.02 vs. 33.57 ± 1.32 mg/10 g) compared with NCG group (Table 3). To compared with the CyG group, all the indexes in CCP2 treatment groups remarkable increased. The result implicated that the organic damage and immune function of immunocompromised mice might be recovered after CCP2 treatments.

Effects of CCP2 on the spleen investigated *via* histological examinations in the BALB/c mice

The destruction of the immune system, lead to autoimmune diseases and inflammatory diseases, always accompanied the organic damage (40). As an vital extrinsic diagnostic technology, HE image is easily available to assess the immunosuppressive status of organism (41, 42).

In this study, the HE stained was performed to evaluate the effect of CCP2 on colon tissues ultrastructure. As shows in Figure 4, histological analysis showed that the ultrastructure of spleen cells in the NCG were dense and arrange regularly. To compared with NCG group, CyG group (B) showed unclear red and white pulp structure and obvious intercellular spaces dilatation. However, the administration of CCP2 could significantly decreased the extent of macroscopic and microscopic intestinal irregular arrangement of cells induced by Cy. As the ultrastructure of spleen cells in CCP2 + Cy (M) (200 mg kg^{-1} day^{-1}) and CCP2 + Cy (H) (400 mg kg^{-1} day^{-1}) groups were dense, arrange regularly with clear nuclei, red and white pulp structure, which were similar to the case of NCG group. Likewise, the microscopic structure of CCP2 + Cy (L) (100 mg kg^{-1} day^{-1}) group also recovered slightly. The histopathological analysis showed that CCP2 could attenuate the immune lesions of spleen in immunosuppression mice after Cy intervention.

Effects of CCP2 on the secretion of cytokines of the immunosuppressive BALB/c mice

Cytokines are synthesized and secreted by immune cells (macrophages, monocytes, B and T cells, DCs and neutrophils, etc.) and non-immune cells (endothelial cells, epidermal and

TABLE 3 The thymus and spleen index of immunocompromised mice.

	Group	Dosage (mg·kg^{-1}·day^{-1})	Thymus index (mg 10 g^{-1})	Spleen index (mg 10 g^{-1})
	NCG	–	16.27 ± 0.89	33.57 ± 1.32
	CyG	–	6.94 ± 0.51$^{\#\#}$	20.11 ± 1.02$^{\#\#}$
Prevent	CCP2 + Cy (L)	100	9.46 ± 0.56**	22.97 ± 1.35**
	CCP2 + Cy (M)	200	13.32 ± 0.74**	29.47 ± 0.78**
	CCP2 + Cy (H)	400	11.27 ± 0.34**	26.38 ± 0.68**

Data are presented as mean ± SD, $n = 6$.
$^{\#\#}p < 0.01$ was significant when compared to the NCG group.
$^{**}p < 0.01$ was significant when compared to the CyG group.

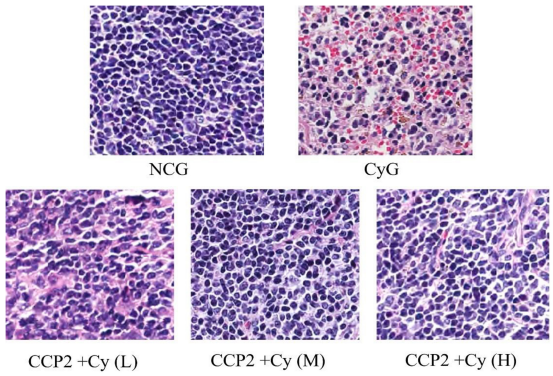

FIGURE 4
Effects of CCP2 on the spleen tissues showed in HE-stained histopathological images (scale bar = 100 μm, objective: 20×). NCG, normal control group; CyG, cyclophosphamide treatment group; CCP2 + Cy(L), Cy + CCP2 treatment group (100 mg kg^{-1} day^{-1}); CCP2 + Cy(M): Cy + CCP2 treatment group (200 mg kg^{-1} day^{-1}), CCP2 + Cy(H): Cy + CCP2 treatment group (400 mg kg^{-1} day^{-1}).

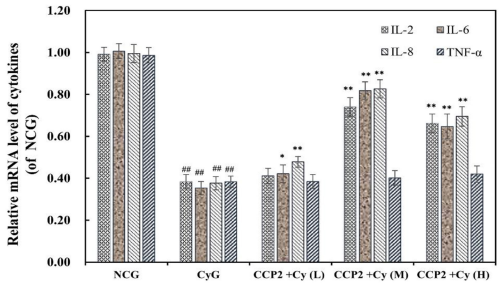

FIGURE 5
Effects of CCP2 on the secretion of cytokines (IL-2, IL-6, IL-8, and TNF-α) in the peritoneal macrophage of immunosuppressive mice induced by Cy. RT-qPCR analysis was relative to that of the reference gene (GAPHD). NCG: Normal control group, CyG: Cyclophosphamide treatment group, CCP2 + Cy (L): Cy + CCP2 treatment group (100 mg kg^{-1} day^{-1}), CCP2 + Cy (M): Cy + CCP2 treatment group (200 mg kg^{-1} day^{-1}), CCP2 + Cy (H): Cy + CCP2 treatment group (400 mg kg^{-1} day^{-1}), $^{\#\#}p < 0.01$ vs. the NCG group, $^{*}p < 0.05$, $^{**}p < 0.01$ vs. the CyG group. Data were expressed as mean ± SD, $n = 6$.

fibroblasts, etc.) after stimulation by immunogen, inflammatory factors, and exogenous stimulant with the biological activities on regulating inflammatory, innate or adaptive immune response (43). Such as TNF-α and IL-1β were released robustly by monocytes and macrophages after treated with LPS or Tripalmitoyl-S-glyceryl-cysteine (Pam3Cys, a lipopeptide). ECs granulocyte-monocyte-colony stimulating factor (GM-CSF), secreted granulocyte-colony stimulating factor (G-CSF), IL-6, IL-10, and IL-1α as major cytokines upon TLR stimulation (44, 45).

To evaluate the immunosuppressive regulation capacity of CCP2, the mRNA expressions of immunological cytokines (IL-2, IL-6, TNF-α, and IL-8) in peritoneal macrophage of various treatment groups were analyzed (**Figure 5**). To compare with the NCG group, the expressions of IL-2, IL-6, IL-8, and TNF-α were suppressed significantly after Cy intervention ($p < 0.01$). As the comparison, CCP2 alleviated Cy-induced immunosuppression at a molecular level by promoting the production of IL-2, IL-6, and IL-8, but to different degrees in a dose-dependent manner. The CCP2 + Cy (M) and CCP2 + Cy (H) (200 and 400 mg kg^{-1} day^{-1}) groups significantly enhanced the mRNA expression of above cytokines to compare with the CyG groups ($p < 0.01$) except TNF-α. Current data suggested that CCP2 capable of reversing the down-regulation of mRNA expressions to relieve the immunosuppressive.

Effects of *Craterellus cornucopioides* on protein expressions in abdominal macrophages in BALB/c mice

Reportedly, TLRs and NF-κBs were involved in the stimulation of gene expression [such as Inducible Nitric Oxide Synthase (iNOS), IL-6, TNF-α mRNA] and cytokine secretion (such as NO, IL-6 and TNF-α) in immune responses. In view of the immunosuppression of Cy-induced injury as mentioned above, we elucidated an underlying mechanism of CCP2 effect *via* the TLR4-NF-κBp65 signal pathways, which were commonly involved in immune signaling cascades. The level of TLR4, TRIF, and TRAF6, and the phosphorylation of P- NFkB p65 were determined. As a result of Cy administration, the level of TLR4, TRIF, TRAF6, and P-NFκB p65 declined significantly, compared

with those of mice in the NCG group. After administrating with CCP2, the phenomena (decrease of TLR4, TRIF, and TRAF6) were all alleviated significantly in a dose dependent manner, especially at the dose of 200 mg kg^{-1} day^{-1}. Next, we evaluated the effect of CCP2 on the phosphorylation of p65. As shown in Figure 6, treatment with CCP2 increased the phosphorylation of p65 in a concentration-dependent manner. The CCP2 + Cy (M) and CCP2 + Cy (H) (200 and 400 mg kg^{-1} day^{-1}) groups significantly enhanced the protein expression compared with the CyG groups ($p < 0.01$). Results suggested that CCP2 activated NF-κB signaling pathway which was implicated in transcriptional activation.

The main experiments contents and the sketch map was showed in Figure 7. In the light of the analysis conducted, we concluded that the receptor TLR4 plays a key role in the CCP2-modulated immunoregulation in immunosuppression mice model. Moreover, we showed that TLR4 in the pathogenesis of CCP2 modulated NF-κB pathways.

Discussion

Macrofungus (mushroom) has been extensively applied as traditional oriental medicine and food component for centuries (46, 47). Several reports revealed the importance of Split gill mushroom [*Schizophyllum commune* (Fr.:Fr.)], Lingzhi (in China) [*Ganoderma lucidum* (W.Curt.:Fr.) P. Karst.], Shiitake mushrooms [*Lentinus edodes* (Berk.) Sing], among other (48, 49). Nowadays, mushrooms are used as natural product-based pharmaceuticals with higher treatment potential and lower toxic effects in different pathological processes.

Polysaccharides are made up of identical or different monosaccharides together with glycosidic linkages to be linear or branching structure, which have been produced as the first biopolymer on earth (50, 51). The macrofungus polysaccharides and polysaccharide complexes components attract considerable attention due to their bioactive [such as efficient immunomodulatory, anti-cancer (52) and anti-inflammatory effects (53, 54)]. However, the structural information of different functional polysaccharides needs to be analyzed to supply and to expand the application of macro-fungus polysaccharides. Thus, in this study, we obtained a polysaccharide that principally comprised of mannose, galactose, glucose, and xylose in the ratio of 1.86:1.57:1.00:1.14, obtained from *C. cornucopioides* (CCP2) that widely distributed around the world (China, Japan, Korea, North America and Europe).

There was a clear correlation between allowed conformations and linking pattern (55). As confirmed by reports, polysaccharides extracted from MAE showed excellent biological properties owing to their complete structure, functional glycosidic linkages with a higher Mw and uronic acid content. In this study, The CCP2 was a catenarian pyranose with the Mw of 8.28×10^4 Da. The high structural diversity reflects the functional diversity of these molecules (55, 56). The number of structural factors such as monosaccharide composition, uronic acids content, molecular weight (Mw), glycosidic bond type in the backbone chain, and the esterification degree are profoundly affected on the antiradical, antioxidant, and

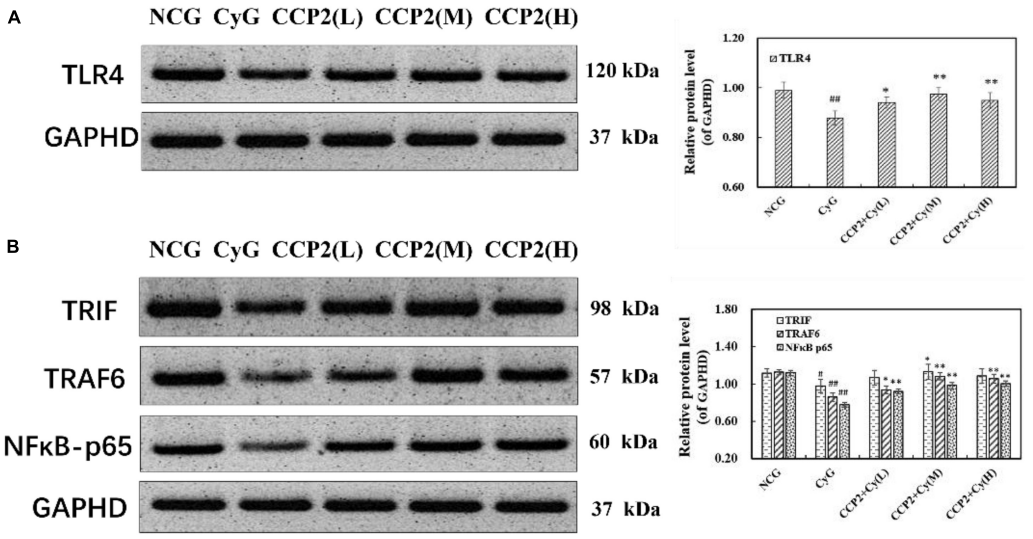

FIGURE 6
Detection of the protein expressions of TLR4, TRIF, TRAF6, and phosphor-NFκB-p65 by western blotting. **(A)** Effect of CCP on the expression of TLR4 in BALB/c mouse. **(B)** Effect of CCP on the expression of TRIF, TRAF6 and phosphor-NFκB-p65 in BALB/c mouse. GAPHD was used as an equal loading control. $^{\#}p < 0.05$, $^{\#\#}p < 0.01$ vs. the NCG group, $^{*}p < 0.05$, $^{*}p < 0.01$ vs. the CyG group. Data were expressed as means ± SD, $n = 10$.

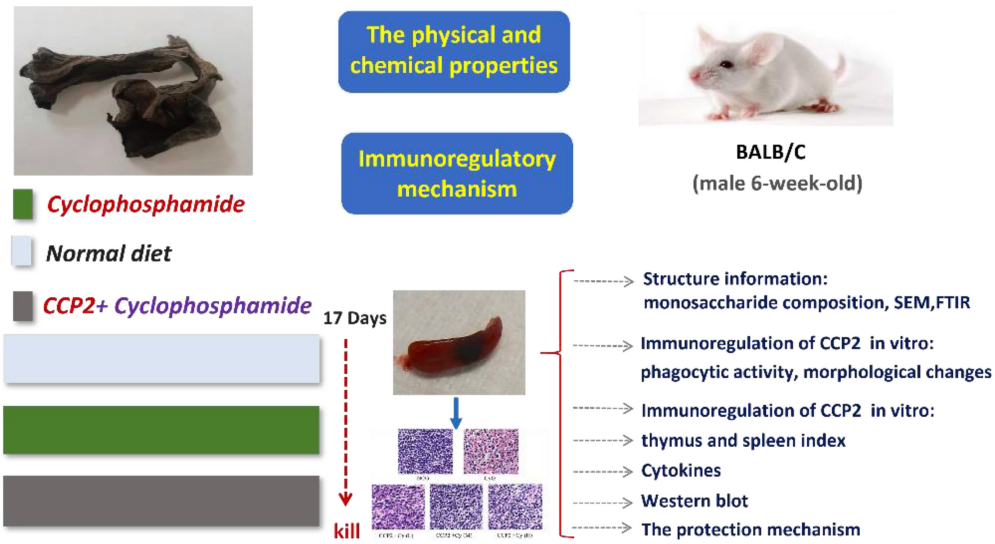

FIGURE 7
The sketch map of the immunoregulatory induced by CCP.

antimicrobial activities of polysaccharides extracted from biological sources (5, 57).

Recently, the structure of numbers of different heteropolysaccharides had been precisely defined. It indicated that the heteropolysaccharides in mushrooms revealed prominently biological activities, in which β-D-glucan was mainly relative to immunomodulatory and anti-tumor activity. The most conversant polysaccharide in medicinal mushroom is β-glucan due to their ability on stimulating cytokine secretion ability of T cells, NK cells, and macrophage (proliferation and differentiation) (47, 58, 59). The water soluble β-glucan isolated from edible mushroom *Entoloma lividoalbum*, contains (1→3,6)-β-D-Glc*p*, (1→3)-β-D-Glc*p*, (1→6)-β-D-Glc*p*, and terminal β-D-Glc*p* glucosides, showed antioxidant and immune-stimulate activities on thymocyte, splenocyte, and macrophage (44). Based on the result of monosaccharide composition, CCP2 composed of mannose, glucose and galactose showed potential utilization in hypoimmunity population, might be a potential immunomodulatory.

In our previous study, we obtained a polysaccharide (CCP) with a molecular weight of 1.97×10^3 kDa from edible *C. cornucopioides* fruiting bodies (21, 23). It was a heteroglycan with (1→3)-linked-β-D-Manp-(1→6)-linked-α-D-Galp backbone distributed by (1→4)-linked-α-D-Xylp-t-α-D-Manp and t-β-D-Glup units at O-6 and composed of mannose (48.73%), galactose (17.37%), glucose (15.97%), and xylose (17.93%), and stimulated macrophage function, rising phagocytosis, and activated cell morphology of RAW264.7 cells by TLR4-NFκB pathway. In the present paper, we investigated the chemical structure and biological activity of another *C. cornucopioides* polysaccharide. This study reported the isolation, structure analysis, and immunoregulatory activity of CCP2. Similarly, the immunomodulatory capacity was also found in CCP2. indicating the efficacy. Further studies including clinical trials need to be carried out to ascertain the safety of these compounds as adequate alternatives to conventional medicine. Our results showed that CCP2 could promote the phagocytosis of RAW264.7 cells in a concentration-dependent potency manner.

Cy has wide-spreading side-effects, such as hepatotoxicity and nephrotoxicity (60, 61). According to our results of thymus and spleen index (**Table 2**), and histological examination on the spleen of immunocompromised mice. We hypothesized that the immunosuppression in this group probably attributed to Cy side-effects on organic damage.

The stimulating factors affected adaptive immune cells (Th1, Th2, Th17, Tgd17, and CD8 T cells) to secrete IL-4, IL-5, IL-15, TNF-α, and chemokine CXCL8 (IL-8), which influenced neutrophils, macrophages (M1 and M2), and other granulocytes to fight against extracellular bacteria, tumors, viruses or extracellular parasites involved in immunologic processes of infection resistance, autoimmunity and allergic disease. It has previously been described that Cy polarizes the immune response from Th1 to Th2 (62). In the current study, mRNA and protein levels of all targeted elements were severely decreased in three CCP2-treatment immunosuppressed mice groups.

Some polysaccharides, characterized from plants, animals, fungi, etc., with various pharmacological properties by inducing cytokine secretion in immune cells, causing its segments similar to the cell membrane which were predominantly composed of various polysaccharides with species-specific monosaccharides or structures. The present data demonstrated that CCP2 significantly stimulated the mRNA expression of IL-2, IL-8, IL-6 to modulate immune response.

The western blot was used to explain the phenomenon. As an integral membrane protein in cytoplasmic domain,

the toll protein is the first identified in D. melanogaster as potent classes of PRRs (63). It is an essential factor involve in the survival and development of the embryo along with patterning, and characterize in recognizing the polysaccharide structures of cell walls. Among TLRs, TLR4 is known to induce production of TNF-α and IL-6. In this study, the expression of cell surface receptor TLR4 was elevated significantly. Moreover, the production of TRIF, TRAF6, and phosphorylation of NF-κBp65 were detected after administration of CCP2, indicating the activation of TLR4- NF-kBp65 signaling pathway.

These results indicated the impact of Cy in suppressing immune system through diminishing immune cells production, circulation and infiltration. The chemotherapy might cause an overall depletion of adaptive immune system cells.

Nevertheless, the administration of CCP2 reversed the immunosuppression side-effects that caused by Cy, which provided us a better understanding of the molecular mechanisms of the activation of immune system. Further understanding of the signaling pathways might provide novel insights into the mechanisms of immunomodulation and new opportunities on rational application of CCP2.

Conclusion

Polysaccharides obtained from fungi have attracted considerable attention due to their unique biological activities. In the present study, we investigated the chemical structure and immunoregulatory activity of CCP2 for the first time. Available data indicated CCP2 possessed immune-enhancing effect *in vivo* and *in vitro* to alleviate immunosuppression, which could be considered as a functional component of *C. cornucopioides* and an immunological modulator in the food nutrition industry.

Data availability statement

The original contributions presented in this study are included in the article/supplementary material, further inquiries can be directed to the corresponding author/s.

Ethics statement

This animal study was reviewed and approved by the Animal Ethical and Welfare Committee (AEWC).

Author contributions

CZ designed and conceived the experiments. MG performed the experiments and wrote the manuscript. YS and YL contributed the reagents, materials, and analysis tools and analyzed the data. All authors have read and approved the final manuscript.

Funding

This study was supported by the Science and Technology Research Project of University in Hebei Province (QN2021072), Introduced Talent Research Project of Hebei Agricultural University (YJ2021003), and Key Research and Development projects of Hebei Province (22327310D).

Conflict of interest

The authors declare that the research was conducted in the absence of any commercial or financial relationships that could be construed as a potential conflict of interest.

Publisher's note

All claims expressed in this article are solely those of the authors and do not necessarily represent those of their affiliated organizations, or those of the publisher, the editors and the reviewers. Any product that may be evaluated in this article, or claim that may be made by its manufacturer, is not guaranteed or endorsed by the publisher.

References

1. Pearce EL, Pearce EJ. Metabolic pathways in immune cell activation and quiescence. *Immunity.* (2013) 38:633–43.

2. Goulopoulou S, McCarthy CG, Webb RC. Toll-like receptors in the vascular system: Sensing the dangers within. *Pharmacol Rev.* (2016) 68:142–67.

3. van Dijk RA, Rijs K, Wezel A, Hamming JF, Kolodgie FD, Virmani R, et al. Systematic evaluation of the cellular innate immune response during the process of human *Atherosclerosis*. *J Am Heart Assoc.* (2016) 5:e002860. doi: 10.1161/JAHA.115.002860

4. Ohta T, Kusano K, Ido A, Miura C, Miura T. Silkrose: A novel acidic polysaccharide from the silkmoth that can stimulate the innate immune response. *Carbohydr Polym.* (2016) 136:995–1001.

5. Ferreira SS, Passos CP, Madureira P, Vilanova M, Coimbra MA. Structure-function relationships of immunostimulatory polysaccharides: A review. *Carbohydr Polym.* (2015) 132:378–96.

6. Jin M, Zhao K, Huang Q, Shang P. Structural features and biological activities of the polysaccharides from *Astragalus membranaceus*. *Int J Biol Macromol.* (2014) 64:257–66. doi: 10.1016/j.ijbiomac.2013.12.002

7. Cao J, Tang D, Wang Y, Li X, Hong L, Sun C. Characteristics and immune-enhancing activity of pectic polysaccharides from sweet cherry (*Prunus avium*). *Food Chem.* (2018) 254:47–54. doi: 10.1016/j.foodchem.2018.01.145

8. Kumar V. Corrigendum to 'Toll-like receptors in immunity and inflammatory diseases: Past, present, and future' [International Immunopharmacology 59 (2018) 391-412]. *Int Immunopharmacol.* (2018) 62:338. doi: 10.1016/j.intimp.2018.06.044

9. Bernareggi D, Pouyanfard S, Kaufman DS. Development of innate immune cells from human pluripotent stem cells. *Exp Hematol.* (2019) 71:13–23.

10. Gao L, Han Y, Deng H, Hu W, Zhen H, Li N, et al. The role of a novel C-type lectin-like protein from planarian in innate immunity and regeneration. *Dev Comp Immunol.* (2017) 67:413–26. doi: 10.1016/j.dci.2016.08.010

11. Zdorovenko EL, Shashkov AS, Kadykova AA, Kiseleva EP, Savich VV, Novik GI, et al. Structural analysis of the O-polysaccharide from the lipopolysaccharide of *Pseudomonas* putida BIM B-1100. *Carbohydr Res.* (2018) 457:8–13. doi: 10.1016/j.carres.2017.12.009

12. Zeng YJ, Yang HR, Wang HF, Zong MH, Lou WY. Immune enhancement activity of a novel polysaccharide produced by *Dendrobium officinale* endophytic fungus *Fusarium solani* DO7. *J Funct Foods.* (2019) 53:266–75.

13. Liu Y, Duan X, Zhang M, Li C, Zhang Z, Liu A, et al. Cooking methods effect on the nutrients, bioaccessibility and antioxidant activity of *Craterellus cornucopioides*. *Lwt.* (2020) 131:109768.

14. Liu Y, Duan X, Zhang M, Li C, Zhang Z, Hu B, et al. Extraction, structure characterization, carboxymethylation and antioxidant activity of acidic polysaccharides from *Craterellus cornucopioides*. *Ind Crops Prod.* (2021) 159:113079.

15. Guo H, Diao QP, Hou DY, Li ZH, Zhou ZY, Feng T, et al. Sesquiterpenoids from cultures of the edible mushroom *Craterellus cornucopioides*. *Phytochem Lett.* (2017) 21:114–7.

16. Yang WW, Wang LM, Gong LL, Lu YM, Pan WJ, Wang Y, et al. Structural characterization and antioxidant activities of a novel polysaccharide fraction from the fruiting bodies of *Craterellus cornucopioides*. *I Int J Biol Macromol.* (2018) 117:473–82. doi: 10.1016/j.ijbiomac.2018.05.212

17. Yi Y, Lamikanra O, Sun J, Wang LM, Min T, Wang HX. Activity diversity structure-activity relationship of polysaccharides from lotus root varieties. *Carbohydr Polym.* (2018) 190:67–76. doi: 10.1016/j.carbpol.2017.11.090

18. Zhang S, Pang G, Chen C, Qin J, Yu H, Liu Y, et al. Effective cancer immunotherapy by *Ganoderma lucidum* polysaccharide-gold nanocomposites through dendritic cell activation and memory T cell response. *Carbohydr Polym.* (2019) 205:192–202. doi: 10.1016/j.carbpol.2018.10.028

19. Wei YJ, Fang RE, Ou JY, Pan CL, Huang CH. Modulatory effects of Porphyra-derived polysaccharides, oligosaccharides and their mixture on antigen-specific immune responses in ovalbumin-sensitized mice. *J Funct Foods.* (2022) 96:105209.

20. Wusiman A, Rexiati S, Aziz M, Cheng X, Mai Z, Abulaiti A, et al. Preparation and sulfate modified of *Lagenaria siceraria* (Molina) Standl polysaccharide and its immune-enhancing adjuvant activity. *Poult Sci.* (2022) 101:102112. doi: 10.1016/j.psj.2022.102112

21. Guo MZ, Meng M, Duan SQ, Feng CC, Wang CL. Structure characterization, physicochemical property and immunomodulatory activity on RAW264.7 cells of a novel triple-helix polysaccharide from *Craterellus cornucopioides*. *Int J Biol Macromol.* (2019) 126:796–804. doi: 10.1016/j.ijbiomac.2018.12.246

22. Guo M, Meng M, Zhao J, Wang X, Wang C. Immunomodulatory effects of the polysaccharide from *Craterellus cornucopioides* via activating the TLR4-NFkappaB signaling pathway in peritoneal macrophages of BALB/c mice. *Int J Biol Macromol.* (2020) 160:871–9. doi: 10.1016/j.ijbiomac.2020.05.270

23. Guo MZ, Meng M, Feng CC, Wang X, Wang CL. A novel polysaccharide obtained from *Craterellus cornucopioides* enhances immunomodulatory activity in immunosuppressive mice models via regulation of the TLR4-NF-kappaB pathway. *Food Funct.* (2019) 10:4792–801. doi: 10.1039/c9fo00201d

24. Guo M, Yu H, Meng M, Wang C. Research on the structural characteristics of a novel Chinese Iron Yam polysaccharide and its gastroprotection mechanism against ethanol-induced gastric mucosal lesion in a BALB/c mouse model. *Food Funct.* (2020) 11:6054–65. doi: 10.1039/c9fo02642h

25. Zhu Z.-y, Liu R.-q, Si C.-l, Zhou F, Wang Y.-x, Ding L.-n, et al. Structural analysis and anti-tumor activity comparison of polysaccharides from Astragalus. *Carbohydre Polym.* (2011) 85:895–902.

26. Zhu Z, Dong F, Liu X, Lv Q, Yang Y, Liu F, et al. Effects of extraction methods on the yield, chemical structure and anti-tumor activity of polysaccharides from *Cordyceps gunnii* mycelia. *Carbohydr Polym.* (2016) 140:461–71. doi: 10.1016/j.carbpol.2015.12.053

27. Yan JK, Li L, Wang ZM, Wu JY. Structural elucidation of an exopolysaccharide from mycelial fermentation of a *Tolypocladium* sp. fungus isolated from wild *Cordyceps sinensis*. *Carbohydr Polym.* (2010) 79:125–30.

28. He LX, Ren JW, Liu R, Chen QH, Zhao J, Wu X, et al. Ginseng (*Panax ginseng* Meyer) oligopeptides regulate innate and adaptive immune responses in mice via increased macrophage phagocytosis capacity, NK cell activity and Th cells secretion. *Food Funct.* (2017) 8:3523–32. doi: 10.1039/c7fo00957g

29. Yang Z, Wang J, Li J, Xiong L, Chen H, Liu X, et al. Antihyperlipidemic and hepatoprotective activities of polysaccharide fraction from *Cyclocarya paliurus* in high-fat emulsion-induced hyperlipidaemic mice. *Carbohydr Polym.* (2018) 183:11. doi: 10.1016/j.carbpol.2017.11.033

30. Price SJ, Pangloli P, Dia VP. Pepsin-pancreatin hydrolysis reduced the ability of lunasin-enriched material to inhibit activation of the inflammasomes in THP-1 human macrophages. *Food Funct.* (2017) 8:4449–58. doi: 10.1039/c7fo00992e

31. Ren D, Lin D, Alim A, Zheng Q, Yang X. Chemical characterization of a novel polysaccharide ASKP-1 from Artemisia sphaerocephala Krasch seed and its macrophage activation via MAPK, PI3k/Akt and NF-kappaB signaling pathways in RAW264.7 cells. *Food Funct.* (2017) 8:1299–312. doi: 10.1039/c6fo01699e

32. Xie J, Wang Z, Shen M, Nie S, Gong B, Li H, et al. Sulfated modification, characterization and antioxidant activities of polysaccharide from *Cyclocarya paliurus*. *Food Hydrocoll.* (2016) 53:7–15.

33. Hu WB, Zhao J, Chen H, Xiong L, Wang WJ. Polysaccharides from *Cyclocarya paliurus* : Chemical composition and lipid-lowering effect on rats challenged with high-fat diet. *J Funct Foods.* (2017) 36:262–73.

34. Wang T, He H, Liu X, Liu C, Liang Y, Mei Y. Mycelial polysaccharides of *Lentinus edodes* (shiitake mushroom) in submerged culture exert immunoenhancing effect on macrophage cells via MAPK pathway. *Int J Biol Macromol.* (2019) 130:745–54. doi: 10.1016/j.ijbiomac.2019.03.023

35. Rong Y, Yang R, Yang Y, Wen Y, Liu S, Li C, et al. Structural characterization of an active polysaccharide of longan and evaluation of immunological activity. *Carbohydr Polym.* (2019) 213:247–56. doi: 10.1016/j.carbpol.2019.03.007

36. Deng Y, Xie J, Luo Z, Li SP, Zhao J. Synergistic immunomodulatory effect of complex polysaccharides from seven herbs and their major active fractions. *Int J Biol Macromol.* (2020) 165 (Pt A):530–41. doi: 10.1016/j.ijbiomac.2020.09.199

37. Perera N, Yang FL, Chiu HW, Hsieh CY, Li LH, Zhang YL, et al. Phagocytosis enhancement, endotoxin tolerance, and signal mechanisms of immunologically active glucuronoxylomannan from Auricularia auricula-judae. *Int J Biol Macromol.* (2020) 165 (Pt A):495–505. doi: 10.1016/j.ijbiomac.2020.09.171

38. Gan T, Feng C, Lan H, Yang R, Zhang J, Li C, et al. Comparison of the structure and immunomodulatory activity of polysaccharides from fresh and dried longan. *J Funct Foods.* (2021) 76:104323.

39. Wufuer R, Bai J, Liu Z, Zhou K, Taoerdahong H. Biological activity of *Brassica rapa* L. polysaccharides on RAW264.7 macrophages and on tumor cells. *Bioorg Med Chem.* (2020) 28:115330. doi: 10.1016/j.bmc.2020.115330

40. Li WJ, Zhang XY, Wu RT, Song YH, Xie MY. *Ganoderma atrum* polysaccharide improves doxorubicin-induced cardiotoxicity in mice by regulation of apoptotic pathway in mitochondria. *Carbohydr Polym.* (2018) 202:581–90. doi: 10.1016/j.carbpol.2018.08.144

41. Xu C, Ding C, Zhou N, Ruan X-M, Guo B-X. A polysaccharide from *Aloe vera* L. var. chinensis (Haw.) Berger prevents damage to human gastric epithelial cells in vitro and to rat gastric mucosa in vivo. *J Funct Foods.* (2016) 24:501–12.

42. Yun L, Wu T, Li Q, Zhang M. Dietary supplementation with purified wheat germ glycoprotein improve immunostimulatory activity in cyclophosphamide induced Balb/c mice. *Int J Biol Macromol.* (2018) 118 (Pt A):1267–75. doi: 10.1016/j.ijbiomac.2018.06.199

43. Dehghan P, Tolouie S, Baradaran B, Nami S, Morovati H. TLR-2, IL-10 and IL-17-mediated immunity in experimental chemotherapy murine model of systemic candidiasis, cyclophosphamides' impact and roles. *Microb Pathog.* (2018) 119:183–92. doi: 10.1016/j.micpath.2018.04.026

44. Maity P, Sen IK, Maji PK, Paloi S, Devi K, Acharya K, et al. Structural, immunological, and antioxidant studies of β-glucan from edible mushroom *Entoloma lividoalbum*. *Carbohydr Polym.* (2015) 123:350–8. doi: 10.1016/j.carbpol.2015.01.051

45. Vijay K. Toll-like receptors in immunity and inflammatory diseases: Past, present, and future. *Int Immunopharmacol.* (2018) 59:391–412.

46. Vetvicka V, Gover O, Karpovsky M, Hayby H, Danay O, Ezov N, et al. Immune-modulating activities of glucans extracted from *Pleurotus ostreatus* and *Pleurotus eryngii*. *J Funct Foods.* (2019) 54:81–91.

47. Mirzadeh M, Arianejad MR, Khedmat L. Antioxidant, antiradical, and antimicrobial activities of polysaccharides obtained by microwave-assisted extraction method: A review. *Carbohydr Polym.* (2020) 229:115421. doi: 10.1016/j.carbpol.2019.115421

48. Yz A, Hk A, Yfa B, Kna C, Gopa B. Schizophyllan: A review on its structure, properties, bioactivities and recent developments. *Bioact Carbohydr Diet Fibre.* (2013) 1:53–71.

49. Chakraborty I, Sen IK, Mondal S, Rout D, Bhanja SK, Maity GN, et al. Bioactive polysaccharides from natural sources: A review on the antitumor and immunomodulating activities. *Biocatal Agric Biotechnol.* (2019) 22:101425.

50. Maity P, Nandi AK, Sen IK, Pattanayak M, Chattopadhyay S, Dash SK, et al. Heteroglycan of an edible mushroom *Entoloma lividoalbum*: Structural characterization and study of its protective role for human lymphocytes-ScienceDirect. *Carbohydr Polym.* (2014) 114:157–65. doi: 10.1016/j.carbpol.2014.07.080

51. Manna DK, Maity P, Nandi AK, Pattanayak M, Panda BC, Mandal AK, et al. Structural elucidation and immunostimulating property of a novel polysaccharide extracted from an edible mushroom *Lentinus fusipes*. *Carbohydr Polym.* (2017) 157:1657–65. doi: 10.1016/j.carbpol.2016.11.048

52. Han L, Suo Y, Yang Y, Jing M, Na H. Optimization, characterization, and biological activity of polysaccharides from *Berberis dasystachya* Maxim. *Int J Biol Macromol.* (2016) 85:655–66. doi: 10.1016/j.ijbiomac.2015.10.038

53. Tamiello CS, Nascimento G, Iacomini M, Cordeiro L. Arabinogalactan from edible jambo fruit induces different responses on cytokine secretion by THP-1 macrophages in the absence and presence of proinflammatory stimulus. *Int J Biol Macromol.* (2018) 107 (Pt A):35. doi: 10.1016/j.ijbiomac.2017.08.148

54. Weichao H, Zhao Y, Yang Y, Zhang H, Ding C. Microwave-assisted extraction, physicochemical characterization and bioactivity of polysaccharides from *Camptotheca acuminata* fruits. *Int J Biol Macromol.* (2019) 133:127–36. doi: 10.1016/j.ijbiomac.2019.04.086

55. Liu H, Xu J, Xu X, Yuan Z, Zhu D. Structure/function relationships of bean polysaccharides: A review. *Crit Rev Food Sci Nutr.* (2021) 13:1–15. doi: 10.1080/10408398.2021.1946480

56. Li S, Li M, Yue H, Zhou L, Huang L, Du Z, et al. Structural elucidation of a pectic polysaccharide from Fructus Mori and its bioactivity on intestinal bacteria strains. *Carbohydr Polym.* (2018) 186:168–75. doi: 10.1016/j.carbpol.2018.01.026

57. Chen X, Yang J, Shen M, Chen Y, Yu Q, Xie J. Structure, function and advance application of microwave-treated polysaccharide: A review. *Trends Food Sci Technol.* (2022) 123:198–209.

58. Song HN. Functional cordyceps coffee containing cordycepin and β-glucan. *Prev Nutr Food Sci.* (2020) 25:184–93. doi: 10.3746/pnf.2020.25.2.184

59. Zong S, Li J, Ye Z, Zhang X, Yang L, Chen X, et al. Lachnum polysaccharide suppresses S180 sarcoma by boosting anti-tumor immune responses and skewing tumor-associated macrophages toward M1 phenotype. *Int J Biol Macromol.* (2020) 144:1022–33. doi: 10.1016/j.ijbiomac.2019.09.179

60. Yu Y, Zhu H, Shen M, Yu Q, Chen Y, Xie J. Sulfation modification enhances the intestinal regulation of Cyclocarya paliurus polysaccharides in cyclophosphamide-treated mice via restoring intestinal mucosal barrier function and modulating gut microbiota. *Food Funct.* (2021) 12:12278–90. doi: 10.1039/d1fo03042f

61. Jeelani R, Khan SN, Shaeib F, Kohan-Ghadr HR, Aldhaheri SR, Najafi T, et al. Cyclophosphamide and acrolein induced oxidative stress leading to deterioration of metaphase II mouse oocyte quality. *Free Radic Biol Med.* (2017) 110:11–8. doi: 10.1016/j.freeradbiomed.2017.05.006

62. Viaud S, Flament C, Zoubir M, Pautier P, LeCesne A, Ribrag V, et al. Cyclophosphamide induces differentiation of Th17 cells in cancer patients. *Cancer Res.* (2011) 71:661–5. doi: 10.1158/0008-5472.CAN-10-1259

63. Wei W, Xiao HT, Bao WR, Ma DL, Leung CH, Han XQ, et al. TLR-4 may mediate signaling pathways of Astragalus polysaccharide RAP induced cytokine expression of RAW264.7 cells. *J Ethnopharmacol.* (2016) 179:243–52. doi: 10.1016/j.jep.2015.12.060

frontiers | Frontiers in Nutrition

TYPE Original Research
PUBLISHED 09 November 2022
DOI 10.3389/fnut.2022.1041655

Check for updates

OPEN ACCESS

EDITED BY
Wenjie Sui,
Tianjin University of Science and Technology, China

REVIEWED BY
Ahmed A. Zaky,
National Research Centre, Egypt
Cristiane Canan,
Universidade Tecnológica Federal do Paraná, Brazil

*CORRESPONDENCE
Daodong Pan
daodongpan@163.com

SPECIALTY SECTION
This article was submitted to Nutrition and Food Science Technology, a section of the journal Frontiers in Nutrition

RECEIVED 11 September 2022
ACCEPTED 28 October 2022
PUBLISHED 09 November 2022

CITATION
Xu J, Chen Y, Fan X, Shi Z, Liu M, Zeng X, Wu Z and Pan D (2022) Isolation, identification, and characterization of corn-derived antioxidant peptides from corn fermented milk by *Limosilactobacillus fermentum*. *Front. Nutr.* 9:1041655. doi: 10.3389/fnut.2022.1041655

COPYRIGHT
© 2022 Xu, Chen, Fan, Shi, Liu, Zeng, Wu and Pan. This is an open-access article distributed under the terms of the Creative Commons Attribution License (CC BY). The use, distribution or reproduction in other forums is permitted, provided the original author(s) and the copyright owner(s) are credited and that the original publication in this journal is cited, in accordance with accepted academic practice. No use, distribution or reproduction is permitted which does not comply with these terms.

Isolation, identification, and characterization of corn-derived antioxidant peptides from corn fermented milk by *Limosilactobacillus fermentum*

Jue Xu[1,2], Yingyan Chen[3], Xiankang Fan[1,2], Zihang Shi[1,2], Mingzhen Liu[1,2], Xiaoqun Zeng[1,2], Zhen Wu[1,2] and Daodong Pan[1,2]*

[1]Key Laboratory of Animal Protein Food Deep Processing Technology of Zhejiang Province, College of Food and Pharmaceutical Sciences, Ningbo University, Ningbo, China, [2]State Key Laboratory for Managing Biotic and Chemical Threats to the Quality and Safety of Agro-products, Ningbo University, Ningbo, China, [3]Department of Food Science and Technology, School of Food Science and Pharmaceutical Engineering, Nanjing Normal University, Nanjing, China

Dairy-derived peptides and corn-derived peptides have been identified as essential ingredients for health promotion in the food industry. The hydrolysis based on lactic acid bacteria (LAB) protease system is one of the most popular methods to prepare bioactive peptides. The objectives of this paper are to develop antioxidant fermented milk and to obtain natural antioxidant peptides. In our study, LAB with antioxidant capacity were screened *in vitro*, and the corn fermented milk with antioxidant capacity was achieved by the traditional fermentation method. Fermented milk was purified by ultrafiltration and molecular sieve, and identified by liquid chromatography-tandem mass spectrometry (LC-MS/MS). Our findings demonstrate that *Limosilactobacillus fermentum* L15 had a scavenging capacity of more than 80% of DPPH radicals, Trolox equivalent antioxidant capacity (TEAC) of 0.348 ± 0.005 mmol/L. Meanwhile, the peptide content of corn fermented milk prepared with *L. fermentum* L15 was 0.914 ± 0.009 mg/mL and TAEC of 0.781 ± 0.020 mmol/L. Particularly important, IGGIGTVPVGR and LTTVTPGSR isolated and extracted from fermented milk were found to have antioxidant capacity for the first time. The synthetic peptides IGGIGTVPVGR and LTTVTPGSR demonstrated a scavenging capacity of 70.07 ± 2.71% and 70.07 ± 2.77% for DPPH radicals and an antioxidant capacity of 0.62 ± 0.01 mmol/L and 0.64 ± 0.02 mmol/L Trolox equivalent, respectively. This research provides ideas and basis for the development and utilization of functional dairy products.

KEYWORDS

lactic acid bacteria, antioxidant peptide, fermented milk, corn (maize), LC-MS/MS

Introduction

Oxidation is an inevitable process in the oxidative metabolism of all organisms (1). However, the imbalance between oxidation and antioxidation causes oxidative stress, which is one of the major causes of various chronic diseases such as aging, cardiovascular diseases, diabetes, Alzheimer's disease, and cancer (2, 3). Synthetic antioxidants, although having strong antioxidant activity, are potentially risky in the organism, so attention has been turned to natural antioxidants, and many studies revealed that peptides produced by the hydrolysis of various proteins or by microbial fermentation have antioxidant activity (4). Therefore, the development of antioxidant products from natural foods has become a current research hotspot for antioxidants. Fermented dairy products are becoming increasingly popular with consumers, especially those who have special nutritional requirements. In addition to the rich nutrients in milk, the bioactive peptides produced by lactic acid bacteria (LAB) breaking down milk proteins are also an excellent resource. Fermentation is an effective way to produce target bioactive peptides at this stage, and numerous studies have demonstrated the production of bioactive peptides by LAB through a protein hydrolysis system, and these active peptides have anticoagulant, angiotensin-converting enzyme activity inhibition and antioxidant capacity (5). These natural exogenous antioxidants have received attention from the food industry and the medical field, and the fact that they can be supplemented without limit and do not cause dangerous immune reactions in the body provides an effective way to alleviate oxidation.

In fermented milk, the content of antioxidant peptides was dependent on the type of probiotics used. It is well-known that probiotics contain a lot of enzymes. LAB is the most widely used probiotic microorganisms. The proteins in milk were degraded into different polypeptides by the cell envelope protease (CEP) on the surface of LAB during fermentation process (6). Degradation products are transported across the cell membrane by different peptide transport systems, including oligopeptide (Opp), dipeptide (DtpP), and tripeptide (DtpT) transport carriers (7). They are then hydrolyzed into amino acids or small peptides by intracellular peptidase, and produce a series of bioactive peptides. Our previous study demonstrated that fermented milk of *Lactobacillus delbrueckii* subsp. *bulgaricus* has an antioxidant capacity and the hydrolysis of casein and whey proteins by *Lactobacillus reuteri* released bioactive peptides with more potential antioxidant capacity compared to *Lactobacillus brevis* and *Lactobacillus plantarum* (8). Other studies have also illustrated that the fermentation of milk by *Lactobacillus acidophilus* increases the production of bioactive peptides, especially antioxidant peptides (9). The peptides extracted from *kefir*, a fermenting agent rich in probiotics (LAB, acetate bacteria, and yeast), had also shown potent and excellent functional properties (10). Screening of LAB that produce antioxidant peptides is essential to obtain bioactive peptides in fermentation.

Plant foods not only offer many potential health benefits, but they are also rich in protein. Plant ingredients are typically added to foods to increase nutritional value (11). Corn is one of the most important foods and industrial crops in the world, and has a comprehensive nutritional profile. Corn contains active oxidizing substances such as phenolic acids, anthocyanins, carotenoids, etc. (12). The antioxidant capacity of corn had been well-known. Corn silk polysaccharide had a good antioxidant capacity and protects oxidatively damaged renal epithelial cells (13). Zeaxanthin and lutein in corn had also been reported to have strong antioxidant activity, significantly reducing visual fatigue and reducing the risk of macular degeneration and cataracts (14). Corn also contains 10–15% protein. Corn has a protein content of 60–70% after crushing. The relatively low content of certain essential amino acids such as lysine and tryptophan results in poor-quality corn protein lacking desirable functional properties (15). Hence it is crucial to hydrolyze corn protein to improve protein utilization. Hu et al. (16) reported the enhancement of corn protein amount using hydrolyzed corn protein powder such as papain. Jorge et al. (17) measured the antioxidant capacity of corn alcohol-soluble protein on hepatocytes. Zhuang et al. (18) obtained antioxidant peptides by hydrolyzing corn protein powder with alkaline protease and flavored protease, which improved the deficiency of poor protein quantity of corn. Jang et al. (19) improved the nutrition, antioxidant, and bioavailability of corn bran and wheat bran mix by fermenting them with LAB and acid protease. However, it is rare to find studies on the fermentation of corn proteins in combination with milk proteins by LAB.

Due to the outstanding antioxidant potential of milk and corn proteins and the limited information on the production of bioactive peptides from milk fermented with *Limosilactobacillus fermentum*. This study expected to develop a corn fermented milk with the hope that its antioxidant capacity would fill the gap in developing a healthy antioxidant product from natural foods. Furthermore, the potential antioxidant peptides in the fermented milk were identified by ultrafiltration purification and LC-MS/MS. Finally, the structure-activity characteristics of the peptides were analyzed and validated.

Materials and methods

Screening of antioxidant peptides production capacity of LAB from fermented milk

Fermented milk preparation and peptide content assay

The 20 strains of LAB preserved in our laboratory were activated. The activated bacteria were inoculated into sterile skim milk at an inoculum level of 5.0% (v/v), mixed thoroughly,

and then placed in a constant temperature incubator at 42°C to ferment until all the milk was curdled, and stored at 4°C for subsequent experiments.

Glutathione was used as the standard, and the peptide content was determined by the precipitation of macromolecular protein with trichloroacetic acid (TCA) and the biuret method (20). Concretely, glutathione was prepared as standard solutions with different concentrations (0, 0.4, 0.6, 0.8, 1, 1.2 mg/mL), and the absorbance values at 540 nm were measured by the biuret method and the standard curves were plotted. The peptide content of each fermented milk sample was calculated by precipitating the macromolecular proteins in the fermented milk samples with 10% trichloroacetic acid, centrifuging (4 × 103 *g*, 20 min) the supernatant, and adding bicarbonate reagent to determine the absorbance value at 540 nm.

Total acid and free acid in fermented milk assay

The titration acidity was determined in accordance with the National Standard of the People's Republic of China (GB 5413.34-2010) (21). Briefly, 10 *g* of fermented milk sample was mixed with 20 mL of boiled deionized water and titrated with 0.1 mol/L NaOH and phenolphthalein as an indicator. Titratable acidity was expressed as milliliters of NaOH (0.1 mol/L) consumed for the acidity value of fermented milk. The pH of the fermented milk sample was measured by recording by pH meter (Shanghai Yimai Instrument Technology Co., Shanghai, China).

Water-holding capacity and antioxidant activity of fermented milk

Based on the measurements by Sodini et al. (22), the WHC of the sample was measured. A homogenized sample of fermented milk (Y) was centrifuged at 4 × 10^3 *g* for 10 min at 4°C, and the whey supernatant, removed from the sample, was weighed (WE). The WHC is calculated as follows:

$$WHC\ (\%) = \frac{Y - WE}{Y} \times\ 100\%$$

The antioxidant capacity of LAB fermented milk was determined by the Trolox equivalent antioxidant capacity assay using the colorimetric Total Antioxidant Capacity Assay kit (Nanjing Jiancheng Bioengineering Institute, Nanjing, China). Results were obtained by interpolation to a Trolox (reference antioxidant) standard curve and expressed as Trolox equivalent antioxidant capacity (TEAC) (23). In addition, 2,2-Diphenyl-1-picrylhydrazyl (DPPH) radical scavenging activity was chosen to assess the antioxidant capacity of fermented milk (24).

LAB cell-envelope-proteinase assay

Lactobacillus can use cell-envelope-proteinase (CEP) to hydrolyze milk proteins into a series of short peptides, which is important for screening antioxidant peptide-producing LAB. We modified the CEP assay method, based on Sinsuwan et al. (25). After lysis of the bacterium using lysozyme, protease activity was measured at an absorbance of 410 nm using MeOsuc-Arg-Pro-Tyr-pNA (MS-Arg) as a specific substrate. Enzyme activity was defined as an increase of 0.10 per hour at 410 nm at 37°C indicating one unit of activity.

Identification of target LAB

LAB with superior fermentability and high production of antioxidant peptides were further identified by 16S rRNA analysis. The 16S rRNA sequence analysis procedure was as follows: total DNA of a strain was extracted using a bacterial genomic DNA extraction kit. The general primers 1492R and 27F were used for amplification. The PCR fragments (1,500 bp) were purified using a quick PCR purification kit and sequenced by Sangon Biotech (Shanghai, China). Then, a phylogenetic tree was constructed by generating a complete alignment of the 16S rRNA gene of the selected members in GenBank by using MEGA software (https://www.megasoftware.net/) bootstrap values. The identified strains were finally selected for subsequent testing.

Fermented milk with corn preparation

Alkaline protease was added to the milled corn to prepare corn digest A. Add 6% (v/v) Bacillus subtilis to A, ferment at 37°C for 18 h to fully hydrolyze the corn protein, and sterilize to prepare fermentation broth B. In the milk fermentation process, 9% (v/v) corn fermentation solution B was added to fresh milk and sterilized at 121°C for 5 min, then yogurt fermenter *Lactobacillus bulgaricus* and *Streptococcus thermophilus* (3% (v/v) inoculum), and *Limosilactobacillus fermentum* L15 (2% (v/v) inoculum) were added to make corn fermented milk at 42°C (26).

Purification of antioxidant peptides

Preparation of whey

The pH of the fermented milk was adjusted to 3.4–3.6 with 1 mol/L HCl, centrifuged at 8 × 10^3 *g* for 15 min, and the supernatant was taken, then the pH of the fermented milk was adjusted to 8.3 with 1 mol/L NaOH, centrifuged at 8 × 10^3 *g* for 15 min, and the supernatant was collected for the subsequent extraction of peptides.

Ultrafiltration

Protein was concentrated by centrifugal ultrafiltration. The above samples were purified using centrifugal ultrafiltration

with 3 and 10 kDa molecular weight cutoff filters to obtain fractions of different molecular weights and freeze-dried them (27). The antioxidant capacity of freeze-dried samples was assessed by two well-established methods, including DPPH radical scavenging activity and TEAC (28). The fraction with the highest antioxidant activity was selected for the next step of isolation and purification.

Sephadex G-25 gel filtration

A gel chromatographic column filled with Sephadex G25 was used to separate the peptides. The chromatographic column was equilibrated and the filtered sample was loaded at a flow rate of 1 mL/min. The fractions with absorption peaks at 280 nm were collected and lyophilized (29). The lyophilized peptides were dissolved in water and assayed for their antioxidant activity. The fraction with the highest antioxidant activity was selected for subsequent analysis.

Identification of antioxidant peptides by LC-MS/MS and evaluation of antioxidant activity

To determine the peptide sequences, the Q Exactive Plus liquid mass spectrometry system (Thermo Fisher Scientific, Waltham, MA, USA) was used for analysis. Briefly, peptide samples were aspirated by the autosampler and bound to a C18 capture column (3 μm 120 Å, 100 μm 20 mm) and eluted to an analytical column (2 μm, 120 Å, 750 μm × 150 mm) for separation. Analytical gradients were established at a flow rate of 300 μL/min using two mobile phases (mobile phase A: 3% dimethyl sulphoxide (DMSO), 0.1% formic acid, 97% H_2O, and mobile phase B: 3% DMSO, 0.1% formic acid, 97% ACN). The most abundant precursor ions were dynamically selected from a survey scan (350–1,800 m/z) of HCD fragments during mass spectrometry DDA mode analysis. The automatic gain control (AGC) target was set to 3×10^6 with a maximum injection time of 20 ms and a dynamic exclusion time of 35 s. Survey scans were performed at a resolution of 70,000 at m/z 200, HCD spectral resolution was set to 17,500 at m/z 200, normalized collision energy was 28 eV, and the screening window of the four-stage rod was set to 1.6 Da. The instrument was run with the peptide recognition mode enabled.

The mass spectrometry data generated by Q Exactive Plus is retrieved through ProteinPilot (V4.5) using the database retrieval algorithm Paragon. Search the proteome reference database using Maize_Bovine_Lab in UniProt. Search parameters were as follows: Sample Type selected Identification; Cys Alkylation selected Iodoacetamide; Digestion selected Trypsin; Search Effort set to Rapid ID. Search results were filtered by Unused $\geq$ 1.3, entries retrieved from the inverse library and contaminating proteins were deleted, and the remaining identification information was used for subsequent analysis. The identified peptides were sent to Shanghai Botai Biotechnology Co., Ltd. for synthesis according to their sequences. The synthesized peptides were verified by HPLC-MS to determine their molecular weight. The antioxidant capacity of the synthetic peptides was assessed by the DPPH radical scavenging activity and TEAC.

In silico analysis

ChemDraw online tools were used to map peptide chemical structures. The iso-electric point (pI) was analyzed by the online Innovagen server, available at www.innovagen.com/proteomics-tools. The PepDraw server (http://www.tulane.edu/$\sim$biochem/WW/PepDraw/) was used to evaluate the hydrophobicity and net charge (at neutral pH) of the peptides.

Statistical analysis

All experiments were repeated 3 times. All statistical analyses were performed by GraphPad Prism 7.0 software. Data were expressed as mean ± SD and analyzed by repeated measures with the one-way analysis of variance (ANOVA). Bonferroni's test group comparisons were also adopted in the group data analysis. $p < 0.05$ was considered to be statistically significant, and $p < 0.01$ was considered extremely significant.

Results and discussion

Quality analysis of fermentation strains

In order to assess the quality of the fermented strains, this study examined the fermentation characteristics of fermented milk samples in terms of both pH and titratable acidity. The pH value of fermented milk during its shelf life is generally 4.0–4.6, and the titratable acidity is generally between 70 and 110 mL NaOH/kg (30). A higher pH value indicates inappropriate fermentation and does not effectively inhibit the growth of negative microorganisms. Islam et al. (31) examined different varieties of fermented milk marketed and found a significant difference ($p < 0.05$) in the pH of fermented milk, the average pH of the fermented milk samples remained slightly acidic, averaging between 5.28 and 6.33. In this study, there were 10 strains of milk fermented by bacteria with pH values in the range of 4.0–4.6, but all the pH values of fermented milk were below 5.5, which may be related to single bacteria fermentation (Figure 1A). Total titratable acidity is the total amount of hydrogen ions in the fermented milk sample, except for binding to basic ions (32). Therefore, titratable acidity measurements are more relevant in the evaluation of microbial fermentation

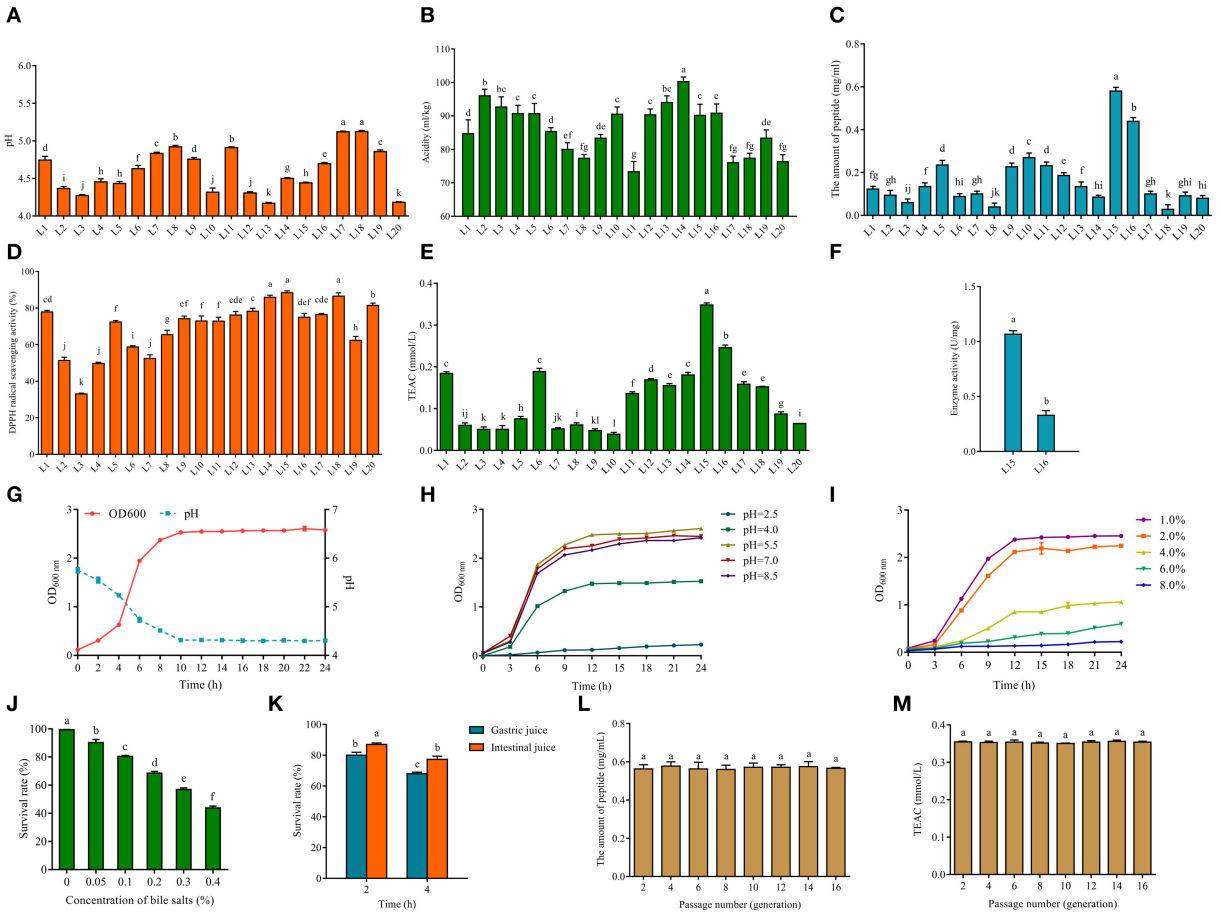

FIGURE 1
pH **(A)** and acidity **(B)** of fermented milk produced from screened LAB (L1-20). The amount of peptide **(C)** of fermented milk of 20 screened LAB (L1-20). The DPPH radical scavenging ability **(D)** and Trolox equivalent antioxidant capacity (TEAC) **(E)** of fermented milk of 20 screened LAB (L1-20). Enzyme activity **(F)** of fermented milk of L15 and L16. Growth curve and acid production capacity of *L. fermentum* L15 **(G)**. **(H)** Growth characteristics (optical density, OD_{600nm}) of *L. fermentum* L15 grown in MRS medium at different pH values (F; 2.5, 4.0. 5.5, 7.0, and 8.5). **(I)** Growth characteristics (optical density, OD_{600nm}) of *L. fermentum* L15 grown in MRS medium at different NaCl concentrations (w/v; 1, 2, 4, 6, and 8%). **(J)** The survival rate of *L. fermentum* L15 treated for different concentrations of bile salts. **(K)** The simulated gastrointestinal fluid environment *in vitro* on *L. fermentum* L15 growth. Genetic stability of peptide production **(L)** and TEAC **(M)** of fermented milk of *L. fermentum* L15. Different lowercase letters indicate significant differences between groups ($p < 0.05$).

capacity. Figure 1B indicates that the acidity values of each fermented buttermilk ranged from 70 to 110 mL NaOH/kg. These data show that all strains of fermented milk were of good quality and could be used for subsequent experiments.

Isolation, identification, and preservation of antioxidant peptides producing LAB from fermented milk

The antioxidant peptide is a bioactive peptide that can maintain the balance of free radicals and enhance the anti-aging ability of the body (33). Milk contains rich protein and is one of the main sources of bioactive peptides. LAB can produce antioxidant peptides using milk proteins. Thus, it is crucial to find excellent strains for preparing antioxidant peptides. Research has demonstrated that proteolytic strains contribute to the availability of free amino acids and peptides in fermented milk (34). The main production methods of bioactive peptides are protein enzymatic digestion and dairy product fermentation (35). Thus, 20 strains of LAB were selected to ferment milk to produce peptides and to determine the peptide content and their antioxidant capacity, respectively, in this study. Figure 1C clearly showed that L15 produced the highest amount of peptides (close to 0.6 mg/mL) from fermented milk and L16 produced more than 0.4 mg/mL of peptides. The fermented milk of strain L15 showed the strongest capability of scavenging DPPH radicals (Figure 1D), and all strains except strain L3 showed excellent

scavenging capability of DPPH radicals. TEAC experiments further confirmed that strain L15 fermented milk exhibited the strongest antioxidant activity among all 20 isolates (Figure 1E). The screening of *Lactobacillus delbrueckii* subsp. *bulgaricus* L7 from Xinjiang cheese in our previous study showed a good antioxidant capacity. The DPPH radical scavenging capacity of L7 fermented milk was around 80% and the TEAC was around 0.15 mmol/L. In this study, strain L15 fermented milk had a DPPH radical scavenging capacity of >80% and TEAC of 0.348 ± 0.005 mmol/L, which is better than our previous study (36).

Besides, Cell-Envelope-Proteinase (CEP) is an enzyme in the protein system of LAB, which is a key enzyme for the hydrolysis of proteins into oligopeptides and then translocation into the cell. It is also an essential component for the utilization of bovine milk proteins by LAB (37). Figure 1F reveals that the CEP enzyme activity of L15 is more than two times higher than that of L16. Therefore, L15 was selected for subsequent physiological characterization of the strain in this study (Figures 1G–K). Figure 1G showed that strain L15 reached the logarithmic stage in 2 h and reached its lowest value in 10 h, which was beneficial for fermented milk fermentation. To function in the acidic environment of the stomach, LAB must have a considerable acid tolerance (38). It was evident from Figure 1H that strain L15 was still in a growth condition even if growth of strain L15 was hindered at pH 2.5 as compared to pH 4.0. This was superior to the acid tolerance of *Lactiplantibacillus plantarum* subsp. *plantarum* F8 that we previously reported (39). Strain L15 maintained a growth trend at NaCl concentrations up to 6% (Figure 1I) and had a survival rate >40% at 0.4% bile salt (Figure 1J). This strain showed better osmotic stress tolerance and bile salt tolerance than we previously screened *Levilactobacillus brevis* 54 (26). Besides, the survival rate of L15 was more than 60% after 4 h of gastrointestinal fluid stress (Figure 1K). Moreover, the antioxidant stability of L15 was found to remain consistent over 16 h of growth in this study (Figures 1L,M, $p > 0.05$). Taking into account the antioxidant capacity and fermentation ability of the strain, strain L15 was applied in subsequent studies.

The 16S rRNA gene sequence was submitted to the National Center of Biotechnology Information with accession number OP616039. 16S rRNA-directed phylogenetic analysis primarily supported the delimitation of strain L15 as *Limosilactobacillus fermentum* (formerly named *Lactobacillus fermentum*) (Figure 2). *L. fermentum* has been identified as one of the probiotics that can be used in food, indicating that the L15 strain can be safely used as a dietary supplement.

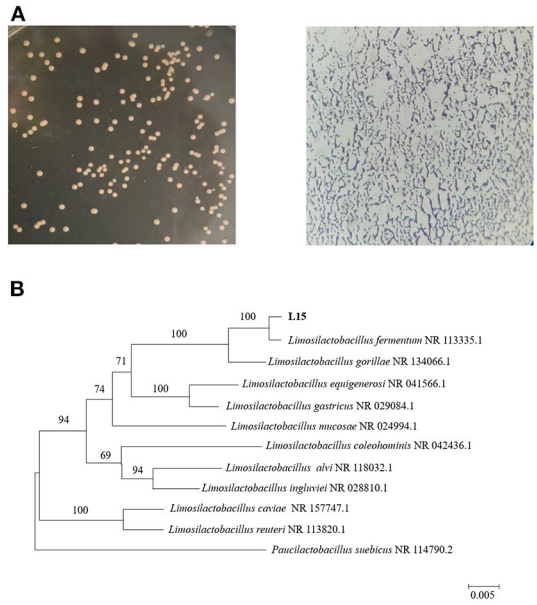

FIGURE 2
Identification of strain L15. **(A)** Morphology of screened strain L15 on MRS plate and under the microscope. **(B)** Phylogenetic tree based on 16S rRNA gene sequences of strain L15. The evolutionary history was inferred using the Neighbor-Joining method, scale bar represents 0.01 nucleotide substitution per position.

Preparation and optimization of corn fermented milk

Maize proteins and their derived peptides have become an essential source of bioactive peptides (40). The protein content is increased to 60% in the crushed corn. In addition to physical fragmentation, enzymatic, chemical hydrolysis, and biofermentation are also used to produce protein hydrolysates (41). In order to improve the antioxidant capacity of corn fermentation also, in this paper, corn was fermented with *Bacillus subtilis*, which was enzymatically digested by alkaline protease and they were fermented into fermented milk. Optimal conditions for corn enzymatic digestion were obtained by single-factor experiments with response surface optimization (Supplementary Table S1). The optimal enzymatic solution for corn (OEC) was determined as follows: 9.82% maize addition, 6.53% alkaline protease addition, pH = 9.19, and temperature 49.53°C (Supplementary Figure S1). The optimal fermentation protocol for *Bacillus subtilis* (OFB) was 6% inoculum, 18 h fermentation time, pH = 8, 37°C fermentation temperature, and TEAC of the ferment solution was 0.748 ± 0.016 mM (Supplementary Figure S2). The orthogonal results are shown in Supplementary Table S2. The optimal conditions for fermented milk were 9% (v/v) for OFB addition, 3% (v/v) for the first fermenting agent (*L. fermentum* L15), 2% (v/v) for the second fermenting agent (direct injection fermenting agent), and 8% (w/v) for sucrose addition. The peptide content and TAEC of fermented milk were 0.914 ± 0.009 mg/mL and 0.781 ± 0.020 mmol/L, respectively (Supplementary Figures S3A–D). The pH and viable cell count of corn fermented milk during fermentation were determined. As shown in Supplementary Figure S3E, following 6 h of

fermentation, the pH of the fermented milk dropped to below 4.5. The rate of viable bacteria in the fermented milk was increasing, and the content of viable bacteria reached about 10 $\log_{10}$ CFU, and the water-holding capacity of the fermented milk was 57.48 ± 0.01%, all of which were in accordance with the reported requirements of the marketed fermented milk (42).

Purification of antioxidant peptides

The antioxidant activity of protein hydrolysates and peptides was related to their molecular weight (18). Antioxidant peptides in fermented milk were purified by centrifugal ultrafiltration and gel chromatography separation in this study. After centrifugal ultrafiltration, three fractions, named Y1, Y2, and Y3, were separated according to their molecular weights of 3 and 10 kDa, and their antioxidant properties were evaluated. Figures 3A,B showed the DPPH radical scavenging rate and TEAC content of these fractions. There was no significant difference in the DPPH radical scavenging rate of three fractions in Figure 3A ($p > 0.05$), while Y2 had a stronger antioxidant capacity in Figure 3B ($p < 0.05$), which might be related to the fact that the DPPH radical scavenging rate method was more suitable for alcohol-soluble substances (43). The supernatant of the fermented milk sample was used for subsequent analysis, and the results of the DPPH tests were not as significant as TEAC after centrifugation.

Subsequently, Y2 was separated by gel chromatography Sephadex G-25, and we collected fractions A and B in Figure 3C to evaluate their antioxidant capacity. Among them, the shortest retention time of component A indicated the largest molecular weight, while the longest retention time of B indicated the smallest molecular weight. Figures 3D,E clearly showed that the antioxidant capacity of component B was stronger. Similarly, Hernández-Ledesma et al. (44) isolated 10 different peptide fractions from commercial fermented milk by reversed-phase high-performance liquid chromatography and showed that one of the fractions with significant antioxidant activity consisted of antioxidant peptides. In addition, it was shown that the antioxidant activity of hydrolysates was closely related to their molecular weight distribution, and peptides or protein hydrolysates with small molecular weight could react better and more fully with free radicals during the oxidation process (45), which was consistent with the results of this study.

Sequence and activities of the antioxidant peptides

The sequence identification of the isolated and purified fraction B was performed by LC-MS/MS. Due to the complex protein composition in corn fermented milk, a large number of peptide sequences were observed in this fraction. The antioxidant peptide capacity is related to the antioxidant peptide length. Lower molecular weight peptides had been reported to have higher antioxidant capacity. This is because lower molecular weight can readily react with lipid radicals, thus reducing free radical-mediated lipid peroxidation (35). We selected peptides with no more than 15 amino acids for further screening. Most of the peptides were derived from casein, glycoprotein, and lactoglobulin in milk, and a small percentage was derived from maize. We selected two peptides synthesized from maize and selected antioxidant peptides of bovine milk origin that have been reported as positive controls (Supplementary Table S3). The antioxidant peptide activity was related to the composition and sequence of amino acids, which had a significant effect on the antioxidant activity of the peptide (35). The peptides containing His, Leu, Tyr, Met, Pro, Trp, Phe, and Val were reported to have stronger antioxidant activity (46). Four peptides showed the presence of these amino acids in our study, namely FPKYPVEPF, HLPLPLLQSWM, IGGIGTVPVGR, and LTTVTVTPGSR, named B1, B2, B3, and B4. Therefore, the four peptides were resynthesized and their antioxidant activities were verified, and it was found that all four sequences of the peptides had more than 60% DPPH radical scavenging rate and more than 0.6 mmol/L TEAC content (Figure 4). Analysis of peptide data from the BIOPEP database showed that FPKYPVEPF and HLPLPLLQSWM were derived from bovine milk proteins. Among them, peptides FPKYPVEPF (47), and HLPLPLLQSWM (48) had been identified as antioxidant peptides by different researchers. Antioxidant peptides isolated from soybean hydrolysate and egg white hydrolysate have also been reported to be attributed to histidine due to the protons providing the ability of the imidazole moiety (49). It has also been reported that the antioxidant activity of peptides in β-casein trypsin hydrolysates VKEAMAPK is derived from methionine (50). Methionine residues in β-casein are preferred targets for oxidation, and these may be due to the release of -SH groups contributing to the antioxidant properties (51). Aromatic amino acids, such as Tyr and Phe, enhance antioxidant activity by effectively scavenging free radicals by providing protons like electron-deficient free radicals (52). Moreover, it has been demonstrated in our previous studies that bioactive peptide sequences containing two proline and one valine contribute to antioxidant activity (8).

The antioxidant capacity of IGGIGTVPVGR was predicted but not verified by Lu et al. (53) through the characterization and quantification of functional proteins and bioactive peptides produced during the enzymatic digestion of *Hermetia illucens* larvae fed with food wastes. Similarly, Karami et al. (54) isolated IGGIGTVPVGR peptide by proteinase K digestion of wheat germ and demonstrated its ability to inhibit angiotensin-converting enzyme (ACE). Interestingly, the present study found that IGGIGTVPVGR derived from maize proteins showed better antioxidant capacity, indicating adequate hydrolysis of maize by L. fermentum and alkaline proteases (serine protease) (Figures 4I,J). Besides, the peptide LTTVTVTVTPGSR from *L.*

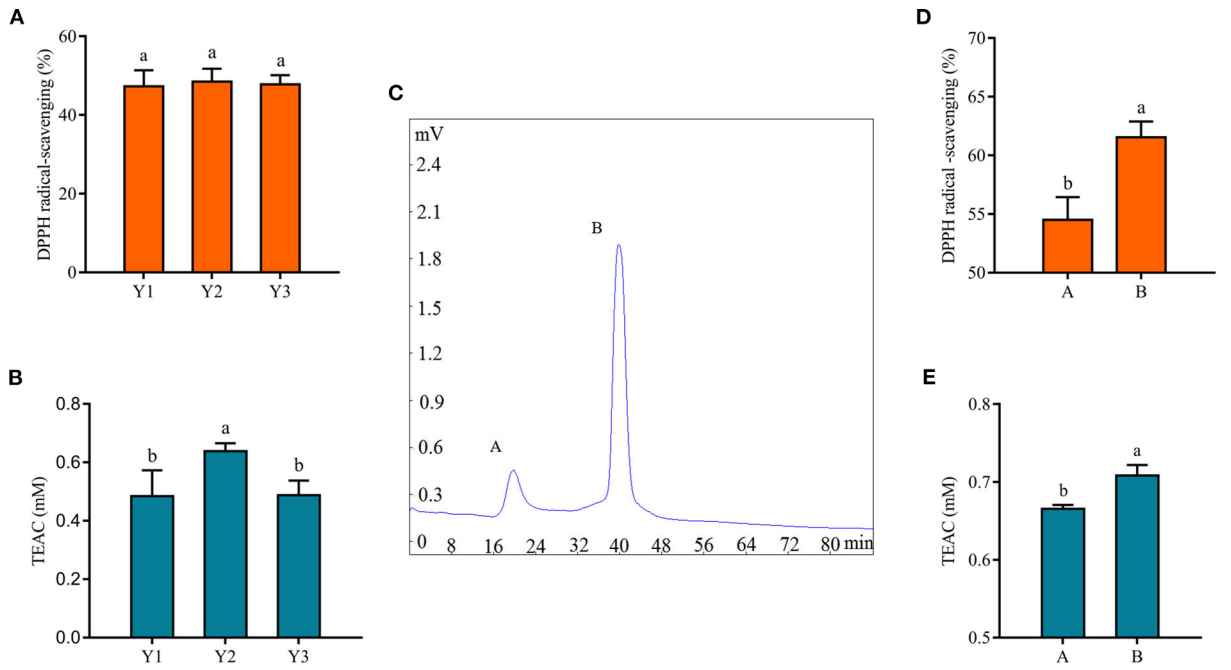

FIGURE 3
Isolation of antioxidant peptides from fermented yogurt. The DPPH radical scavenging ability **(A)** and TEAC **(B)** of each fraction are separated by centrifugal ultrafiltration. **(C)** Gel chromatogram of component Y2. The DPPH radical scavenging ability **(D)** and TEAC **(E)** of component Y2 are separated by centrifugal ultrafiltration. Different lowercase letters indicate significant differences between groups ($p < 0.05$).

fermentum L15 fermented corn cow's milk protein hydrolysate, derived from corn protein, had strong antioxidant activity, which was consistent with previous studies that the free radical scavenging ability of proteins or peptides was related to serine content (55). Similarly, n-termini containing hydrophobic amino acids, including valine or leucine, had been reported as strong oxidants (56). Hydrophobic amino acid residues such as valine or leucine also contribute to the formation of antioxidant peptides.

At the same time, alkaline proteases could digest proteins from maize into peptides with antioxidant activity. Based on the digestion site, we found that the formation of IGGIGTVPVGR, and LTTVTVTPGSR matched perfectly with Arg (R), the digestion site of a serine protease (alkaline protease). In addition, the duplication of 2–3 amino acid residues in the peptide might be related to its antioxidant activity (57). Interestingly, our study revealed that the peptide IGGIGTVPVGR had successive repeating hydrophobic amino acid residues and in our identification results, 1 mg/mL of IGGIGTVPVGR showed a scavenging rate of 70.07 ± 2.71% of DPPH radicals and a total antioxidant capacity (ABTS method) measured at 0.62 ± 0.01 mmol/L (Figures 4I,J).

Moreover, the difference in antioxidant activity of the experimental samples could be attributed to the ability of the cultures to produce antioxidant peptides during the fermentation process, which contributes to the antioxidant activity. Virtanen et al. (58) found that the antioxidant activity was dependent on the strain used and increased during the fermentation process. Ferments of *L. casei* enhanced the antioxidant activity of cheddar cheese during ripening (59). It has also been observed that the antioxidant activity of fermented milk was strain dependent, and that fermented milk could be used as a carrier of antioxidant probiotic LAB from non-dairy sources (60). Farvin et al. (61) found that the high antioxidant activity of fermented milk may be due to the release of antioxidant peptides by lactic acid bacteria during fermentation, which is consistent with our results. LAB has a rich enzyme system that can effectively break down proteins. Both corn and bovine milk are rich in proteins, and this study found that the antioxidant peptides from bovine milk protein and those from corn protein both have superior antioxidant capacity. Except for IGGIGTVPVGR, LTTVTVTPGSR showed a scavenging rate of 70.07 ± 2.77% for DPPH radicals and total antioxidant capacity (ABTS method) was determined to be 0.64 ± 0.02 mmol/L (Figures 4I,J). The primary structures of corn-derived peptides IGGIGTVPVGR and LTTVTPGSR isolated from corn fermented milk were shown in Figure 5.

Conclusion

Overall, *L. fermentum* L15, a high antioxidant peptide-producing bacteria, was screened to ferment corn enzymatic digest and milk to produce an artificial corn fermented milk. Two novel maize-derived antioxidant peptides, IGGIGTVPVGR and LTTVTVTPGSR, were extracted

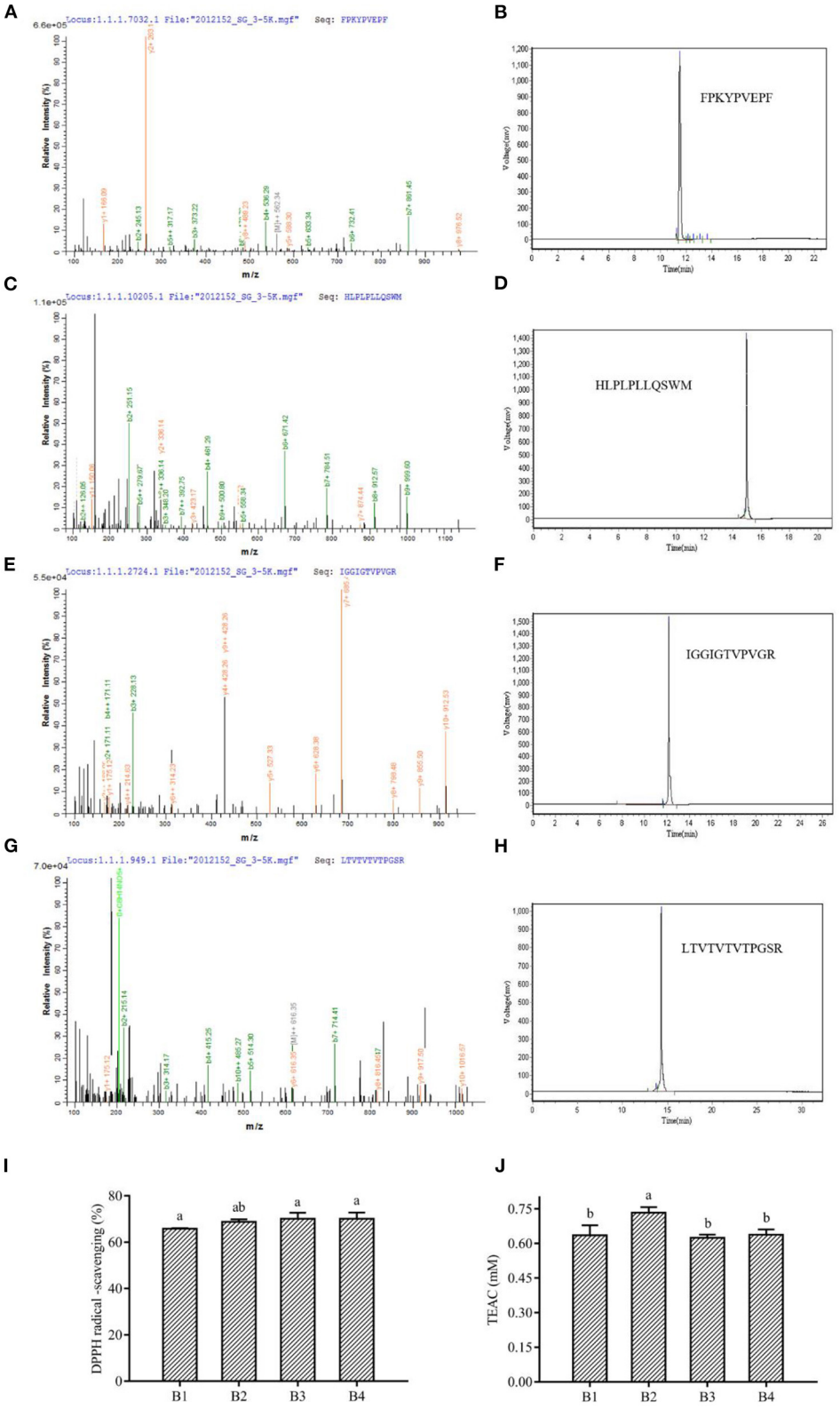

FIGURE 4
Mass spectrum and the primary structure of the peptide **(A)** FPKYPVEPF, **(C)** HLPLPLLQSWM, **(E)** IGGIGTVPVGR, and **(G)** LTVTVTVTPGSR. HPLC of synthetic peptides FPKYPVEPF **(B)**, HLPLPLLQSWM **(D)**, IGGIGTVPVGR **(F)**, and LTVTVTVTPGSR **(H)**. The DPPH radical scavenging ability **(I)** and TEAC **(J)** of peptides. B1, peptide FPKYPVEPF. B2, peptide HLPLPLLQSWM. B3, peptide IGGIGTVPVGR. B4, peptide LTVTVTVTPGSR. Different lowercase letters indicate significant differences between groups ($p < 0.05$).

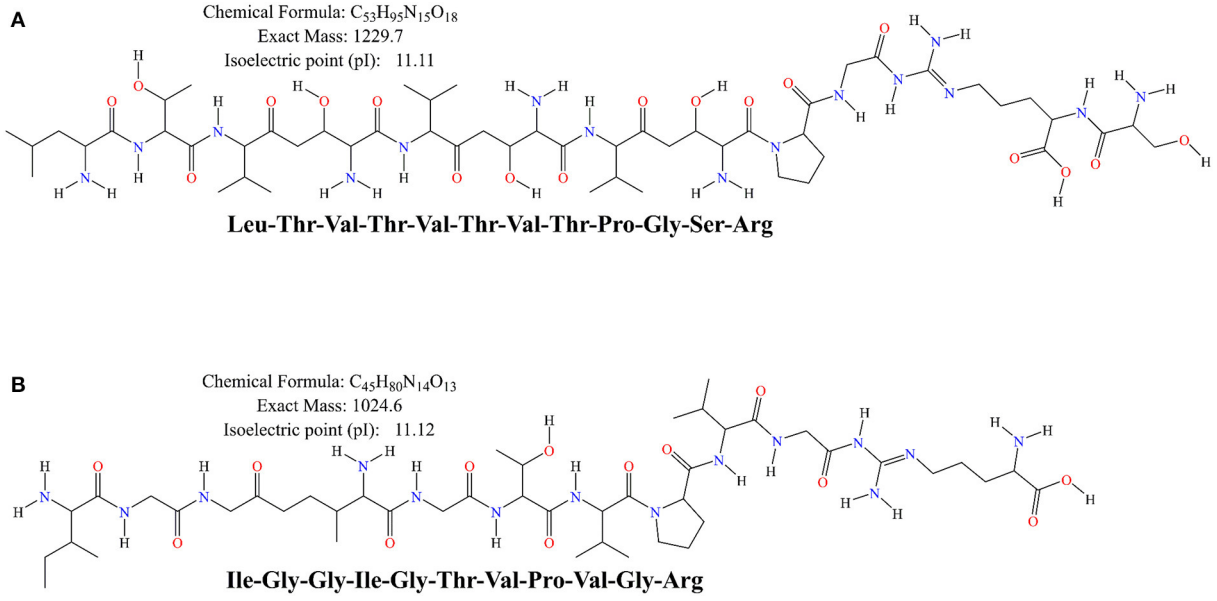

FIGURE 5
The primary structure of the peptides LTVTVTVTPGSR **(A)** and IGGIGTVPVGR **(B)** was generated by ChemBioDraw Ultra (13.0) software.

from fermented milk by ultrafiltration purification and LC-MS/MS and were validated for their activity. This research has the potential to be applied to the development of healthy antioxidant products from natural foods, and it provides a theoretical basis for functional food development and also offers a new practical basis for exploring bioactive food-derived peptides.

Data availability statement

The original contributions presented in the study are publicly available. The data presented in the study are deposited in the NCBI repository, accession number OP616039. This data can be found here: https://www.ncbi.nlm.nih.gov/nuccore/OP616039.1/.

Author contributions

JX: writing—original draft, data curation, investigation, methodology, and formal analysis. YC: conceptualization, writing—review and editing, data curation, formal analysis, investigation, and project administration. DP: conceptualization, project administration, funding acquisition, validation, and supervision. XF: data curation, methodology, and supervision. ZS: formal analysis, visualization, resources, and methodology. ML: resources and methodology. XZ: conceptualization and project administration. ZW: conceptualization and formal analysis. All authors contributed to the article and approved the submitted version.

Funding

This work was financially supported by Natural Science Funding of China (31972048), the National Key R&D Program of China (2021YFD2100104), and the National Natural Science Foundation of China (32272339).

Conflict of interest

The authors declare that the research was conducted in the absence of any commercial or financial relationships that could be construed as a potential conflict of interest.

Publisher's note

All claims expressed in this article are solely those of the authors and do not necessarily represent those of their affiliated organizations, or those of the publisher, the editors and the reviewers. Any product that may be evaluated in this article, or claim that may be made by its manufacturer, is not guaranteed or endorsed by the publisher.

Supplementary material

The Supplementary Material for this article can be found online at: https://www.frontiersin.org/articles/10.3389/fnut.2022.1041655/full#supplementary-material

References

1. Balasubramanian T, Arumugam M, Vimalraj V, Meenakshi S, Umayaparvathi SJP, Letters P. Isolation and structural elucidation of antioxidant peptides from Oyster (*Saccostrea cucullata*) protein hydrolysate. *Protein Pept Lett.* (2014) 21:1073–83. doi: 10.2174/0929866521666140417121616

2. Lobo V, Patil A, Phatak A, Chandra N. Free radicals, antioxidants and functional Foods: Impact on human health. *Pharmacogn Rev.* (2010) 4:118–26. doi: 10.4103/0973-7847.70902

3. Martínez-Martínez E, Souza-Neto FV, Jiménez-González S, Cachofeiro V. Oxidative stress and vascular damage in the context of obesity: the hidden guest. *Antioxidants.* (2021) 10:406. doi: 10.3390/antiox10030406

4. Janssen L, Allard NAE, Saris CGJ, Keijer J, Hopman MTE, Timmers S. Muscle toxicity of drugs: when drugs turn physiology into pathophysiology. *Physiol Rev.* (2020) 100:633–72. doi: 10.1152/physrev.00002.2019

5. Suetsuna K, Ukeda H, Ochi H. Isolation and characterization of free radical scavenging activities peptides derived from casein. *J Nutr Biochem.* (2000) 11:128–31. doi: 10.1016/S0955-2863(99)00083-2

6. Kieliszek M, Pobiega K, Piwowarek K, Kot AM. Characteristics of the proteolytic enzymes produced by lactic acid bacteria. *Molecules.* (2021) 26:1858. doi: 10.3390/molecules26071858

7. Pasolli E, De Filippis F, Mauriello IE, Cumbo F, Walsh AM, Leech J, et al. Large-scale genome-wide analysis links lactic acid bacteria from food with the gut microbiome. *Nat Commun.* (2020) 11:2610. doi: 10.1038/s41467-020-16438-8

8. Cui L, Yang G, Lu S, Zeng X, He J, Guo Y, et al. Antioxidant peptides derived from hydrolyzed milk proteins by Lactobacillus strains: a BIOPEP-UWM database-based analysis. *Food Res Int.* (2022) 156:111339. doi: 10.1016/j.foodres.2022.111339

9. Padghan PV, Mann B, Hati S. Purification and characterization of antioxidative peptides derived from fermented milk (*Lassi*) by lactic cultures. *Int J Pept Res Ther.* (2018) 24:235–49. doi: 10.1007/s10989-017-9608-2

10. Sodanlo A, Azizkhani M. Evaluation of antioxidant and antimicrobial activity of water-soluble peptides extracted from iranian traditional *Kefir*. *Int J Pept Res Ther.* (2021) 27:1441–9. doi: 10.1007/s10989-021-10181-4

11. Kumar S, Rajendran K, Kumar J, Hamwieh A, Baum M. Current knowledge in lentil genomics and its application for crop improvement. *Front Plant Sci.* (2015) 6:78. doi: 10.3389/fpls.2015.00078

12. Žilić S, Serpen A, Akillioglu G, Gökmen V, Vančetović J. Phenolic compounds, carotenoids, anthocyanins, and antioxidant capacity of colored maize (Zea mays L) kernels. *J Agr Food Chem.* (2012) 60:1224–31. doi: 10.1021/jf204367z

13. Chen JY, Sun XY, Ouyang JM. Modulation of calcium oxalate crystal growth and protection from oxidatively damaged renal epithelial cells of corn silk polysaccharides with different molecular weights. *Oxid Med Cell Longevity.* (2020) 2020:6982948. doi: 10.1155/2020/6982948

14. Wang L, Lu W, Li J, Hu J, Ding R, Lv M, et al. Optimization of ultrasonic-assisted extraction and purification of zeaxanthin and lutein in corn gluten meal. *Molecules.* (2019) 24:2994. doi: 10.3390/molecules24162994

15. Li Y, Liu H, Liu Q, Kong B, Diao X. Effects of zein hydrolysates coupled with sage (salvia officinalis) extract on the emulsifying and oxidative stability of myofibrillar protein prepared oil-in-water emulsions. *Food Hydrocoll.* (2019) 87:149–57. doi: 10.1016/j.foodhyd.2018.07.052

16. Hu R, Chen G, Li Y. Production and characterization of antioxidative hydrolysates and peptides from corn gluten meal using papain, ficin, and bromelain. *Molecules.* (2020) 25:4091. doi: 10.3390/molecules25184091

17. Jorge DG, Margarita OM, Oscar A, Silverio GL, Fabiola TJM. Antioxidant activity of zein hydrolysates from zea species and their cytotoxic effects in a hepatic cell culture. *Molecules.* (2018) 23:312. doi: 10.3390/molecules23020312

18. Zhuang H, Tang N, Yuan Y. Purification and identification of antioxidant peptides from corn gluten meal. *J Funct Foods.* (2013) 5:1810–21. doi: 10.1016/j.jff.2013.08.013

19. Jiang X, Liu X, Xu H, Sun Y, Zhang Y, Wang Y. Improvement of the nutritional, antioxidant and bioavailability properties of corn gluten-wheat bran mixture fermented with lactic acid bacteria and acid protease. *LWT.* (2021) 144:111161. doi: 10.1016/j.lwt.2021.111161

20. Karlsson JO, Ostwald K, Kabjorn C, Andersson M. A method for protein assay in Laemmli buffer. *Anal Biochem.* (1994) 219:144–6. doi: 10.1006/abio.1994.1243

21. The Ministry of Health of the People's Republic of China. GB 5413.34-2010. *Determination of Acidity in Milk and Milk Products*. The Ministry of Health of the People's Republic of China: Beijing, China (2010).

22. Sodini I, Montella J, Tong PS. Physical properties of yogurt fortified with various commercial whey protein concentrates. *J Sci Food Agric.* (2005) 85:853–9. doi: 10.1002/jsfa.2037

23. Aubi O, Prestegard KS, Jung-Kc K, Shi TS, Ying M, Grindheim AK, et al. The Pah-R261Q mouse reveals oxidative stress associated with amyloid-like hepatic aggregation of mutant phenylalanine hydroxylase. *Nat Commun.* (2021) 12:2073. doi: 10.1038/s41467-021-22107-1

24. Conlon M, Poltorack CD, Forcina GC, Armenta DA, Mallais M, Perez MA, et al. Compendium of kinetic modulatory profiles identifies ferroptosis regulators. *Nat Chem Biol.* (2021) 17:665–74. doi: 10.1038/s41589-021-00751-4

25. Sinsuwan S, Rodtong S, Yongsawatdigul J. Hydrolytic activity of *Virgibacillus* sp. SK37, a starter culture of fish sauce fermentation, and its cell-bound proteinases. *World J Microbiol Biotechnol.* (2012) 28:2651–9. doi: 10.1007/s11274-012-1075-5

26. Wu Z, Wang P, Pan D, Zeng X, Guo Y, Zhao G. Effect of adzuki bean sprout fermented milk enriched in gamma-aminobutyric acid on mild depression in a mouse model. *J Dairy Sci.* (2021) 104:78–91. doi: 10.3168/jds.2020-19154

27. Hueso D, Fontecha J, Gómez-Cortés P. Comparative study of the most commonly used methods for total protein determination in milk of different species and their ultrafiltration products. *Front Nutr.* (2022) 9:925565. doi: 10.3389/fnut.2022.925565

28. Yuan L, Chu Q, Wu X, Yang B, Zhang W, Jin W, Gao R. Anti-inflammatory and antioxidant activity of peptides from ethanol-soluble hydrolysates of sturgeon (*Acipenser schrenckii*) cartilage. *Front Nutr.* (2021) 8:689648. doi: 10.3389/fnut.2021.689648

29. Villa O, Brookes SJ, Thiede B, Heijl L, Lyngstadaas SP, Reseland JE. Subfractions of enamel matrix derivative differentially influence cytokine secretion from human oral fibroblasts. *J Tissue Eng.* (2015) 6. doi: 10.1177/2041731415575857

30. Zhong J, Yang R, Cao X, Liu X, Qin X. Improved physicochemical properties of yogurt fortified with fish Oil/γ-Oryzanol by nanoemulsion technology. *Molecules.* (2018) 23:56. doi: 10.3390/molecules23010056

31. Islam SMR, Tanzina AY, Foysal MJ, Hoque MN, Rumi MH, Siddiki A, et al. Insights into the nutritional properties and microbiome diversity in sweet and sour yogurt manufactured in Bangladesh. *Sci Rep.* (2021) 11:22667. doi: 10.1038/s41598-021-01852-9

32. Geidam YA, Ambali AG, Onyeyili P. Phytochemical screening and antibacterial properties of organic solvent fractions of psidium guajava aqueous leaf extracts. *Int J Pharmacol.* (2007) 3:68–73. doi: 10.3923/ijp.2007.68.73

33. Chen ML, Ning P, Jiao Y, Xu Z, Cheng YH. Extraction of antioxidant peptides from rice dreg protein hydrolysate via an angling method. *Food Chem.* (2021) 337:128069. doi: 10.1016/j.foodchem.2020.128069

34. Bachmann H, Pronk JT, Kleerebezem M, Teusink B. Evolutionary engineering to enhance starter culture performance in food fermentations. *Curr Opin Biotech.* (2015) 32:1–7. doi: 10.1016/j.copbio.2014.09.003

35. Sah B, Vasiljevic T, Mckechnie S, Donkor O. Antioxidative and antibacterial peptides derived from bovine milk proteins. *Crit Rev Food Sci Nutr.* (2016) 24:726–40. doi: 10.1080/10408398.2016.1217825

36. Liu M, Liu M, Yang S, Shen C, Wang X, Liu W, et al. Fermented milk of cheese-derived *Lactobacillus delbrueckii* subsp. bulgaricus displays potentials in alleviating alcohol-induced hepatic injury and gut dysbiosis in mice. *Food Res Int.* (2022) 157:111283. doi: 10.1016/j.foodres.2022.111283

37. Law BA, Kolstad J. Proteolytic systems in lactic acid bacteria. *Antonie Van Leeuwenhoek.* (1983) 49:225–45. doi: 10.1007/BF00399500

38. Kudo H, Sasaki Y. Intracellular pH determination for the study of acid tolerance of lactic acid bacteria. *Methods Mol Biol.* (2019) 1877:33—41. doi: 10.1007/978-1-4939-8907-2_4

39. Fan X, Li X, Zhang T, Guo Y, Shi Z, Wu Z, Zeng X, Pan D. Novel millet-based flavored yogurt enriched with superoxide dismutase. *Front Nutr.* (2022) 8:791886. doi: 10.3389/fnut.2021.791886

40. Ortiz-Martinez M, Winkler R, García-Lara S. Preventive and therapeutic potential of peptides from cereals against cancer. *J Proteomics.* (2014) 111:165–83. doi: 10.1016/j.jprot.2014.03.044

41. Zhu B, He H, Hou T, Safety F. A comprehensive review of corn protein-derived bioactive peptides: Production, characterization, bioactivities, transport pathways. *Compr Rev Food Sci Food Saf.* (2018) 22:329–45. doi: 10.1111/1541-4337.12411

42. Balthazar CF, Guimarães JF, Coutinho NM, Pimentel TC, Ranadheera CS, Santillo A, et al. The future of functional food: Emerging technologies application

on prebiotics, probiotics and postbiotics. *Compr Rev Food Sci Food Saf.* (2022) 21:2560–86. doi: 10.1111/1541-4337.12962

43. Pein H, Ville A, Pace S, Temml V, Garscha U, Raasch M, et al. Endogenous metabolites of vitamin E limit inflammation by targeting 5-lipoxygenase. *Nat Commun.* (2018) 9:3834. doi: 10.1038/s41467-018-06158-5

44. Hernández-Ledesma B, Miralles B, Amigo L, Ramos M, Recio I. Identification of antioxidant and ACE-inhibitory peptides in fermented milk. *J Sci Food Agric.* (2010) 85:1041–8. doi: 10.1002/jsfa.2063

45. Onuh JO, Girgih AT, Aluko RE, Aliani M. *In vitro* antioxidant properties of chicken skin enzymatic protein hydrolysates and membrane fractions. *Food Chem.* (2014) 150:366–73. doi: 10.1016/j.foodchem.2013.10.107

46. Li YW, Bo L, He J, Ping Q. Quantitative structure–activity relationship study of antioxidative peptide by using different sets of amino acids descriptors. *J Mol Struct.* (2011) 998:53–61. doi: 10.1016/j.molstruc.2011.05.011

47. Tonolo F, Fiorese F, Moretto L, Folda A, Scalcon V, Grinzato A, et al. Identification of new peptides from fermented milk showing antioxidant properties: mechanism of action. *Antioxidants.* (2020) 9:117. doi: 10.3390/antiox9020117

48. Rana S, Bajaj R, Mann B. Characterization of antimicrobial and antioxidative peptides synthesized by *L. rhamnosus* C6 fermentation of milk. *Int J Pept Res Ther.* (2017) 24:1–13. doi: 10.1007/s10989-017-9616-2

49. Qi Q, Zhang G, Wang W, Sadiq FA, Zhang Y, Li X, Chen Q, Xia Q, Wang X, Li Y. Preparation and antioxidant properties of germinated soybean protein hydrolysates. *Front Nutr.* (2022) 9:866239. doi: 10.3389/fnut.2022.866239

50. Rival SG, Fornaroli S, Boeriu CG, Wichers H. Caseins and casein hydrolysates. 1 Lipoxygenase inhibitory properties. *J Agric Food Chem.* (2001) 49:287–94. doi: 10.1021/jf000392t

51. Rajapakse N, Mendis E, Jung WK, Je JY, Kim S. Purification of a radical scavenging peptide from fermented mussel sauce and its antioxidant properties. *Food Res Int.* (2005) 38:175–82. doi: 10.1016/j.foodres.2004.10.002

52. Chen Y, Zheng Z, Ai Z, Zhang Y, Tan CP, Liu Y. Exploring the antioxidant and structural properties of Black Bean protein hydrolysate and Its peptide fractions. *Front Nutr.* (2022) 9:884537. doi: 10.3389/fnut.2022.884537

53. Lu J, Guo Y, Muhmood A, Zeng B, Qiu Y, Wang P, et al. Probing the antioxidant activity of functional proteins and bioactive peptides in *Hermetia illucens* larvae fed with food wastes. *Sci Rep.* (2022) 12:2799. doi: 10.1038/s41598-022-06668-9

54. Karami Z, Peighambardoust SH, Hesari J, Akbari Adergani B, Andreu D. Identification and synthesis of multifunctional peptides from wheat germ hydrolysate fractions obtained by proteinase K digestion. *J Food Biochem.* (2019) 43:e12800. doi: 10.1111/jfbc.12800

55. Pownall TL, Udenigwe CC, Aluko R, Chemistry F. Amino acid composition and antioxidant properties of pea seed (*Pisum sativum* L) enzymatic protein hydrolysate fractions. *J Agric Food Chem.* (2010) 58:4712. doi: 10.1021/jf904456r

56. Elias RJ, Kellerby SS, Decker E. Antioxidant activity of proteins and peptides. *Crit Rev Food Sci Nutr.* (2008) 48:430–41. doi: 10.1080/10408390701425615

57. Siow HL, Gan C. Extraction of antioxidative and antihypertensive bioactive peptides from *Parkia speciosa* seeds. *Food Chem.* (2013) 141:3435–42. doi: 10.1016/j.foodchem.2013.06.030

58. Virtanen T, Pihlanto A, Akkanen S, Korhonen H. Development of antioxidant activity in milk whey during fermentation with lactic acid bacteria. *J Appl Microbiol.* (2010) 102:106–15. doi: 10.1111/j.1365-2672.2006.03072.x

59. Gupta A, Mann B, Kumar R, Sangwan RB. Antioxidant activity of Cheddar cheeses at different stages of ripening. *Int J Dairy Technol.* (2009) 62:339–47. doi: 10.1111/j.1471-0307.2009.00509.x

60. Ali E, Nielsen SD, Abd-El Aal S, El-Leboudy A, Saleh E, LaPointe G. Use of mass spectrometry to profile peptides in whey protein isolate medium fermented by *Lactobacillus helveticus* LH-2 and *Lactobacillus acidophilus* La-5. *Front Nutr.* (2019) 6:152. doi: 10.3389/fnut.2019.00152

61. Farvin K, Baron CP, Nielsen NS, Jacobsen C. Antioxidant activity of yoghurt peptides: Part 1-*in vitro* assays and evaluation in ω-3 enriched milk. *Food Chem.* (2010) 123:1081–9. doi: 10.1016/j.foodchem.2010.05.067

frontiers | Frontiers in Nutrition

TYPE Review
PUBLISHED 06 December 2022
DOI 10.3389/fnut.2022.1036295

Check for updates

OPEN ACCESS

EDITED BY
Wenjie Sui,
Tianjin University of Science and Technology, China

REVIEWED BY
Paucean Adriana,
University of Agricultural Sciences and Veterinary Medicine of Cluj-Napoca, Romania
Dmitriy Shcherbakov,
Altai State University, Russia
Khalid Z. Masoodi,
Sher-e-Kashmir University of Agricultural Sciences and Technology, India
Songfeng Diao,
Chinese Academy of Forestry, China

*CORRESPONDENCE
Xiaoyun Chai
chaixy1207@smmu.edu.cn
Guige Hou
houyun820424@bzmc.edu.cn
Qingguo Meng
qinggmeng@ytu.edu.cn

SPECIALTY SECTION
This article was submitted to Nutrition and Food Science Technology, a section of the journal Frontiers in Nutrition

RECEIVED 04 September 2022
ACCEPTED 22 November 2022
PUBLISHED 06 December 2022

CITATION
Wang Z, Zhao F, Wei P, Chai X, Hou G and Meng Q (2022) Phytochemistry, health benefits, and food applications of sea buckthorn (*Hippophae rhamnoides* L.): A comprehensive review.
Front. Nutr. 9:1036295.
doi: 10.3389/fnut.2022.1036295

COPYRIGHT
© 2022 Wang, Zhao, Wei, Chai, Hou and Meng. This is an open-access article distributed under the terms of the Creative Commons Attribution License (CC BY). The use, distribution or reproduction in other forums is permitted, provided the original author(s) and the copyright owner(s) are credited and that the original publication in this journal is cited, in accordance with accepted academic practice. No use, distribution or reproduction is permitted which does not comply with these terms.

Phytochemistry, health benefits, and food applications of sea buckthorn (*Hippophae rhamnoides* L.): A comprehensive review

Zhen Wang[1], Fenglan Zhao[1], Panpan Wei[1], Xiaoyun Chai[2]*, Guige Hou[3]* and Qingguo Meng[1]*

[1]Key Laboratory of Molecular Pharmacology and Drug Evaluation (Yantai University), Ministry of Education, Collaborative Innovation Center of Advanced Drug Delivery System and Biotech Drugs in Universities of Shandong, School of Pharmacy, Yantai University, Yantai, China, [2]Department of Organic Chemistry, School of Pharmacy, Naval Medical University, Shanghai, China, [3]School of Pharmacy, Binzhou Medical University, Yantai, China

Sea buckthorn (*Hippophae rhamnoides* L.), an ancient miraculous plant, is of great interest because of its tenacity, richness in nutritional active substances, and biological activity. Sea buckthorn is a deciduous shrub or tree of the genus *Hippophae* in the family *Elaeagnaceae*. It is a pioneer tree species for soil improvement, wind and sand control, and soil and water conservation. Sea buckthorn contains many nutritional active components, such as vitamins, carotenoids, polyphenols, fatty acids, and phytosterols. Moreover, sea buckthorn has many health benefits, such as antioxidant, anticancer, anti-hyperlipidemic, anti-obesity, anti-inflammatory, antimicrobial, antiviral, dermatological, neuroprotective, and hepatoprotective activities. Sea buckthorn not only has great medicinal and therapeutic potential, but also is a promising economic plant. The potential of sea buckthorn in the human food industry has attracted the research interest of researchers and producers. The present review mainly summarizes the phytochemistry, nutrients, health benefits, and food applications of sea buckthorn. Overall, sea buckthorn is a dietary source of bioactive ingredients with the potential to be developed into functional foods or dietary supplements for the prevention and treatment of certain chronic diseases, which deserves further research.

KEYWORDS

sea buckthorn, phytochemistry, nutrients, health benefits, food applications

Introduction

Sea buckthorn (*Hippophae rhamnoides* L.) is a deciduous shrub or tree that is also known as Siberian pineapple, sand thorn, sea berry, and sallow thorn (1). *Hippophae* L. originated in the Hengduan Mountains and East Himalayas area and is widely distributed in the temperate regions of Eurasia (2). Every part of this plant (fruits, leaves, stems, branches, roots, and thorns) has been traditionally used in medicine, nutritional supplement, soil and moisture conservation, and the establishment of wildlife habitats. Therefore, sea buckthorn is popularly known as "Wonder Plant," "Golden Bush," or "Gold Mine" (3).

Since the 1940s, Russian scientists have researched the bioactive substances in the berries, leaves and bark of sea buckthorn, leading to the development of sea buckthorn foods and radiation protection creams for Russian cosmonauts (4). Sea buckthorn contains nearly 200 nutritional and bioactive compounds and is known as a "natural vitamin treasure house" and a "source of nutrition and health care" (5, 6). Sea buckthorn is therefore widely used by the food industry in the preparation of breads, yogurts, jams, beverages, teas and other products (7–9). The medicinal value of sea buckthorn has been recorded in the Tibetan medical classic "Somaratsa," dating back to as early as the first half of the eighth century (10). Sea buckthorn has been extensively exploited in the folklore treatment of slow digestion, stomach malfunctioning, cardiovascular problems, liver injury, skin diseases, and ulcers (11). In recent years, there have been numerous reports on the pharmacological activities of sea buckthorn, including its anticancer, anti-inflammatory, antimicrobial and antiviral activities, and its ability to act in cardiovascular protection (12–16). There is no doubt that sea buckthorn has great medicinal and therapeutic potential, which may be attributed to the fact that sea buckthorn contains several vitamins, carotenoids, polyphenols, and fatty acids (17–20).

Sea buckthorn is a plant of ecological and economic importance. To promote the role of sea buckthorn in environmental protection, economic development, and human health, the International Sea Buckthorn Association (ISA) was established in 1999 by China, India, Canada, and other countries. In recent years, more countries have become aware of the therapeutic potential of sea buckthorn, and many countries are beginning to recognize and develop a sea buckthorn industry. According to statistics, as of December 2020, sea buckthorn had been distributed to 52 countries around the world, with a total area of 2.33 million hm^2. Among this distribution, about 2.1 million hm^2 is found within China and the rest is in other countries (21). With the increase of sea buckthorn planting and production, more attention should be paid to the exploitation and utilization of sea buckthorn. Thus, the present review aims to provide a comprehensive overview of the phytochemistry, nutritional and bioactive compounds, health benefits and food applications of sea buckthorn for reference by industrial manufacturers and researchers.

Botanical description

Morphology

Sea buckthorn is a deciduous tree or shrub of the *Elaeaceae* family and *Hippophae* L. genus (**Figure 1**). It is generally 1–8 m high, with some plants growing up to 18 m tall. The leaves are lanceolate or linear, usually 3–8 cm long and less than 7 mm wide. The upper surface of the leaves is dark gray, and the lower surface is distinct silver-gray (22). The fruits are spherical or oblate with a diameter of 5–8 mm. There are usually several fruits stuck together. The fruit is orange-yellow or brownish-red in color and has a ruffled surface. The pulp is oily and soft in texture. The seeds of sea buckthorn are about 4 mm long, 2 mm wide, and obliquely ovate. The seeds are brown and shiny, with a longitudinal groove in the middle. The seed coat is hard, and the seed kernel is creamy white (**Figure 1**) (23).

Taxonomy

On the basis of the analysis of morphological variation, Arne Rousi classified *Hippophae* L. ($2n = 24$) into three species, *H. rhamnoides* L., *H. salicifolia* D. Don, and *H. tibetana* Schlecht. *H. rhamnoides* is divided into nine subspecies, which include the ssp. *carpatica* Rousi, ssp. *caucasica* Rousi, ssp. *gyantsensis* Rousi, ssp. *mongolica* Rousi, ssp. *sinensis* Rousi, ssp. *turkestanica* Rousi, ssp. *yunnanensis* Rousi, ssp. *rhamnoides*, and ssp. *fluviatilis* van Soest (24). Liu and He described a fourth species, *H. neurocarpa.* Liu and He, found on the Qinghai-Tibet Plateau of China (25). However, taxonomists still disagree on the precise classification of the genus *Hippophae*. Chinese scientist Hu has updated and improved the classification system and revised *Hippophae* L. into 6 species and 17 subspecies (**Table 1**) (26).

Nutrients and bioactive compounds

Sea buckthorn contains nearly 200 nutrients and bioactive components (5). Many of the components are well known for their health benefits. Vitamin C is a very important nutrient in sea buckthorn. Carotenoids and polyphenolic compounds, especially phenolic acids and flavonoids, are the main bioactive and antioxidant components of sea buckthorn (27). The fatty acids, phytosterols, organic acids, amino acids, and minerals contained in sea buckthorn also play an important role. The nutrients and bioactive composition content of sea buckthorn influence its health value (28). The nutritional and

FIGURE 1
Sea buckthorn in different periods.

bioactive composition of sea buckthorn fruit varies considerably depending on genetic variation, the part analyzed, climatic, and growth conditions, year of harvest, degree of maturity, storage conditions, harvest time, and processing and analytic methods (29). **Tables 2, 3** show the main nutrients and bioactive components in sea buckthorn fruits, respectively.

TABLE 1 Classification of *Hippophae* Linn.

Genus	Section	Species	Subspecies
Hippophae L.	*Hippophae*	*Hippophae salicifolia*	
		Hippophae rhamnoides	ssp. *sinensis*
			ssp. *yunnanensis*
			ssp. *turkestanica*
			ssp. *mongolica*
			ssp. *caucasica*
			ssp. *carpatica*
			ssp. *rhamnoides*
			ssp. *fluviatilis*
	Gyantsenses	*Hippophae goniocarpa*	ssp. *litangensis*
			ssp. *goniocarpa*
		Hippophae gyantsensis	ssp. *litangensis*
			ssp. *gyantsensis*
		Hippophae neurocarpa	ssp. *stellatopilosa*
			ssp. *neurocarpa*
		Hippophae tibetana	ssp. *tibetana*

Nutrients

Vitamins and minerals

The quality of sea buckthorn fruit is often based on its nutritional value (29). Known as a "natural treasure trove of vitamins," sea buckthorn is undoubtedly rich in vitamins (6). The vitamin C content of sea buckthorn fruits ranges from 52.86 to 896 mg/100 g (28, 29). It has been showed that the vitamin C content of 100 g of sea buckthorn berries (275 mg) is much higher than the equivalent quantity of mango (27.7 mg), apricot (10 mg), banana (8.7 mg), orange (50 mg), and peach (6.6 mg) (17). In addition, sea buckthorn berries contain vitamin A, vitamin E, riboflavin, niacin, pantothenic acid, vitamin B_6, and vitamin B_{12}. Mineral elements are involved in the formation of human tissues and the maintenance of normal physiological functions. Sea buckthorn berries contain many minerals, e.g., phosphorus, iron, magnesium, boron, calcium, aluminum, potassium and others (30, 31). Significant differences in the mineral content of sea buckthorn fruits have been reported at its different stages of maturity. The highest content of calcium, magnesium and phosphorus was found in ripe sea buckthorn fruits with 68.28, 145.67, and 457.7 mg/kg, respectively (32).

Carbohydrates

As the main component of dry matter, carbohydrates play numerous essential roles in living organisms. Monosaccharides are the main source of energy for human metabolism with

TABLE 2 Nutrients in sea buckthorn fruits.

Class	Compounds	Content	Analytical method	Specie/varieties	Location	References
Vitamin (mg/100 g)	Vitamin C	275	HPLC	–	Ladakh	(17)
	Vitamin E	3.54				
	Vitamin B_{12}	5.4				
	Riboflavin	1.45				
	Vitamin B_6	1.12				
	Niacin	68.4				
	Vitamin A	432.4 IU/100 g				
	Pantothenic acid	0.85 mcg/100 g				
Mineral	Phosphorus (P)	491	HPLC	Wild	Iran	(30)
(mg/kg DW)	Potassium (K)	1,674				
	Calcium (Ca)	1,290				
	Magnesium (Mg)	990				
	Iron (Fe)	291				
	Zinc (Zn)	29.77				
	Manganese (Mn)	108.37				
	Copper (Cu)	17.87				
(mg/kg DM)	Boron (B)	13.61–16.3	ICP-AES	Wild ssp. *rhamnoides* and Mažeikiai	Lithuania	(31)
	Nickel (Ni)	0.41–0.49	GFAAS			
	Cadmium (Cd)	0.023–0.045				
	Lead (Pb)	0.034–0.038				
Organic acid (mg/100 g)	L-malic acid	26.45	HPLC	Botanicheskaya	Japan	(38)
	D-malic acid	22.90				
	Succinic acid	6.96				
	Citric acid	2.01				
	Tartaric acid	5.39				
	Quininic acid	16.00				
	Pyruvic acid	0.32				
	Acetic acid	0.08				
	Formic acid	1.94				
	Oxalic acid	10–20	HPLC, UPLC	Aromatnaja, Botaniczeskaja-Lubitelskaja, Józef, Luczistaja, Moskwiczka, and Podarok Sadu	Poland	(34)
	Isocitric acid	20–21				
Amino acid (mg/100 g)	Aspartic acid	240–560	HPLC	Shenqiuhong, Wucifeng, Xinjiyihao, Xinjierhao	China	(37)
	Serine	11–80				
	Glutamic acid	260–360				
	Glycine	60–80				
	Alanine	56–92				
	Cysteine	20–41				
	Tyrosine	38–51				
	Histidine	56–62				
	Arginine	130–180				
	Proline	64–130				
	Threonine	47–63				
	Valine	74–92				
	Methionine	11–20				
	Isoleucine	52–80				
	Leucine	90–130				
	Phenylalanine	60–82				
	Lysine	78–93				
	Total	1,460–2,190				

"–" indicates that the value is not available. DW, dry weight basis; DM, dry matter basis.

TABLE 3 Main bioactive components in sea buckthorn fruits.

Class	Compounds	Content	Analytical method	Specie/varieties	Location	References
Carotenoids (mg/100 g DW)	Lutein	1.4–2.1	HPLC-PAD	ssp. *Carpatica* (Victoria, Tiberiu, Sf. Gheorghe, Serpenta, Serbanesti 4, and Ovidiu)	Carpathians	(18)
	Zeaxanthin	1.8–2.5				
	β-Cryptoxanthin	1.3–1.6				
	δ-Carotene	1.4–1.9				
	α-Carotene	0.9–1.6				
	γ-Carotene	1.6–1.8				
	Cis β-Carotene	1.3–2.1				
	β-Carotene	1.9–7.5				
(mg/100 g)	Lycopene	13–20	UV/VIS	–	Iran	(29)
(mg/100 g DM)	Xanthophylls	37.76–80.73	UPLC	Aromatnaja, Botaniczeskaja-Lubitelskaja, Józef, Luczistaja, Moskwiczka, and Podarok Sadu	Poland	(34)
	Total carotenoids	53–97		ssp. *Carpatica*	Carpathians	(18)
Polyphenols (mg/kg DM)	Phenolic acid	51.8–89.4	UPLC	Aromatnaja, Botaniczeskaja-Lubitelskaja, Józef, Luczistaja, Moskwiczka, and Podarok Sadu	Poland	(34)
		3,570–4,439	GC-MS	Nadba, ltycka, Nevlejena, Otradnaja, Podarok, Sadu, Trofimowskaja, and Hybrid 29–88	Poland and Byelorussia	(46)
	Ferulic acid	5.1–17.8				
	Gallic acid	1.0–4.6				
	Vanillic acid	1.4–8.4				
	Caffeic acid	0.9–6.7				
	Protocatechuic acid	0.7–4.3				
	m-Coumaric	0.3–6.1				
	o-Coumaric	2.2–13.3				
	p-Coumaric acid	1.4–9.8				
	Quinic	3.5–193.9				
	Cinnamic	0.8–803.9				
	2,5-Dihydroxybenzoic	0.1–3.1				
	3,4-Dihydroxycinnamic	5.9–27.3				
	Pyrocatechuic	0.2–32.1				
	Salicylic	21–47.5				
	p-Hydroxyphenyl-lactic	5.3–24.7				
	Veratric	3.3–63				
	Hydroxycaffeic	9.1–58.5				
	Syringic	2.5–12.8				
(mg/kg FW)	flavonoid	381–616	RP-HPLC	Avgustinka, Botanièeskaja, Botanièeskaja Liubitelskoje, Hibrid perèika, Julia, Nivelena-1, Nivelena-2, Otradnaja, Padarok sadu, Trofimovskaja, Vorobjevskaja	Lithuania	(49)
	quercetin-3-O-rutinoside	99–280				
	isorhamnetin-3-O-rutinoside	102–229				
	isorhamnetin-3-O-glucoside	83–195				
(mg/mL)	Catechin	8.51	HPLC	Botanicheskaya	Japan	(38)
	Rutin	9.45				
	Quercetin	5.16				
(mg/100 g DW)	Isorhamnetin	10.3–15.1	RP-HPLC	ssp. *sinensis*, ssp. *yunnanensis*, ssp. *mongolica*, ssp. *turkestanica*	China	(48)
	Kaempferol	1.02–1.5				

(Continued)

TABLE 3 (Continued)

Class	Compounds	Content	Analytical method	Specie/varieties	Location	References
	Quercetin-3-*O*-rutinoside	23–44.6				
	Quercetin-3-*O*-glucoside	31.2–49.5				
	Isorhamnetin-3-*O*-rutinoside	38.7–84.0				
	Isorhamnetin-3-*O*-glucoside	7.61–26.0				
	Kaempferol-3-*O*-sophoroside-7-*O*-rhamnoside	34.1–61.6				
	Isorhamnetin-3-*O*-sophoroside-7-*O*-rhamnoside	15.2–74.6				
	Isorhamnetin-3-*O*-glucoside-7-*O*-rhamnoside	112–187				
Fatty acids (g/kg)	Myristic (C14:0)	2–2.6	GC	wild ssp. *rhamnoides* and Mažeikiai	Lithuania	(31)
	Pentadecanoic (C15:0)	0.93–2.23				
	Palmitic (C16:0)	223.2–227.2				
	Margaric (C17:0)	0.56–0.86				
	Stearic (C18:0)	13.25–17.86				
	Arachidic (C20:0)	2.81–3.72				
	Henicosanoic (C21:0)	0.73–1.54				
	Behenic (C22:0)	1.09–2.28				
	Lignoceric (C24:0)	0.60–0.93				
	Myristoleic (C14:1)	0.31–1.53				
	Pentadecenoate (C15:1)	0.00–0.60				
	Palmitoleic (C16:1 n-7)	134.6–185.0				
	Hexadecenoic (C16:1 n-9)	0.80–0.91				
	Margaroleic (C17:1)	0.44–0.71				
	Oleic (C18:1 n-9)	255.5–264.1				
	cis-Vaccenic (C18:1 n-7)	56.52–65.61				
	Eicosenoic (C20:1 n-9)	2.50–2.73				
	Erucic (C22:1 n-9)	1.06–1.07				
	Nervonic (C24:1 n-9)	1.00–1.51				
	Linoleic (C18:2 n-6)	127.0–163.5				
	γ-Linolenic (C18:3 n-6)	0.30–0.60				
	α-Linolenic (C18:3 n-3)	100.3–109.8				
	Docosatetraenoic (C22:4 n-6)	3.90–4.41				
	Docosapentaensyre (C22:5 n-3)	2.53–2.60				
Phytosterols (μg/100 mL)	Squalene	885.71–2714.37	GC	ssp. *Mongolica* (Aromatnaja, Avgustinka, Botaniczeskaja, Botaniczeskaja Ljubitelskaja, Luczistaja, Moskwiczanka, Podarok Sadu, and Porozrachnaja)	Poland	(28)
	Kampesterol	44.37–201.32				
	Stigmasterol	24.08–68.22				
	β-Sitosterol	2036.14–6145.58				
	Sitostanol	96.50–254.67				
	Δ^5-Avenasterol	114.93–377.56				
	α-Amyrin	110.48–314.52				
	Cycloarteno	293.49–474.38				
	Δ^7-Avenasterol	80.80–194.97				
	28-Methylobtusifoliol	70.88–251.85				
	24-Methylenecycloartanol	1454.21–4048.89				
	Erythrodiol	284.02–818.75				
	Citrostadienol	212.97–663.22				
	Friedelan-3-ol	232.89–737.28				
	Total	6168.24–13378.22				

FW, fresh weight basis; DW, dry weight basis; DM, dry matter basis.

polysaccharides acting as structural components and the main storage form of energy (33). Sugar content determines the sweetness of the juice. It has been reported that sea buckthorn fruits contain 1.34–2.87 g/100 g FW of sugar. The sugar with the highest content is glucose, accounting for 86.58–92.68% of the total sugar content (34). A study on the sugar composition of three German sea buckthorn varieties reported that the contents of glucose, fructose, and mannitol are 11.95–15.26 mg/mL, 1.75–6.75 mg/mL, and 1.32–6.21 mg/mL, respectively. The sugar content varies among varieties (35).

Organic acids and amino acids

Sea buckthorn fruit contains several organic acids and their derivatives. These organic acid derivatives can promote bone differentiation and contribute to the differentiation of mesenchymal stem cells into osteoblasts (36). Different species of sea buckthorn have different types and concentrations of organic acids. For example, subspecies of Russian sea buckthorn exhibit relatively low total acidity, with organic acid concentrations of 2.1–3.2 g/100 mL. Finnish genotypes were in the middle, ranging from 4.2 to 6.5 g/100 mL, whereas Chinese genotypes showed the highest organic acid concentration, with values between 3.5 and 9.1 g/100 mL (37). It has been reported that sea buckthorn juice contains nine organic acids, namely quinic acid, L-malic acid, D-malic acid, succinic acid, pyruvic acid, tartaric acid, acetic acid, formic acid, and citric acid (38). Another study on six sea buckthorn varieties in Poland detected oxalic acid and isocitric acid (34).

Furthermore, sea buckthorn is rich in amino acids, which are indispensable to the human body. Amino acids are the basic units that make up proteins and are closely related to life activities. Seventeen amino acids, including seven essential amino acids (threonine, valine, methionine, isoleucine, leucine, phenylalanine, and lysine), have been detected in sea buckthorn fruits (39), leaves, branches and seeds (40). The amino acid content in sea buckthorn seeds is 18.63%, in leaves 15.41%, in branches 11.62%, and in fruits 6.89%. The content of aspartic acid and glutamic acid were highest in sea buckthorn fruits, leaves, and branches, with 1.11 and 1.24% in fruits, 2.42 and 1.60% in leaves, and 3.71 and 0.97% in branches. The highest content of tyrosine and glutamic acid can be found in sea buckthorn seeds, at 4.72 and 3.42%, respectively (40).

Bioactive compounds

Carotenoids

Sea buckthorn fruits contain high levels of carotenoids, which give sea buckthorn its characteristic orange-yellow color. Carotenoids mainly act as antioxidants, although they also have other roles. For example, β-carotene is the precursor of vitamin A, and lutein/zeaxanthin constitutes the macular pigment of the eye (41). Carotenoids are considered to have health benefits and can reduce the risk of diseases, especially cancers and eye diseases (42). The content of carotenoids in different species and different parts of sea buckthorn varies greatly. Teleszko et al. (28) detected an average of 11 mg/100 g FW of total carotenoids in eight species of Russian sea buckthorn. In another study on six Romanian sea buckthorn varieties (*H. rhamnoides* ssp. *carpatica*), total carotenoid content ranged from 53 to 97 mg/100 g DW in berries, and ranged from 3.5 to 4.2 mg/100 g DW in leaves (18). β-Carotene is the main carotenoid in sea buckthorn. The percentage of β-carotene is 15–55% in berries, and 26–34% in the peel, pulp, and seed oil (28, 43). In addition, carotenoids include γ-carotene, *cis*-lycopene, lycopene, *cis*-γ-carotene, β-cryptoxanthin, α-carotene, and so on.

Polyphenols

Polyphenols are the main compounds with antioxidant activity in sea buckthorn. It has been reported that the polyphenol content in the fruit ranges from 12.36 to 34.6 mg GAE/g (GAE, gallic acid equivalents), higher than that in oranges (1.27 mg GAE/g) mandarins (1.16 mg GAE/g), blueberries (2.19 mg GAE/g), sour cherries (2.56 mg GAE/g), and strawberries (1.12 mg GAE/g) (29, 44, 45). A recent review showed that nearly 100 polyphenolic compounds have been isolated and identified from sea buckthorn (27). Polyphenols mainly include phenolic acids and flavonoids. Seventeen phenolic acids have been reported in sea buckthorn berries. Salicylic acid is the main phenolic acid in berries, accounting for 55–74.3% of the total phenolic acids (46). However, another study reported that gallic acid is the main phenolic acid in sea buckthorn fruit and leaves (27).

Flavonoids may have potential roles in the prevention of chronic diseases, such as diabetes, cardiovascular disease, and cancer (47). Guo et al. (48) found that the total phenols and flavonoid aglycones in sea buckthorn extract had antioxidant and anti-proliferative activities. To date, 95 flavonoids have been identified from sea buckthorn, including 75 flavonols, 2 dihydroflavones, 6 catechins, 1 leucocyanidin, 9 anthocyanidins, 1 proanthocyanidin, and 1 chalcone (49). Raudonis et al. (50) detected the total flavonoid content in 11 sea buckthorn varieties grown in Lithuania and found that total flavonoid content ranged 385–616 μg/g FW. Flavonols are the major constituents of flavonoids and are mainly present in the glycosylated forms of quercetin, isorhamnetin, and kaempferol (49). Flavonols range from 463.14 mg to 893.92 mg/100 g DM, accounting for approximately 99% of the total phenolic compounds (34). The content and composition of polyphenolic compounds are significantly influenced by geographical factors, climatic conditions and berry varieties. Chemical structures of the main phenolic compounds in sea buckthorn are shown in **Figure 2**.

Fatty acids

Sea buckthorn is rich in a variety of fatty acids that play an important role in human health, such as treating

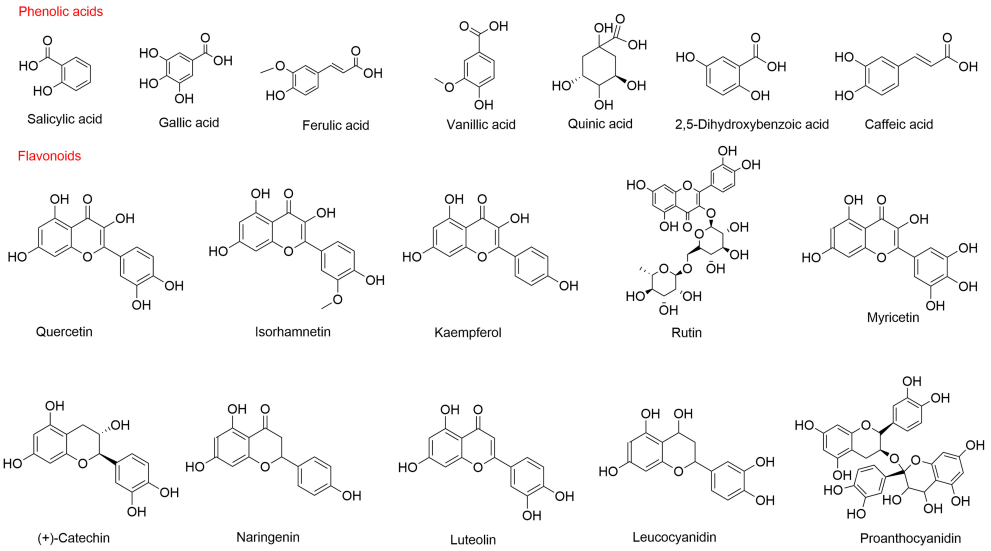

FIGURE 2
Structure of the main phenolic compounds in sea buckthorn.

skin and mucous membrane disorders and dry eyes syndrome and reducing the risk of cardiovascular disease (30). Teleszko et al. (28) identified 11 fatty acids in sea buckthorn pulp oil. At present, 24 fatty acids have been identified in wild and cultivated sea buckthorn berries in Lithuania (**Table 3**). There were differences in the content of fatty acids between wild and cultivated sea buckthorn. The monounsaturated fatty acid content of wild sea buckthorn berries was significantly higher than that of cultivated berries, while the levels of polyunsaturated and saturated fatty acids were higher in cultivated berries (31). The main fatty acids in sea buckthorn berries are palmitic, palmitoleic, and oleic acids.

Phytosterols

Phytosterols, as a bioactive component, can prevent cardiovascular diseases. A recent study found that the total phytosterol content of berry lipids from eight Russian sea buckthorn species ranged from 6168.24 to 13378.22 μg/100 mL. Fourteen sterol compounds have been detected in sea buckthorn pulp lipids, namely 4-desmethyl sterols (cholestanol derivatives, including β-sitosterol, stigmasterol, campesterol, and Δ^5-avenasterol), 4α-monomethyl sterols (e.g., citrostadienol), and 4,4-dimethylsterols (e.g., 24-methylenecycloartanol) (**Table 3**) (28).

Health benefits

Sea buckthorn contains a variety of bioactive components, including vitamins, carotenoids, polyphenols, fatty acids, and phytosterols. These components exert a wide range of health benefits by exerting antioxidant, anticancer, anti-inflammatory, antimicrobial and antiviral effects, as well as exerting protective cardiovascular, dermatological, neuroprotective, and hepatoprotective effects. The health benefits of sea buckthorn are categorized and summarized in **Table 4**, which highlights the study type, main results and potential bioactive components.

Antioxidant activity

Many studies have confirmed the antioxidant activity of sea buckthorn *in vitro* and *in vivo*. Phenolic fraction from sea buckthorn fruits inhibits hydrogen peroxide (H_2O_2) or H_2O_2/Fe stimulated plasma lipid peroxidation and protein carbonylation. In fact, protein carbonylation is a relatively stable biomarker of oxidative stress. The phenolic constituents of sea buckthorn fruit reduced the concentration of carbonyl groups in plasma protein treated with H_2O_2 or H_2O_2/Fe. When plasma was treated with sea buckthorn phenolic fractions at a concentration of 50 g/mL for 60 min, the inhibition rate of plasma lipid peroxidation was as high as 60% (51). *In vitro* trials have shown that sea buckthorn extract with or without atorvastatin for the treatment of hyperlipidemia helped reduce the oxidative damage caused by lipid peroxidation (52). In addition, sea buckthorn leaf extract attenuates intracellular oxidative stress in a dose-dependent manner, thereby increasing neuronal PC-12 cell viability and membrane integrity (53). Serban et al. (54) retrieved 3,145 results from six databases, including PubMed, Scopus, Web of Science and others, among which 101 studies on cardiovascular disease showed that sea buckthorn fruit lowered blood cholesterol levels and reduced inflammation and oxidative stress parameters. Sea

TABLE 4 Health benefits of sea buckthorn.

Sea buckthorn	Effective concentration/time	Study type	Experimental model	Main results	Bioactive compounds	References
Antioxidant						
Phenolic fraction from sea buckthorn fruits	0.5–50 μg/mL	*In vitro*	H_2O_2 or H_2O_2/Fe-treated human plasma or blood platelets	↓ Plasma lipid peroxidation and protein carbonylation. At 50 μg/mL, the inhibition rate of plasma lipid peroxidation was 60%	Flavonoids	(52)
Sea buckthorn extract	100 mg/kg·bw	*In vivo*	Hyperlipidemic rats	↓ Oxidative damage provoked by the lipid peroxidation	Polyphenols	(53)
Sea buckthorn leaf extracts	5, 10, 20 μg/mL	*In vitro*	PC-12 cells	↓ Relative proportion of total apoptotic PC-12 cells	Ellagic acid, gallic acid, isorhamnetin, kaempferol, and quercetin	(54)
Sea Buckthorn seed oil	500 ng/mL	*In vitro*	UV-Induced human skin cells	↓ ROS generation by approximately 25%	Fatty acids, phytosterols, vitamins A and E, β-carotene.	(55)
Anticancer						
Polyphenols extraction	80 and 120 μg/mL	*In vitro*	Human colon cancer cell	↓ Expression of cyclins and cell proliferation	Kaempferol and its derivatives	(56)
	50 mg/kg	*In vivo*	Xenograft BALB/c nude mice model	↓ Tumor volume and kinetic tumor growth		
Leaf aqueous extract	3.12, 6.25, 12.5, 25, 50 μg/mL	*In vitro*	LNCaP and C4-2 cell	↓ Proliferation and migration of prostate cancer cells	–	(12)
Leaf extract	6.2, 62 μg/mL	*In vitro*	Rat C6 glioma cells	↓ Intracellular ROS ↑ Pre-apoptosis in rat C6 glioma cells	Phenolics	(57)
Isorhamnetin	12.5, 15 μmoL/L	*In vitro*	Hypoxia model of $CoCl_2$ (100 μmol/L) promoting maximal proliferation of MKN-45 cells	↓PI3K AKT mTOR-mediated adaptive autophagy ↑ MKN-45 gastric cancer cell apoptosis in a hypoxic environment	Isorhamnetin	(58)
Anti-hyperlipidemia						
Flavonoid-enriched extract from sea buckthorn seed	100 and 300 mg/kg	*In vivo*	High fat diet (HFD)-induced obese mouse model	↓ Serum and liver triglyceride concentrations in dose-dependent manner	Flavonoid	(64)
Sea buckthorn fruit oil	50, 100, 200 mg/kg	*In vivo*	Hypercholesterolemic golden syrian hamster model	↓ TC, TG, non-HDL-C ↑ HDL-C ↓ Oxidative stress and liver impairment caused by hyperlipemia through regulating antioxidant enzyme	Palmitoleic acid	(65)
Anti-obesity						
Sea buckthorn polysaccharide	0.1%	*In vivo*	High fat diet (HFD) induced C57BL/6 male mice	↓ Accumulation of lipids and weight gain	Polysaccharide	(66)
Sea buckthorn fruit oil	50, 100, 200 mg/kg	*In vivo*	Hypercholesterolemic golden syrian hamster model	↓ Weight and blood sugar elevation	Palmitoleic acid	(65)

(Continued)

10.3389/fnut.2022.1036295

TABLE 4 (Continued)

Sea buckthorn	Effective concentration/time	Study type	Experimental model	Main results	Bioactive compounds	References
Flavonoid-enriched extract from sea buckthorn seed	100 and 300 mg/kg	*In vivo*	High fat diet (HFD)-induced obese mouse model	↓ Serum and liver triglyceride concentrations in dose-dependent manner	Flavonoid	(64)
Sea buckthorn freeze-dried powder	4 mg/(g.d. body weight)	*In vivo*	High-fat induced obesity mice	↓ Body weight gain	–	(67)
Antiplatelet						
Polyphenols rich fraction from fruits	50 g/mL	*In vitro*	Healthy human blood platelet	↓ Platelet activation	Polyphenols	(68)
Non-polar fraction from twigs	10 μg/mL	*In vitro*	Healthy human blood platelet	↓ Platelet adhesion and platelet aggregation	Triterpenoids	(69)
Sea buckthorn fraction	0.5–50 μg/mL	*In vitro*	Human blood platelet	↓ Adhesion of resting platelets and thrombin-activated platelets to fibrinogen	Phenolic compounds	(70)
Dermatological						
Sea buckthorn extract	8 weeks (twice daily)	Clinical trial	10 psoriasis patients	↓ Psoriasis Area Severity Index (PASI) and Dermatology Life Quality Index (DLQI) scores	–	(71)
Sea buckthorn oil	100, 200 mg/kg p.o. 20 μL topical application (T.A.)	*In vivo*	TPA stimulated CD-1 mice psoriasis-like model	↓ Ear edema by 34.05 ± 7.65%, 30.45 ± 8.90%, respectively ↓Ear epidermal thickness by 31.80 ± 6.90 μm and 21.91 ± 5.07 μm, respectively,	Fatty acids	(72)
Sea buckthorn oil	1 mL/kg 4 weeks	*In vivo*	DNCB-induced AD-like lesions mice model	↓ DNCB-induced AD severity	–	(73)
Sea buckthorn cream	3-mm thickness (once a day)	Clinical trial	55 patients with second-degree burns	↓Period of wound healing and the course of treatment of second-degree burns	–	(74)
Sea Buckthorn seed oil	500 ng/mL	*In vitro*	UV-Induced human skin cells	↓ UV-induced disorders of redox and lipid metabolism in skin fibroblasts and keratinocytes	Fatty acids, phytosterols, vitamins A and E, β-carotene.	(55)
Anti-inflammatory						
Sea buckthorn peel extract	500 mg/kg	*In vivo*	48/80-induced rat paw edema models	↓ Edema volume	Ursolic acid, oleanolic acid	(75)
Sea buckthorn branches, berries, and leaves extracts	10 μg/mL	*In vitro*	RAW 264.7 macrophages	NO inhibition rates increased from 73 to 98%	Phenolic compounds	(76)
Sea buckthorn leaves extracts	0.05, 5, 50 μg/Ml	*In vivo*	Mouse peritoneal macrophages	↓ Pro-inflammatory cytokine level (TNF-α, IFN-γ and IL-6)	Tannins, proteins and carbohydrate groups	(15)
Sea buckthorn fruits powder	5, 10, 25, 50, and 100 μM	*In vitro*	RAW 264.7 (the mouse macrophage cell line)	↓ LPS-induced NO production	1,5-Dimethyl Citrate	(77)
Sea buckthorn flavonoids (Shanghai Yuan Ye Biotechnology, Ltd.)	0.06%, 0.31% w/w	*In vitro*	HFFD-induced obese mice	↓ Inflammatory mediators/cytokines, iNOS, COX-2, and IL-1β	Flavonoids	(78)

(Continued)

10.3389/fnut.2022.1036295

TABLE 4 (Continued)

Sea buckthorn	Effective concentration/time	Study type	Experimental model	Main results	Bioactive compounds	References
Antimicrobial						
Sea buckthorn leaf extracts	5%	*In vitro*	Common skin and wound pathogens	↓ Gram positive bacteria (*S. aureus, S. epidermidis, S. intermedius, and S. pyogenes*)	–	(16)
Sea buckthorn berries extract	0.15 mg/mL	*In vitro*	Human keratinocytes (HaCaT) cells	↓ Various proinflammatory cytokines and apoptotic pathways	–	(81)
Sea buckthorn berries and leaves extracts	6 mg/mL	*In vitro*	*Staphylococcus aureus* (MRSA)	Inhibits the growth of MRSA	–	(82)
Antiviral						
Sea buckthorn fruit peel extract	12.5 μM	*In vitro*	HSV-2 virus infected Vero cells	↓ Herpes simplex type 2 virus yield	14-Noreudesmanes and a phenylpropane heterodimer	(14)
Sea buckthorn leaf extract	100 mg/kg body weight	*In vivo*	Healthy Swiss albino mice	↑ RVNA titers and CTL population ↑ Memory T cells, plasma cells	Isorhamnetin and other flavonoids	(84)
Neuroprotective						
Sea buckthorn powder	1.5 g/mL	*In vitro*	Aβ-induced Neuroblastoma cells	↓ Intracellular Aβ depositions and Aβ-induced toxicity	–	(86)
Sea buckthorn flavonoids (Shanghai Yuan Ye Biotechnology, Ltd.)	0.06%, 0.31% w/w	*In vitro*	HFFD-induced obese mice	↓ Insulin resistance, neuroinflammation, and cognitive impairment in the CNS	Flavonoids	(80)
Sea buckthorn berries extract	mL/kg	*In vivo*	Iron-induced epileptic rats	↓ Memory impairment, anxiety-like behavior, histological impairments	–	(87)
Hepatoprotective						
Sea buckthorn flavonoids extracted by MCAE	200 mg/kg, po	*In vivo*	Tetracycline-induced ICR mice fatty liver model	↓ Liver Index, serum Index, TG, TC, LDL-C, AST, ALT	Flavonoids	(90)
Sea buckthorn fermentation liquid	1.75, 2.675, 5.35 g/kg	*In vivo*	Alcoholic liver disease mice model	↓ Kidney and spleen injury caused by alcohol, liver hypertrophy, and alcoholic fatty liver	Flavonoids, triterpenes and related SCFAs	(91)
Sea buckthorn berries extracts	20 and 40 mg/kg	*In vivo*	BDL-induced liver fibrosis model in rats	↓ liver fibrosis by inhibiting HSC activation	Flavonoids, phenolic acids	(92)
Sea buckthorn flavonoids from seeds	100 and 300 mg/kg	*In vivo*	High-fat diets-induced obese mice model	↓ Fat infiltration of liver tissues caused by high-fat diet and the expression of PPARγ in liver and white adipose tissues	Flavonoids	(93)

10.3389/fnut.2022.1036295

buckthorn seed oil inhibits ultraviolet (UV)-induced redox balance disturbance in skin cells. Gęgotek et al. (55) reported that fibroblast incubation with sea buckthorn oil causes decreases in reactive oxygen species (ROS) generation by approximately 25%. Sea buckthorn may be used as a natural source of antioxidants to prevent and treat diseases related to oxidative stress.

Anticancer activity

At present, many studies have shown that the bioactive components in sea buckthorn have anticancer activity. Sea buckthorn polyphenols, the active ingredient of kaempferol and its derivatives, have shown significant anti-colon cancer activity *in vitro* and *in vivo*. Sea buckthorn polyphenols upregulate expression of microRNA (miR)-195-5p and miR-497-5p and down-regulate the expression of miR-1247-3p to suppress cyclins expression, thereby arresting the cell cycle in the G1 phase and affecting further proliferation of colon cancer. In addition, sea buckthorn polyphenols (50 mg/kg) significantly reduced tumor volume and control tumor growth in xenografted BALB/c nude mice *in vivo* (56). Sea buckthorn leaf aqueous extract effectively targeted androgen receptor (AR) and significantly downregulated androgen response genes, prostate specific antigen (PSA), eleven-nineteen lysine-rich leukemia 2 (ELL2), ELL-associated factor 2 (EAF2), calreticulin (CALR) *in vitro*. Sea buckthorn leaf aqueous extract can effectively inhibit proliferation and migration of prostate cancer cells. Therefore, sea buckthorn leaves hold promise as a functional food that may play a key role in the prevention of prostate cancer in high-risk populations. However, the potential bioactive compounds in sea buckthorn leaves are yet to be investigated for the development of new treatment options for prostate cancer (12).

Kim et al. (57) reported that sea buckthorn leaf extract at concentrations of 6.2 and 62 μg/mL significantly reduced the production of intracellular ROS by 16.3 and 42.3%, respectively, up-regulated expression of the pro-apoptotic protein B-cell lymphoma-2 (BCL2)-associated X (Bax) and inhibited the rapid proliferation of C6 glioma cells (11 and 49.5%). Therefore, sea buckthorn may be a potential source of pharmacological interventions for glioma treatment. In addition, isorhamnetin, the active component of sea buckthorn, increased expression of the mitochondrial pathway pro-apoptotic protein (cytochrome c-caspase 9-caspase 3) in gastric cancer cells in a hypoxic environment. It also significantly inhibited the autophagy of MKN-45 gastric cancer cells and promoted the apoptosis of gastric cancer cells by activating the Phosphoinositide 3-kinase (PI3K)-protein kinase B (AKT)-mammalian target of rapamycin (mTOR) signaling pathway (58).

In short, these studies support the anticancer effect of sea buckthorn and suggest that polyphenolic compounds may be responsible for its anticancer activity. The anticancer mechanisms of sea buckthorn are related to the expression of cyclin, proapoptotic proteins, autophagy of cancer cells, and related signaling pathways. However, there are few *in vivo* experiments and clinical trials on the anticancer effects of sea buckthorn. Thus, further research on the anticancer effects of sea buckthorn in humans is needed. A growing number of studies have found that carotenoids, especially lycopene, can reduce the risk of prostate, breast, lung, cervical and other cancers (59). However, there are almost no studies on the anticancer activity of sea buckthorn carotenoids. The anticancer activity of sea buckthorn carotenoid extracts is a promising research direction.

Anti-hyperlipidemia activity

Hypercholesterolemia is an important risk factor for cardiovascular disease (60). The bioactive substance in the lipids of sea buckthorn pulp, phytosterols, plays an important role in the prevention of cardiovascular diseases, especially hypercholesterolemia (28). Numerous clinical trials have shown that spreads with added phytosterols have a stronger cholesterol-lowering effect, reducing low-density lipoprotein cholesterol (LDL-C) levels by about 10–15% (61). The mechanism of the hypocholesterolemic effect of phytosterols may be *via* the inhibition of endogenous cholesterol reabsorption and the promotion of its excretion in the form of neutral steroids (62). A meta-analysis from 11 independent randomized controlled trials concluded that supplementation with sea buckthorn berries/extracts significantly improved total cholesterol, triglyceride (TG), LDL-C, and high-density lipoprotein cholesterol (HDL-C) in subjects with hyperlipidemia, but not in healthy subjects (63).

In vivo animal trials showed that sea buckthorn has anti-hyperlipidemic effects. Flavonoid-enriched extract from sea buckthorn seed (FSH) at a dose of 100 and 300 mg/kg reduced serum and liver triglyceride concentrations by 16.67 and 49.56% in high fat diet (HFD)-induced obese mouse, respectively. FSH may improve lipid metabolism by inhibiting peroxisome proliferator-activated receptor gamma (PPARγ) expression, promoting PPARα expression, and suppressing adipose tissue inflammation (64). In addition, sea buckthorn fruit oil extract dose-dependently attenuated metabolic dysfunction in hamsters with hyperlipemia, including improving blood lipid composition (total cholesterol (TC), TG, HDL-C, and non-HDL-C levels), and relieving oxidative stress and liver impairment through the AMP-activated protein kinase (AMPK) and Akt pathways (65). In summary, sea buckthorn fruit, seed and oil are a source of phenolic compounds (especially flavonoids) and phytosterols. Sea buckthorn may be a valuable source of important bioactive compounds for the prevention and treatment of cardiovascular disease, which requires further research support.

Anti-obesity activity

Sea buckthorn polysaccharide promotes expression of PPARγ-coactivator 1α (PGC1α), uncoupling protein-1 (UCP-1), and PR domain containing 16 (PRDM 16) in adipocytes to activate the brown adipocytes and improve thermogenesis, thus inhibiting the accumulation of lipids and weight gain (66). Palmitic acid-rich sea buckthorn fruit oil extract reduces the weight of hypercholesterolemic hamsters and blood sugar elevation caused by dyslipidemia. Therefore, sea buckthorn fruit oil can relieve obesity caused by hyperlipidemia (65). It has been reported that FSH at doses of 100 and 300 mg/kg significantly reduced body weight gain in HFD-induced obese mice by 33.06 and 43.51%, respectively (64). Sea buckthorn freeze-dried powder is made by low-temperature freeze-drying technology, allowing the powder to retain all of the plant's useful nutrients and functional ingredients. Sea buckthorn powder improves HFD-induced obesity by altering the composition and structure of gut microbiome (67). Sea buckthorn is likely to develop into functional foods and dietary supplements for obese people.

Antiplatelet activity

Anticoagulant and antiplatelet agents play an important role in the prevention and treatment of cardiovascular thrombotic events caused by various mechanisms. The polyphenols rich fraction of sea buckthorn fruit at the highest used concentration (50 μg/mL) has potent antiplatelet activity compared to polyphenol and triterpenic acid rich fractions from leaves and twigs. It has been shown to inhibit the expression of PAC-1 in three models of non-activated platelets, platelets activated by 10 μM adenosine diphosphate (ADP), and platelets activated by 10 μg/mL of collagen. This may be due to the inhibition of platelet aggregation as a result of the low expression of GPIIb/IIIa (68). Another report indicated that the non-polar fraction of sea buckthorn twigs showed stronger antiplatelet activity than the phenolic and non-polar fractions of leaves. This activity may be related to the regulation of arachidonic acid metabolism, changes in ROS concentration, and expression of platelet receptors (69). The 50 g/mL sea buckthorn fraction inhibited the adhesion of resting platelets and thrombin-activated platelets to fibrinogen by 65 and 55%, respectively (70).

Dermatological effect

Sea buckthorn has been reported to have a wide range of dermatological effects. Clinical trials have demonstrated the anti-psoriasis effects of sea buckthorn. Boca et al. (71) treated 10 patients diagnosed with mild to moderate psoriasis with topical sea buckthorn fruit extract. When compared with placebo-treated patients, the Psoriasis Area Severity Index (PASI) score and Dermatology Life Quality Index (DLQI) scores in the treatment group were improved at both the fourth and eighth weeks of treatment. Sea buckthorn also exhibits anti-psoriatic and anti-atopic dermatitis activities in animal models. In the 12-*O*-tetradecanoylphorbol-13-acetate (TPA)-induced psoriasis-like lesion CD-1 mouse model, simultaneous oral (100 and 200 mg/kg) and topical (20 μL) application of sea buckthorn oil significantly inhibited ear edema (34.05 ± 7.65%, and 30.45 ± 8.90%, respectively) and reduced ear biopsy weights. Sea buckthorn oil has anti-inflammatory and anti-psoriatic properties. The possible mechanism for these effects may be that the high levels of fatty acids in sea buckthorn oil acts to inhibit reactive nitrogen and down-regulate nuclear factor kappa-B (NF-κB) protein and pro-inflammatory cytokines (72). Studies have suggested that 4 weeks of consecutive use of sea buckthorn oil decreases 2,4-dinitrochlorobenzene (DNCB)-induced atopic dermatitis (AD) severity in mice. This effect was due to inhibition of the thymus activation regulated chemokine (TARC) and macrophage-derived chemokine (MDC) in Interferon-γ (IFN-γ)/tumor necrosis factor-α (TNF-α)-stimulated HaCaT cells, which occurred by blocking activation of the NF-κB/signal transducerand activator of transcription 1 (STAT1) signaling pathway, thereby inhibiting the development of AD-like skin lesions. Sea buckthorn oil may be an effective therapeutic agent in the treatment of patients with AD (73).

Moreover, a randomized triple-blind clinical trial demonstrated that the healing period for second-degree burns in patients treated with 40% sea buckthorn cream was about 5 days shorter than for patients treated with 1% silver sulfadiazine dressings. The sea buckthorn cream had better clinical efficacy and shortened the healing time for second-degree burns (74). It was found that sea buckthorn seed oil promoted wound contraction by increasing hydroxyproline, hexosamine, DNA, and total protein content, which in turn promoted full-layer burn wound healing. The wound healing potential of sea buckthorn seed oil is dependent on the presence of omega-3 and omega-6 fatty acids, tocopherols and carotenoids (75). In addition, the palmitic acid-rich fraction purified from sea buckthorn seed oil has cell proliferation properties that promote growth of keratinocytes and dermal fibroblasts, which can be used to develop skin preparations and skin care products (76). UV light induces damage to the redox system and impairs lipid metabolism in skin fibroblasts and keratin-forming cells, and sea buckthorn oil can inhibit this effect and sea buckthorn seed oil may be a promising natural substance for skin photoprotection (55).

Overall, sea buckthorn has a therapeutic role in dermatology due to the high levels of saturated, monounsaturated and polyunsaturated fatty acids and other biological compounds that exert their effects. Determining the specific bioactive compounds and their mechanisms of action, however, requires further research.

Anti-inflammatory activity

Sea buckthorn is widely used in traditional medicine to treat inflammatory diseases. The anti-inflammatory activity of sea buckthorn has been demonstrated in many *in vivo* studies. For example, 70% methanolic extract of sea buckthorn (500 mg/kg) inhibited 48/80-induced edematous inflammation and significantly reduced the volume of foot swelling in rats (0.660 ± 0.082 mL, compared to 0.935 ± 0.041 mL in the control). The anti-inflammatory effect of the peel extract was greatest (0.470 ± 0.124 mL, compared with 0.920 ± 0.111 mL for the control). Ursolic acid and oleanolic acid were the main active compounds in the peel extract. They may cause membrane stabilization by inhibiting mast cell degranulation (77). The anti-inflammatory activity of sea buckthorn branches, leaves, and fruits was measured by nitric oxide (NO) production, and it was found that treatment with 10 μg/mL sea buckthorn extracts inhibited NO by 73–98%. Cytotoxic effects of sea buckthorn have not been observed in 3-(4,5-dimethylthiazol-2-yl)-2,5-diphenyltetrazolium bromide (MTT) assays. Sea buckthorn extracts displayed good anti-inflammatory activities in RAW 264.7 macrophages (78). Sea buckthorn leaves extract exhibited potent anti-inflammatory activity against lipopolysaccharide (LPS) stimuli by inhibiting the expression of NO, inducible nitric oxide synthase (iNOS) and cyclooxygenase-2 (COX-2), and by decreasing levels of pro-inflammatory cytokines (15). Furthermore, sea buckthorn fruit extract, identified as a citric acid derivative, inhibited LPS-induced NO production in RAW 264.7 cells by inhibiting the expression of IκB kinase alpha/beta (IKKα/β), inhibitor of kappa Bα (I-κBα), NF-κB p65, iNOS, and COX-2, and the activities of interleukin 6 (IL-6) and TNF-α (79). Similarly, Mulati et al. (80) reported that sea buckthorn flavonoids significantly reversed high-fat and high-fructose diet (HFFD)-induced iNOS overexpression and reduced interleukin 1β (IL-1β) and COX-2 mRNA levels in the hippocampus of mice, suppressing the HFFD-induced inflammation reaction.

Therefore, the anti-inflammatory activity of sea buckthorn may be attributed to ursolic acid, oleanolic acid, citric acid derivatives and flavonoids. Its anti-inflammatory mechanism of action may be related to inhibition of the expression of pro-inflammatory cytokines (IL-6, IL-1β, and TNF-α) and a reduction in the production of pro-inflammatory mediators (NF-κB, iNOS, and COX-2). Sea buckthorn has shown promise as a source of bioactive compounds for the treatment of inflammatory diseases, but more *in vivo* and clinical studies are still needed to support this.

Antimicrobial and antiviral activity

It has been reported that sea buckthorn exhibits antimicrobial activities *in vitro*. Verma et al. (16) found that sea buckthorn leaf extract was significantly effective against all 67 gram-positive bacteria recovered from clinical samples. Sea buckthorn leaf extract at a 5% concentration inhibited *S. aureus*, *S. epidermidis*, *S. intermedius*, and *S. pyogenes* growth by almost 50%. Sea buckthorn extract may reverse the detrimental effects of *S. aureus* on human keratinocytes by down-regulating various pro-inflammatory cytokines and apoptotic pathways, such as ILs, TNFs, transforming growth factors (TGFs), IFNs, fibroblast growth factors (FGFs), MAPKs, matrix metalloproteinases (MMPs), and caspases and Wnts molecular pathways (81). Additionally, a study showed that 6 mg/mL of sea buckthorn berry and leaf extract significantly inhibits the growth of Methicillin-resistant *S. aureus* (MRSA) (82). Smida et al. (83) reported that an experimentally designed mouthwash based on sea buckthorn pulp oil had bactericidal effects on some periodontal pathogens and had the ability to inhibit the formation of single-strain and multi-strain biofilms.

Moreover, sea buckthorn exhibits significant antiviral activity. 14-Noreudesmanes and a phenylpropane heterodimer isolated from the 70% methanol extract of sea buckthorn fruit inhibited the replication of herpes simplex type 2 (HSV-2) virus. Therefore, sea buckthorn may be a potential source of antiviral agents with anti-HSV-2 activity and may provide an alternative drug candidate for the treatment of patient populations infected with acyclovir- and penciclovir-resistant strains of HSV-2 (14). In addition, it has been shown that immunization with sea buckthorn leaf extract and inactivated rabies virus antigens (SBTE + Rb) increases rabies virus neutralizing antibody (RVNA) titers and the cytotoxic T lymphocytes (CTLs) response. Compared with the Rb immunized group, memory T cells and plasma cells in the SBTE + Rb immunized group were significantly increased by 5.5 and 1.9%, respectively. The components of sea buckthorn leaf extract that exert adjuvant activity may be isorhamnetin and other flavonoids (84).

Neuroprotective activity

Alzheimer's disease is a neurodegenerative disorder in which the typical histopathological changes are extracellular amyloid-β (Aβ) deposition and neurofibrillary tangles due to Tau protein hyperphosphorylation (85). Sea buckthorn removes intracellular Aβ deposits, with sea buckthorn powder at 1.5 g/mL being the most effective. This finding may be attributed to the higher levels of antioxidants present in sea buckthorn berry powder. Antioxidants inhibit Aβ-induced toxicity and prevent cell death by exerting a neuroprotective effect. Sea buckthorn holds promise as a potential therapeutic agent for the treatment of Alzheimer's disease (86). Another study showed that sea buckthorn flavonoids stimulated insulin receptor substrate (IRS)/AKT activation, reduced protein tyrosine phosphatase 1B (PTP1B) expression and normalized insulin signaling pathways, neurogenic damage

and ERK/CREB/BDNF signaling pathways. It inhibited insulin resistance and neuroinflammation, attenuated HFD-induced cognitive impairment, and effectively prevented memory loss (80). In addition, sea buckthorn improved epileptiform activity in the cerebral cortex and hippocampus in iron-induced epilepsy rats and reduced anxiety-like behavior, and improved memory impairment and histological damage in rats (87). In conclusion, sea buckthorn has been demonstrated to possess neuroprotective effects. The mechanisms include the removal of Aβ deposits, inhibition of Aβ-induced toxicity, and inhibition of insulin resistance and neuroinflammation. These effects may be attributed to the presence of flavonoids and other antioxidant compounds in sea buckthorn. In the future, it is necessary to investigate the neuroprotective effect of sea buckthorn on humans using clinical trials.

Hepatoprotective activity

Sea buckthorn extract and sea buckthorn oil have significant hepatoprotective activities. Sea buckthorn oil is rich in carotenoids and may be an important source of bioavailable lutein (88). Carotenoids such as β-carotene, lycopene, lutein, and β-cryptoxanthin exhibit hepatoprotective activity by reducing oxidative stress and regulating lipid metabolism in hepatocytes (89). Biochemical and histopathological studies have shown that sea buckthorn flavonoid extract significantly improves biomarkers, including TG, TC, LDL-C, aspartate aminotransferase (AST), and alanine aminotransferase (ALT) in the serum and liver of non-alcoholic fatty liver mice. The therapeutic effects of sea buckthorn were superior to that of curcumin (90). Furthermore, sea buckthorn fruit fermentation solution regulates hepatic lipid metabolism and oxidative stress by modulating the composition of the intestinal microbiota. Thus, sea buckthorn prevents alcoholic liver disease and exerts hepatoprotective effect (91). Another study found that the active ingredients in sea buckthorn inhibited the activation of hepatic stellate cells, reduced inflammatory cytokine levels, and reduced the development of bile duct ligation (BDL)-induced fibrosis in rats in a dose-dependent manner. Thus, sea buckthorn reduces liver injury and inflammation, and restored liver function (92). It has been reported that a flavonoid extract from sea buckthorn seed residues reduces the number of adipocytes in the liver of obese mice, which significantly reduces HFD-induced fatty infiltration in the liver tissue, and reduces expression of PPARγ in the liver and adipose tissue, resulting in reduced of fat accumulation (93). In general, the flavonoids and carotenoids in sea buckthorn have hepatoprotective effects. The mechanisms for these effects may be associated with the regulation of lipid metabolism and oxidative stress and a reduction in inflammatory factor levels. It is necessary to conduct more *in vivo* studies to explore the hepatoprotective activity of sea buckthorn.

Food applications

In addition to medical biological activities, sea buckthorn is also widely used in food, and has high economic value. Sea buckthorn is rich in nutritional value and contains a variety of biologically active compounds. Sea buckthorn is currently used as an antioxidant, antimicrobial and other natural additives in a variety of food products. The application of sea buckthorn in the food industry is more and more extensive, such as sea buckthorn oil, freeze-dried powder, fruit juice, fruit wine, milk tablets, fruit vinegar drinks, tea (94), preserved fruit, yogurt, and jam. The maximum utilization of sea buckthorn to improve the sensory properties and nutritional value of sea buckthorn products is currently being pursued by food industry manufacturers and researchers.

Food additives

The meat processing industry is currently seeking natural additives to replace chemical additives in their products. Kozhakhiyeva et al. (95) found that the new functional cooked and smoked horse meat Jaya product, produced by adding 5.0% sea buckthorn fruit powder extract, is rich in 1.0% bioactive substances. The samples showed a 38% reduction in lipolysis and a significant 24% reduction in lipid hydroperoxides after 21 days of storage. This improved the oxidative stability and quality of new functional horsemeat delicacies. The addition of 3% ethanolic extract of sea buckthorn fruit to pork sausage effectively inhibited lipid oxidation and reduced the total bacterial count. Total sausage colonies were reduced by approximately 7 times, improving the microbiological content of the sausage (96).

The addition of sea buckthorn fruit powder to wheat bread extends the shelf life of the bread by 1–3 days. It also improves the antioxidant and organoleptic properties of the bread (8). The addition of 0.8 g/L of sea buckthorn leaf powder to white wine increased its free radical scavenging activity from 28.4 to 55.8%. The reducing ability of white wine, as measured by the amount of reduced ferric ion in an antioxidant power assay, increased from 35.3 to 62.1% with the addition of sea buckthorn. The total phenolic content of white wine increased from 11 to 23.7% and the color intensity increased from 39.9 to 50.7%, which contributed to the antioxidant capacity of the wines without sulfites (97). Sea buckthorn leaves have significant antioxidant capacity (98), and can be used as an alternative to increase the antioxidant capacity of wines.

Studies have found that sea buckthorn juice and its by-products could be used in chewing gum formulations and significantly improve the antioxidant activity. It showed antimicrobial properties against MRSA, *Klebsiella pneumoniae*, *Salmonella enterica*, *Pseudomonas aeruginosa*, *Bacillus cereus*, etc. Sea buckthorn juice and its by-products have great potential as antimicrobial agents in the food industry (99).

Furthermore, sea buckthorn seeds used to purify chitinase, *via* its action on the antifreeze protein HrCHI4 preserved the integrity of frozen green pea membranes and helped preserve sample freshness by retaining volatile compounds. This study opens up the possibility of using edible products to preserve food and preserve its texture and freshness by natural means (100).

All in all, sea buckthorn has a promising future as a natural food additive. The bioactive compounds contained in sea buckthorn, such as polyphenols (especially flavonoids), ascorbic acid, vitamins, carotenoids, and antifreeze proteins exert antioxidant, antibacterial and antifreeze effects. In the future, it will be necessary to investigate these mechanisms of action in depth for better application in food production.

Sea buckthorn yogurt

Sea buckthorn, as a new plant-based additive, is becoming increasingly popular in dairy production worldwide due to its healthful, nutritional benefits. This is exactly the kind of nutritional quality that consumers are happy to seek. Sea buckthorn is rich in nutritional active substances and its addition to yogurt enhances the nutritional value of yogurt. Developed from sea buckthorn berries, sea buckthorn yogurt is rich in fat, protein, carbohydrates and antioxidants (vitamin C, vitamin E, carotenoids, phenols, etc.) meeting people's nutritional needs. The yogurt can be stored safely at 4°C for 12 days and at 15°C for 3 days without losing its microbiological quality (9). In addition to adding sea buckthorn to yogurt, carrot (101), tomato (102), water chestnut (103), yellow peach, and passion fruit have also been added to sea buckthorn yogurt to develop novel healthy yogurt. The different additions add to the unique natural flavor of fruits and vegetables, enriching the yogurt with a variety of functional ingredients and making up for the nutritional deficiencies of plain yogurt (101).

Sea buckthorn jam and jelly

Sea buckthorn berries have a sour taste and a short shelf life. Therefore, processing berries into jam is an effective means to improve sensory characteristics and increase berry utilization. The jam, produced using sea buckthorn fruit at 102°C with stevia, contains high levels of total carotenoids and polyphenols and exhibits antioxidant activity. After 21 days of storage at room temperature, the value of yeast and mold was less than 100 CFU/g, and the value of Enterobacteriaceae was less than 5 CFU/g (104). Ordinary jam has a single flavor. In the *Elaeagnus angustifolia* and sea buckthorn compound jam, sea buckthorn was used both as a raw material and as an acidulant instead of citric acid. The jam has a shelf life of 177 days at 20°C without the addition of preservatives (105). In addition, sea buckthorn can be combined with sweet potatoes, pumpkins and carrots in a certain ratio to make novel, nutritious and healthy compound jam (106). A reasonable mixture of sea buckthorn juice with other fruit juices (papaya, watermelon, grape) can produce a delicious and nutritious jelly. Among them, sea buckthorn mixed jelly prepared in certain ratios with grapes has shown good organoleptic characteristics. The shelf life of sea buckthorn-grape jelly is 6 months at room temperature and its microbial load is also within the specified limits (107). Sea buckthorn has the potential to be a potentially rich source of bioactive compounds for the production of sugar-based products.

Sea buckthorn beverages

Sea buckthorn berry wastes are inevitably generated in the sea buckthorn processing industry, and improper disposal of these wastes will cause environmental pollution. Fermentation and reuse of these wastes can improve the utilization rate of sea buckthorn and increase the economic value of these wastes. Waste from the sea buckthorn processing industry can be used as a suitable substrate for fermentation. Fermentation under optimal fermentation conditions resulted in 3% ethanolic sea buckthorn beverage. This beverage contains high levels of phenolic compounds (including gallic acid, protocatechuic acid, vanillic acid, chlorogenic acid, etc.) and high antioxidant activity, and contains carbon dioxide and low levels of ethanol. So it is a refreshing and healthy functional drink (108). In addition to fermentation, a waste-free whole fruit pulp juice of sea buckthorn can be developed using the micro-wet milling (MWM) process. Compared to mixed milled and commercial sea buckthorn juice, MWM sea buckthorn juice has a better color (bright yellow tint, highest total carotenoid content of 145 $\pm$ 0.10 mg/mL), smaller particle size, higher ascorbic acid value (67.67 $\pm$ 1.15 mg/mL), total phenolic content and antioxidant activity. The process minimizes the loss of heat-sensitive bioactive compounds. It also provides a fiber-rich juice, showing great promise for processing sea buckthorn juice in the food industry (109). Sea buckthorn is rich in nutrients and bioactive compounds. The potential of sea buckthorn as a botanical ingredient for novel functional food applications is obvious. It is promising to make full use of sea buckthorn fruits, peels, and seeds and to explore new ways of processing sea buckthorn.

Toxicity and safety

Despite the long nutritional and medicinal history of sea buckthorn, there is still relatively little information available on the toxicity and safety of sea buckthorn. Wen et al. (110) reported that sea buckthorn berry oil was not a genotoxic or teratogenic substance. He found that sea buckthorn berry oil showed no mutagenic activity against histidine-dependent

strains of *Salmonella typhimurium* at exposure concentrations ranging from 8 to 5,000 μg/plate. At a dose up to 9.36 g/kg body weight, sea buckthorn berry oil had no significant effect on sperm morphology and the micronucleus rate of polychromatic erythrocytes in mice. In addition, 4.68 g/kg of sea buckthorn fruit oil did not cause maternal toxicity or embryotoxicity in pregnant mice. The no-observed-adverse-effect level (NOAEL) for rats was determined to be 4.68 g/kg of body weight. A 90-day safety study showed that the NOAEL in rats was 100 mg/kg body weight/day of aqueous fruit extract of sea buckthorn (111). Furthermore, Zhao et al. (112) reported that the maximum tolerated dose of sea buckthorn oil in the acute toxicity study in mice was bigger than 18.72 g/kg. Ninety-day repeated oral toxicity tests in rats showed that the NOAEL was 9.36 g/kg body weight. Sea buckthorn is healthy and non-toxic enough to be used as a human food, medicinal product, or dietary supplement.

Conclusion and outlooks

Sea buckthorn is a unique and highly valuable plant with a wide distribution covering more than 2 million hectares of land worldwide. It contains nearly 200 bioactive compounds and has great benefits to human health, and *in vivo*, *in vitro*, and clinical trials in the past 5 years have demonstrated the health benefits of sea buckthorn. These biological activities include antioxidant, anticancer, anti-inflammatory, anti-hyperlipidemic, anti-obesity, antimicrobial and antiviral, dermatological, neuroprotective, and hepatoprotective effects. Moreover, sea buckthorn has created enormous economic value in the food industry and is a promising dietary source of bioactive components.

As a versatile economic and ecological plant, sea buckthorn undoubtedly has a bright future. This ancient plant has powerful therapeutic synergies and has made many contributions to humankind. Sea buckthorn has an outstanding ability to help with economic development and improve the ecological environment. In order to rationally develop and utilize sea buckthorn resources, further research should focus on: (1) Developing mechanical harvesting and reasonable preservation technology. Sea buckthorn is a berry plant and manual harvesting is inefficient. The berries have high moisture content and are easily squeezed leading to deformation and mold. It is necessary to improve the efficiency at the harvesting stage; (2) Isolation and identification of more specific bioactive compounds and further study of their health promoting mechanisms; (3) Conducting more clinical trials to verify the health benefits of sea buckthorn for humans; (4) Applying sea buckthorn in the prevention and treatment of diseases; (5) Developing functional foods and other products based on sea buckthorn; (6) Adhering to the mode of combining economy and ecology, and developing the sea buckthorn industry in a scientific, reasonable and sustainable manner.

Author contributions

QM conceptualized the topic. FZ and PW reviewed the literature and collected the data. ZW drafted the manuscript. GH and XC revised and edited the manuscript. All authors contributed to the article and approved the submitted version.

Funding

This work was financially supported by the National Natural Science Foundation of China (grant no. 81473104).

Conflict of interest

The authors declare that the research was conducted in the absence of any commercial or financial relationships that could be construed as a potential conflict of interest.

Publisher's note

All claims expressed in this article are solely those of the authors and do not necessarily represent those of their affiliated organizations, or those of the publisher, the editors and the reviewers. Any product that may be evaluated in this article, or claim that may be made by its manufacturer, is not guaranteed or endorsed by the publisher.

References

1. Singh B, Peter K. . *Indian sea buckthorn. New age herbals*. Singapore: Springer (2018). p. 29–54. doi: 10.1007/978-981-10-8291-7_3

2. Chen X, Lian Y. The geographical distribution patterns and its formative factors on the genus *Hippophae* L. *Acta Bot Boreali Occident Sin.* (1994) 14:105–10.

3. Stobdan T, Targais K, Lamo D, Srivastava R. Judicious use of natural resources: a case study of traditional uses of seabuckthorn (*Hippophae rhamnoides* L.) in trans-himalayan ladakh. *India Natl Acad Sci Lett.* (2013) 36:609–13. doi: 10.1007/s40009-013-0177-4

4. Piłat B, Bieniek A, Zadernowski R. Common sea buckthorn (*Hippophae rhamnoides* L.) as an alternative orchard plant. *Pol J Nat Sci.* (2015) 30:417–30.

5. Wang K, Xu Z, Liao X. Bioactive compounds, health benefits and functional food products of sea buckthorn: a review. *Crit Rev Food Sci Nutr.* (2021) 2021:1–22. doi: 10.1080/10408398.2021.1905605

6. Wang X, Xu T, Liu Y, Liu Y, Liu J, Li M, et al. Research progress on the relative theory of medicinal plants of *Hippophae* L World. *Chin Med.* (2021) 16:2217–27. doi: 10.3969/j.issn.1673-7202.2021.15.002

7. Gâtlan A, Gutt G. Sea buckthorn in plant based diets. an analytical approach of sea buckthorn fruits composition: nutritional value, applications, and health benefits. *Int J Environ Res Public Health.* (2021) 18:8986. doi: 10.3390/ijerph18178986

8. Ghendov-Mosanu A, Cristea E, Patras A, Sturza R, Padureanu S, Deseatnicova O, et al. Potential application of *Hippophae rhamnoides* in wheat bread production. *Molecules.* (2020) 25:1272. doi: 10.3390/molecules25061272

9. Selvamuthukumaran M, Farhath K. Evaluation of shelf stability of antioxidant rich seabuckthorn fruit yoghurt. *Int Food Res J.* (2014) 21:759–65.

10. Wang H, Sun X, Hua S, Teng X. Historical record and current sistuation of pharmaceutical R&D about seabuckthorn in China. *Glob Seabuckthorn Res Dev.* (2012) 10:25–8.

11. Suryakumar G, Gupta A. Medicinal and therapeutic potential of Sea buckthorn (*Hippophae rhamnoides* L.). *J Ethnopharmacol.* (2011) 138:268–78. doi: 10.1016/j.jep.2011.09.024

12. Masoodi K, Wani W, Dar Z, Mansoor S, Anam-ul-Haq S, Farooq I, et al. Sea buckthorn (*Hippophae rhamnoides* L.) inhibits cellular proliferation, wound healing and decreases expression of prostate specific antigen in prostate cancer cells in vitro. *J Funct Foods.* (2020) 73:104102. doi: 10.1016/j.jff.2020.104102

13. Olas B. Sea buckthorn as a source of important bioactive compounds in cardiovascular diseases. *Food Chem Toxicol.* (2016) 97:199–204. doi: 10.1016/j.fct.2016.09.008

14. Rédei D, Kúsz N, Rafai T, Bogdanov A, Burián K, Csorba A, et al. 14-noreudesmanes and a phenylpropane heterodimer from sea buckthorn berry inhibit Herpes simplex type 2 virus replication. *Tetrahedron.* (2019) 75:1364–70. doi: 10.1016/j.tet.2019.01.050

15. Tanwar H, Singh D, Singh S, Ganju L. Anti-inflammatory activity of the functional groups present in *Hippophae rhamnoides* (seabuckthorn) leaf extract. *Inflammopharmacology.* (2018) 26:291–301. doi: 10.1007/s10787-017-0345-0

16. Verma H, Chahota R, Palial A, Sharma M. Antibacterial properties of seabuckthorn (*Hippophae rhamnoides* L.) leaf extracts against common skin and wound bacteria. *Indian J Vet Res.* (2011) 20:38–41.

17. Stobdan T, Chaurasia O, Korekar G, Yadav A, Singh S. Attributes of seabuckthorn (*Hippophae rhamnoides* L.) to meet nutritional requirements in high altitude. *Def Sci J.* (2010) 60:226–30. doi: 10.14429/dsj.60.344

18. Pop R, Weesepoel Y, Socaciu C, Pintea A, Vincken J, Gruppen H. Carotenoid composition of berries and leaves from six romanian sea buckthorn (*Hippophae rhamnoides* L.) varieties. *Food Chem.* (2014) 147:1–9. doi: 10.1016/j.foodchem.2013.09.083

19. Yang F, Suo Y, Chen D, Tong L. Protection against vascular endothelial dysfunction by polyphenols in sea buckthorn berries in rats with hyperlipidemia. *Biosci Trends.* (2016) 10:188–96. doi: 10.5582/bst.2016.01056

20. Marsiñach S, Cuenca A. The impact of sea buckthorn oil fatty acids on human health. *Lipids Health Dis.* (2019) 18:145. doi: 10.1186/s12944-019-1065-9

21. ISA. The annual report of international seabuckthorn development for the year of 2020. Beijing: China WaterPower Press (2021).

22. Government of Ontario. *Minist agric food rural aff ont canda*. (2022). Available online at: http://www.omafra.gov.on.ca/english/crops/facts/seabuckthorn.htm (accessed May 5, 2022).

23. ChinesePharmacopoeia. *Pharmacopoeia of the people's republic of china 2020*. Beijing: China Medical Science Press (2020). 191 p.

24. Rousi A. The genus *Hippophaë* L. A taxonomic study. *Ann Bot Fenn.* (1971) 8:177–227.

25. Liu S, He T. The genus hippophae from qing-zang plateau. *J Syst Evol.* (1978) 16:106–8.

26. Hu J. Main achievements of systematic planting and development of seabuckthorn in china in past 35 years (1985˜2020). *Int J Ecol.* (2021) 10:500–8.

27. Ji M, Gong X, Li X, Wang C, Li M. Advanced research on the antioxidant activity and mechanism of polyphenols from hippophae species—a review. *Molecules.* (2020) 25:917. doi: 10.3390/molecules25040917

28. Teleszko M, Wojdyło A, Rudzińska M, Oszmiański J, Golis T. Analysis of *Lipophilic* and *Hydrophilic* bioactive compounds content in sea buckthorn (*Hippophaë rhamnoides* L.) berries. *J Agric Food Chem.* (2015) 63:4120–9. doi: 10.1021/acs.jafc.5b00564

29. Kuhkheil A, Badi H, Mehrafarin A, Abdossi V. Chemical constituents of sea buckthorn (*Hippophae rhamnoides* L.) fruit in populations of central alborz mountains in Iran. *Res J Pharmacogn.* (2017) 4:1–12.

30. Saeidi K, Alirezalu A, Akbari Z. Evaluation of chemical constitute, fatty acids and antioxidant activity of the fruit and seed of sea buckthorn (*Hippophae rhamnoides* L.) grown wild in Iran. *Nat Prod Res.* (2016) 30:366–8. doi: 10.1080/14786419.2015.1057728

31. Vaitkevièienë N, Jarienë E, Danilèenko H, Kulaitienë J, Mažeika R, Hallmann E, et al. Comparison of mineral and fatty acid composition of wild and cultivated sea buckthorn berries from lithuania. *J Elem.* (2019) 24:1101–13. doi: 10.5601/jelem.2019.24.1.1759

32. Arif S, Ahmed S, Shah A, Hassan L, Awan S, Hamid A, et al. Determination of optimum harvesting time for vitamin C, oil and mineral elements in berries sea buckthorn (*Hippophae rhamnoides*). *Pak J Bot.* (2010) 42:3561–8.

33. Biel W, Jaroszewska A. The nutritional value of leaves of selected berry species. *Sci Agric.* (2017) 74:405–10. doi: 10.1590/1678-992x-2016-0314

34. Tkacz K, Wojdyło A, Turkiewicz I, Bobak Ł, Nowicka P. Anti-oxidant and anti-enzymatic activities of sea buckthorn (*Hippophaë rhamnoides* L.) fruits modulated by chemical components. *Antioxidants.* (2019) 8:618. doi: 10.3390/antiox8120618

35. Ficzek G, Mátravölgyi G, Furulyás D, Rentsendavaa C, Jócsák I, Papp D, et al. Analysis of bioactive compounds of three sea buckthorn cultivars (*Hippophaë rhamnoides* L. 'askola', 'leikora', and 'orangeveja') with HPLC and spectrophotometric methods. *Eur J Hortic Sci.* (2019) 84:31–8. doi: 10.17660/eJHS.2019/84.1.5

36. Lee Y, Jang H, Park K, Kim S, Kim J, Kim J, et al. Phytochemical analysis of the fruits of sea buckthorn (*Hippophae rhamnoides*): identification of organic acid derivatives. *Plants.* (2021) 10:860. doi: 10.3390/plants10050860

37. Bal L, Meda V, Naik S, Satya S. Sea buckthorn berries: a potential source of valuable nutrients for nutraceuticals and cosmoceuticals. *Food Res Int.* (2011) 44:1718–27. doi: 10.1016/j.foodres.2011.03.002

38. Odgerel U, Islam M, Kitamura Y, Kokawa M, Odbayar T. Effect of micro wet milling process on particle sizes, antioxidants, organic acids, and specific phenolic compounds of whole sea buckthorn (*Hippophae rhamnoides* L.) juices. *J Food Process Preserv.* (2021) 45:1–14. doi: 10.1111/jfpp.15474

39. Ma C, Zheng X, Deng S, Erdake A, He H. Determination and analysis of amino acids in fruits of *Hippophae rhamnoide*. *Protect Forest Sci Technol.* (2019) 9:39–40.

40. Tan L, Zhao J, Ma J, Ji T, Dong Q, Shen J. Analysis of nutritional compositions and nutritional quality evaluation in different parts of yushu hippophae (*Hippophae rhamnoides* L. subsp. sinensis). *Nat Prod Res Dev.* (2018) 30:807–16. doi: 10.16333/j.1001-6880.2018.5.014

41. Eggersdorfer M, Wyss A. Carotenoids in human nutrition and health. *Arch Biochem Biophys.* (2018) 652:18–26. doi: 10.1016/j.abb.2018.06.001

42. Johnson E. The role of carotenoids in human health. *Nutr Clin Care.* (2002) 5:56–65. doi: 10.1046/j.1523-5408.2002.00004.x

43. Seglioà D, Krasnova I, Grygier A, Radziejewska—Kubzdela E, Rudzińska M, Górnaś P. Unique bioactive molecule composition of sea buckthorn (*Hippophae rhamnoides* L.) oils obtained from the peel, pulp, and seeds via physical "solvent—free" approaches. *J Am Oil Chem Soc.* (2021) 98:1009–20. doi: 10.1002/aocs.12524

44. Dragović-Uzelac V, Bursać Kovačević D, Levaj B, Pedisić S, Mezak M, TomljenovićAna A. Polyphenols and antioxidant capacity in fruits and vegetables common in the croatian diet. *Agric Conspec Sci Cus.* (2009) 74:175–9.

45. Li N, Hu Y, Ge X. Determination of contents of total flavonoids and total polyphenols in *Hippophae rhamnoides* L. from different origins and their antioxidant activity. *Chem Bioeng.* (2021) 38:64–8. doi: 10.3969/j.issn.1672-5425.2021.08.010

46. Zadernowski R, Naczk M, Czaplicki S, Rubinskiene M, Szałkiewicz M. Composition of phenolic acids in sea buckthorn (*Hippophae rhamnoides* L.) berries. *J Am Oil Chem Soc.* (2005) 82:175–9. doi: 10.1007/s11746-005-5169-1

47. Ciesarová Z, Murkovic M, Cejpek K, Kreps F, Tobolková B, Koplík R, et al. Why is sea buckthorn (*Hippophae rhamnoides* L.) so exceptional? A review. *Food Res Int.* (2020) 133:109170. doi: 10.1016/j.foodres.2020.109170

48. Guo R, Guo X, Li T, Fu X, Liu R. Comparative assessment of phytochemical profiles, antioxidant and antiproliferative activities of Sea buckthorn (*Hippophaë rhamnoides* L.) berries. *Food Chem.* (2017) 221:997–1003. doi: 10.1016/j.foodchem.2016.11.063

49. Liu S, Xiao P, Kuang Y, Hao J, Huang T, Liu E. Flavonoids from sea buckthorn: a review on phytochemistry, pharmacokinetics and role in metabolic diseases. *J Food Biochem.* (2021) 45:e13724. doi: 10.1111/jfbc.13724

50. Raudonis R, Raudone L, Janulis V, Viskelis P. Flavonoids in cultivated berries of sea buckthorn (*Hippophaë rhamnoides* L.). *Planta Med.* (2014) 80:24. doi: 10.1055/s-0034-1395082

51. Olas B, Kontek B, Malinowska P, Żuchowski J, Stochmal A. *Hippophae rhamnoides* L. Fruits reduce the oxidative stress in human blood platelets and plasma. *Oxid Med Cell Longev.* (2016) 2016:1–8. doi: 10.1155/2016/4692486

52. Mohamed E, Tulcan C, Alexa E, Morar D, Dumitrescu E, Muselin F, et al. Sea buckthorn and grape extract might be helpful and sustainable phyto-resources as associated hypolipidemic agents-preliminary study. *Sustainability.* (2020) 12:9297. doi: 10.3390/su12219297

53. Cho C, Jang H, Lee M, Kang H, Heo H, Kim D. Sea buckthorn (*Hippophae rhamnoides* L.) leaf extracts protect neuronal PC-12 cells from oxidative stress. *J Microbiol Biotechnol.* (2017) 27:1257–65. doi: 10.4014/jmb.1704.04033

54. Serban M, Serban A, Ursoniu S, Dragan S. Systematic review on the potential of sea buckthorn *Hippophae rhamnoides* L. for a possible novel enriched bread for the patients with cardiovascular diseases. *Atherosclerosis.* (2019) 287:285. doi: 10.1016/j.atherosclerosis.2019.06.882

55. Gęgotek A, Jastrząb A, Jarocka-Karpowicz I, Muszyńska M, Skrzydlewska E. The effect of sea buckthorn (*Hippophae rhamnoides* L.) seed oil on UV-induced changes in lipid metabolism of human skin cells. *Antioxidants.* (2018) 7:110. doi: 10.3390/antiox7090110

56. Wu H, Li C, Cui M, Guo H, Chen S, Du J, et al. Polyphenols from *Hippophae rhamnoides* suppressed colon cancer growth by regulating miRNA-mediated cell cycle arrest and apoptosis in vitro and in vivo. *J Funct Foods.* (2021) 87:104780. doi: 10.1016/j.jff.2021.104780

57. Kim S, Hwang E, Yi S, Song K, Lee H, Heo T, et al. Sea buckthorn leaf extract inhibits glioma cell growth by reducing reactive oxygen species and promoting apoptosis. *Appl Biochem Biotechnol.* (2017) 182:1663–74. doi: 10.1007/s12010-017-2425-4

58. Li C, Li J, Li Y, Li L, Luo Y, Li J, et al. Isorhamnetin promotes MKN-45 gastric cancer cell apoptosis by inhibiting PI3K-mediated adaptive autophagy in a hypoxic environment. *J Agric Food Chem.* (2021) 69:8130–43. doi: 10.1021/acs.jafc.1c02620

59. Rao A, Rao L. Carotenoids and human health. *Pharmacol Res.* (2007) 55:207–16. doi: 10.1016/j.phrs.2007.01.012

60. Zhou F, Zhang J, Zhao A, Zhang Y, Wang P. Effects of sea buckthorn puree on risk factors of cardiovascular disease in hypercholesterolemia population: a double-blind, randomized, placebo-controlled trial. *Anim Biotechnol.* (2020) 2020:1–9. doi: 10.1080/10495398.2020.1853139

61. Ntanios F, Duchateau GS. A healthy diet rich in carotenoids is effective in maintaining normal blood carotenoid levels during the daily use of plant sterol-enriched spreads. *Int J Vitam Nutr Res.* (2002) 72:32–9. doi: 10.1024/0300-9831.72.1.32

62. Basu M, Prasad R, Jayamurthy P, Pal K, Arumughan C, Sawhney R. Anti-atherogenic effects of seabuckthorn (*Hippophaea rhamnoides*) seed oil. *Phytomedicine.* (2007) 14:770–7. doi: 10.1016/j.phymed.2007.03.018

63. Guo X, Yang B, Cai W, Li D. Effect of sea buckthorn (*Hippophae rhamnoides* L.) on blood lipid profiles: a systematic review and meta-analysis from 11 independent randomized controlled trials. *Trends Food Sci Technol.* (2017) 61:1–10. doi: 10.1016/j.tifs.2016.11.007

64. Yang X, Wang Q, Pang Z, Pan M, Zhang W. Flavonoid-enriched extract from *Hippophae rhamnoides* seed reduces high fat diet induced obesity, hypertriglyceridemia, and hepatic triglyceride accumulation in C57BL/6 mice. *Pharm Biol.* (2017) 55:1207–14. doi: 10.1080/13880209.2016.1278454

65. Gao S, Hu G, Li D, Sun M, Mou D. Anti-hyperlipidemia effect of sea buckthorn fruit oil extract through the AMPK and Akt signaling pathway in hamsters. *J Funct Foods.* (2020) 66:103837. doi: 10.1016/j.jff.2020.103837

66. Ma Z, Sun Q, Chang L, Peng J, Zhang M, Ding X. A natural anti-obesity reagent derived from sea buckthorn polysaccharides: structure characterization and anti-obesity evaluation in vivo. *Food Chem.* (2022) 375:131884. doi: 10.1016/j.foodchem.2021.131884

67. Guo C, Han L, Li M, Yu L. Seabuckthorn (*Hippophaë rhamnoides*) freeze-dried powder protects against high-fat diet-induced obesity, lipid metabolism disorders by modulating the gut microbiota of mice. *Nutrients.* (2020) 12:265. doi: 10.3390/nu12010265

68. Skalski B, Rywaniak J, Szustka A, Żuchowski J, Stochmal A, Olas B. Anti-platelet properties of phenolic and nonpolar fractions isolated from various organs of *Elaeagnus rhamnoides* (L.) a. nelson in whole blood. *Int J Mol Sci.* (2021) 22:3282. doi: 10.3390/ijms22063282

69. Skalski B, Stochmal A, Żuchowski J, Grabarczyk Ł, Olas B. Response of blood platelets to phenolic fraction and non-polar fraction from the leaves and twigs of *Elaeagnus rhamnoides* (L.) a. Nelson in vitro. *Biomed Pharmacother.* (2020) 124:109897. doi: 10.1016/j.biopha.2020.109897

70. Olas B, Kontek B, Szczesna M, Grabarczyk L, Stochmal A, Zuchowski J. Inhibition of blood platelet adhesion by phenolics' rich fraction of *Hippophae rhamnoides* L. fruits. *J Physiol Pharmacol.* (2017) 68:223–9.

71. Boca A, Ilies R, Saccomanno J, Pop R, Vesa S, Tataru A, et al. Sea buckthorn extract in the treatment of psoriasis. *Exp Ther Med.* (2019) 17:1020–3. doi: 10.3892/etm.2018.6983

72. Balkrishna A, Sakat S, Joshi K, Joshi K, Sharma V, Ranjan R, et al. Cytokines driven anti-inflammatory and anti-psoriasis like efficacies of nutraceutical sea buckthorn (*Hippophae rhamnoides*) oil. *Front Pharmacol.* (2019) 10:1186. doi: 10.3389/fphar.2019.01186

73. Hou D, Di Z, Qi R, Wang H, Zheng S, Hong Y, et al. Sea buckthorn (*Hippophaë rhamnoides* L.) oil improves atopic dermatitis-like skin lesions via Inhibition of NF-κB and STAT1 activation. *Skin Pharmacol Physiol.* (2017) 30:268–76. doi: 10.1159/000479528

74. Abdullahzadeh M, Shafiee S. To compare the effect of sea buckthorn and silver sulfadiazine dressing on period of wound healing in patients with second−degree burns: a randomized triple−blind clinical trial. *Wound Repair Regen.* (2021) 29:732–40. doi: 10.1111/wrr.12916

75. Upadhyay N, Kumar R, Mandotra S, Meena R, Siddiqui M, Sawhney R, et al. Safety and healing efficacy of sea buckthorn (*Hippophae rhamnoides* L.) seed oil on burn wounds in rats. *Food Chem Toxicol.* (2009) 47:1146–53. doi: 10.1016/j.fct.2009.02.002

76. Dudau M, Codrici E, Tarcomnicu I, Mihai S, Siddiqui M, Popescu I, et al. A fatty acid fraction purified from sea buckthorn seed oil has regenerative properties on normal skin cells. *Front Pharmacol.* (2021) 12:737571. doi: 10.3389/fphar.2021.737571

77. Rédei D, Kúsz N, Jedlinszki N, Blazsó G, Zupkó I, Hohmann J. Bioactivity-guided investigation of the anti-inflammatory activity of *Hippophae rhamnoides* fruits. *Planta Med.* (2018) 84:26–33. doi: 10.1055/s-0043-114424

78. Zheng W, Bai H, Han S, Bao F, Zhang K, Sun L, et al. Analysis on the constituents of branches, berries, and leaves of *Hippophae rhamnoides* L. by UHPLC-ESI-QTOF-MS and their anti-inflammatory activities. *Nat Prod Commun.* (2019) 14:1934578X1987140. doi: 10.1177/1934578X19871404

79. Baek S, Lee D, Jo M, Lee K, Lee Y. Inhibitory effect of 1,5-dimethyl citrate from sea buckthorn (*Hippophae rhamnoides*) on lipopolysaccharide-induced inflammatory response in RAW 264.7 mouse macrophages. *Foods.* (2020) 9:269. doi: 10.3390/foods9030269

80. Mulati A, Ma S, Zhang H, Ren B, Zhao B, Wang L, et al. Sea-buckthorn flavonoids alleviate high-fat and high-fructose diet-induced cognitive impairment by inhibiting insulin resistance and neuroinflammation. *J Agric Food Chem.* (2020) 68:5835–46. doi: 10.1021/acs.jafc.0c00876

81. Shah H, Shakir H, Safi S, Ali A. Hippophae rhamnoides mediate gene expression profiles against keratinocytes infection of *Staphylococcus aureus*. *Mol Biol Rep.* (2021) 48:1409–22. doi: 10.1007/s11033-021-06221-3

82. Qadir M, Abbas K, Younus A, Shaikh R. Antibacterial activity of sea buckthorn (*Hippophae rhamnoides* L.) against methicillin resistant *Staphylococcus aureus* (MRSA). *Pak J Pharm Sci.* (2016) 29:1711–3.

83. Smida I, Pentelescu C, Pentelescu O, Sweidan A, Oliviero N, Meuric V, et al. Benefits of sea buckthorn (*Hippophae rhamnoides*) pulp oil−based mouthwash on oral health. *J Appl Microbiol.* (2019) 126:1594–605. doi: 10.1111/jam.14210

84. Singh D, Jayashankar B, Mishra K, Tanwar H, Madhusudana S, Belludi A, et al. Adjuvant activity of ethanol extract of *Hippophae rhamnoides* leaves with inactivated rabies virus antigen. *Pharm Biol.* (2018) 56:25–31. doi: 10.1080/13880209.2017.1413662

85. Zhang P, Ji H, Hu Q. Research progress in clinical treatment of Alzheimer's disease and potential drugs from natural products. *Acta Pharm Sin.* (2022) 2022:1–21. doi: 10.16438/j.0513-4870.2022-0226

86. Dong K, Fernando W, Durham R, Stockmann R, Jayatunga D, Jayasena V. A role of sea buckthorn on Alzheimer's disease. *Int J Food Sci Technol.* (2020) 55:3073–81. doi: 10.1111/ijfs.14571

87. Ladol S, Sharma D. The effects of *Hippophae rhamnoides* in neuroprotection and behavioral alterations against iron-induced epilepsy. *Epilepsy Res.* (2021) 175:106695. doi: 10.1016/j.eplepsyres.2021.106695

88. Tudor C, Bohn T, Iddir M, Dulf F, Focsan M, Ruginã D, et al. Sea buckthorn 0il as a valuable source of bioaccessible xanthophylls. *Nutrients.* (2020) 12:76. doi: 10.3390/nu12010076

89. Elvira-Torales L, García-Alonso J, Periago-Castón M. Nutritional importance of carotenoids and their effect on liver health: a review. *Antioxidants.* (2019) 8:229. doi: 10.3390/antiox8070229

90. Guo Z, Cheng J, Zheng L, Xu W, Xie Y. Mechanochemical-assisted extraction and hepatoprotective activity research of flavonoids from sea buckthorn

(*Hippophaë rhamnoides* L.) pomaces. *Molecules.* (2021) 26:7615. doi: 10.3390/molecules26247615

91. Ran B, Guo C, Li W, Li W, Wang Q, Qian J, et al. Sea buckthorn (*Hippophae rhamnoides* L.) fermentation liquid protects against alcoholic liver disease linked to regulation of liver metabolome and the abundance of gut microbiota. *J Sci Food Agric.* (2021) 101:2846–54. doi: 10.1002/jsfa.10915

92. Zhang G, Liu Y, Liu P. Active components from sea buckthorn (*Hippophae rhamnoides* L.) regulate hepatic stellate cell activation and liver fibrogenesis. *J Agric Food Chem.* (2018) 66:12257–64. doi: 10.1021/acs.jafc.8b05306

93. Hao Y, Zhou F, Dong J, Wang Y, Lang Z, Li S, et al. Study on the role of flavonoids derived extract from seed residues of hippophae rhamnoides on high-fat diet induced obese mice. *J King Saud Univ Sci.* (2020) 32:1597–603. doi: 10.1016/j.jksus.2019.12.017

94. Ma C, Du L, Cai G. Investigation and research on the distribution of seabuckthorn germplasm resources in changji prefecture. *Mod Agric Sci Technol.* (2022) 2022:139–41. doi: 10.3969/j.issn.1007-5739.2022.02.046

95. Kozhakhiyeva M, Dragoev S, Uzakov Y, Nurgazezova A. Improving the oxidative stability and quality of new functional horse meat delicacy enriched with sea buckthorn (*Hippophae rhamnoides*) fruit powder extract or seed kernel pumpkin (*Cucurbita pero* L.) flour. *Comptes Rendus L'Academie Bulg Sci.* (2018) 70:132–40. doi: 10.7546/CRABS.2018.01.18

96. Salejda A, Nawirska-Olszańska A, Janiewicz U, Krasnowska G. Effects on quality properties of pork sausages enriched with sea buckthorn (*Hippophae rhamnoides* L.). *J Food Qual.* (2017) 2017:1–7. doi: 10.1155/2017/7123960

97. Tzachristas A, Pasvanka K, Liouni M, Calokerinos A, Tataridis P, Proestos C. Effect of *Hippophae rhamnoides* L. leaves treatment on the antioxidant capacity, total phenol content and sensory profile of moschofilero wines vinified with and without added sulphites. *Appl Sci.* (2020) 10:3444. doi: 10.3390/app10103444

98. Haq S, Mir M, Lone S, Banoo A, Shafi F, Mir S, et al. Explicating genetic diversity based on ITS characterization and determination of antioxidant potential in sea buckthorn (*Hippophae* spp.). *Mol Biol Rep.* (2022) 49:5229–40. doi: 10.1007/s11033-021-06619-z

99. Lele V, Monstaviciute E, Varinauskaite I, Peckaityte G, Paskeviciute L, Plytnikaite M, et al. Sea buckthorn (*Hippophae rhamnoides* L.) and quince (*Cydonia oblonga* L.) juices and their by-products as ingredients showing antimicrobial and antioxidant properties for chewing candy: nutraceutical formulations. *J Food Qual.* (2018) 2018:1–8. doi: 10.1155/2018/3474202

100. Kashyap P, Kumar S, Singh D. Performance of antifreeze protein HrCHI4 from *Hippophae rhamnoides* in improving the structure and freshness of green beans upon cryopreservation. *Food Chem.* (2020) 320:126599. doi: 10.1016/j.foodchem.2020.126599

101. Gu Y, Chen Z, Fu L. Development of yogurt mixed with sea buckthorn and carrot. *China Brew.* (2008) 12:113–8.

102. Gu Y, Chen X, Fu L. Preparation of yogurt mixed with *Hippophae rhamnoides* and tomoto. *China Brew.* (2008) 29:66–8.

103. Liu H, Wang R, Gao Z. Study on the process of compound yoghurt with sea buckthorn and water chestnut. *J Shanxi Datong Univ.* (2019) 35:59–62.

104. Nistor O, Bolea C, Andronoiu D, Cotârleț M, Stănciuc N. Attempts for developing novel sugar-based and sugar-free sea buckthorn marmalades. *Molecules.* (2021) 26:3073. doi: 10.3390/molecules26113073

105. Yuan L, Liu J, Wu T, Wu H, Liu L. Optimization of technology of *Elaeagnus angustifolia* and *Hippophae rhamnoides* compound jam by response surface methodology and prediction of storage period. *Storage Proc.* (2022) 22:37–44. doi: 10.3969/j.issn.1009-6221.2022.07.006

106. Sun L, Xu X. Preferred research on technology and materials of sea buckthorn composite jam. *Storage Proc.* (2014) 20:52–4.

107. Selvamuthukumaran M, Khanum F, Bawa A. Development of sea buckthorn mixed fruit jelly. *Int J Food Sci Technol.* (2007) 42:403–10. doi: 10.1111/j.1365-2621.2006.01233.x

108. Gâtlan A, Gutt G, Naghiu A. Capitalization of sea buckthorn waste by fermentation: optimization of industrial process of obtaining a novel refreshing drink. *J Food Proc Pres.* (2020) 44:14565. doi: 10.1111/jfpp.14565

109. Xin Y, Zhao S, Yang J, Zhang T, Zhang J, Wang Y. Effect of microwave-drying on the quality and antioxidant properties of *Ganoderma lucidum* fermented sea-buckthorn tea. *Int J Food Eng.* (2021) 17:65–74. doi: 10.1515/ijfe-2019-0271

110. Wen P, Zhao P, Qin G, Tang S, Li B, Zhang J, et al. Genotoxicity and teratogenicity of seabuckthorn (*Hippophae rhamnoides* L.) berry oil. *Drug Chem Toxicol.* (2020) 43:391–7. doi: 10.1080/01480545.2018.1497047

111. Tulsawani R. Ninty day repeated gavage administration of *Hipphophae rhamnoides* extract in rats. *Food Chem Toxicol.* (2010) 48:2483–9. doi: 10.1016/j.fct.2010.06.018

112. Zhao P, Wang S, Liang C, Wang Y, Wen P, Wang F, et al. Acute and subchronic toxicity studies of seabuckthorn (*Hippophae rhamnoides* L.) oil in rodents. *Regul Toxicol Pharmacol.* (2017) 91:50–7. doi: 10.1016/j.yrtph.2017.10.002

frontiers | Frontiers in Nutrition

TYPE Original Research
PUBLISHED 22 December 2022
DOI 10.3389/fnut.2022.1055725

Check for updates

OPEN ACCESS

EDITED BY
Bin Liang,
Ludong University, China

REVIEWED BY
Zhiguo Ma,
Jinan University, China
Peng Wang,
Ocean University of China, China

*CORRESPONDENCE
Jiayu Zhang
✉ zhangjiayu0615@163.com
Long Dai
✉ 2665275709@qq.com
Shaoping Wang
✉ wsp.0104@163.com

†These authors have contributed equally to this work

SPECIALTY SECTION
This article was submitted to Nutrition and Food Science Technology, a section of the journal Frontiers in Nutrition

RECEIVED 28 September 2022
ACCEPTED 06 December 2022
PUBLISHED 22 December 2022

CITATION
Jiang S, Dong W, Zhang Z, Xu J, Li H, Zhang J, Dai L and Wang S (2022) A new iron supplement: The chelate of pig skin collagen peptide and Fe^{2+} can treat iron-deficiency anemia by modulating intestinal flora. *Front. Nutr.* 9:1055725. doi: 10.3389/fnut.2022.1055725

COPYRIGHT
© 2022 Jiang, Dong, Zhang, Xu, Li, Zhang, Dai and Wang. This is an open-access article distributed under the terms of the Creative Commons Attribution License (CC BY). The use, distribution or reproduction in other forums is permitted, provided the original author(s) and the copyright owner(s) are credited and that the original publication in this journal is cited, in accordance with accepted academic practice. No use, distribution or reproduction is permitted which does not comply with these terms.

A new iron supplement: The chelate of pig skin collagen peptide and Fe^{2+} can treat iron-deficiency anemia by modulating intestinal flora

Shan Jiang[1,2†], Weichao Dong[1,3†], Zhen Zhang[1], Jing Xu[1,3], Haoran Li[1,3], Jiayu Zhang[1*], Long Dai[1*] and Shaoping Wang[1*]

[1]School of Pharmacy, Binzhou Medical University, Yantai, China, [2]Institute of Chinese Materia Medica, China Academy of Chinese Medical Sciences, Beijing, China, [3]School of Pharmacy, Shandong University of Traditional Chinese Medicine, Jinan, China

Introduction: Iron deficiency anemia (IDA) is one of the most common nutritional diseases encountered all over the world. Nowadays, oral iron supplementation is still the mainstay of IDA treatment.

Methods: In this study, a new iron nutritional supplement named pig skin collagen peptides ferrous chelates (PSCP-Fe) was prepared, and its structure was characterized by the scanning electron microscopy, sykam amino acid analyzer and Fourier transform infrared spectroscopy (FTIR). The anti-IDA activity of PSCP-Fe was evaluated in low-Fe^{2+} diet-induced IDA in rats. 16S amplicon sequencing technology was then used to reveal the mechanism of PSCP-Fe against IDA.

Results: The results of amino acid analysis and FTIR showed that aspartic acid (Asp), arginine (Arg), histidine (His), glutamic acid (Glu), cystine (Cys), and lysine (Lys) residued in PSCP chelated readily with Fe^{2+} through their functional groups. PSCP-Fe treated reversed the hematology-related indexes, such as red blood cells (RBC), hemoglobin (HGB), hematocrit (HCT), mean corpuscular volume (MCV), mean corpuscular hemoglobin (MCH), mean corpuscular hemoglobin concentrate (MCHC), serum ferritin (SF), serum hepcidin (HEPC) and serum transferrin receptor (TFR). And its regulatory action was better than that of $FeSO_4$. Moreover, PSCP-Fe alleviated the hepatocyte apoptosis and necrosis, Fe^{2+} loss, and injury in IDA rats. In addition, PSCP-Fe could significantly retrace the disturbed profile of gut microbiota in IDA rats ($p < 0.05$) and significantly up-regulated the relative abundances of nine bacterial genus, including *Lactobacillus, Alloprevotella, unclassified_of_Oscillospiraceae,* and *NK4A214_group* ($p < 0.05$). It could also downgrade the relative abundances of *Subdoligranulum* and *Coriobacteriaceae_UCG-002* ($p < 0.05$). The results of Spearman's correlation analysis and distance-based redundancy analysis (db-RDA) revealed that *Subdoligranulum* and *Christensenellaceae*_R-7_group may be potential microbial markers for effective PSCP-Fe action in the treatment of IDA.

Discussion: Overall, our results elucidate the interactions between gut bacteria and related cytokines and reveal the mechanisms underlying the anti-IDA effect of PSCP-Fe. They will thus provide a theoretical foundation for PSCP-Fe as a new iron nutritional supplement.

KEYWORDS

iron deficiency anemia, iron nutritional supplement, peptides-ferrous chelate, structural characterization, gut flora

Introduction

Iron deficiency anemia (IDA) is the most common nutritional deficiency in the world (1). The World Health Organization (WHO) estimates that two billion individuals, mostly residing in low- and middle-income countries, are influenced by IDA due to a variety of causes, including parasitic infections, nutritional deficiencies, chronic diseases, hemoglobinopathies, and lead poisoning (2). Moreover, IDA is frequently identified in high-risk groups in developed countries, such as infants, women of childbearing age, and pregnant women (3, 4). Clinical research indicates that IDA is an independent risk in multiple diseases. Children with IDA often suffer from intellectual disability, non-specific immune deficiency, inflammation, and cognitive impairment. Adults suffering from IDA may face tumors, paralysis, tissue ischemia, and digestive system diseases (3). Although physiological and nutritional studies have confirmed that many factors can cause IDA, an insufficient intake of iron through diet and malabsorption of iron are predominant causes for the occurrence of IDA. Therefore, the global incidence of IDA can be reduced by increasing the intake of iron-rich foods and improving iron absorption.

Oral iron supplements are the mainstay of treatment for IDA. Iron can be supplemented as inorganic and organic salts of iron, amino acid-iron, and peptide-iron chelates (3, 4). However, inorganic iron salts have many disadvantages, such as lower iron bioavailability, lower absorption, and poor stability, which severely restrict their clinical application. In addition, inorganic iron salts can also cause colitis and liver damage. Recently, many studies have shown that bioactive peptides from animals, plants, and marine algae, exhibit numerous merits, such as low toxicities, chelation sites, and excellent bioactivities as compared to prototype proteins. These peptides can be released from their parent protein *via* gastrointestinal digestion or enzymatic hydrolysis (5). Usually, food-derived bioactive peptides, containing between 2 and 20 amino acids, can be used to prepare nutritional supplements with iron chelates. Some ferrous-peptide chelates have been reported and applied to treat IDA, such as chickpea peptide-iron chelates and ferrous-hairtail peptide chelates (6, 7).

Improvement in the microenvironment for iron to be absorbed effectively is another approach to the treatment of IDA. The gut bacteria, i.e., the "new organ of the human body," may act as a key modulator of iron homeostasis (8). In the intestine, despite its pivotal role in cellular proliferation, free Fe^{2+} may generate toxic reactive oxygen species (ROS), which can affect intestinal integrity by inducing oxidative stress (9). In addition, unabsorbed Fe^{2+} can stimulate virulence of pathogenic bacteria (e.g., *Escherichia coli*, *Clostridium Welchii*, *Enterococcus faecalis*), which contributes to an oxidative proinflammatory environment. Gut probiotics, including *Lactobacillus*, *Bacillus*, *Bacteroides,* and *Clostridium*, can inhibit the expression of transferrin receptor (TFR), thereby reducing the proportion of Fe^{2+} in gut and blood, which reverses the above-mentioned adverse reactions (10). In addition, the gut probiotics can release multiple metabolites [e.g., branched-chain amino acids, bile acids, short-chain fatty acids (SCFAs), and nucleosides] by fermenting nutrients, which can improve intelligence and immunity by increasing the release of neurotransmitters and immune factors (11). Therefore, gut probiotics may help overcome the challenges in IDA treatment by modulating intestinal bacteria.

Pig skin, which is often used as a by-product from meat processing premises, is associated with environmental problem and low economic value. Thus, the high value-added utilization of pig skin needs to be valued and solved (12). Based on morphology and physiological functions, domestic pig skin seems to be the closest to human skin in composition (13). For this reason, it is a good model for studies on wound healing and permeability (13, 14). It is rich in collagen, and thus, is marked as a good source of active peptides. Pig skin is also used as a raw material for the preparation of new Ejiao—a blood tonic in Traditional Chinese Medicine that has been used for 2000 years. However, there are only a few studies that explore the use of pig skin collagen peptides (PSCP) for the preparation of ferrous chelates. The therapeutic effect of these chelates on IDA has never been reported, and thus, the modulation of gut microbiota in the IDA model remains ambiguous. In this study, we first prepared PSCP by enzymatic hydrolysis of pig skin with trypsin and pepsin. PSCP was then chelated with Fe^{2+} to obtain the PSCP-ferrous chelates (PSCP-Fe). The microstructure and chelation sites in PSCP-Fe were identified *via* multiple analytical

instruments. An IDA rat model was then established to evaluate the potential of PSCP-Fe for the treatment of IDA. The related mechanisms of PSCP-Fe against IDA were also revealed by correlation analysis of gut microbiota structure and cytokines.

Materials and methods

Materials and reagents

Fresh pig skin was purchased from Jinluo Foods Co., Ltd. (Yantai, China) and was stored at −20°C until further experimentation. Pepsin (3,000 U/mg) and trypsin (1,000–1,500 U/mg) were obtained from Shanghai Lanji Technology Development Co., Ltd. (Shanghai, China). Ferrous chloride (molecular weight 126.75 Da) was purchased from Shanghai Biological Technology of Vibration Spectrum Co., Ltd. (Shanghai, China). Ferrous sulfate tables were purchased from Shanxi Lijiu Pharmaceutical Co., Ltd. (Shanxi, China). Ascorbic acid, anhydrous ethanol, and other reagents used in this study were of analytical grade. The Prussian Blue Stain Kit and hematoxylin-eosin/HE staining kit were obtained from Solarbio Technology Co., Ltd. (Beijing, China).

Preparation and characterization of PSCP-Fe

Preparation of PSCP-Fe

Collagen was extracted from pig skin according to the method described by He et al. (15). After being defatted by petroleum ether, collagen was added to deionized water to obtain a concentration of 10% (weight/volume, w/v). The mixture was subjected to continuous enzymatic hydrolysis with pepsin (1.0% of the substrate, pH 1.5, 2 h) and trypsin (1.0% of the substrate, pH 8.0, 3 h) at 40°C. Finally, the enzyme solution was soaked in boiling water for 15 min to inactivate the enzymes. Samples were then centrifuged at 4,000 rpm for 10 min, and the supernatant was subjected to ultrafiltration using a 3 kDa cut-off membrane (Millipore Corporation, Bedford, MA, USA). The filtrate solution was lyophilized (−80°C, 48 h) to obtain the PSCP powder.

The PSCP-Fe was prepared following the procedure described by Ma et al. with minor adjustments (16). The PSCP (5%) were suspended in distilled water (20 mL, pH 7.0), mixed with 300 μL of $FeCl_2$ (0.01%, w/v) and 75 μL of ascorbic acid (0.01%, w/v) at pH 5.0. The mixture was stirred at 40°C for 40 min, and anhydrous ethanol (6 of the solution) was added to remove unnecessary peptides. The mixture was centrifuged at 4,000 rpm for 10 min, and the precipitate, referred to as PSCP-Fe, was lyophilized (−80°C, 48 h). After the binding treatment, ferrous content in PSCP-Fe was measured by inductively coupled plasma atomic emission spectroscopy (ICP-AES, Perkin Elmer, Waltham, MA, USA) according to the method of Li et al. (17).

Structural characterization of PSCP-Fe

The occurrence of chelation reactions often alters the apparent structure of the peptide. Hence, the scanning electron microscopy (Phenom XL, Phenom-World BV, Eindhoven, Holland) was used to distinguish PSCP-Fe and PSCP by applying 10 mA current and 5 kV voltage. The chelating ability of peptides and Fe^{2+} is closely associated with the types of amino acid residues present. The amino acid composition of PSCP-Fe was characterized by a known method (16) with minor modifications. 100 mg of PSCP-Fe was hydrolyzed with 6 M HCl at 110°C for 24 h. The mixture was then analyzed using a Sykam amino acid analyzer (S-433D, Sykam Corporation, Munich, Germany). The chelation sites on PSCP and ferrous could be more easily diagnosed using a Fourier transform infrared spectroscopy (FTIR), whose experimental design was as follows: 5.0 mg each of PSCP and PSCP-Fe mixed with potassium bromide were flaked and then analyzed using an FTIR spectrometer (Shimadzu IRTracer-100, JPN) in the wavelength range of 4,000–400 cm^{-1} at 30°C.

Evaluation of the effect of PSCP-Fe in the IDA rat model

Animals, diets, and experimental design

Forty-eight male Sprague-Dawley (SD) rats (SPF weighing 110 ± 10 g) were purchased from Jinan Pengyue Laboratory Animal Breeding Co., Ltd. (Shandong, China, SYXK (RU) 2019–0003). All rats were housed at room temperature (24 ± 2°C) with humidity (50 ± 5%) and 12 h light/12 h dark cycle. The animal usage protocol was approved by the Institutional Animal Care and Use Committee at Bin Zhou Medical University (approval certificate number: 2020–090). The animal facilities and protocols complied with the Guide for the Care and Use of Laboratory Animals [USA National Research Council, 1996 (18)].

Deionized water was provided continuously to all rats. After 7 days, all rats were randomly divided into control group (Control, 8 rats) and IDA groups (40 rats) based on body weights (BW). Rats in the control group were fed normal rodent chow (45 mg Fe kg^{-1} of diet, Pengyue, Shandong, China), and those in the IDA groups were fed a low-Fe^{2+} diet (4.93 mg Fe kg^{-1} of diet, Beijing Keao Xieli Animal Feed Co., Ltd., Beijing, China) for 5 weeks (6, 16). The health of the IDA model rats was assessed by hemoglobin (HGB), BW, and mental state of rats compare with those in the control group. Rats in the IDA groups were again allocated into five groups: the model group (Model, $n = 8$), the $FeSO_4$ group ($FeSO_4$, 1.62 mg Fe/100 g BW, $n = 8$), the low dose PSCP-Fe group (LPSCP-Fe, 0.81 mg Fe/100 g BW, $n = 8$), the medium dose PSCP-Fe group (MPSCP-Fe, 1.62 mg

Fe/100 g BW, $n = 8$) and the high dose PSCP-Fe group (HPSCP-Fe, 3.24 mg Fe/100 g BW, $n = 8$). PSCP-Fe solutions were freshly prepared in distilled deionized water and intragastric administration was performed once per day for 3 weeks.

Biological sample collection and preservation

At the end of the experimental period, fresh feces of all rats were collected in sterile plastic tubes and then stored at −80°C until further analysis. The rats were fasted for 12 h before being anesthetized with 10% chloral hydrate. Blood samples from the abdominal aorta were collected and divided into two components. A component was used to analyze blood-related parameters associated with IDA, and another component was centrifuged at 4,500 rpm/min for 10 min at 4°C. Liver and colon tissues were stored in a 4% paraformaldehyde solution for histological analysis.

Determination of hematology-related indexes in IDA rats

The levels of red blood cells (RBC), HGB, hematocrit (HCT), mean corpuscular volume (MCV), mean corpuscular hemoglobin (MCH), and mean corpuscular hemoglobin concentrate (MCHC) were determined using an automated hematology analyzer (BC-3000, Tokyo Mairui Co., Tokyo, Japan). Serum ferritin (SF), serum hepcidin (HEPC), and TFR were measured using enzyme-linked immunosorbent assay (ELISA) kits (Shanghai Enzyme-linked Biotechnology Co., Ltd., Shanghai, China).

Evaluation of liver and colon damage

A long-term iron-deficient diet causes the imbalance of liver function and iron loss. In this research, hepatic tissues fixed in 4% paraformaldehyde solution were dehydrated, embedded in paraffin, and cross-sectioned into 4-μm thick slices. The slices were then treated with HCl (5%) to release ferric ions, followed by treatment with 5% potassium ferrocyanide (Sigma, MO, USA) to produce insoluble ferric ferrocyanide and counterstained with the neutral red (18, 19). In addition, the H&E staining of colon tissue was carried out according to the previous method (20). Briefly, colon tissues were cut into 5 μm-thick sections and stained with the H&E kit (Solarbio Science and Technology, Beijing, China). All the stained samples were observed under the microscope (DM1000, Leica Microsystems, Wetzlar, Germany).

Gut bacteria analysis by 16S rRNA gene-based amplicon sequencing

Fecal DNA extraction and PCR amplification

The total bacterial DNA was isolated from fecal samples using the cetyltrimethylammonium bromide (CTAB) method. The specific experimental protocol was as follows: DNA concentration in all samples was detected by1% agarose gel. DNA was diluted to 1 ng/μL using sterile water. Extracted DNA from each sample was then used as a template to amplify the *V3-V4* region of 16S rRNA genes using PCR (21). All PCRs were performed as 30 μL reactions containing 15 μL of Phusion® High-Fidelity PCR Master Mix with GC Buffer (New England Biolabs), 0.2 μM of forward and reverse primers each, and 10 ng of template DNA. The purity of PCR products was examined using electrophoresis (2% agarose gel).

16S rRNA gene-based amplicon sequencing and bioinformatics analysis

The sequencing libraries were generated using TruSeq® DNA PCR-Free Sample Preparation Kit (Illumina, USA) according to the manufacturer's recommendations. Index codes were also added. The library quality was assessed on the Qubit @ 2.0 Fluorometer (Thermo Scientific). The library was then sequenced on an Illumina NovaSeq platform.

Analytical methods were used to identify bacteria and their abundances in the samples and among groups. The alpha diversity index of samples was evaluated using Mothur (Version 1.30) (22). Other related indexes, such as observed operational taxonomic units (OTUs), Chao1 richness estimator, Shannon diversity index, and Faith's phylogenetic distance, were calculated to estimate microbial diversity within individual samples. The observed OTUs and Chao1 indexes reflect the abundance of species, while the Shannon and Simpson indexes represent the abundance and diversity of species constituting the samples. The QIIME analysis was used to analyze beta diversity, and the similarity in species diversity across the different groups of samples was compared. The beta diversities were visualized by PCoA (principal coordinate analysis) and NMDS (Non-metric multidimensional scaling, NMDS) frameworks. PCoA with Bray-Curtis distance was used to examine the separation of species and metabolites in the different samples (23). Differences in the relative abundance of the microbial features were determined by linear discriminant analysis (LDA) effect size (LEfSe) (24).

Spearman correlation analysis

The Spearman correlation coefficient[1] was calculated to determine the potential correlations between the intestinal flora and different biochemical indicators. The correlations determined between the variables were displayed using heat maps. Finally, a network revealing the gut microbiota, associated markers, and disease relationships was drawn to evaluate the beneficial effects of PSCP-Fe against IDA.

Statistical analysis

All results were analyzed using the Statistical Product and Service Solutions (SPSS) 23.0 software (SPSS Inc., Chicago,

1 https://www.bioincloud.tech/

IL, USA), and were presented as Mean ± standard deviation (SD). One-way ANOVA and Student's *t*-test were used to assess statistical significance for multiple comparisons among the different groups. $P < 0.05$ and $p < 0.01$ were defined as statistically significant. Data visualization of results was performed using GraphPad Prism 8.0.2 software (San Diego, CA, USA).

Results

Structural characterization of PSCP-Fe

As shown in **Figures 1A, B**, the microstructure of PSCP-Fe was significantly different from that of PSCP. The PSCP surface was relatively flat, smooth, and voluminous. A few cracks were seen, which could have been carved by drying PSCP in the electron microscope. Conversely, the surface of PSCP-Fe was irregular and rough. The significant difference in the surface structures of PSCP and PSCP-Fe suggested the success of the chelation reaction. Amino acid composition analysis showed that PSCP and PSCP-Fe contained 17 amino acids, illustrating the integrity of amino acids during the chelation reaction (**Supplementary Table 1**). The contents of some amino acids, including aspartic acid (Asp), arginine (Arg), histidine (His), glutamic acid (Glu), cystine (Cys), and lysine (Lys), were increased in PSCP-Fe as compared to PSCP (**Figure 1C**). It has been reported that the composition and sequence of amino acids in peptides determine their ferrous-binding capacities (25). Thus, our results suggested that peptides containing the above amino acids may exhibit higher ferrous-chelating capacities (25–30).

FTIR spectroscopy was applied to reveal the chelation sites on PSCP for Fe^{2+}. PSCP could generate several infrared-active vibrational modes: −NH (−3,300 cm^{-1}), −OH (−3,100 cm^{-1}), C-O (−1,400 cm^{-1}), and C = O (−1,500 cm^{-1}) (31). As shown in **Figure 1D**, the FTIR spectrum of PSCP-Fe presented interesting features as compared to the spectrum of PSCP. Firstly, the C-O and C = O bands at 1393.92 and 1521.18 cm^{-1} in the PSCP spectrum were shifted to 1331.62 and 1535.59 cm^{-1} after binding with Fe^{2+}, which might be caused by the combination of −COO and Fe^{2+}. The amide (−NH) band at 3272.64 cm^{-1} in PCSP was shifted to 3306.69 cm^{-1} in PSCP-Fe, indicating that −NH was also involved in the chelation reaction. The Amide I peak was observed at 1,600–1,700 cm^{-1}, which was the absorption band of C = O stretching. In this study, the band of amide I was shifted from 1633.71 to 1647.51 cm^{-1} after Fe^{2+} chelation. Moreover, the broad absorption bands at 900, 922, and 1,020 cm^{-1}, which were generated by the benzene ring of tyrosine, remained consistent in PSCP and PSCP-Fe, excluding the possibility of tyrosine being coordinated to Fe^{2+}. As the above results, Asp, Arg, His, Glu, Cys, and Lys in PSCP should be more easily chelated with Fe^{2+} through functional groups of −NH and −COO.

PSCP-Fe attenuates Low-Fe^{2+} diet-induced dysplasia and promotes iron absorption in IDA rats

Iron deficiency usually affects the growth and development of the body. In this study, rats that were given a low-Fe^{2+} diet indeed presented many undesirable morphological features as compared to the control rats. For instance, the BWs of IDA rats were significantly decreased ($p < 0.05$), this was accompanied by negative symptoms, such as dullness, unresponsiveness, and roughness of skin. These results suggested that the low-Fe^{2+} diet adversely affected the growth of rats. After 21 days of iron supplementation, the BWs in all PSCP-Fe treatment groups were significantly increased ($p < 0.05$), while the untreated IDA model and the $FeSO_4$ treatment group, showed no significant difference ($p > 0.05$). In addition, there were no significant differences in BW among the three PSCP-Fe treatments (low, medium, and high), indicating that PSCP-Fe had a positive effect on the growth of IDA rats (**Figure 2A**).

The serum indicators in the rat groups are shown in **Figure 2B**. The levels of RBC and HGB, MCHC, MCH, HCT, and MCV were significantly lower in the model group compared to the control group ($p < 0.001$). After iron supplementation, these serum indicators were significantly raised ($p < 0.05$). The RBC and HGB, MCHC, HCT, and MCV were significantly increased by 1.058, 1.026, 1.028, 1.010, and 1.004% in the MPSCP-Fe group compared to the $FeSO_4$ group ($p < 0.05$). In addition, RBC, HGB, MCHC, MCH, HCT, and MCV were also increased by 1.075, 1.061, 1.028, 1.002, 1.050, and 1.015% in the HPSCP-Fe group compared to the $FeSO_4$ group ($p < 0.05$). Therefore, PSCP-Fe can effectively improve anemia symptoms.

Simultaneously, the SF, HEPC, and TFR levels were also determined. The contents of SF and HEPC in the Model group were significantly decreased, while TFR was up-regulated compared to the control group ($p < 0.001$). However, all iron supplement significantly reversed the above situations ($p < 0.05$). Additionally, SF and HEPC levels were increased significantly (by 1.021 and 1.335%), while TFR levels were decreased (by 1.098%) in the MPSCP-Fe group compared with $FeSO_4$ group. These results showed the effective effect of PSCP-Fe resist IDA.

PSCP-Fe can alleviate Fe^{2+} loss in the liver and colon damage

The iron deposition and pathological changes in liver tissues in each group of rats were assessed *via* Prussian blue staining assay. The rats in the IDA model group exhibited a

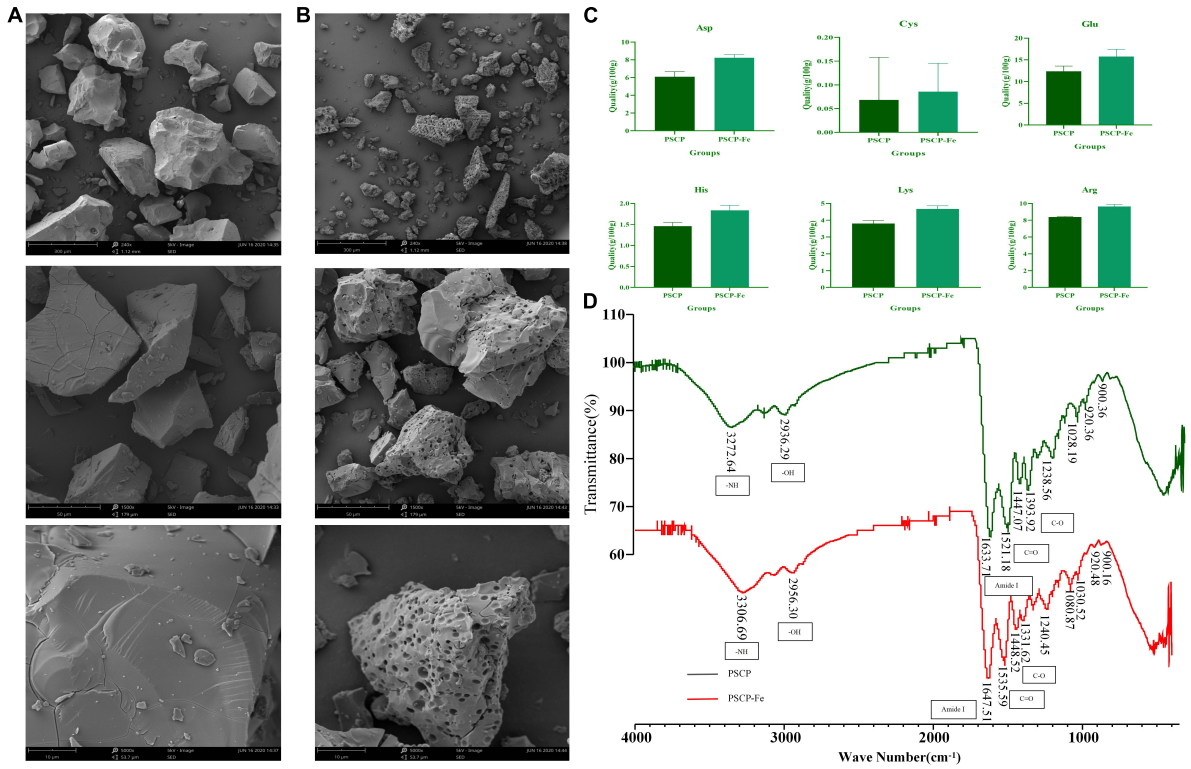

FIGURE 1
The scanning electron microscopy of PSCP **(A)** and PSCP-Fe **(B)**. Differences in amino acid content between PSCP and PSCP-Fe **(C)**. The FTIR spectroscopy of PSCP and PSCP-Fe **(D)**.

series of adverse symptoms, including hepatocyte apoptosis and necrosis, nucleus pyknosis, hepatocyte edema, and ballooning degeneration. These pathological injuries were clearly alleviated upon supplementation with Fe^{2+}, especially in MPSCP-Fe and HPSCP-Fe groups. Simultaneously, Fe^{2+} was scarcely observed in IDA rats, indicating a low-Fe^{2+} diet restricted the accumulation of Fe^{2+} in the liver. After treatment, all Fe^{2+} supplements reversed the above problem. PSCP-Fe revealed better enrichment effects of iron than $FeSO_4$ at all doses. In addition, the reversal effect of HPSCP-Fe was better than that of LPSCP-Fe and MPSCP-Fe (Figure 2C), suggesting that PSCP-Fe could effectively promote the transportation and enrichment of Fe^{2+} to some extent.

The colon is critical for the transportation of Fe^{2+} from the intestine into the circulatory system (32). Fe^{2+} deficient diet caused colon damage, accelerating the process of IDA. In this study, IDA rats induced by a low-Fe^{2+} diet developed diarrhea, suggesting the occurrence of colon injury (33). HE staining was used to analyze the histology of the colon. Colon damage in the supplementary ferrous groups was much less than that observed in the IDA model group. Furthermore, colon morphology in the PSCP-Fe groups was the same as that observed in the control group, whereas colon morphology in the $FeSO_4$ group was not the same as that observed in the control group (Figure 2D). These observations suggested that PSCP-Fe administration was beneficial to the colon or caused less irritation to the intestinal tract.

The PSCP-Fe treatment restored dysbiosis in the gut microbiota in IDA rats

In this study, 24 fecal samples from the Control, Model, HPSCP-Fe, and LPSCP-Fe groups were used to evaluate the ameliorative effect of PSCP-Fe against IDA. The composition and diversity of the bacterial communities were assessed through 16S rRNA gene sequencing. After quality filtering and trimming, 1,355,946 high-quality sequences were obtained with an average of 56,497 reads per sample. The Pan/Core and rarefaction curves showed the presence of clear asymptotes, confirming the completeness of the sampling (Supplementary Figure 1).

Illumina MiSeq 16S rRNA amplicon sequencing was conducted to determine the effects of PSCP-Fe treatment on gut microbiota. As shown in Figures 3A–C, the Sobs Chao index and Ace revealed that the alpha diversity in the model rats was significantly lower than that in the other groups ($p < 0.05$).

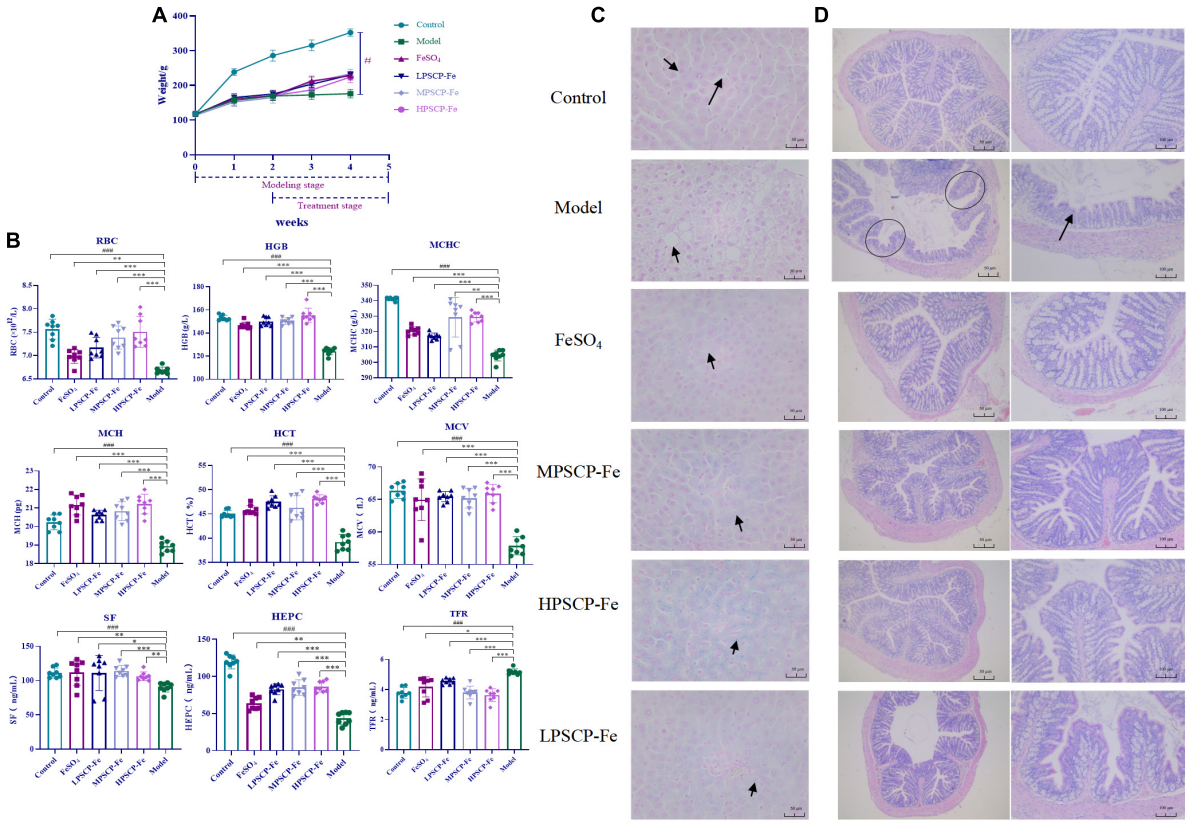

FIGURE 2
Effects of PSCP-Fe on body weight **(A)** and blood routine parameters **(B)** in IDA rats. The data in the columns are expressed as the mean ± SD ($n = 8$). Different marks ($^{\#}$, *) indicate differences at the $p < 0.05$ level. $^{\#\#\#}p < 0.001$: Control vs. Model; $^{*}p < 0.05$, $^{**}p < 0.01$, and $^{***}p < 0.001$: Treatments vs. Model. Liver iron staining evaluation by Prussian blue staining method **(C)**, × 400 magnification. Evaluate the histopathology changes of the rats colon tissues by H&E staining **(D)**.

However, PSCP-Fe recovered the alpha diversity relative to the IDA rats. The Venn plots showed the structural similarity and overlap of species in different groups. 728 OTUs were identified in the Control group, while only 517 OTUs were in Model group, indicating that the low-Fe^{2+} diet directly affected the composition of the intestinal flora (Figure 3D). With PSCP-Fe treatment, the numbers of OTUs were increased to 739 and 711 in HPSCP-Fe and LPSCP-Fe, respectively. Overall, the model, control, LPSCP-Fe, and HPSCP-Fe groups shared 299 OTUs with the following percentages: 41.07, 57.83, 40.46, and 42.05, indicating that the gut microbiota of the IDA model group changed significantly compare with the control group, while PSCP-Fe administration ameliorated this issue.

The beta diversity was described by PCoA analysis and NMDS, it showed that there were different clusters among the four groups, with significant differences among the clusters (Figures 3E, F). The low-Fe^{2+} diet led to a decrease in the number of OTUs in IDA rats, but the situation could be reversed with PSCP-Fe intervention. Taken together, the results suggested that PSCP-Fe treatment could modulate the IDA-induced dysbiosis of intestinal flora and restored a microbial community similar to that in the control.

Comparison of gut microbiome at phylum and genus levels

At the phylum level (Figure 3G), *Firmicutes* and *Bacteroidota* were the two most dominant phylum with a relative abundance of 97.1% in the control group, 81.4% in the model group, 97.1% in the HPSCP-Fe group, and 98.4% in the LPSCP-Fe group. The differently abundant taxa among the experimental samples were identified using LEfSe performed at the taxonomic levels from phylum to genus, the above results is shown at Figure 3I. In addition, the low-Fe^{2+} diet could decrease the relative abundances of *Firmicutes* and *Bacteroidota*, yet PSCP-Fe fixed this deficiency. At the same time, microbiota composition at the genus levels were also identified (Figure 3H). For genus analysis, the composition of gut microbiota (greater than 0.1% abundance) is presented and

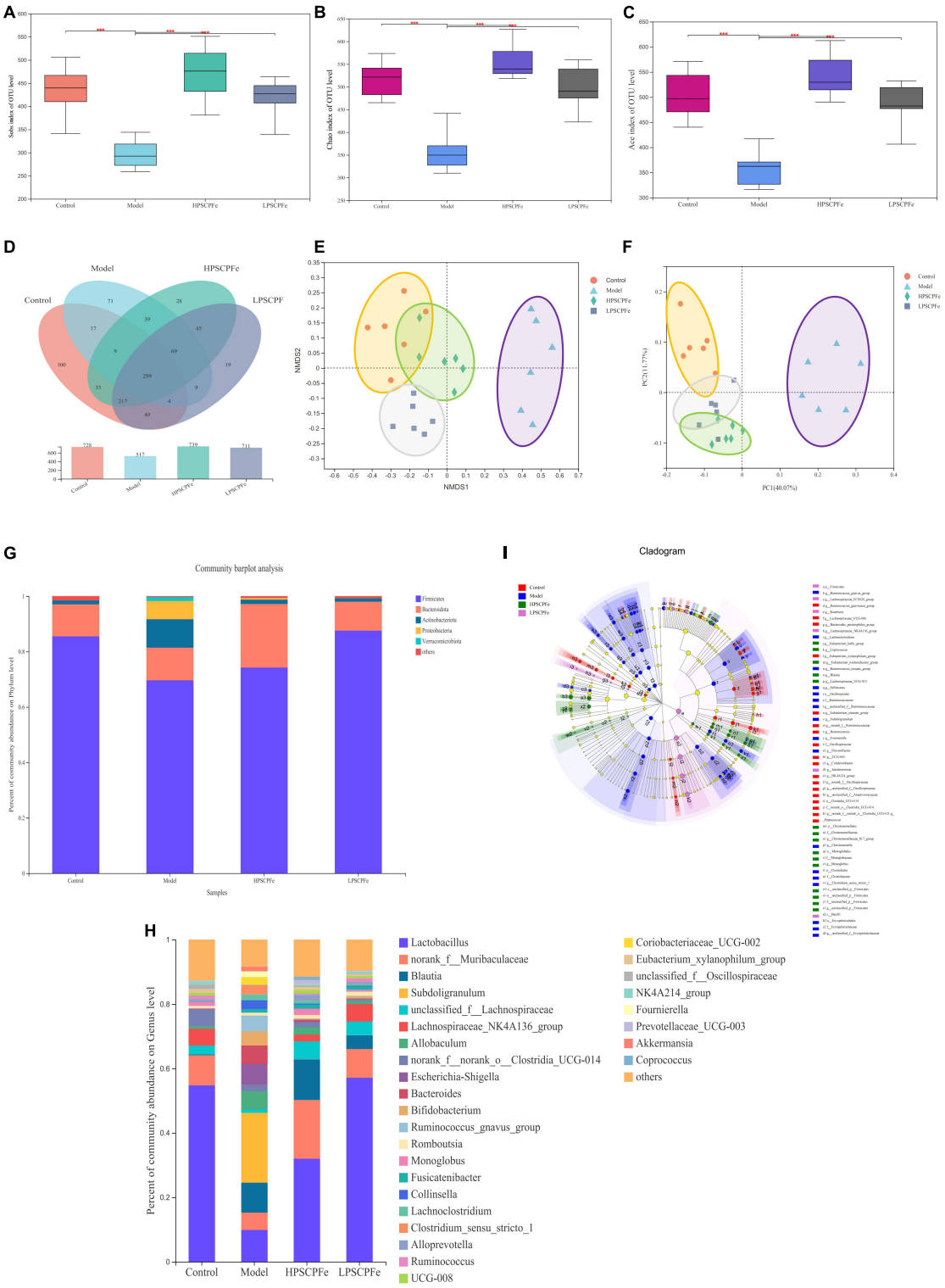

FIGURE 3
PSCP-Fe treatment restored the distribution of gut flora composition in IDA rat. **(A)** The Sobs index of OTU level. **(B)** The Chao index of OTU level. **(C)** The Ace index of OTU level. In each group, $n = 6$. $^{***}p < 0.001$: control or treatment vs. model group. **(D)** Venn diagram of 16S rRNA based profiling. **(E)** Non-metric multidimensional scaling (NMDS) based on the Bray-Curtis dissimilarity. **(F)** Bray-Curtis PCoA of 16S rRNA based profiling. **(G)** Relative abundance of bacterial phylum. **(H)** Relative abundance of bacterial genus. **(I)** Taxonomic cladogram generated by LEfSe analysis showing taxa significantly enriched in control (red), model (blue), HPSCP-Fe (green), LPSCP-Fe (purple), respectively. Each ring represents a taxonomic level from phylum to genus. The diameter of each dot on the ring represents the relative abundance of the taxon.

summarized in Figure 4. 20 gut bacteria, such as *Lactobacillus*, *norank_f_Muribaculaceae*, *Blautia*, *Subdoligranulum*, *unclassified_f Lachnospiraceae*, *NK4A214_group*, *Fournierella*, *Prevotellaceae_UCG-003*, *Akkermansia,* and *Coprococcus*, were significantly altered ($p < 0.05$). The Kruskal Wallis test for the significance of difference was performed on genus-level OTUs and genera ($p < 0.05$). The 13 bacteria in IDA rats were significantly reduced as compared to the control ($p < 0.05$), and 7 bacteria had increased ($p < 0.05$). *Lactobacillus, Alloprevotella, unclassified_of_Oscillospiraceae, NK4A214_group, Prevotellaceae_UCG-003, Colidextribacter, Coriobacteriaceae_UCG-005, Enterorhabdus,* and *Christensenellaceae_R-7_group* were reduced in IDA rats upon PSCP-Fe treatment. However, two simultaneous doses of PSCP-Fe significantly increased the relative abundances of 5 out of 9 bacteria ($p < 0.05$). In addition, LPSCP-Fe and HPSCP-Fe could downgrade the relative abundances of *Subdoligranulum* and *Coriobacteriaceae_UCG-002* ($p < 0.05$). *Lactobacillus, Alloprevotella, unclassified_of_Oscillospiraceae, NK4A214_group, Prevotellaceae_UCG-003, Colidextribacter, Coriobacteriaceae_UCG-005, Enterorhabdus,* and *Christensenellaceae_R-7_group* might benefit the action of PSCP-Fe in the treatment of IDA. However, *Subdoligranulum* and *Coriobacteriaceae_UCG-002* contribute to the occurrence of IDA.

The correlation between hematological indicators and intestinal microbiota

To determine the regulatory mechanisms of different microbiota, the Spearman's correlation analysis was used. The relative abundances of specific microflora were correlated with hematology-related indicators as shown in Figure 5A. Eighteen bacterial genus showed correlations with cytokines at different levels, among which five bacteria correlated positively with TFR ($p < 0.05$). Based on the correlation coefficients, correlations with TFR of different species were in the order of *Subdoligranulum* ($p \approx 0.003$) > *Faecalibaculum* ($p \approx 0.009$) > *Coriobacteriaceae_UCG-002* ($p \approx 0.027$) > *Lachnoclostridium* ($p \approx 0.046$) > *Adlercreutzia* ($p \approx 0.047$). In addition, these gut bacteria presented negative correlations with RBC, HGB, HEPC, and SF. However, only *Subdoligranulum* was significantly negatively correlated with all four factors ($p < 0.05$), where the correlation coefficients were 0.009 (RBC), 0.002 (HGB), 0.01 (HEPC), and 0.002 (SF), showing that *Subdoligranulum* strongly promoted the occurrence of IDA. In addition, *Faecalibaculum*, *Coriobacteriaceae_UCG-002, Adlercreutzia,* and *Lachnoclostridium* showed significantly negative correlations with RBC. These five gut bacteria might be regarded as inhibitors of RBC recovery in IDA rats.

For the next analysis, 13 gut bacteria showed negative correlations with TFR and positive correlations with RBC, HGB, SF, and HEPC. Among these, *Christensenellaceae*_R-7_group, unclassified_f_*Oscillospiraceae*, *Prevotellaceae*_UCG-003, and *Colidextribacter* presented significantly negative correlations ($0.0001 < p < 0.001$) compared to the other 9 bacteria, indicating that these microbes seemed to be closely related to the inhibition of TFR expression. Nevertheless, 8 of the 13 bacteria, including *Christensenellaceae*_R-7_group, norank_f_*Oscillospiraceae*, unclassified_f_*Oscillospiraceae*, *Prevotellaceae*_UCG-003, *Colidextribacter*, *Roseburia*, *Ruminococcus,* and *Alloprevotella*, showed significantly positive correlations with RBC, HGB, HEPC, and SF ($p < 0.05$). The above bacteria might offer incredible functions for the recovery of active factors. Based on these correlation data, we found that different bacteria might play different roles in regulating cytokines. For cytokines, the correlations between HGB and *Christensenellaceae*_R-7_group, norank_f_*Oscillospiraceae*, unclassified_f_*Oscillospiraceae,* and *Prevotellaceae*_UCG-003 ($0.0001 < p < 0.001$) were 10 times stronger than the correlations with other bacteria ($0.001 < p < 0.01$). Moreover, norank_f_*Oscillospiraceae* and unclassified_f_*Oscillospiraceae* ($0.0001 < p < 0.001$) were more focused on restoring the RBC levels than the other 5 bacterial phyla ($0.001 < p < 0.05$). However, for SF, only unclassified_f_*Oscillospiraceae* showed a more intensive correlation ($p < 0.01$) than the other bacteria. Next, *Christensenellaceae*_R-7_group, unclassified_f_*Oscillospiraceae*, *Roseburia*, and *Ruminococcus* were found to have obviously correlations with HEPC ($0.001 < p < 0.01$).

Putting aside the above phenomenon, we found that the same bacteria revealed differential correlations with different cytokines. The negative correlation parameters of *Subdoligranulum* and SF, RBC, and HGB ($0.001 < p < 0.01$) were significantly higher than the correlation with HEPC ($0.01 < p < 0.05$). Thus, this bacterium was able to inhibit the expression of SF, RBC, and HGB, while inhibiting the expression of HEPC. In addition, *Christensenellaceae*_R-7_group could reverse HGB levels more ($0.0001 < p < 0.001$) than the levels of SF, RBC, and HEPC ($0.001 < p < 0.05$). Norank_f_*Oscillospiraceae* also exhibited the same property ($0.0001 < p < 0.001$). Both unclassified_f_*Oscillospiraceae* and *Prevotellaceae*_UCG-003, restored the levels of HGB and RBC ($0.0001 < p < 0.001$), rather than the levels of SF and HEPC ($p < 0.01$). The correlation gradation of *Roseburia* and cytokines was RBC ($p \approx 0.004$) > HEPC ($p \approx 0.005$) > HGB ($p \approx 0.007$) > SF ($p \approx 0.02$), illustrating that these genera might be of importance in increasing the levels of RBC, HEPC, and HGB. However, *Ruminococcus* seemed to be more associated with the regulation of HEPC ($0.001 < p < 0.01$). *Alloprevotella* did not offer significant correlations with any of the four factors.

In addition to the above-mentioned microbiota, some probiotics were found to be associated with sporadic cytokines.

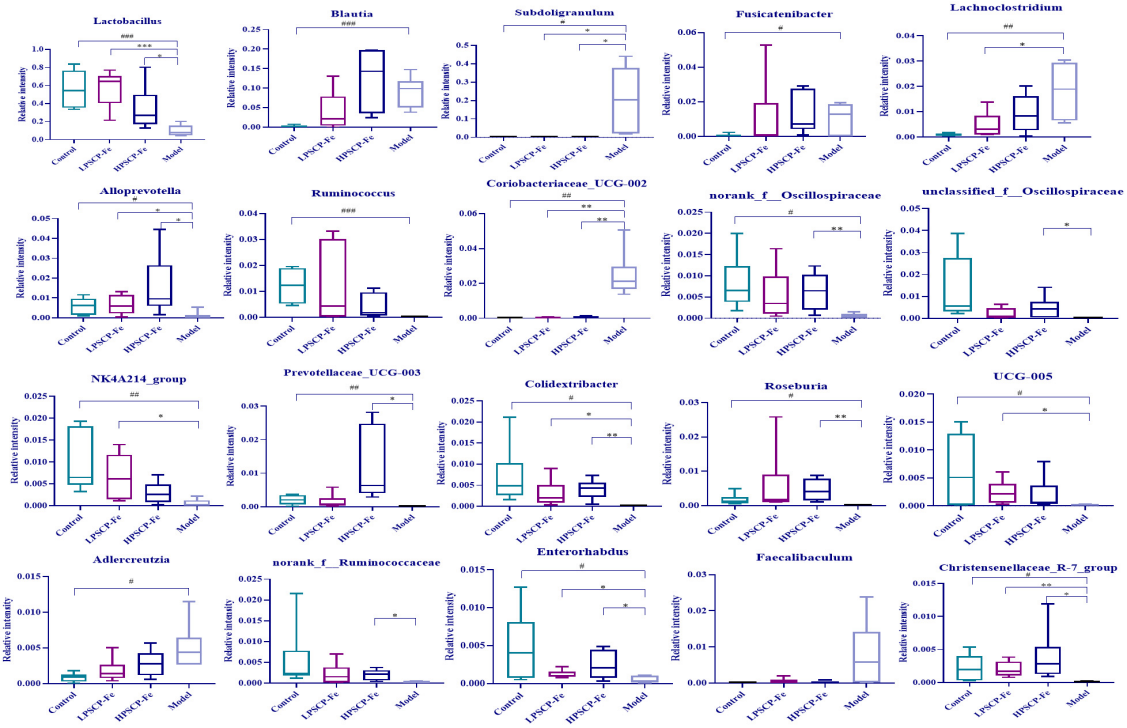

FIGURE 4
Average relative abundance of difference features flora in feces of all groups. Data are presented as mean ± SD, $n = 6$. $^{\#}p < 0.05$, $^{\#\#}p < 0.01$, $^{\#\#\#}p < 0.001$: control vs. model; $^{*}p < 0.05$, $^{**}p < 0.01$, $^{***}p < 0.001$: treatment vs. model.

Lactobacillus showed a positive correlation between RBC and HGB ($0.001 < p < 0.05$), and its ability to regulate RBC might be more prominent than HGB. *Coriobacteriaceae*_UCG-005, a Gram-negative bacterium, was significantly positively correlated with HGB and SF ($p < 0.05$). Coincidentally, two bacteria were negatively correlated with TFR ($p < 0.05$). These results suggested that *Coriobacteriaceae*_UCG-005 and *Lactobacillus* should alleviate IDA by inhibiting the expression of TFR and increasing the levels of HGB, RBC, and SF.

The distance-based redundancy analysis (db-RDA) was performed to determine whether the cytokines correlated with microbiota (**Figures 5B, C**). The levels of SF, HGB, RBC, and HEPC were positively associated with each other, and negatively correlated with TFR. In addition, *Subdoligranulum* and *Christensenellaceae*_R-7_group ($p < 0.05$) were closely associated with cytokines ($p < 0.05$) than the other microbiota. Thus, the *Subdoligranulum* and *Christensenellaceae*_R-7_group should be potential microbial markers for PSCP-Fe action in the treatment of IDA.

Discussion

The active peptides from natural sources, such as wheat, egg white, and soy, often carry trace elements with incredible functions (4, 34). In this study, we chose pig skin as the chelating agent of Fe^{2+} to obtain PSCP-Fe. A range of analytical methods was then used to determine the chelating property of PSCP and Fe^{2+}. It was found that the surface structure of PSCP-Fe was significantly different from that of PSCP. Pore traces of PCSP-Fe were likely to be left by the chelation reaction of PSCP with Fe^{2+}, which has been reported in previous literature (35). Peptides containing Asp, Arg, His, Glu, Cys, and Lys residues exhibit higher iron-chelating capacity. Among these, Asp and Glu are acidic amino acids that can contribute more −COO to achieve chelation with Fe^{2+} compared to neutral amino acids. These chelating abilities have been confirmed in Fe^{2+}-binding peptides in whey protein hydrolysates and soy protein (34, 36). Similarly, Arg, His, and Lys are basic amino acids that can provide −NH groups to combine with Fe^{2+} (37). These results are similar to the observation of Greve et al. (27), Johnson et al. (29), and De la Hoz et al. (30). Interestingly, Cys has been recognized as an important amino acid that has excellent ferrous binding capacity because of its functional groups (−NH, −COO, and −SH), especially when it is derived from digested meat protein (38, 39). FTIR analysis confirmed that the functional groups of these amino acids were involved in chelation with Fe^{2+}. The absorption bands of −NH and −COO were changed significantly, showing the authenticity of the functional groups involved in the chelation reaction.

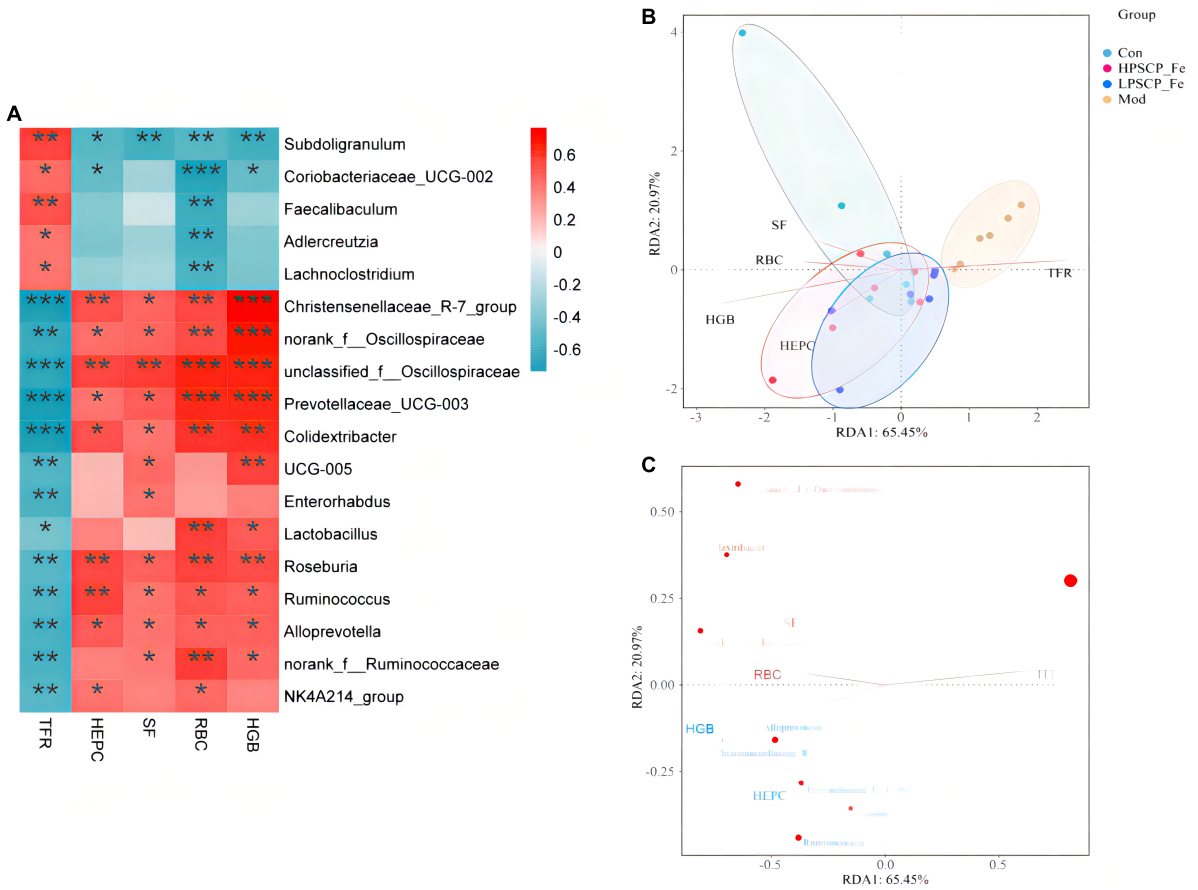

FIGURE 5
Correlation analysis between related factors and microbiota at the genus level **(A)**. Spearman's correlation analyses were used to analyze the relative abundance (%) between the specific genus in each treatment group. $0.01 < *p \leq 0.05$, $0.001 < **p \leq 0.01$, $***p \leq 0.001$. **(B)** The db-RDA analysis result in different groups. **(C)** The db-RDA analysis result of gut flora and the related factors.

An early meta-analysis revealed that 42.7% of women in developing countries experience anemia during pregnancy, which is associated with a significantly higher risk of low birth weight in infants (40). Underweight and malnourished infants and toddlers are more susceptible to IDA. In this experiment, 4-week-old SD rats (weighing 110 g) were equivalent to a 4–6-years-old human child,[2] and thus, were used to evaluate the effect of PSCP-Fe against IDA. The levels of RBC, HGB, HCT, MCV, and MCH in the blood can provide diagnostic evidence of IDA. We found that the low-Fe^{2+} diet could indeed cause significant changes in the above parameters ($p < 0.05$), while PSCP-Fe could reverse their deficiencies ($p < 0.05$). These results indicated that PSCP-Fe may treat IDA by interfering with the production of HGB and RBCs.

In addition, the levels of the secreted factors, including HEPC, TFR, and SF, were determined. HEPC is an antimicrobial peptide found in blood and urine. It is predominantly expressed in the liver and is regulated based on the hepatic iron stores (41). TFR is a liver-derived protein that can bind up to two iron atoms. Iron-laden transferrin delivers the metal to most cells upon binding to TFR (42). TFR mediates cellular iron uptake through clathrin-dependent endocytosis of iron-loaded transferrin, thus playing a key role in iron homeostasis. Moreover, SF is synthesized by the liver and can transport iron to all tissues through an affinity reaction, while transporting excess iron to the liver for storage. SF level is also widely measured as an indicator of iron status (43). The present study showed that PSCP-Fe could significantly increase the levels of HEPC and SF, while downgrading the levels of TFR ($p < 0.05$) compared to untreated IDA rats; its effect was thus better than $FeSO_4$. These results were similar to the observations of Mantadakis et al. (3) and Xiao et al. (44). Certainly, the colonic damage caused by additive should not be ignored. The free Fe^{2+} can cause side effects, such as colon and liver damage and inflammation. Compared with the free Fe^{2+}, the chelate of peptide and Fe^{2+} shows miraculous stability in a series of biomimetic experiments, and this chelate can only be degraded

2 https://www.taletn.com/rats/age/

reluctantly in the duodenum. This suggests that the destruction of colon and intestine by chelate of Fe^{2+} and peptide is negligible (45, 46). In this research, we found that PSCP-Fe was beneficial to the colon or caused less irritation to the intestinal tract, and the reversal was much better than $FeSO_4$, which was recommended by pharmacopeias and food additive regulations in many countries. These results indicated the security of PSCP-Fe. Surprisingly, in histopathology experiments, more Fe^{2+} was noted to be transported to the liver after supplementation by PSCP-Fe, confirming the therapeutic effect on IDA. Two possible mechanisms for the enhancement effect of peptides in the non-heme Fe^{2+} bioavailability have been reported, on the one hand, the peptide can intercept the incorporation between Fe^{2+} and non-nutritional factors in diet, such as phatic acid, oxalate or tannin. On the other hand, peptide can increase Fe^{2+} absorption by maintaining the morphology of Fe^{2+} and enhancing chelating capacity with Fe^{2+} (47). However, the role of PSCP in Fe^{2+} absorption was ambiguous in this study. In addition, whether the gut microbiota is related to the absorption of PSCP-Fe was not discussed in this study. These problems will be deeply dissected in our next work.

Neurological analysis suggested that the key role of iron absorption should be the intestinal solubility of oral iron (48). Gut microbiota is critical for maintaining iron homeostasis in the intestine. *Escherichia*, *Salmonella*, *Faecalibaculum,* and *Vibrio cholerae* have reported the ability to lock iron by generating siderophores, therefore, iron from daily diets cannot be transported into the circulatory system, leading to IDA (49). In addition, the imbalance in iron content caused by intestinal flora may increase the levels of fecal calprotectin, which is released by neutrophils and phagocytes, causing inflammation of the intestine (50). Specific bacterial genera that mediate the development of intestinal inflammation, such as *Adlercreutzia*, *Coriobacteriaceae*, *Faecalibaculum,* and *Clostridium*, can release many harmful metabolites (e.g., secondary bile salts, hydrogen sulfide, and indoles), accelerating inflammation and cancer-induction in intestinal tissue (51). These pathological conditions may also reduce the expression of the duodenal cytochrome B (DcytB) and divalent metal transporter 1 (DMT1) by disrupting the intestinal mechanical barrier, and their coupled action is required for Fe^{2+} absorption. It must be noted that the above bacteria are able to restrain the conversion of Fe^{3+}

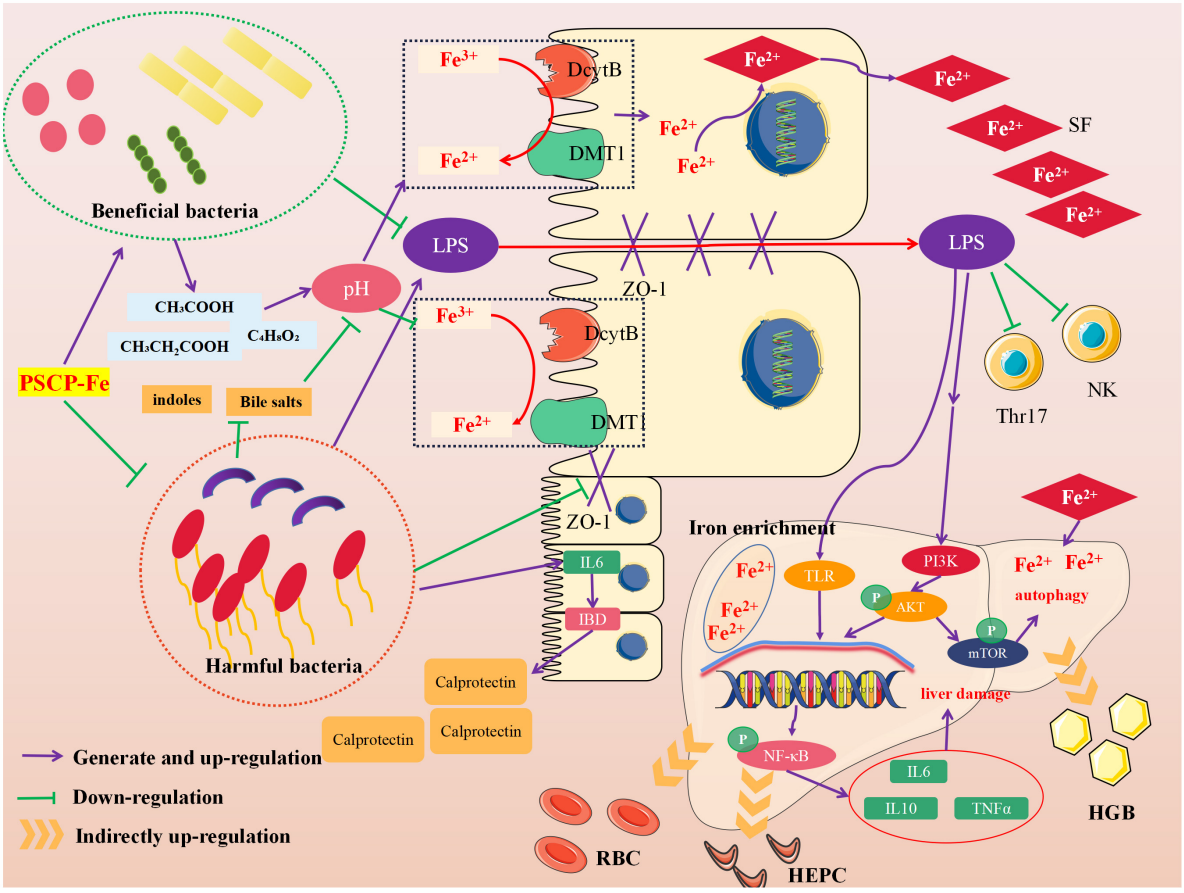

FIGURE 6
Intervention mechanism of PSCP-Fe on IDA rats.

to Fe^{2+} by mediating intestinal pH, indirectly causing Fe^{2+} deficiency *in vivo*. In addition, the zonula occludens-1 (ZO-1) and occludin, which reflect the integrity of the intestinal mechanical barrier, can also be destroyed due to long-term erosion by harmful bacteria and their metabolites. In this case, lipopolysaccharide (LPS) entering the body can lead to tissue inflammation by increasing inflammatory factors, such as interleukin 6 (IL-6), interleukin 10 (IL-10), and tumor necrosis factor α (TNF-α). The latter activates the TLR/NF-κB pathway and inhibits the differentiation of immune cells, such as Thr17 and NK (52). **Figure 6** shows the intervention mechanism of PSCP-Fe on IDA rats. In this study, we found that a low-Fe^{2+} diet altered the structure of gut microbiota and increased the relative abundances of *Lachnoclostridium*, *Adlercreutzia*, *Faecalibaculum, Coriobacteriaceae*_UCG-002, and *Subdoligranulum*, which is consistent with the literature (53). Some beneficial bacteria were also recovered by administering PSCP-Fe. Probiotics can alleviate IDA by making use of compound pathways that promote Fe^{2+} absorption. For instance, bacteria that produce (SCFAs) and lactic acid derivatives can restore the pH of the intestinal lumen, thereby promoting the conversion of Fe^{3+} to Fe^{2+}, and they can also repair intestinal tissue and up-regulate the expression of related receptors to increase Fe^{2+} absorption. Surprisingly, SCFAs can inhibit the spread of LPS, and thus, eliminate inflammation. Here, PSCP-Fe increased the relative abundances of *Blautia*, *Alloprevotella*, *Ruminococcus*, *Oscillospiraceae*, *Prevotellaceae*_UCG-003, *Roseburia*, norank_f_*Ruminococcaceae,* and *Christensenellaceae*_R-7_group, which are producers of SCFAs, including butyric acid, propionic acid, and acetic acid. A previous report has indicated that *Lactobacillus*, which is the main probiotic found in human microbiota, exhibits a remarkable Fe^{3+}-reducing activity due to its metabolite, P-hydroxyphenyllactic acid, and increases Fe^{2+} absorption through DMT1. Coincidentally, PSCP-Fe increased the relative abundance of *Lactobacillus* in IDA rats. Liver histopathology should reveal liver damage caused by harmful bacteria and their metabolites, along with injury to intestinal tissue. After PSCP-Fe treatment, the relative abundances of beneficial bacteria were positively correlated with iron enrichment and tissue repair. The fortification of iron also contributes to the reduction in beneficial bacteria and is directly associated with intestinal inflammation. However, beneficial bacteria did not decrease upon intervention with PSCP-Fe, demonstrating the safety of PSCP-Fe and the potential activities of PSCP.

Red blood cells, HGB, and SF are important indicators of iron in the body. HEPC and TFR are critical parameters for iron homeostasis and immune response *in vivo*. The Spearman correlation analysis was utilized to determine whether the five factors were associated with differential microflora. Five gut bacteria were positively correlated with TFR, and 13 gut bacteria showed positive correlations in RBC, HGB, SF, and HEPC. *Subdoligranulum and Christensenellaceae*_R-7_group were more closely related to the above five factors. *Subdoligranulum* is a butyric acid-producing bacteria, which plays an important role in alleviating obesity and Type-2 diabetes (54). However, we found that this bacterium did not increase iron content in the body by producing butyric acid; instead, it promoted iron release based on the positive correlation with TFR, highlighting its indistinct function in *Subdoligranulum*. Conversely, *Christensenellaceae*_R-7_group, which is known as special probiotics, has also been related to a healthy status in the context of different diseases, including obesity and inflammation. In a study on intestinal inflammation, *Christensenellaceae* _R-7_group remained depleted in individuals with Crohn's disease (CD) and ulcerative colitis (UC), which are two major subtypes of inflammatory bowel disease (IBD) (55). Therefore, *Christensenellaceae* _R-7_group may increase Fe^{2+} absorption by repairing intestinal mucosa and upregulating receptor expression. These changes would in turn alleviate the low levels of HGB, RBC, and SF caused by IDA. This group can also up-regulate the expression of certain factors and increase HEPC levels. However, the mechanisms behind these changes have not yet been revealed, and the correlation between *Christensenellaceae* _R-7_group, PSCP and Fe^{2+} has been also hidden. Therefore, the relevant problems should be studied in follow-up experiments.

Data availability statement

The original contributions presented in this study are publicly available. This data can be found here: https://www.ncbi.nlm.nih.gov/bioproject/PRJNA796635.

Ethics statement

The animal study was reviewed and approved by the Institutional Animal Care and Use Committee at Bin Zhou Medical University (approval certificate number: 2020-090).

Author contributions

SW, LD, and JZ developed the idea and designed the research. SJ and WD performed the experiments and wrote the draft of the manuscript. SW, ZZ, JX, and HL contributed to the revise the writing. All authors read and approved the submitted version.

Funding

This work was financially supported by the Shandong Province Chinese Herbal Medicine and Decoction Piece Standard Research Topic (2020–201), the Yantai Campus

Integration Development Project (No. 2019XDRHXMPT18), the Binzhou Medical University Scientific Research Fund for High-level Talents (Nos. BY2018KYQD11, 2019KYQD05, and 2019KYQD06), the Young and Creative Team for Talent Introduction of Shandong Province (No. 10073004), the Project of Shandong Provincial Natural Fund (Nos. ZR2021QH009, ZR2020MH371, and ZR2020MH372), and the Medical and Health Technology Development Plan at Shandong Province (No. 202006031281).

Conflict of interest

The authors declare that the research was conducted in the absence of any commercial or financial relationships that could be construed as a potential conflict of interest.

Publisher's note

All claims expressed in this article are solely those of the authors and do not necessarily represent those of their affiliated organizations, or those of the publisher, the editors and the reviewers. Any product that may be evaluated in this article, or claim that may be made by its manufacturer, is not guaranteed or endorsed by the publisher.

Supplementary material

The Supplementary Material for this article can be found online at: https://www.frontiersin.org/articles/10.3389/fnut.2022.1055725/full#supplementary-material

References

1. Stelle I, Kalea A, Pereira D. Iron deficiency anaemia: experiences and challenges. *Proc Nutr Soc.* (2019) 78:19–26. doi: 10.1017/S0029665118000460

2. Baumgartner J, Barth-Jaeggi T. Iron interventions in children from low-income and middle-income populations: benefits and risks. *Curr Opin Clin Nutr Metab Care.* (2015) 18:289–94. doi: 10.1097/MCO.0000000000000168

3. Mantadakis E, Chatzimichael E, Zikidou P. Iron deficiency anemia in children residing in high and low-income countries: risk factors, prevention, diagnosis and therapy. *Mediterr J Hematol Infect Dis.* (2020) 12:e2020041. doi: 10.4084/MJHID.2020.041

4. Li B, He H, Shi W, Hou T. Effect of duck egg white peptide-ferrous chelate on iron bioavailability in vivo and structure characterization. *J Sci Food Agric.* (2019) 99:1834–41. doi: 10.1002/jsfa.9377

5. Zarei M, Ghanbari R, Tajabadi N, Abdul-Hamid A, Bakar F, Saari N. Generation, fractionation, and characterization of iron-chelating protein hydrolysate from palm kernel cake proteins. *J Food Sci.* (2016) 81:C341–7. doi: 10.1111/1750-3841.13200

6. Lin H, Deng S, Huang S, Li Y, Song R. The effect of ferrous-chelating hairtail peptides on iron deficiency and intestinal flora in rats. *J Sci Food Agric.* (2016) 96:2839–44. doi: 10.1002/jsfa.7452

7. Torres-Fuentes C, Alaiz M, Vioque J. Iron-chelating activity of chickpea protein hydrolysate peptides. *Food Chem.* (2012) 134:1585–8. doi: 10.1016/j.foodchem.2012.03.112

8. Das N, Schwartz A, Barthel G, Inohara N, Liu Q, Sankar A, et al. Microbial metabolite signaling is required for systemic iron homeostasis. *Cell Metab.* (2020) 31:115.e–30.e. doi: 10.1016/j.cmet.2019.10.005

9. Qi X, Zhang Y, Guo H, Hai Y, Luo Y, Yue T. Mechanism and intervention measures of iron side effects on the intestine. *Crit Rev Food Sci Nutr.* (2020) 60:2113–25. doi: 10.1080/10408398.2019.1630599

10. Yilmaz B, Li H. Gut microbiota and iron: the crucial actors in health and disease. *Pharmaceuticals.* (2018) 11:98. doi: 10.3390/ph11040098

11. Oliphant K, Allen-Vercoe E. Macronutrient metabolism by the human gut microbiome: major fermentation by-products and their impact on host health. *Microbiome.* (2019) 7:91. doi: 10.1186/s40168-019-0704-8

12. Jiang H, Zhang W, Chen F, Zou J, Chen W, Huang G. Purification of an iron-binding peptide from scad (*Decapterus maruadsi*) processing by-products and its effects on iron absorption by Caco-2 cells. *J Food Biochem.* (2019) 43:e12876. doi: 10.1111/jfbc.12876

13. Rosenberg L, Bagger C, Janfelt C, Haedersdal M, Olesen U, Lerche CMA. Comparison of human and porcine skin in laser-assisted drug delivery of chemotherapeutics. *Lasers Surg Med.* (2021) 53:162–70. doi: 10.1002/lsm.23344

14. Hwang J, Jeong H, Lee N, Hur S, Lee N, Han J, et al. Ex vivo live full-thickness porcine skin model as a versatile in vitro testing method for skin barrier research. *Int J Mol Sci.* (2021) 22:657. doi: 10.3390/ijms22020657

15. He L, Lan W, Zhao Y, Chen S, Liu S, Cen L, et al. Characterization of biocompatible pig skin collagen and application of collagen-based films for enzyme immobilization. *RSC Adv.* (2020) 10:7170–80. doi: 10.1039/c9ra10794k

16. Ma X, Liu C, Song W, Che S, Wang C, Feng X, et al. Evaluating the efficacy of a ferrous-ion-chelating peptide from Alaska pollock frame for the improvement of iron nutritional status in rats. *Food Funct.* (2019) 10:4888–96. doi: 10.1039/c9fo00310j

17. Li C, Cui Z, Li Z, Gao L, Zhang C, Li D, et al. Determination of mineral elements in nanyang mugwort (*Artemisia argyi*) leaves harvested from different crops by inductively coupled plasma mass spectrometry and inductively coupled plasma atomic emission spectrometry. *Chem Pharm Bull.* (2021) 69:411–3. doi: 10.1248/cpb.c20-00875

18. Lee ES, Kwon M-H, Kim HM, Woo HB, Ahn CM, Chung CH. Curcumin analog CUR5-8 ameliorates nonalcoholic fatty liver disease in mice with high-fat diet-induced obesity. *Metabolism.* (2020) 103:154015. doi: 10.1016/j.metabol.2019.154015

19. Nagappan A, Kim J, Jung D, Jung M. Cryptotanshinone from the *Salvia miltiorrhiza* bunge attenuates ethanol-induced liver injury by activation of AMPK/SIRT1 and Nrf2 signaling pathways. *Int J Mol Sci.* (2019) 21:265. doi: 10.3390/ijms21010265

20. Jun J, Choi J, Bae S, Oh S, Kim G. Decreased C-reactive protein induces abnormal vascular structure in a rat model of liver dysfunction induced by bile duct ligation. *Clin Mol Hepatol.* (2016) 22:372–81. doi: 10.3350/cmh.2016.0032

21. Pang J, Ma S, Xu X, Zhang B, Cai Q. Effects of rhizome of *Atractylodes* Koreana (Nakai) Kitam on intestinal flora and metabolites in rats with rheumatoid arthritis. *J Ethnopharmacol.* (2021) 281:114026. doi: 10.1016/j.jep.2021.114026

22. Li Q, Cui Y, Xu B, Wang Y, Lv F, Li Z, et al. Main active components of Jiawei Gegen Qinlian decoction protects against ulcerative colitis under different dietary environments in a gut microbiota-dependent manner. *Pharmacol Res.* (2021) 170:105694. doi: 10.1016/j.phrs.2021.105694

23. Erawijantari P, Mizutani S, Shiroma H, Shiba S, Nakajima T, Sakamoto T, et al. Influence of gastrectomy for gastric cancer treatment on faecal microbiome and metabolome profiles. *Gut.* (2020) 69:1404–15. doi: 10.1136/gutjnl-2019-319188

24. Yang X, Liu D, Ren H, Zhang X, Zhang J, Yang X. Effects of sepsis and its treatment measures on intestinal flora structure in critical care patients. *World J Gastroenterol.* (2021) 27:2376–93. doi: 10.3748/wjg.v27.i19.2376

25. Sun N, Cui P, Li D, Jin Z, Zhang S, Lin S. Formation of crystalline nanoparticles by iron binding to pentapeptide (Asp-His-Thr-Lys-Glu) from egg white hydrolysates. *Food Funct.* (2017) 8:3297–305. doi: 10.1039/c7fo00843k

26. Kim S, Seo I, Khan M, Ki K, Lee W, Lee H, et al. Enzymatic hydrolysis of heated whey: iron-binding ability of peptides and antigenic protein fractions. *J Dairy Sci.* (2007) 90:4033–42. doi: 10.3168/jds.2007-0228

27. Greve J, Pinkham A, Thompson Z, Cowan J. Active site characterization and activity of the human aspartyl (asparaginyl) β-hydroxylase. *Metallomics.* (2021) 13:mfab056. doi: 10.1093/mtomcs/mfab056

28. Efsa Panel on Additives and Products or Substances used in Animal Feed (Feedap), Bampidis V, Azimonti G, Bastos M, Christensen H, Dusemund B, et al. Efficacy of iron chelates of lysine and glutamic acid as feed additive for all animal species. *EFSA J.* (2020) 18:e06164. doi: 10.2903/j.efsa.2020.6164

29. Johnson E, Russo M, Nye D, Schlessman J, Lecomte J. Lysine as a heme iron ligand: a property common to three truncated hemoglobins from *Chlamydomonas reinhardtii*. *Biochim Biophys Acta Gen Subj.* (2018) 1862:2660–73. doi: 10.1016/j.bbagen.2018.08.009

30. De la Hoz L, Ponezi A, Milani R, Nunes da Silva V, Sonia de Souza A, Bertoldo-Pacheco M. Iron-binding properties of sugar cane yeast peptides. *Food Chem.* (2014) 142:166–9. doi: 10.1016/j.foodchem.2013.06.133

31. Yang S, Zhang Q, Yang H, Shi H, Dong A, Wang L, et al. Progress in infrared spectroscopy as an efficient tool for predicting protein secondary structure. *Int J Biol Macromol.* (2022) 206:175–87. doi: 10.1016/j.ijbiomac.2022.02.104

32. Anderson G, Frazer D. Current understanding of iron homeostasis. *Am J Clin Nutr.* (2017) 106(Suppl. 6):1559S–66S. doi: 10.3945/ajcn.117.155804

33. Jie F, Xiao S, Qiao Y, You Y, Feng Y, Long Y, et al. Kuijieling decoction suppresses NLRP3-mediated pyroptosis to alleviate inflammation and experimental colitis in vivo and in vitro. *J Ethnopharmacol.* (2021) 264:113243. doi: 10.1016/j.jep.2020.113243

34. Zhu S, Zheng Y, He S, Su D, Nag A, Zeng Q, et al. Novel zn-binding peptide isolated from soy protein hydrolysates: purification, structure, and digestion. *J Agric Food Chem.* (2021) 69:483–90. doi: 10.1021/acs.jafc.0c05792

35. Sun R, Liu X, Yu Y, Miao J, Leng K, Gao H. Preparation process optimization, structural characterization and in vitro digestion stability analysis of Antarctic krill (*Euphausia superba*) peptides-zinc chelate. *Food Chem.* (2021) 340:128056. doi: 10.1016/j.foodchem.2020.128056

36. Athira S, Mann B, Sharma R, Pothuraju R, Bajaj R. Preparation and characterization of iron-chelating peptides from whey protein: an alternative approach for chemical iron fortification. *Food Res Int.* (2021) 141:110133. doi: 10.1016/j.foodres.2021.110133

37. Wu J, Cai X, Tang M, Wang S. Novel calcium-chelating peptides from octopus scraps and their corresponding calcium bioavailability. *J Sci Food Agric.* (2019) 99:536–45. doi: 10.1002/jsfa.9212

38. Park K, Sim I, Ko H, Lim Y. Gamma aminobutyric acid increases absorption of glycine-bound iron in mice with iron deficiency anemia. *Biol Trace Elem Res.* (2020) 197:628–38. doi: 10.1007/s12011-020-02027-9

39. Ye J, Wang S, Zhang P, Nabi M, Tao X, Zhang H, et al. L-cysteine addition enhances microbial surface oxidation of coal inorganic sulfur: complexation of cysteine and pyrite, inhibition of jarosite formation, environmental effects. *Environ Res.* (2020) 187:109705. doi: 10.1016/j.envres.2020.109705

40. Rahman M, Abe S, Rahman M, Kanda M, Narita S, Bilano V, et al. Maternal anemia and risk of adverse birth and health outcomes in low- and middle-income countries: systematic review and meta-analysis. *Am J Clin Nutr.* (2016) 103:495–504. doi: 10.3945/ajcn.115.107896

41. Böser P, Mordashova Y, Maasland M, Trommer I, Lorenz H, Hafner M, et al. Quantification of hepcidin-related iron accumulation in the rat liver. *Toxicol Pathol.* (2016) 44:259–66. doi: 10.1177/0192623315623866

42. Gammella E, Buratti P, Cairo G, Recalcati S. The transferrin receptor: the cellular iron gate. *Metallomics.* (2017) 9:1367–75. doi: 10.1039/c7mt00143f

43. Wang F, Xie Z, Ye X, Deng S, Hu Y, Guo X, et al. Effectiveness of treatment of iron deficiency anemia in rats with squid ink melanin-Fe. *Food Funct.* (2014) 5:123–8. doi: 10.1039/c3fo60383k

44. Xiao C, Lei X, Wang Q, Du Z, Jiang L, Chen S, et al. Effects of a tripeptide iron on iron-deficiency anemia in rats. *Biol Trace Elem Res.* (2016) 169:211–7. doi: 10.1007/s12011-015-0412-6

45. Udechukwu M, Collins S, Udenigwe C. Prospects of enhancing dietary zinc bioavailability with food-derived zinc-chelating peptides. *Food Funct.* (2016) 7:4137–44. doi: 10.1039/c6fo00706f

46. Qu W, Feng Y, Xiong T, Li Y, Wahia H, Ma H. Preparation of corn ACE inhibitory peptide-ferrous chelate by dual-frequency ultrasound and its structure and stability analyses. *Ultrason Sonochem.* (2022) 83:105937. doi: 10.1016/j.ultsonch.2022.105937

47. Li Y, Jiang H, Huang G. Protein hydrolysates as promoters of non-haem iron absorption. *Nutrients.* (2017) 9:609. doi: 10.3390/nu9060609

48. Milto I, Suhodolo I, Prokopieva V, Klimenteva T. Molecular and cellular bases of iron metabolism in humans. *Biochemistry.* (2016) 81:549–64. doi: 10.1134/S0006297916060018

49. Seyoum Y, Baye K, Humblot C. Iron homeostasis in host and gut bacteria – a complex interrelationship. *Gut Microbes.* (2021) 13:1–19. doi: 10.1080/19490976.2021.1874855

50. Liu B, Pan X, Liu Z, Han M, Xu G, Dai X, et al. Fecal microbiota as a noninvasive biomarker to predict the tissue iron accumulation in intestine epithelial cells and liver. *FASEB J.* (2020) 34:3006–20. doi: 10.1096/fj.201901635RR

51. Schepici G, Silvestro S, Bramanti P, Mazzon E. The gut microbiota in multiple sclerosis: an overview of clinical trials. *Cell Transplant.* (2019) 28:1507–27. doi: 10.1177/0963689719873890

52. Low K, Smith S, Abbott D, Boraston A. The glycoconjugate-degrading enzymes of *Clostridium perfringens*: tailored catalysts for breaching the intestinal mucus barrier. *Glycobiology.* (2021) 31:681–90. doi: 10.1093/glycob/cwaa050

53. Lin H, Zeng C, Shui S, Zhang B. Effects of Fe (II)-chelating hairtail protein hydrolysates on the immune characteristics and intestinal microorganisms in loach (*Misgurnus anguillicaudatus*). *Aquac Rep.* (2021) 19:100630. doi: 10.1016/j.aqrep.2021.100630

54. Chen W, Zhang M, Guo Y, Wang Z, Liu Q, Yan R, et al. The profile and function of gut microbiota in diabetic nephropathy. *Diabetes Metab Syndr Obes.* (2021) 14:4283–96. doi: 10.2147/DMSO.S320169

55. Mancabelli L, Milani C, Lugli G, Turroni F, Cocconi D, van Sinderen D, et al. Identification of universal gut microbial biomarkers of common human intestinal diseases by meta-analysis. *FEMS Microbiol Ecol.* (2017) 93:fix153. doi: 10.1093/femsec/fix153

frontiers | Frontiers in Nutrition

TYPE Original Research
PUBLISHED 06 January 2023
DOI 10.3389/fnut.2022.1093277

Check for updates

OPEN ACCESS

EDITED BY
Wenjie Sui,
Tianjin University of Science and Technology, China

REVIEWED BY
Weihua Qiu,
Institute of Process Engineering (CAS), China
Junhua Zhang,
Nanjing Forestry University, China
Kun Wang,
Beijing Forestry University, China

*CORRESPONDENCE
Guanhua Li
✉ liguanhua1984@126.com
Dejian Zhang
✉ zhangdejian00@163.com

†These authors have contributed equally to this work

SPECIALTY SECTION
This article was submitted to Nutrition and Food Science Technology, a section of the journal Frontiers in Nutrition

RECEIVED 08 November 2022
ACCEPTED 13 December 2022
PUBLISHED 06 January 2023

CITATION
Zhao Z-M, Yu W, Huang C, Xue H, Li J, Zhang D and Li G (2023) Steam explosion pretreatment enhancing enzymatic digestibility of overground tubers of tiger nut (*Cyperus esculentus* L.). *Front. Nutr.* 9:1093277. doi: 10.3389/fnut.2022.1093277

COPYRIGHT
© 2023 Zhao, Yu, Huang, Xue, Li, Zhang and Li. This is an open-access article distributed under the terms of the Creative Commons Attribution License (CC BY). The use, distribution or reproduction in other forums is permitted, provided the original author(s) and the copyright owner(s) are credited and that the original publication in this journal is cited, in accordance with accepted academic practice. No use, distribution or reproduction is permitted which does not comply with these terms.

Steam explosion pretreatment enhancing enzymatic digestibility of overground tubers of tiger nut (*Cyperus esculentus* L.)

Zhi-Min Zhao[1,2†], Wenqing Yu[1†], Caitong Huang[1], Huiting Xue[3], Juan Li[1], Dejian Zhang[1*] and Guanhua Li[1*]

[1]State Key Laboratory of Reproductive Regulation and Breeding of Grassland Livestock, School of Life Sciences, Inner Mongolia University, Hohhot, China, [2]Inner Mongolia Key Laboratory of Environmental Pollution Control & Wastes Reuse, School of Ecology and Environment, Inner Mongolia University, Hohhot, China, [3]College of Basic Medicine, Inner Mongolia Medical University, Hohhot, China

Introduction: Tiger nut (TN) is recognized as a high potential plant which can grow in well-drained sandy or loamy soils and provide food nutrients. However, the overground tubers of TN remain unutilized currently, which limits the value-added utilization and large-area cultivation of this plant.

Methods: In the present study, the overground tubers of TN were subjected to enzymatic hydrolysis to produce fermentable sugars for biofuels production. Steam explosion (SE) was applied to modify the physical-chemical properties of the overground tubers of TN for enhancing its saccharification.

Results and discussion: Results showed that SE broke the linkages of hemicellulose and lignin in the TN substrates and increased cellulose content through removal of hemicellulose. Meanwhile, SE cleaved inner linkages within cellulose molecules, reducing the degree of polymerization by 32.13–77.84%. Cellulose accessibility was significantly improved after SE, which was revealed visibly by the confocal laser scanning microscopy imaging techniques. As a result, enzymatic digestibility of the overground tubers of TN was dramatically enhanced. The cellulose conversion of the SE treated TN substrates reached 38.18–63.97%, which was 2.5–4.2 times higher than that without a SE treatment.

Conclusion: Therefore, SE pretreatment promoted saccharification of the overground tubers of TN, which paves the way for value-added valorization of the TN plants.

KEYWORDS

lignocellulosic biomass, tiger nut, enzymatic hydrolysis, steam explosion pretreatment, biorefinery

Introduction

Energy security is essential for the development of global economy. Traditional fossil fuels (e.g., oil, coal) are still the main energy sources in the world currently. However, the consumption of fossil fuels leads to severe environmental deterioration (1). Broad consensus on fossil fuel reduction and pollution minimization stipulates great research

interest to renewable fuels (2). Nearly all cellulose is produced by photosynthetic higher plants and algae in the nature, and is considered to participate in the most vital global carbon flows. Additionally, cellulose is the only origin of "green" fixed carbon source and widely available worldwide (3). Biofuels from inedible cellulose are deemed as clean and renewable alternatives to the traditional fossil fuels, which mitigate climate change and reduce greenhouse gas emission. Commercial biofuels require cheap resources that are easy to harvest and collect. Tiger nut (*Cyperus esculentus* L., TN), a *Corsa sedge* genus perennial herb, is dated back to ∼4,000 years ago and now widely cultivated in the tropic or temperate regions, with an annual mass of 9,000 metric tons (4). TN can be a major grower in well-drained sandy or loamy soils to achieve a high productivity and economic efficiency. The underground tubers of TN contain unsaturated fatty acids, protein, and vitamin E, which are commonly regarded as a "health" food. However, there is seldom report regarding the utilization of the overground tubers, despite more than 90 cm in height of the solitary stems growing from a tuber. Overground tubers of TN represent promising resources for biofuels production.

The key step in biofuels production is to release fermentable sugars form cellulose with economic competitiveness (5). Compared to chemical strategies, biological conversion of cellulose exhibits more attractiveness owing to the lower energy input and less environment pollution (6). Enzymatic hydrolysis of cellulose needs valid binding between the surface of substrate and cellulase. Cellulose is a linear polymer condensed by D-anhydroglucopyranose through β-1,4-glycosidic bonds, which exists as successive and stacked sheets of anhydroglucopyranose on top of each other, forming a three-dimensional particle. This particle exhibits distinct "faces" that interact with the aqueous environment and enzymes (7). The "faces" can be deemed as both external and internal surfaces. The former is closely related to crystallinity index (CrI), degree of polymerization (DP), and pore size, whereas the latter is correlated with shape or particle size. For example, it is reported that crystalline cellulose hydrolysis rates are commonly 3–30 times faster than amorphous cellulose (8). Additionally, other components, such as hemicellulose, lignin, and pectin, are commonly interconnected through non-covalent and covalent linkages, forming a complicated structural and chemical network coats the "faces" or generates non-productive enzyme binding. This physical and chemical complexity makes cellulose recalcitrant to enzymatic hydrolysis. Additionally, the recalcitrance presents substantial differences according to different biomass, organs, and maturity stages. Therefore, establishing appropriate pretreatment and saccharification technologies to improve the cellulose accessibility to cellulases is significantly important for enhancing the enzymatic digestibility.

Pretreatment is considered to be a foundational step to efficiently facilitate enzymatic hydrolysis through removing stubborn components and deconstructing lignocellulosic matrix, which is also a key criterion to determine economic viability of large-scale industrialization (9). Steam explosion (SE), a kind of mechanico-physico-chemical pretreatment, is becoming one of the most commonly used technologies with huge commercial potential, because it needs low capital investment and energy requirements (10). Also, SE is a clean process without any chemical addition. During the SE process, the sample is treated by saturated steam at high temperature and pressure for a short duration time (cooking stage), during which the hydrolytic breakdown occurs. And then a sudden pressure drop (decompression phase) occurs, which results in a vapor expansion inside the "capillary-like" structures and a dislocation of the fibrous structure. SE has been proven efficient for fractionating a broad range of lignocellulosic feedstock, including wheat straw, sugarcane bagasse, and corn stover. The byproducts could be generated during the SE process, which could be toxic for the following valorization processes. These inhibiting compounds are divided into three main groups: weak acids, furan derivatives, and phenolic compounds (11). In detail, acetic acid is formed from hemicellulose, which further reduces the pH of the cooking liquor. The low pH and high temperature during SE could promote monosaccharide degradation to generate furfural, 5-hydroxymethylfurfural (HMF), and levulinic acid. The phenolic compounds are formed from lignin degradation (12). Our previous studies have shown that the redistribution of lignin facilitates the enzymatic digestibility of cellulose (13). However, the precise mechanism from an integral sense, especially, the influence of lignin distribution around the surface of cell wall caused by SE pretreatment on the cellulose accessibility remains ambiguous. To the best of our knowledge, SE pretreatment of TN biomass is seldom studied. In order to facilitate the value-added utilization of the TN plants, SE was applied to modify the physical-chemical properties of the overground tubers of TN. The chemical compositions and physical parameters (e.g., CrI and DP) were measured to investigate the influences of SE on the TN substrates. Meanwhile, the morphological changes of the TN materials during SE processes were also analyzed. Enzymatic digestibility performance of raw and pretreated TN was compared to examine the effects of SE on saccharification efficiency. These findings from the present research would shed some light on the mechanisms of SE pretreatment and promote the valorization of TN biomass.

Materials and methods

Lignocellulosic materials and chemicals

The TN used in this study was cultivated in an experimental field of Inner Mongolia Academy of Agricultural & Animal Husbandry Sciences, China, and was harvested in September 2021. The overground tubers were collected, washed to remove

TABLE 1 Conditions for SE pretreatment.

Pressure (MPa)	Temperature (°C)	Time (min)	Severity factor (SF)
1.2	188	5	3.29
1.5	198	10	3.89
1.8	207	10	4.15
1.5	198	20	4.19

impurity, and air-dried to constant weight. Cellulase cocktail (*Trichoderma viride* G) with average activity of 90.3 filter paper unit per gram was provided by Shanghai Yuanye Co., Ltd. Other chemicals (analytic grade) were purchased from Huhhot Shengkang Biotechnology Company, China.

Steam explosion pretreatment

The dried overground tubers of TN was chopped to smaller sizes (∼10 cm in length) and pre-soaked in water with a solid-liquid ratio of 1:10 (w/v) overnight to guarantee the saturation moisture. The saturated sample was drained off and placed into the SE equipment (Hebi Company, China) which consisted of a steam generator, a 400 mL reaction cylinder, and a collecting tank. As shown in Table 1, four conditions with different severity factor (SF) were selected to obtain various pretreated TN (PTN). SF of each condition was determined according to equation developed by Melissa (14), shown below:

$$SF = log_{10}\left[t * \exp\left(\frac{T-100}{14.75}\right)\right] \quad (1)$$

Where t is the residence time, min; and T is the holding temperature, °C.

After each pretreatment, the PTN was washed in a water bath with a solid-liquid ratio of 1:10 (w/v) at room temperature for 30 min to remove the soluble compounds and then oven-dried at 63°C to a constant weight. The other saturated sample without a SE pretreatment was also oven-dried at 63°C to a constant weight and named as unpretreated TN (UTN). The PTN and UTN were shredded to powders with a particle size of 0.42–0.88 mm. Three repetitions were performed for each treatment.

Chemical analysis

Composition analysis

The lignin and monomeric sugars in solid samples were analyzed using two-stage acid hydrolysis method recommended by National Renewable Energy Laboratory (15). The concentration of monosaccharides were analyzed through HPLC system equipped with a Bio-Rad Aminex HPX-87H column, with 5 mM sulfuric acid as mobile phase, eluted flow rate of 0.6 mL/min, and column temperature of 50°C.

Fourier transform infrared spectroscopy

The Infrared spectra of PTN and UTN in the region 4,000–400 cm^{-1} were obtained by FTIR spectrophotometer (IR-Affinity-1S, Shimadzu) in transmission mode, with 4 cm^{-1} resolution and 32 scans at room temperature. Milled sample powder (1 mg, 60 mesh) was mixed with of KBr (50 mg, spectrum grade) and pressed into a pellet. The characteristic bands were identified and analyzed according to literatures (16).

Physical analysis

Cellulose accessibility

The cellulose accessibility of various solid substrates was determined with the theoretical maximum adsorption amount of Congo Red (17). Precise 200 mg of dry sample was incubated with 4 mL of dye sodium citrate buffer (50 mM, pH 4.8) in a 10 mL centrifuge with gentle agitation at 50°C for 24 h. After centrifugation at 6,200×g for 10 min, the absorbance of the supernatant was measured using UV-visible spectrophotometer (UV-1780, Shimadzu, Japan) at 498 nm. The adsorption isotherm was determined in duplicate with a series of increasing dye concentrations (0, 0.1, 0.5, 2.0, 3.0, and 4.0 g/L) and fitted by linear regression in Excel.

X-ray diffraction

The XRD patterns of various samples were detected on a X-ray diffractometer instrument (X'Pert PRO, PANalytical) using Cu K_α radiation (k = 1.54 Å), with a scattering angle (2θ) ranging from 5° to 40° and scanning increments of 0.02°, at 40 kV and 30 mA. The crystallinity index (CrI) was calculated as follows (18).

$$CrI = (I_{002} - I_{am}) * 100/I_{002} \quad (2)$$

Where I_{002} represents the peak intensity of the crystalline area of the biomass in approximate 2θ between 22° and 23°; I_{am} represents the minimum intensity of the amorphous area in ∼2θ between 18° and 19°.

Microscope imaging analysis

Transverse sections (12 μm) of various samples were obtained by cryostat (Leica, RM2015) at −20°C. Whole and uniform sections were maintained on a glass slide and observed by confocal laser scanning microscopy (CLSM, NIKON, AIR) with the identical condition: 20×/1.40 NA Plan-Apochromatic objective lens, laser source at 20% power, and pinhole size of

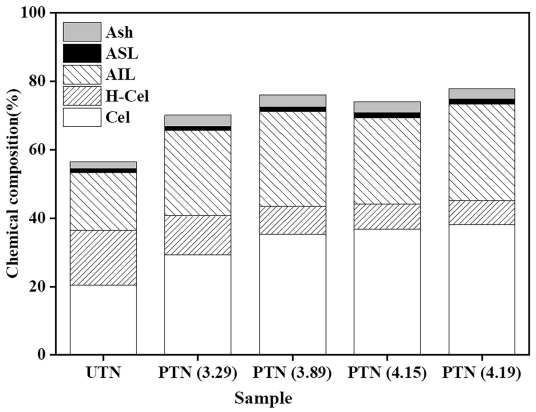

FIGURE 1
Compositions of TN before and after SE pretreatment.

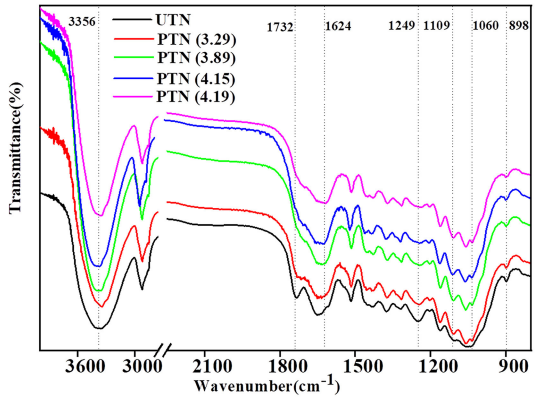

FIGURE 2
FTIR spectra of TN before and after SE pretreatment.

1 AU. Excitation was conducted using a wavelength of 405 nm for lignin autofluorescence, and emissions 410–480 nm (blue fluorescence) was collected. At least five images for each sample were collected.

Enzymatic hydrolysis

Enzymatic hydrolysis was carried out with a cellulase loading of 20 FPU/g in 100 mL Erlenmeyer flasks containing 2 g of solid substrate and 40 ml of sodium citrate buffer (50 mM, pH 4.8, supplementing with 0.01 g/mL sodium azide) in a water–bath. The Erlenmeyer flasks were incubated in a shaker at 50°C and shaken at 150 rpm for 48 h. The generated glucose in enzymatic hydrolysates was analyzed on HPLC. The cellulose conversion based on cellulase mediated hydrolysis was used to express the enzymatic digestibility, which is calculated as the following Equation (19).

$$Cellulose\ conversion\ =\ (m_g{}^*0.9 + m_c{}^*0.95)/m \qquad (3)$$

Where m_g and m_c represents the amount of generated glucose and cellobiose during the enzymatic hydrolysis, respectively; 0.9 and 0.95 represents the conversion factor for glucan to glucose and cellobiose to glucose, respectively; m represents the amount of cellulose in substrate.

Results and discussion

Chemical properties of raw and pretreated tiger nut

Chemical composition

Chemical composition is of great interest as it relates to the pretreatment effectiveness and further conversion performance (20). It was found that the glucan content increased from 20.51% (UTN) to 38.22% (SF = 4.19) with the increment of SF (Figure 1), which was beneficial for increasing the cellulose accessibility and enhancing the enzymatic hydrolysis performance. In contrast, the xylan content gradually decreased from 15.96 to 6.97%, and the declining trend was not obvious when the SF reached 4.15. The results showed that SE removed hemicellulose significantly from the solid biomass materials. The xylan content decreased from 14.51 to 3.51% in the solid substrates as the SE severity increased. Eom and coworkers also reported that SE pretreatment degraded hemicellulose within rubber wood biomass, which was in line with the results in the present study (21). Lignin generally acts as a physical barrier or irreversibly adsorbs cellulases to prevent cellulose hydrolysis (22). However, inconsistent trend of lignin content during SE is often reported. Most published literatures reported that lignin content increased in the SE treated biomass substrates. For example, Nasir et al. found that the lignin content increased by 25.85% in the SE (1.0 MPa, 184°C, 15 min) treated corn stover (23). Whereas, the other party assumed the decreased results of lignin contents during the SE. Besserer and coworkers reported a delignification of 3 to 75% with an average of ∼25% after SE treatments on *Aucoumea klaineana Pierre* sapwood based on both the microscopical data and chemical analysis (24). The lignin profiles after SE pretreatment was investigated in the present study to reveal the effects of SE on TN lignin. Results showed that the lignin content within PTN increased after SE pretreatment. It was deduced that lignin content variation might depend on the SE pretreatment time and temperature. Overall, SE pretreatment altered the compositions of TN materials, which should influence the subsequent enzymatic digestibility performance.

FTIR spectra

The FTIR spectra in band shapes of UTN and PTN samples were presented and compared to clarify the details of chemical

variations, especially for the representative spectral region of 1,800–800 cm^{-1}. As shown in Figure 2, there was a significant peak at 3,356 cm^{-1} (O–H bending in polysaccharides) in all samples, indicating the preservation of cellulose. The mild decrease in the band at 898 cm^{-1} (β-glucosides in cellulose) after SE treatments suggested the breakage of β-1,4 glycosidic bonds in cellulose. Our previous study found that SE could depolymerize cellulose in the wheat bran to release glucose, which benefited to the subsequent biological conversion (25). The disappearance of the band near 1,732 cm^{-1} (C=O stretching in hemicellulose) and 1,249 cm^{-1} (C–O stretching hemicellulose and syringyl ring in lignin) implied the degradation of hemicelluloses and breakage of lignin and hemicellulose, which was in line with the results of hemicellulose content decrease. Slight and continuous increase in the band near 1,109 cm^{-1} (C–OH skeletal vibration) and 1,060 cm^{-1} (C–O deformation vibration in secondary alcohols or aliphatic ethers) suggested the chemical modification of lignin. Maniet and coworkers systematically investigated the influences of SE on lignin structure and revealed that an increase of the SE intensity induced β-O-4 and spirodienone substructure degradations, increase in COOH content and phenolic OH bonds, decrease of aliphatic OH ferulate and *p*-coumarate bonds, and changes in subunits proportions within the organosolv fescue lignin (26). Lignin degradation is an essential step for its bioconversion. Therefore, the SE treated lignin might be suitable for biological valorization for producing value-added products (e.g., lipids and polyhydroxyalkanoates). As the degradation of hemicellulose and lignin was observed, the inhibiting compounds should be generated during the SE treatment. Fortunately, these inhibitors can be removed effectively by facile detoxification methods (e.g., water-washing and drying). Li and Chen reported that water-washing removed 81% of the furfural and 85% of the phenol compounds from SE treated corn straw and hot air-drying can obtained 46% of the furfural removal and 8.1% of the phenol compounds removal, respectively (27). In the present study, the PTN samples were washed in a water bath with a solid-liquid ratio of 1:10 (w/v) at room temperature for 30 min and then oven-dried at 63°C to a constant weight to eliminate the influence of the inhibiting compounds on the following biological valorization processes. Overall, SE removed hemicellulose and broke the linkages of lignin, which mitigated the recalcitrance of the TN biomass to cellulases.

Physical properties of raw and pretreated tiger nut

Cellulose consists of crystalline and amorphous component. Additionally, the lignin and hemicellulose were deemed as amorphous components. XRD patterns depicted typical cellulose Iβ allomorphs in the samples regardless of SE pretreatments. The CrI of UTN (54.15%) was lower than that of PTN samples which ranged from 58.25 to 61.33% (Figure 3). This result revealed the disintegration of the amorphous components (e.g., hemicellulose, lignin, and extractives) by the SE treatments. Ying et al. also found that the degradation of hemicellulose in poplar by an acetic acid hydrolysis pretreatment resulted in an increase of the CrI value, which is in accordance with the present work (28). No significant increase in CrI of PTN was observed as the SF increased from 3.29 to 4.19. This indicated that the crystalline component became correspondingly more exposed despite of little disruption of hydrogen bonds within cellulose, which was responsible for the cellulase adsorption. Cellulose accessibility (CA) correlating to the adsorption behavior of cellulase directly impacts the sugar release. CA increased from 253.53 in UTN to 488.10 of PTN (SF = 4.19) as the severity of SE pretreatment increased, which can be primarily attributed to that the SE allows hemicelluloses solubilization and opens the lignocellulosic structure (26, 29). Thus, SE pretreatment enhanced the accessibility of the cellulose, which could subsequently promote the enzymatic digestibility. An obvious decrease of degree of polymerization (DP) was observed, in detail, the DP decreased from 839.85 (UTN) to 186.08 (SF = 4.19), which represented a 77.84% reduction of cellulose DP. This result suggested the breakage of inner linkages within cellulose chains during the SE process. This was aligned with the above hypothesis that SE could not only degrade the amorphous component but also destroyed basic bonds in cellulose, which resulted in the depolymerization and exposure of the cellulose (30). Huang and coworkers also reported a decrease of cotton stalk cellulose DP by 50–65% after SE (SF = 4.22). Furthermore, they found that the reduction of DP was one of the main factors enhancing the enzymatic hydrolysis (31). Overall, these physical

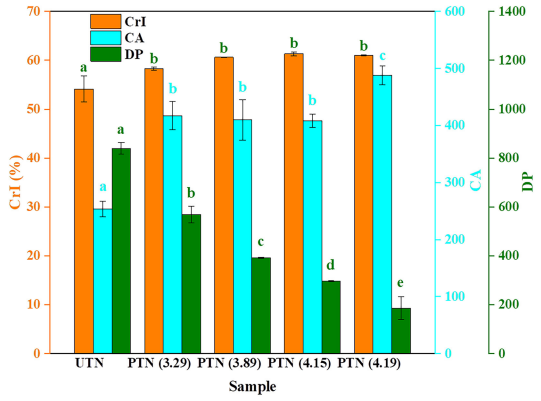

FIGURE 3
Physical properties of TN before and after SE pretreatment. Bars followed by the different superscripts (a–e) show significant difference ($p < 0.05$) according to the Duncan's multiple range test.

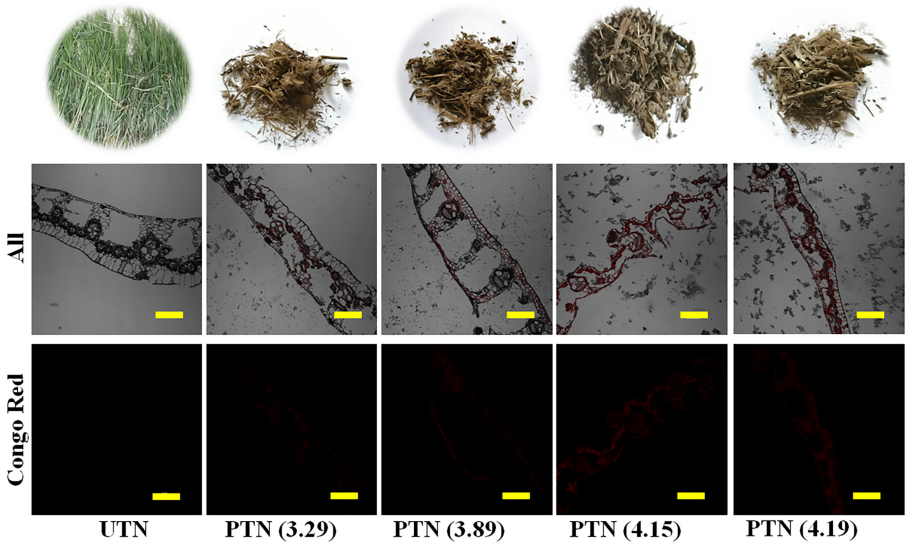

FIGURE 4
Photos (top) and CLSM images of TN before and after SE pretreatment. Red was cellulose labeled with Congo. Scale bar = 100 μm.

parameter changes of TN suggested that more accessible substrates for enzymatic hydrolysis were presented by the SE pretreatment.

Morphological properties of raw and pretreated tiger nut

Morphological alterations of TN during the SE pretreatments were observed using the CLSM imaging techniques. Visual observation suggested that the PTN samples were darker compared to UTN and slightly agglomerated but readily divided (Figure 4). Also, the UTN had rigid and smooth fibers, whereas the PTN looked porous, rough, irregular, and defibrillated. Color variation is a primary indicator of chemical variations in the lignocellulosic biomass. Similar results were also obtained from the SO_2-catalyzed steam treated softwood pellets (32). The enhanced darkness was associated with surface burning and dissolution of extractives, lignin, and hemicellulose, which resulted in the destruction in mechanical strength and dimensional stability, providing readily degraded substrates for enzymes (33).

Based on the microscopic inspection, it was found that SE pretreatment destroyed the rigid structure and dislocated the cell wall. Specially, dramatic structure changes were observed after SE pretreatment with a higher severity. In detail, during the high temperature cooking stage of the SE, the high temperature steam softened the TN biomass matrix structure. Meanwhile, hemicellulose was hydrolyzed by acetic acid derived from acetyl groups and/or other acids. Some inner linkages of lignin were destroyed and cellulose binding was reduced (34). During the subsequent instantaneous decompression stage, the structure of TN substrates was destroyed by the combined effects of water flashing and volume expansion. Furthermore, the TN biomass materials knocked against the inner-wall of the instrument and collided each other, resulting in a destroyed matrix structure of the biomass (30). As shown in Figure 4, when SF reached 4.15 or larger, the TN matrix was disrupted significantly. Therefore, SE treatment reduced the recalcitrance and presented a easily accessible TN substrate for the enzyme attack.

Furthermore, The CLSM images showed that almost no Congo Red was absorbed by the UTN. This phenomenon demonstrated that the cellulose was difficult to access in the raw TN materials, which also confirmed the recalcitrance in the natural plants (35). With the SF increase, it is interesting to note that the signal intensity of Congo Red became stronger. This result suggested that more cellulose were exposed as the SE severity increased. Accordingly, the cellulose could be more accessible by the cellulase, which was in line with the result that CA increased with the SF increase. The CLSM imaging techniques provided a more visible observation and easy understanding regarding the cellulose expose by the SE treatments (36). Therefore, SE pretreatment destructed the rigid structure and exposed cellulose in TN materials, which could facilitate the subsequent saccharification.

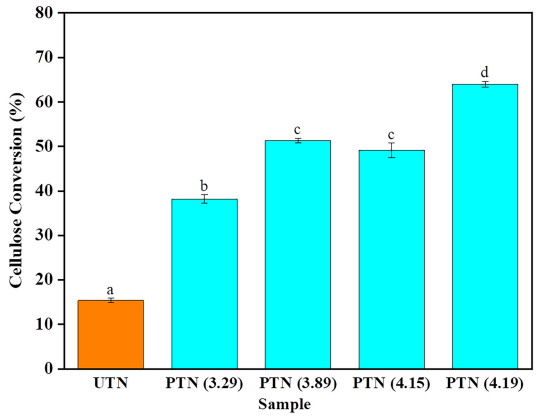

FIGURE 5
Cellulose enzymatic hydrolysis performance of TN before and after SE pretreatment. Bars followed by the different superscripts show significant difference ($p < 0.05$) according to the Duncan's multiple range test.

Enzymatic digestibility performance of raw and pretreated tiger nut

Cellulase was added to the TN substrates regardless of SE pretreatments to release fermentable sugars that can be further used for biofuels production. Previous study reported that a cellulase loading of 20 FPU/g was beneficial to the enzymatic hydrolysis (37). To investigate the effects of SE pretreatment on saccharification of TN biomass, enzymatic hydrolysis was conducted for 48 h with an enzyme loading of 20 FPU/g. As shown in Figure 5, the cellulose conversion of UTN was merely 15.39%. With the SF increased during the SE pretreatment, the cellulose conversion of PTN ranged from 38.18 to 63.97%, which was 2.5–4.2 times larger than that of the UTN. These results implied that SE significantly improved the cellulose conversion efficiency. Interestingly, the difference of cellulose conversion between PTN with SF of 3.89 (1.5 MPa, 10 min) and PTN with SF of 4.15 (1.8 MPa, 10 min) was not significant. Whereas, the cellulose conversion of PTN with SF of 4.19 (1.5 MPa, 20 min) reached 63.97%. These results suggested that the longer boiling time presented more significant impact on enzymatic digestibility than the higher boiling temperature during the SE process. Overall, SE broke the linkages of hemicellulose and lignin and increased the cellulose content within the solid TN substrates. Meanwhile, SE disrupted inner linkages within cellulose chains, reducing the degree of polymerization. As a result, cellulose after SE treatment was more easily accessible by the enzymes (38). Also, the smaller cellulose molecules were more readily degraded, resulting in a significantly improved saccharification efficiency. Enzymatic hydrolysis of cellulose to release fermentable sugars is a prerequisite determining the bioethanol production. Enzymatic digestibility is a significant indicator to evaluate the biorefinery performance of plant materials. For example, Liu et al. examined the enzyme digestibility of corn stover with different particle size to choose the optimal particle size for corn stover biomass utilization. It was found that the utilization of larger biomass particles was desirable for biofuels production and reduced process cost (39). In the present study, the enhanced enzymatic digestibility performance of the steam explosion treated TN demonstrated great potential for the value-added utilization of TN for a biorefinery scenario.

Conclusion

TN grows well in well-drained sandy or loamy soils. The overground tubers of TN represent promising resources for biorefineries. By applying a steam explosion pretreatment, physical-chemical properties of the overground tubers of TN was significantly improved for facilitating the enzymatic hydrolysis to release fermentable sugars. In particular, SE increased cellulose content through removing the hemicellulose from the solid biomass. Moreover, SE reduced the degree of polymerization and improved the accessibility of cellulose, which benefited to the enzymatic adsorption and digestibility. The saccharification efficiency of the TN substrates was significantly enhanced by the SE pretreatment. Therefore, SE is an effective method for promoting the valorization of TN biomass toward a sustainable bioenergy production.

Data availability statement

The original contributions presented in the study are included in the article/supplementary material, further inquiries can be directed to the corresponding authors.

Author contributions

Z-MZ: writing and editing. WY: methodology, investigation, and formal analysis. CH: investigation and data curation. JL: investigation. HX: review and editing. DZ: review, editing, and funding acquisition. GL: conceptualization, design, and writing. All authors contributed to the article and approved the submitted version.

Funding

This study was supported by the National Key Research and Development Program of China (2019YF0507604) and the Science and Technology Planning Proiect of Inner Mongolia Autonomous Region, China (2021GG0212).

Acknowledgments

The authors would like to express thanks to Prof. Guangpeng Li and Yuyin Bao for their constructive direction and kind assistance.

Conflict of interest

The authors declare that the research was conducted in the absence of any commercial or financial relationships that could be construed as a potential conflict of interest.

Publisher's note

All claims expressed in this article are solely those of the authors and do not necessarily represent those of their affiliated organizations, or those of the publisher, the editors and the reviewers. Any product that may be evaluated in this article, or claim that may be made by its manufacturer, is not guaranteed or endorsed by the publisher.

References

1. Raud M, Kikas T, Sippula O, Shurpali NJ. Potentials and challenges in lignocellulosic biofuel production technology. *Renew Sust Energ Rev*. (2019) 111:44–51. doi: 10.1016/j.rser.2019.05.020

2. Velvizhi G, Balakumar K, Nagaraj PS, Ahmad E, Pant KK, Tejraj M, et al. Integrated biorefinery processes for conversion of lignocellulosic biomass to value added materials: paving a path towards circular economy. *Bioresource Technol.* (2022) 343:126151. doi: 10.1016/j.biortech.2021.126151

3. Lin CY, Lu C. Development perspectives of promising lignocellulose feedstocks for production of advanced generation biofuels: a review. *Renew Sust Energ Rev.* (2021) 136:110445. doi: 10.1016/j.rser.2020.110445

4. Elena SZ, Juana FL, Jose APA. Tiger nut (*Cyperus esculentus*) commercialization: health aspects, composition, properties, and food applications. *Compr Rev Food Sci F.* (2012) 34211:366–377. doi: 10.1111/j.1541-4337.2012.00190.x

5. Zerva A, Pentari C, Ferousi C, Nikolaivits E, Karnaouri A, Topakas E. Recent advances on key enzymatic activities for the utilisation of lignocellulosic biomass. *Bioresource Technol.* (2021) 342:126058. doi: 10.1016/j.biortech.2021.126058

6. Zhao L, Sun ZF, Zhang CC, Nan J, Ren NQ, Lee DJ, et al. Advances in pretreatment of lignocellulosic biomass for bioenergy production: challenges and perspectives. *Bioresource Technol.* (2022) 343:126123. doi: 10.1016/j.biortech.2021.126123

7. Zhang YHP, Lynd LR. Toward an aggregated understanding of enzymatic hydrolysis of cellulose: noncomplexed cellulase systems. *Biotechnol Bioeng.* (2004) 88:797–824. doi: 10.1002/bit.20282

8. Lynd LR, Weimer PJ, Van ZWH. Pretorius IS. Microbial cellulose utilization: fundamentals and biotechnology. *Microbiol Mol Biol.* (2002) 66:506–77. doi: 10.1128/MMBR.66.3.506-577.2002

9. Mankar AR, Pandey A, Modak A, Pant KK. Pretreatment of lignocellulosic biomass: a review on recent advances. *Bioresource Technol.* (2021) 334:125235. doi: 10.1016/j.biortech.2021.125235

10. Sarker TR, Pattnaik F, Nanda S, Dalai AK, Meda V, Naik S. Hydrothermal pretreatment technologies for lignocellulosic biomass: a review of steam explosion and subcritical water hydrolysis. *Chemosphere.* (2021) 284:131372. doi: 10.1016/j.chemosphere.2021.131372

11. Hu BB, Wang JL, Wang YT, Zhu MJ. Specify the individual and synergistic effects of lignocellulose-derived inhibitors on biohydrogen production and inhibitory mechanism research. *Renew Energ.* (2019) 140:397–406. doi: 10.1016/j.renene.2019.03.050

12. He J, Huang CX, Lai C, Huang C, Li X, Yong Q. Elucidation of structure-inhibition relationship of monosaccharides derived pseudo-lignin in enzymatic hydrolysis. *Ind Crop Prod*. (2018) 113:368–75. doi: 10.1016/j.indcrop.2018.01.046

13. Li GH, Zhang Y, Zhao C, Xue HT, Yuan L. Chemical variation in cell wall of sugar beet pulp caused by aqueous_ammonia pretreatment influence enzymatic digestibility of cellulose. *Ind Crop Prod.* (2020) 155:112786. doi: 10.1016/j.indcrop.2020.112786

14. Melissa CES, Douglas HF, Pellegrini VOA, Francisco EGG, Eduardo RA, Pereira RL, et al. Physical techniques shed light on the differences in sugarcane bagasse structure subjected to steam explosion pretreatments at equivalent combined severity factors. *Ind Crop Prod.* (2020) 158:113003. doi: 10.1016/j.indcrop.2020.113003

15. Sluiter A, Hames B, Ruiz R, Scarlata C, Sluiter J, Templeton D, et al. *Determination of Structural Carbohydrates and Lignin in Biomass; Laboratory Analytical Procedure (LAP)* (Technical Report) NREL/TP-510-42618.

16. Song WP, Peng LC, Bakhshyar D, He L, Zhang J. Mild O[[sb]]2[[/s]]-aided alkaline pretreatment effectively improves fractionated efficiency and enzymatic digestibility of napier grass stem towards a sustainable biorefinery. *Bioresource Technol.* (2021) 319:124162. doi: 10.1016/j.biortech.2020.124162

17. Inglesby MK, Zeronian SH. Direct dyes as molecular sensors to characterize cellulose substrates. *Cellulose.* (2002) 9:19–29. doi: 10.1023/A:1015840111614

18. Jin KX, Kong LG, Liu XG, Jiang ZH, Tian GL, Yang SM, et al. Understanding the xylan content for enhanced enzymatic hydrolysis of individual bamboo fiber and parenchyma cells. *Acs Sustain Chem Eng.* (2019) 7:18603–11. doi: 10.1021/acssuschemeng.9b04934

19. Li GH, Chen HZ. Synergistic mechanism of steam explosion combined with fungal treatment by *Phellinus baumii* for the pretreatment of corn stalk. *Biomass Bioenerg.* (2014) 67:1–7. doi: 10.1016/j.biombioe.2014.04.011

20. Zhao JK, Yang Y, Zhang M, Rice CW, Wang DG. Elucidating thermochemical pretreatment effectiveness of different particle-size switchgrass for cellulosic ethanol production. *Biomass Bioenerg.* (2022) 164:106561. doi: 10.1016/j.biombioe.2022.106561

21. Tokla E, Sumate C, Boonya C. Enhanced enzymatic hydrolysis and methane production from rubber wood waste using steam explosion. *J Environ Account Ma*. (2019) 235:231–9. doi: 10.1016/j.jenvman.2019.01.041

22. Huang CX, Jiang X, Shen XJ, Hu JG, Tang W, Wu XX, et al. Lignin-enzyme interaction: A roadblock for efficient enzymatic hydrolysis of lignocellulosics. *Renew Sust Energ Rev.* (2022) 154:111822. doi: 10.1016/j.rser.2021.111822

23. Nasir A, Chen HZ, Wang L. Novel single-step pretreatment of steam explosion and choline chloride to de-lignify corn stover for enhancing enzymatic edibility. *Process Biochem.* (2020) 94:273–81. doi: 10.1016/j.procbio.2020.04.036

24. Besserer A, Obame SN, Safou TR, Saker S, Ziegler DI, Brosse N. Biorefining of aucoumea klaineana wood: Impact of steam explosion on the composition and ultrastructure the cell wall. *Ind Crop Prod.* (2022) 177:114432. doi: 10.1016/j.indcrop.2021.114432

25. Zhao ZM, Wang L, Chen HZ. A novel steam explosion sterilization improving solid-state fermentation performance. *Bioresource Technol.* (2015) 192:547–55. doi: 10.1016/j.biortech.2015.05.099

26. Maniet G, Schmetz Q, Jacquet N, Temmerman M, Gofflot S, Richel A. Effect of steam explosion treatment on chemical composition and characteristic of organosolv fescue lignin. *Ind Crop Prod.* (2017) 99:79–85. doi: 10.1016/j.indcrop.2017.01.015

27. Li H, Chen H. Detoxification of steam-exploded corn straw produced by an industrial-scale reactor. *Process Biochem.* (2008) 43:1447–1451. doi: 10.1016/j.procbio.2008.05.003

28. Ying WJ, Fang X, Xu Y, Zhang JH. Combined acetic acid and enzymatic hydrolysis for xylooligosaccharides and monosaccharides production from *Poplar*. *Biomass Bioenerg.* (2022) 158:106377. doi: 10.1016/j.biombioe.2022.106377

29. He LW, Wang C, Shi HH, Zhou W, Zhang Q, Chen XY. Combination of steam explosion pretreatment and anaerobic alkalization treatment to improve enzymatic hydrolysis of Hippophae rhamnoides. *Bioresource Technol.* (2019) 289:121693. doi: 10.1016/j.biortech.2019.121693

30. Zhao ZM, Wang L, Chen ZH. Physical structure changes of solid medium by steam explosion sterilization. *Bioresource Technol.* (2016) 203:204–10. doi: 10.1016/j.biortech.2015.12.043

31. Huang Y, Wei XY, Zhou SG, Liu MY, Tu YY, Li A. Steam explosion distinctively enhances biomass enzymatic saccharification of cotton stalks by largely reducing cellulose polymerization degree in *G. barbadense* and *G. hirsutum*. *Bioresource Technol.* (2015) 181:224–30. doi: 10.1016/j.biortech.2015.01.020

32. Tooyserkani Z, Kumar L, Sokhansanj S, Saddler J, Bi XT, Lim CJ, et al. SO[[sb]]2[[/s]]-catalyzed steam pretreatment enhances the strength and stability of softwood pellets. *Biomass Bioenerg.* (2013) 130:59–68. doi: 10.1016/j.biortech.2012.12.004

33. Vitrone F, Ramos D, Vitagliano V, Ferrando F. Salvadó J. All-lignocellulosic fiberboards from giant reed (Arundo donax L): Effect of steam explosion pre-treatment on physical and mechanical properties. *Constr Build Mater.* (2022) 319:126064. doi: 10.1016/j.conbuildmat.2021.126064

34. Yu Y, Wu J, Ren XY, Lau A, Rezaei H, Takada M, et al. Steam explosion of lignocellulosic biomass for multiple advanced bioenergy processes: a review. *Renew Sust Energ Rev.* (2022) 154:2022. doi: 10.1016/j.rser.2021.111871

35. Omar MMA, Barta K, Beckham GT, Luterbacher JS, Ralph J, Rinaldi R, et al. Guidelines for performing lignin-first biorefining. *Energ Environ Sci.* (2021) 14:262–92. doi: 10.1039/D0EE02870C

36. Mhaske P, Farahnaky A, Kasapis S. Quantification using rheological blending-law analysis and verification with 3D confocal laser scanning microscopy of the phase behaviour in agarose-gelatin co-gels. *Food Hydrocolloid.* (2023) 134:108042. doi: 10.1016/j.foodhyd.2022.108042

37. Li GH, He W, Yuan L. Aqueous ammonia pretreatment of sugar beet pulp for enhanced enzymatic hydrolysis. *Bioproc Biosyst Eng.* (2017) 40:1603–9. doi: 10.1007/s00449-017-1816-9

38. Liu LY, Chandra RP, Tang Y, Huang XY, Bai FW, Liu CG. Instant catapult steam explosion: an efficient preprocessing step for the robust and cost-effective chemical pretreatment of lignocellulosic biomass. *Ind Crop Prod.* (2022) 188:115664. doi: 10.1016/j.indcrop.2022.115664

39. Liu ZH, Qin L, Pang F, Jin MJ, Li BZ, Kang Y, Dale BE, Yuan YJ. Effects of biomass particle size on steam explosion pretreatment performance for improving the enzyme digestibility of corn stover. *Ind Crop Prod.* (2013) 44:176–84. doi: 10.1016/j.indcrop.2012.11.009

frontiers | Frontiers in Nutrition

TYPE Original Research
PUBLISHED 11 January 2023
DOI 10.3389/fnut.2022.1118900

Check for updates

OPEN ACCESS

EDITED BY
Wenjie Sui,
Tianjin University of Science and Technology, China

REVIEWED BY
Zhipeng Yu,
Hainan University, China
Rui Fan,
Peking University, China

*CORRESPONDENCE
Yali Dang
✉ dangyali1978@126.com
Xiuzhi Zhu
✉ zhuxiuzhi13142@163.com

SPECIALTY SECTION
This article was submitted to Nutrition and Food Science Technology, a section of the journal Frontiers in Nutrition

RECEIVED 08 December 2022
ACCEPTED 28 December 2022
PUBLISHED 11 January 2023

CITATION
Li Y, Gao X, Pan D, Liu Z, Xiao C, Xiong Y, Du L, Cai Z, Lu W, Dang Y and Zhu X (2023) Identification and virtual screening of novel anti-inflammatory peptides from broccoli fermented by *Lactobacillus strains*. *Front. Nutr.* 9:1118900. doi: 10.3389/fnut.2022.1118900

COPYRIGHT
© 2023 Li, Gao, Pan, Liu, Xiao, Xiong, Du, Cai, Lu, Dang and Zhu. This is an open-access article distributed under the terms of the Creative Commons Attribution License (CC BY). The use, distribution or reproduction in other forums is permitted, provided the original author(s) and the copyright owner(s) are credited and that the original publication in this journal is cited, in accordance with accepted academic practice. No use, distribution or reproduction is permitted which does not comply with these terms.

Identification and virtual screening of novel anti-inflammatory peptides from broccoli fermented by *Lactobacillus strains*

Yao Li[1], Xinchang Gao[2], Daodong Pan[1], Zhu Liu[3], Chaogeng Xiao[4], Yongzhao Xiong[1], Lihui Du[1], Zhendong Cai[1], Wenjing Lu[4], Yali Dang[1]* and Xiuzhi Zhu[5]*

[1]State Key Laboratory for Managing Biotic and Chemical Threats to the Quality and Safety of AgroProducts, College of Food and Pharmaceutical Sciences, Ningbo University, Ningbo, Zhejiang, China, [2]Department of Chemistry, Tsinghua University, Beijing, China, [3]Zhejiang Institute for Food and Drug Control, Hangzhou, Zhejiang, China, [4]Zhejiang Academy of Agricultural Sciences, Hangzhou, Zhejiang, China, [5]Department of Gynecology and Obstetrics, The Second Affiliated Hospital of Zhejiang Chinese Medical University, Hangzhou, Zhejiang, China

Lactobacillus strains fermentation of broccoli as a good source of bioactive peptides has not been fully elucidated. In this work, the peptide composition of broccoli fermented by *L. plantarum* A3 and *L. rhamnosus* ATCC7469 was analyzed by peptidomics to study the protein digestion patterns after fermentation by different strains. Results showed that water-soluble proteins such as rubisco were abundant sources of peptides, which triggered the sustained release of peptides as the main target of hydrolysis. In addition, 17 novel anti-inflammatory peptides were identified by virtual screening. Among them, SIWYGPDRP had the strongest ability to inhibit the release of NO from inflammatory cells at a concentration of 25 μM with an inhibition rate of 52.32 ± 1.48%. RFR and KASFAFAGL had the strongest inhibitory effects on the secretion of TNF-α and IL-6, respectively. At a concentration of 25 μM, the corresponding inhibition rates were 74.61 ± 1.68% and 29.84 ± 0.63%, respectively. Molecular docking results showed that 17 peptides formed hydrogen bonds and hydrophobic interactions with inducible nitric oxide synthase (iNOS). This study is conducive to the high-value utilization of broccoli and reduction of the antibiotic use.

KEYWORDS

fermented broccoli, anti-inflammatory peptides, peptidomics, virtual screening, *Lactobacillus*

1. Introduction

Inflammation is the aggregate immunoreaction of the body to certain irritants, such as microbiological pollution, and oxidative stress (1). However, long-term inflammation may provocate diabetic mellitus, fat, cardiovascular disease, inflammatory bowel disease, neural inflammation, and other ailments (2). Adjusting mass propagation, swallowing

of macrophages, and secretion of pro-inflammatory cytokines can effectively treat inflammation (3). In general, endocellular nitric oxide (NO) keeps stable at low levels for a long time. However, under the stimulation of various inflammatory conditions, iNOS catalyzes L-arginine oxidation to produce a large amount of NO, which results in tissue damage (4). Inhibition of iNOS could effectively control the inflammatory response in various pathological conditions (5). Therefore, inhibition of iNOS activity has become an important method of treatment of inflammatory diseases. Nevertheless, taking antiphlogistic drug medicines for a long time can easily lead to gastrointestinal diseases, renal insufficiency, and other side effects (6). Moreover, the misuse of antibiotics to treat inflammation caused by bacterial infections can easily make the bacteria resistant, making the infection more difficult to treat and ultimately likely leading to previously preventable deaths (7). In consequence, the evolution of innoxious and easily absorbed natural anti-inflammatory agents has become a research focus.

Fermentation, a microbial physiological process is attracting extensive concern for its effect on improving functional properties (8). Lactic acid bacteria (LAB) are the main microorganisms in fermented food, which have important effects on the quality and physiological activity of fermented food. The main genera of LAB such as *Enterococcus*, *Lactobacillus*, *Streptococcus*, and *Tetragenococcus* have been isolated from fermented foods worldwide (9). Besides the energy and nutritional properties of fermented filtrate, LAB fermentation as an excellent source of bioactive peptides is also well known (10). Many peptides with anti-inflammatory activity or other biological activity have been obtained from various fermented foods, such as fermented milk (11), fermented soybean (12), oyster (13), etc. Fermentation of unprocessed protein-rich organisms has become an important strategy for the production of bioactive peptides in the biotechnology industry.

Broccoli is a variety of *Brassica* species in Cruciferae with green flower balls as products, which is a favorable source of health-promoting nutrients. The most usual bioactive compounds in broccoli are considered to be secondary metabolites such as sulforaphane, phenolic acid, and flavone (14). Therefore, previous research always concentrated on the changes in these metabolites during the fermentation process (15, 16). But few studies have explored the peptide changes of broccoli during fermentation. Plant proteins are modified differently during fermentation to generate a series of hydrolysates with variant bioactivities, such as peptides. It is noteworthy that these hydrolysates are significant for the functions of fermented foods. Among them, bioactive peptides exhibit antihypertensive, hypoglycemic, cholesterol-lowering, anti-inflammatory, and other physiological activities (17). Enzymatic hydrolysis or fermentation to obtain active peptides has been widely used in food processing (18). Broccoli protein could be effectively degraded by its endogenous protease and exogenous protease secreted by microorganisms (19). It is a pity that there are few studies on the identification of peptides and active peptides of LAB fermented broccoli. Previously, active peptides with hypoglycemic and antihypertensive properties have been identified from broccoli, but peptides with anti-inflammatory properties have not been identified (20). Meanwhile, the traditional separation and purification of bioactive peptides are very cumbersome and time-consuming (21). The combination of peptidomics and virtual screening techniques (bioinformatics, molecular docking, etc.) can be used as a tool for the rapid screening of bioactive peptides, thereby effectively improving experimental efficiency.

In this paper, high-flux peptidomic methods were used to study the peptide profiles of fermented and unfermented broccoli of *L. plantarum* A3 and *L. rhamnosus* ATCC7469 and to quickly screen anti-inflammatory peptides. Finally, the molecular mechanism of anti-inflammatory peptides to the iNOS receptor was evaluated. This research will contribute to the high-value utilization of broccoli and provide a new understanding of increasing the functional value of broccoli fermented by LAB.

2. Materials and methods

2.1. Materials

The stems and leaves of broccoli (*Brassica oleracea var. italica*) were obtained from Wumei Market (Ningbo, China). *Lactobacillus plantarum* A3 and *Lactobacillus rhamnosus* ATCC7469 were preserved in our laboratory and used in this study. Peptides from broccoli were synthesized by GL Biochemical, Ltd. (Shanghai, China).

RAW264.7 cells were obtained from the Procell (Wu Han, China). Dulbecco's modified Eagle medium (DMEM), Penicillin/streptomycin solution (P/S), and fetal bovine serum (FBS) were obtained from HyClone (Logan, UT, USA). Lipopolysaccharides (LPS), CCK-8 kits, and nitric oxide test kits were provided by Bey time (Shanghai, China). TNF-α and IL-6 ELISA kits were purchased from Multi Sciences (Hangzhou, China). Pierce^{TM} Quantitative Peptide Assays Kit was purchased from Thermo Fisher Scientific (NY, USA). Other chemicals and reagents are analytically pure.

2.2. Sample preparation

The fresh stems and leaves of broccoli were washed with ultrapure water and juiced, and solid particles were separated by gauze filtration. The juice was transferred into a 200 ml

conical flask and autoclaved at 121°C for 15 min to eliminate the influence of endogenous bacteria.

2.3. Broccoli fermentation

The two strains of lactic acid bacteria were activated in a constant temperature and humidity incubator at 37°C. The activated strains were centrifuged for 5 min at 10,000 × g. And then the precipitate was dissolved in 100 mL of broccoli juice. The initial cell density of the final solution was 10^7 CFU/mL and cultured at 37°C for 24 h. After fermentation, the supernatant was centrifuged and stored at −80°C. All fermentation experiments were repeated three times.

2.4. Peptide extraction

The peptides were rapidly extracted from the hydrolysate of broccoli by ultrafiltration centrifuge tube (*Mw = 10 kDa*, Merck KGaA, Darmstadt, Germany), freeze-dried, and stored at −80°C for further analysis. According to the manufacturer's instructions, the extracted peptides were further cleaned and concentrated using Oasis HLB cartridges (Waters, Milford, MA, USA), which were modified by our research team to remove salt from the sample. The specific program is shown in Supplementary Table S1. The peptide detection kit is used to determine the peptide content in the sample.

2.5. Peptide identification by LC-MS/MS

The detection system was combined with the Thermoelectric Easy-nLC 1200 (Thermo Scientific, P/N LC140) and the orbital trap Exploris 480 (Thermo Scientific, P/N BRE725533) for peptide identification. All mass spectrometer parameters were followed by Zhang et al. (22). The peptide was captured by a capture column (PepMap C18, 100 μm × 25 cm) for 3 min, and then the peptide was separated by gradient elution chromatography on a nano-upgrade analytical column (PepMap C18, 75 μM × 25 cm). Mobile phase A: 0.1% formic acid aqueous solution, mobile phase B: 0.1% formic acid acetonitrile solution; the separation gradient of mobile phase B increased from 5 to 30% within 60 min. The chromatographic flow rate was 300 nL/min. The sample volume was 5 μL; the column temperature was 55°C.

The full scan MS scan range was set to m/z 100–1,600, resolution 70,000 (m/z 200). The maximum ion introduction time was set to 50 ms, the Auto Gain Control was set to 5 $\times 10^5$, the intensity of the first 15 parent ions in the high energy collision dissociation experiment, and the scanning rate was executed at 17,500. Based on the parent ion mass charge ratio automatic control scanning range, the minimum scanning range was set to m/z = 100, up to 2,000. When MS/MS analysis was performed, the minimum ionic strength was set to 13,000, the maximum ion introduction time was set to 100 ms, and the Auto Gain Control was controlled to 2.0×10^5. The parent ion error tolerance was set at 1.6 Da. Finally, ions with charges of 1, 2, 3, and 4 were collected, and the exclusion was set to MS/MS analysis of the parent ion within 10 s, and then 40 s, 30% collision energy was excluded.

PEAKS Studio 8.5 (Bioinformatics Solutions, Waterloo, Canada) was used for mass spectrometry data analysis and broccoli protein database matching (https://www.ncbi.nlm.nih.gov/data-hub/taxonomy/tree/?taxon=36774). The identified protein sequence data were retrieved from the UniProt KB database, and the retrieved sequences were searched locally for homology sequences and their functional annotations. PEAKS Studio was used to quantify the abundance of identified peptides. The false positive rate (FDR) of peptide identification was set at 1%. For the results of *de novo* sequencing, ALC (%) is the full mean local confidence. *De novo* sequencing data are more reliable when the ALC was greater than 80%, and these data were retained. The BIOPEP database was used to retrieve bioactive peptides and identify peptides from samples. Peptide mapping was done using the online tool Peptigram (23). The potential activity of each peptide was identified using the PeptideRanker tool.

2.6. Identification and function prediction of broccoli peptides

PeptideRanker scores above 0.5 were designated as potential bioactive peptides, where the higher the score, the higher probability of the peptide being bioactive. The anti-inflammatory peptides were predicted by AIPpred (24) and Antiinflam (25). The anti-hypertensive peptides were forecast by AHTpin (26), and mATPred (27). The pro-inflammatory activity of the peptides was predicted by VaxinPAD (28). AntiCP 2.0 (29) had access to predict anticancer peptides. The toxicity and major properties of peptides were identified using the ToxinPred13 and Innovagen platforms (http://www.innovagen.com/proteomics-tools).

2.7. Determination of the anti-inflammatory activity of broccoli peptides

2.7.1. Albumin denaturation assay (AI)

The anti-inflammatory properties of broccoli hydrolyzates were preliminarily determined by the albumin denaturation

method (30). The reaction mixture was composed of 5 ml bovine serum albumin (1%, pH = 6.3), 0.5 mL broccoli sample solution, incubated at 37°C for 20 min, and then incubated at 51°C for 20 min. The absorbance at 660 nm was recorded using Tecan microplate reader (Infinite M2000 Pro, Switzerland). Diclofenac sodium was used as the positive control.

2.7.2. Determination of inflammatory factors

RAW264.7 cells were cultured in DMEM medium containing 10% FBS and 1% double antibody at 37°C and 5% CO_2 incubator. CCK-8 reagent was used for cell viability assay.

RAW264.7 cells (3×10^6 cells / mL) seeded into 12-well plates were pretreated with various concentrations of broccoli hydrolyzates or synthetic peptides for 2 h before stimulation by LPS (200 ng/mL). NO was determined using Griess reagent. TNF-α and IL-6 were measured by ELISA kits according to the manufacturer's instructions. More details of the assay are shown in Supplementary Table S2.

2.8. Synthesis of specific sequence peptides

Peptide sequences from broccoli were synthesized by a solid-phase peptide program using a 9-fluorenyl methoxycarbonyl (Fmoc) protected amino acid synthesis method and an AAPPTEC 396 Automatic Peptide Synthesizer (Advanced Automated Peptide Protein technologies, USA). The purity of synthetic peptide was determined by HPLC to be more than 98%.

2.9. Molecular docking with iNOS

Discovery Studio software (Neo Trident Technology Ltd., Shanghai, China) was used for molecular docking. The peptide structure was drawn by Chem Draw Prime 19.1 software. The crystal structure of iNOS (PDB ID 3E6T) complexed with AR-C118901 was prepared. Molecular docking was referenced by Wang et al. (31) with some modifications. Before docking, the protein crystals were treated as required, water and cofactors were removed, hydrogen was added, and other programs were completed as required. Create a receptor region with a radius of 20Å. The docking energy score and interaction force type evaluate the results.

2.10. Statistical analysis

All experiments were repeated 3 times, and the results were expressed as mean ± standard deviation. Excel, SPSS Statistics 23.0 (IBM, NY, USA), and GraphPad Prism 9.0 (GraphPad Software, CA, USA) were used to process the data. $P < 0.05$ was considered significant.

3. Results and discussions

3.1. Proteomics analysis of peptides

3.1.1. General analysis

As a branch of proteomics, peptidomic analysis has access to use to identify the peptide of samples (32). After the raw data processing, 17,581 peptides were retained from all broccoli samples. Among them, 5,901 peptides were obtained by *de novo* sequencing. About 5,081, 6,359, and 4,894 peptides belong to 2,300, 1,982, and 2,126 proteins for broccoli from NC (broccoli hydrolysate fermented for 0 h), *L. plantarum* A3, and *L. rhamnosus* ATCC7469, respectively. Compared with before fermentation, the number of broccoli proteins decreased after fermentation, which indicated that a small cluster of proteins was degraded by *Lactobacillus*. Totally, 595 peptides were commonly found in each broccoli sample, and they belong to 559 accession proteins (Supplementary Figure S1). The major broccoli proteins were identified, such as jacalin (jacalin-related lectin 34-like isoform X1 and X2), photosystem I, rubisco, ribosomal protein, and other proteins. These identified proteins are different from previous studies (20).

Although most proteins were identified in all samples, there were still differences: 1,754 proteins were absent in NC, while 2,072 and 2,332 proteins were detected in *L. plantarum* A3 and *L. rhamnosus* ATCC7469, respectively. The difference may be due to the different processing methods of samples, and the extracellular enzyme of *Lactobacillus* is more complex than a single enzyme. However, their differences at the peptide level are considerable. A total of 6,368 peptides were identified in NC, 9,570 in *L. plantarum* A3, and 8,203 in *L. rhamnosus* ATCC7469.

Figure 1 shows the intersection of the peptides identified from the three samples. There were some differences in the peptide content of broccoli hydrolysate before and after fermentation. The most abundant peptide was from the hydrolysate fermented by *L. plantarum* A3 (16.23%), followed by *L. rhamnosus* ATCC7469 (11.21%). Interestingly, 5,130 peptides (accounting for 21.22% of the total) only existed in unfermented samples and had higher exclusive peptides compared with other groups. During sample treatment, high temperature and pressure might promote the release of peptides (33).

The restricted proteolytic ability of microorganisms is related to the unique sequence and functional peptide fragments produced by the proteolysis of specific residues (34). This indicates that even though different microorganisms of the same genus have different hydrolysis mechanisms, they can still hydrolyze target proteins at the same site and produce peptides with the same sequence (35). It is noteworthy that, all the peptides identified in the three samples were analyzed.

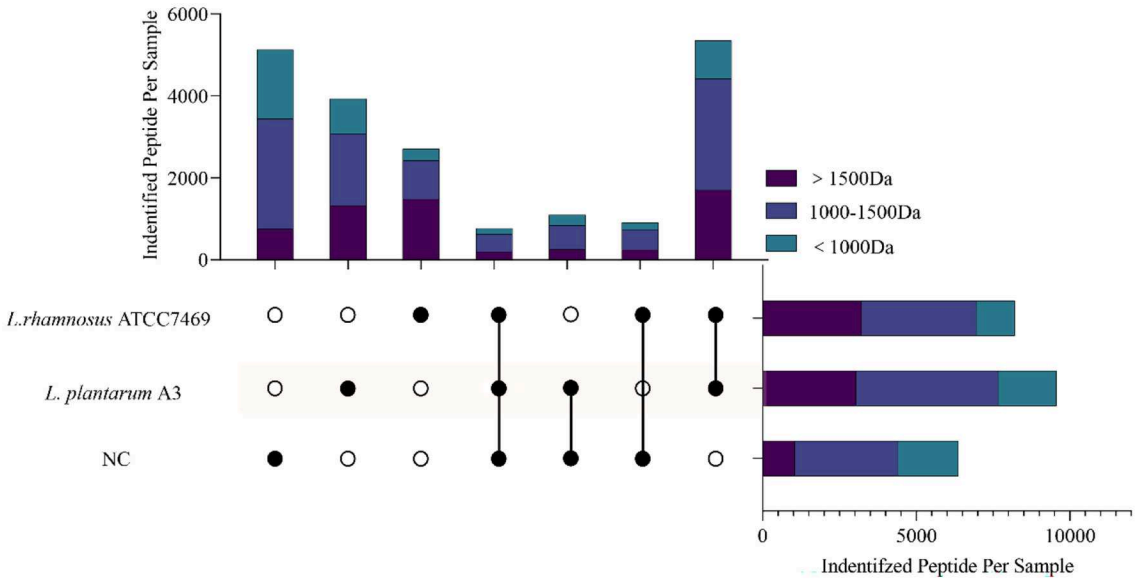

FIGURE 1
The cross plot of peptides identified in broccoli stems and leaves fermentation samples (NC, fermentation for 0 h; *L. plantarum A3*, *Lactobacillus plantarum* fermentation; *L. rhamnosus* ATCC7469, *Lactobacillus rhamnosus* fermentation). Different colors on the strip represent different molecular weights belonging to each cross-group peptide.

As hydrolysates of proteins, amino acids and peptides undergo secondary hydrolysis during fermentation and are consumed by microorganisms (36). Compared with the NC, not only the total number of peptides increased after fermentation, but also the identified peptides were mainly distributed in small molecular weight (<1,000 Da), which was significantly higher than NC. This may indicate that *Lactobacillus* has a good ability to hydrolyze broccoli protein, and can hydrolyze the peptides existing in the NC, resulting in more small molecule active peptides. This proved that *Lactobacillus* fermentation could be a good method for the hydrolysis of plant protein to produce peptides.

3.1.2. Changing of peptides during fermentation in broccoli

During the fermentation process, microorganisms secrete a succession of enzymes that convert macromolecular organic matter in the substrate into small molecules (37). *Lactobacillus plantarum* and *Lactobacillus rhamnosus* are typical LAB for fermentation. It is characterized by high proteolytic activity, extracellular cell wall serine protease, and intracellular peptidase has an extensive range of specificness, including aminopeptidase, carboxypeptidase, and dipeptidase (38). During the fermentation of broccoli, some water-soluble proteins were degraded by LAB, and these proteins were found to be regulatory enzymes in plant physiological metabolism. The peptides on the primary sequence of the identified protein were located and four of the most changed proteins were projected, shown in Figure 2. Among them, ribulose bisphosphate carboxylase was abundant in all samples and increased significantly after fermentation with normalized intensity of 10^8-10^9 (Figure 2A).

This indicates that ribulose bisphosphate carboxylase can be hydrolyzed by microorganisms to become a nitrogen source for its growth and reproduction during microbial proliferation. This result explains the mobile equilibrium of components in the broccoli fermentation broth. Photosystem-I protein same goes for 10^8 (Figure 2B). After fermentation, the sequence almost completely covered the entire protein, and the intensity increased significantly, and the intensity change was more significant in the 60–90 region. In addition, the strength of overlapping peptides at a certain position is proportional to the green depth. The peptides covered in the NC group were the least and the intensity was low, indicating that fermentation could promote protein release. Similar results apply to peptides derived from jacalin and transketolase. The peptides derived from these proteins have a low abundance in NC samples, which may be because these proteins have good thermal stability and are not easy to thermal decomposition. After fermentation, the primary sequence continuously covers the entire mature protein. Only the abundance of peptides at specific locations has been greatly improved. Rubisco is the most abundant protein in plants. Figures 2E–G shows the difference in peptide formation after the fermentation of three different types of rubisco proteins. Discontinuous coverage in the NC sample is

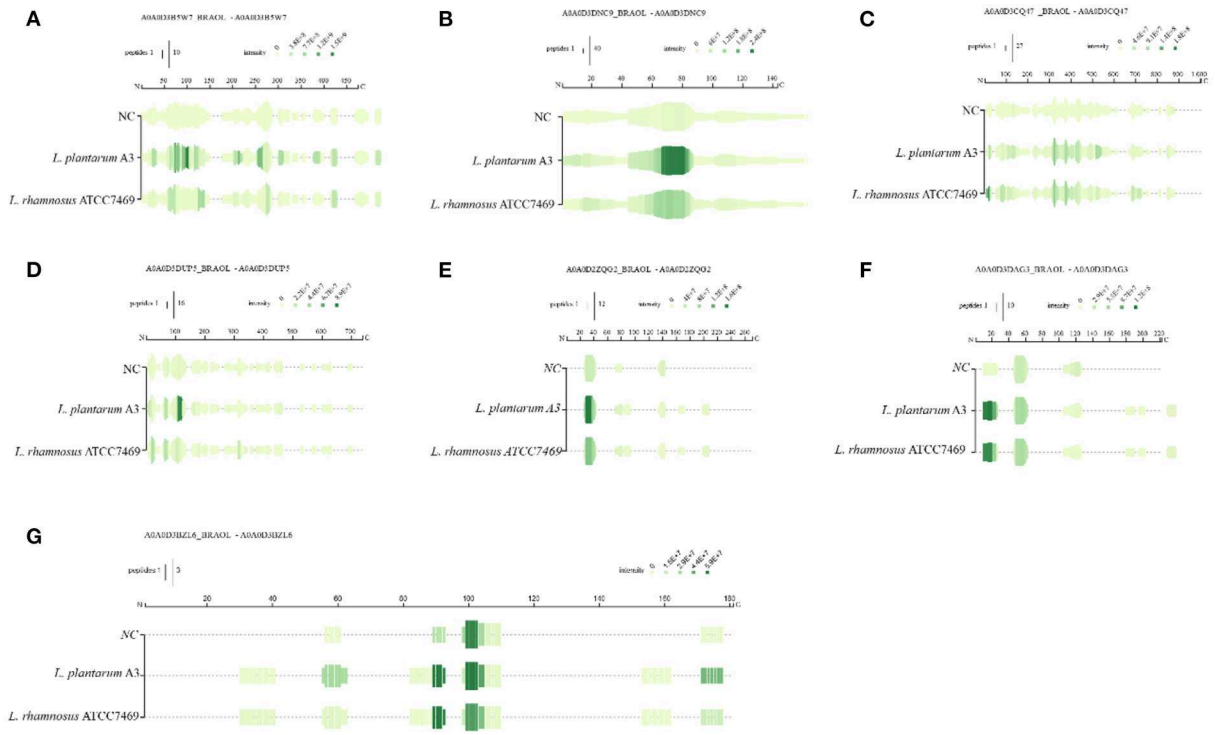

FIGURE 2
Mapping of the identified peptides for the three samples on the sequences of rubisco **(A)** photosystem-I protein **(B)** transketolase **(C)** jacalin **(D)**, rubisco **(E–G)**.

then increased after fermentation and extended to the C-term region. However, there are large gaps between sequences in these regions. Even if they have similar cleavage sites at some positions, the relative strength of the peptides they produce is significantly different. Between 20–40 sites (Figures 2E, F), after fermentation, the green becomes deeper and the strength is significantly improved. In addition, the coverage of *L. plantarum* A3 was wider than that of *L. rhamnosus* ATCC7469 to produce peptides with high intensity. For photosystem-I protein, it was almost completely covered, and its strength was significantly improved after fermentation. After fermentation, its abundance is greatly increased, indicating that microorganisms can also use these two proteins for life activities. Other researchers reported similar results, and they found the most abundant category number was the 'catalytic activity' category of camellia proteins (36). This may provide evidence that the functional properties of proteins in broccoli are highly correlated with substrates.

To better understand the correlation between the digestion process of broccoli protein before and after fermentation and the appearance of its derived peptides, the peptide concentration was normalized and clustered. To reduce the effect of missing values, peptides present in all samples are clustered first. In addition, the second cluster analysis was performed on all peptides that existed in the fermentation group but did not exist in the NC group. Cluster analysis of the co-existing peptides between samples showed that the content of co-existing peptides before and after fermentation was different (Supplementary Figure S2). The small branch distance between *L. plantarum* A3 and *L. rhamnosus* ATCC7469 indicated that the similarity of peptide content between them was high. Additionally, quantitative results showed that the content of most peptides increased significantly after fermentation compared with NC group. In addition, the quantitative levels of broccoli peptides after fermentation with two different strains (FC $\geq$ 2 or $\leq$ 0.5, $p < 0.5$, $n = 260$) were compared, which were not present in NC (Supplementary Figure S3). Compared with *L. plantarum* A3, a total of 75 peptides were significantly enhanced and 185 peptides were significantly reduced. Compared with *L. plantarum* A3, a total of 75 peptides were significantly enhanced and 185 peptides were significantly reduced. This shows that there are significant differences in peptide release ability between different strains. Similarly, peptides from ribiso are the main peptides, but there are also peptides from ATP synthase subunit beta, Jacalin, and other small proteins. The hydrolysis of these proteins may contribute to the release of active peptides (36).

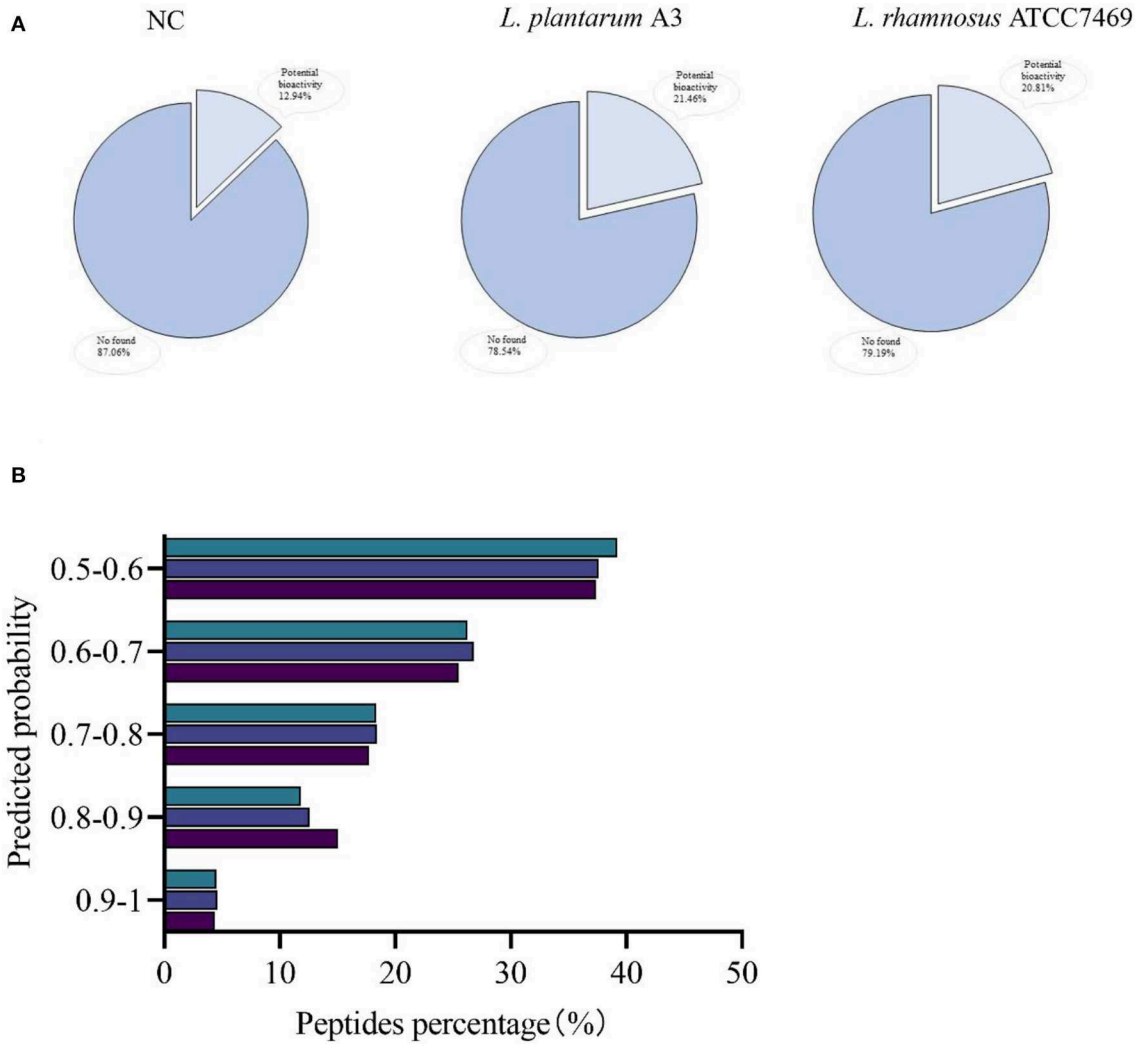

FIGURE 3
Ranked according to the predicted probability of potential biological activity of peptides. Coverage **(A)** and classified **(B)**.

3.1.3. Bioinformatics analysis for the potential bioactivity of broccoli peptides

All peptides were searched in the BIOPEP-UWM database to appraise potential bioactive peptides. Unfortunately, no peptides completely matched with the database were found in this study. Most of the bioactive peptides in BIOPEP database were 2 to 3 amino acids. In our study, most peptides were found to be more than 4 peptides. Therefore, we used PeptideRanker online tool to predict all peptide activity detected in our study (Figure 3). In PeptideRanker, any peptide predicted to exceed 0.5 threshold is considered to have biological activity. Totally, 824 (12.94%), 2,060 (21.46%), and 1,707 (20.81%) peptides with a score of more than 0.5 were found in broccoli from NC, *L. plantarum* A3, and *L. rhamnosus* ATCC7469, respectively (Figure 3A).

The distribution of these potentially bioactive peptides is shown in Figure 3B. The percentage of peptides scored between 0.9 and 1.00 in broccoli from *L. plantarum* A3, and *L. rhamnosus* ATCC7469, was 4.37, 4.61, and 4.51%. In addition, the relative abundances of the potentially active peptides in the three samples were calculated. The standardized intensity of the samples from NC was found 7.98×10^8, the relative abundance of *L. plantarum* A3 was 6.92×10^{10}, and *L. rhamnosus* ATCC7469 was 2.56×10^{10}. Compared with unfermented broccoli, both the proportion and relative abundance of potential bioactive peptides increased significantly after LAB fermentation. And there are differences in strains, *L. plantarum* A3 fermentation than *L. rhamnosus* ATCC7469 fermentation is more obvious. Wei et al. (39) had similar research results to ours. The diversity and abundance of

bioactive peptides increased significantly after fermentation of their furu samples, probably because most of the enzymes secreted during fermentation degraded the proteins to produce more bioactive peptides. This result showed that microbial fermentation could produce bioactive peptides by hydrolysis of proteins from broccoli, thereby improving their potential biological activities.

TABLE 1 Broccoli hydrolysate inhibition albumin denaturation test.

Samples	AI(μg/mL of DSE)
NC	280.89 ± 3.1646^{c}
L. plantarum A3	$1{,}798.39 \pm 1.0014^{a}$
L. rhamnousus ATCC7469	$1{,}403.744 \pm 5.8357^{b}$

Lowercase letters a, b, and c indicate significant differences between samples ($p < 0.05$).

3.2. Functional prediction of bioactive peptides

Bioinformatics, which relies mainly on mathematical and statistical models to accurately predict the likely biological activities of individual peptides, seems to be useful for screening large numbers of peptides and assessing certain functions (35). The broccoli was fermented by LAB, and the protein was degraded by an extracellular protease to produce bioactive peptides, which gave it higher biological activity. To better study the bioactive peptides from broccoli, we selected peptides with PeptideRanker score > 0.5 for functional analysis. Anti-inflammatory, anti-hypertensive, anti-cancer, DPP IV inhibitory, and immunoregulatory activities were screened. The results showed that 84.16% of all predicted peptides had anti-inflammatory effects. In addition, 63.95% of the peptides were predicted to be antihypertensive peptides, 64.56% were considered to have anticancer activity, 47.70% were considered to be potential DPP IV inhibitors, and 7.43% of the peptides were predicted to have immunoregulatory activity (see Supplementary material B).

Computer screening of anti-inflammatory properties of peptides using network servers shows that there are a large number of anti-inflammatory peptides with different prediction probabilities in each hydrolysis station service. About 37.7% of the peptides in the hydrolysates fermented by *L. plantarum* A3 were predicted to be anti-inflammatory. In the hydrolysates fermented by *L. rhamnosus* ATCC7469, 31.83% of the peptides were anti-inflammatory, while only 14.59% of the NC were thought to be anti-inflammatory peptides. These predicted anti-inflammatory peptides contain one or more hydrophobic amino acids at the C- or N-terminus.

Besides, most peptides contain positively charged amino acids. Research has shown that the overall positive charge of peptides may be a chemokine, but their location is not fixed (40). Peptides with highly alkaline N-terminal or N-terminal Arg residues can bind to LPS released by bacteria, thereby blocking the inflammatory response.

To reduce the workload, of all the predicted anti-inflammatory peptides, 395 peptides (PeptideRanker score > 0.8) were retained for molecular docking after the removal of repetitive peptides and peptides longer than 15 amino acids (see Supplementary material B). These potential anti-inflammatory peptides are derived from F-box domain proteins, protein kinase domain-containing proteins, ribosomal proteins, rubisco, and other proteins, including uncharacterized proteins. Among them, the protein sources of most anti-inflammatory peptides have not been characterized. Of the identified proteins, proteins containing the F-box domain are the most abundant source of anti-inflammatory peptides among the three hydrolysates, followed by proteins containing the protein kinase domain. Some peptides were also identified from ribosomal protein and rubisco. F-box protein plays an important role in plant growth and development. Rubisco is the most abundant enzyme in plants and the most extensive source of plant bioactive peptides (41). Ribosomal proteins are also considered an important source of active peptides (42). Water-soluble proteins such as F-box domain protein, ribulose diphosphate carboxylase large chain, and 60S ribosomal protein L13a have a positive effect on the release of anti-inflammatory peptides. This indicates that potential anti-inflammatory peptides can be obtained from broccoli proteins, and increasing the content of active peptides in fermented broccoli will facilitate the degradation of these proteins, thereby improving the bioavailability of broccoli.

3.3. Determination of broccoli peptides activity

Inflammation is an important response of the body to foreign microbial infection and repair damage. But overage and unbounded inflammatory variations often lead to chronic maladies (1). Tissue protein degeneration is one of the causes of inflammation and arthritis (30). Therefore, ground on the prediction results of bioactive peptides, the albumin denaturation test (AI) was used to determine the anti-inflammatory activity of broccoli hydrolysate. The results of AI denaturation were expressed as diclofenac sodium equivalent (DSE) μg/mL, as shown in Table 1.

The results showed that different broccoli hydrolysates could inhibit albumin denaturation. But there are significant differences between them. Compared with NC, the anti-inflammatory potential of the other two hydrolysates was significantly enhanced. Among them, the hydrolysate of *L. plantarum* A3 had the highest anti-inflammatory activity, followed by *L. rhamnosus* ATCC7469, with DSE values of

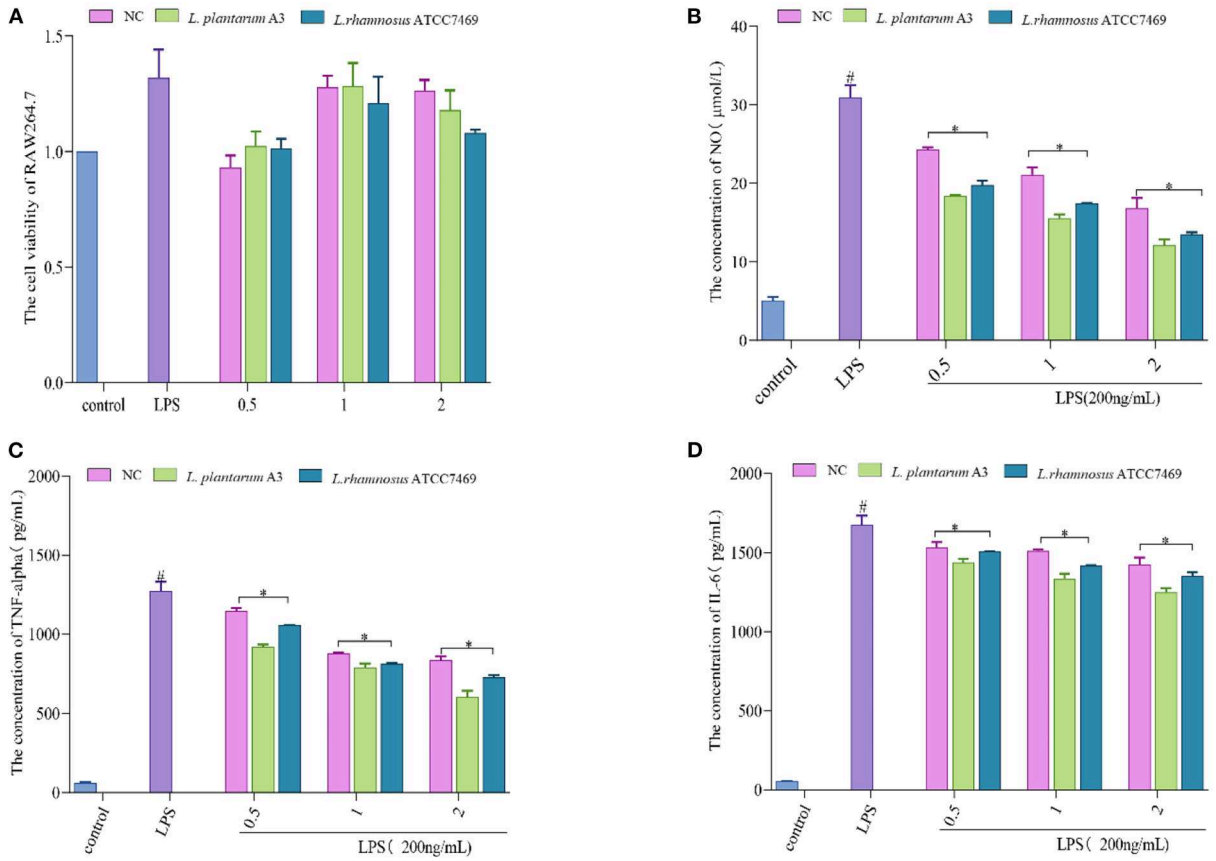

FIGURE 4
(A) Effect of different concentration samples (mg/mL) on the viability of RAW264.7 cells. **(B–D)** represent the effects of different concentrations of samples on the secretion of NO, TNF-α, and IL-6 in RAW264.7 cells after LPS stimulation. #, LPS is significantly different from control; *, The difference between the experimental group and the LPS group was significant ($P < 0.05$).

1,798.39 ± 1.14 and 1,403.744 ± 5.84 μg/mL, respectively. In addition, the anti-inflammatory ability of the samples was further determined by LPS-induced RAW264.7 inflammatory cell model. It found that all three hydrolysates could promote the proliferation of macrophages, and increased first and then decreased with the increase of concentration. However, no significant toxic effects were observed at high concentrations (Figure 4A).

Treatment of macrophages with LPS causes over-immunity, producing large amounts of inflammatory factors (43, 44). Mouse macrophage RAW264.7 cells are commonly used to assess anti-inflammatory properties because their high sensitivity to external stimuli leads to the secretion of inflammatory cytokines (45). The data showed that all of them could prominently inhibit the production of NO, TNF-α, and IL-6. Among them, *L. plantarum* A3 had the strongest anti-inflammatory effect. At the maximum concentration (2 mg/mL), the inhibition rates of NO, TNF-α, and IL-6 were 60.52 ± 2.32%, 55.09 ± 2.87%, and 28.29 ± 1.57%, respectively (Figures 4B–D). This further indicates that LAB fermentation could improve the functional activity of broccoli. This may be because fermentation promotes the release of bioactive peptides and other active substances in broccoli to enhance anti-inflammatory activity. The results also strongly suggested that starter selection is still a major and important step in the development of fermentation-based biological processes. The research of Sun et al. (46) also proved this point. They found that different lactic acid bacteria increase the antioxidant and hypoglycemic activity of pumpkin juice by releasing bioactive substances such as phenols. Among them, *L. plantarum*, *L. acidophilus*, and *L. helveticus* had the strongest antioxidant capacity after fermentation.

3.4. Molecular docking with iNOS

A total of 72 known active anti-inflammatory peptides were docked with iNOS receptors as the positive control (Supplementary Table S3). The docking energy results showed that the docking energy of short peptides was generally higher

than that of long peptides. Since the long-chain peptide has side-chain radicals, it increases the possibility of combining with the reactive site of the receptor. Furthermore, long-chain peptides may have greater flexibility and shorter docking distances to receptors (47). Hence, when utilizing molecular docking to determine whether the peptide has anti-inflammatory activity, peptide chain length and docking energy should be combined for evaluation. In this study, 395 potential anti-inflammatory peptides screened from broccoli were docked by DS software.

Molecular docking results based on reported anti-inflammatory peptides, a total of 251 peptides were found to bind to iNOS. Among them, the samples fermented by *L. plantarum* A3 had the most peptides that could bind to iNOS, followed by the samples fermented by *L. rhamnosus* ATCC7469. As a result, 13 unique peptides in NC products were also found. Besides, 85 and 56 unique peptides were found in the hydrolysates of *L. plantarum* A3 and *L. rhamnosus* ATCC7469, respectively. These peptides are predicted to be non-toxic, providing the possibility for safe use. Wen et al. (48) predicted four anti-inflammatory peptides using the computer prediction method of Net MHC II pan 4.0. However, almost all anti-inflammatory peptides screened by this method are peptides longer than 10, which may be because MCII has an open binding cleft and interacts mainly with long peptides of 13–25 lengths, which may be a defect of the model (49). The use of machine learning and docking of iNOS receptors in this work avoids the disadvantage of not being able to screen short peptides, which indicates that selecting appropriate targets will help screen more anti-inflammatory peptides. Finally, following the docking results of peptides, anti-inflammatory peptides were further screened and combined with the synthesis cost of peptides. The peptides with the lowest docking energy were synthesized under the same chain length. Table 2 shows the 17 peptides obtained from broccoli, which are mostly derived from water-soluble proteins such as F-box domain-containing protein, rubisco (Supplementary Table S4). The results of the remaining molecularly docked peptides are in Supplementary material C. To further research the anti-inflammatory action of broccoli-derived peptides, these 17 peptides were verified by cell experiments.

3.5. Effect of synthetic broccoli peptides on the production of NO, TNF-α, and IL-6

The anti-inflammatory action of synthetic broccoli peptides was further verified by using an inflammatory cell model. Based on the cell viability test (Figure 5A), low concentrations (25, 50, and 100 μM) were selected as the test concentrations (cell viability >90%). It is well known that the release of NO is related to the expression of iNOS. When iNOS is inhibited, NO production is reduced, thereby reducing inflammation (4) Therefore, the Griess test was adopted to verify the inhibition of peptides screened by molecular docking on iNOS. The results showed that 17 peptides could inhibit the secretion of NO by macrophages after LPS stimulation. Among them, SIWYGPDRP had the strongest ability to inhibit the release of NO from inflammatory cells at a concentration of 25 μM, with an inhibition rate of 52.32 ± 1.48%. DGRYW reduced NO content in inflammatory cells in a dose-dependent manner. At the concentration of 100 μM, the inhibition rate of NO release was 53.94 ± 2.49% (Figure 5B). This indicates that the peptides may inhibit the production of NO by inhibiting the expression of iNOS to achieve the purpose of treating inflammation. This is identical to the anti-inflammatory effect of hazelnut peptides reported by Ren et al. (43).

When the inflammation generates, iNOS inhibitors can attenuate the inflammatory reaction by restraining iNOS activity. In addition, it can also regulate the inflammatory pathway affecting the release of cytokines to inhibit the inflammatory reaction (50). TNF-α and IL-6 are representative inflammatory cytokines. The ability of 17 peptides to inhibit the secretion of inflammatory factors TNF-α and IL-6 was further explored and shown in Figures 5C, D. It is found that the ability of cells to secrete inflammatory cytokines (TNF-α and IL-6) was significantly enhanced after LPS induction. The production rates of TNF-α and IL-6 were significantly decreased after synthetic peptide treatment. GDRW and ADLAHLPF significantly inhibited the production of TNF-α and IL-6 and relieved the inflammatory response. ADLAHLPF, FGDFNPGGRL, and CKVWPPLH dose-dependently decreased TNF-α. At a concentration of 100 μM, their inhibition rates on TNF-α were 73.19 ± 5.31%, 68.44 ± 5.63%, and 73.83 ± 0.81%, respectively.

In addition, we found that the ability of some peptides to inhibit the release of TNF-α or IL-6 gradually decreased with the increase in concentration, and even there was almost no inhibition rate at high doses. Some peptides showed a U-shaped dose relationship only at medium concentrations. The peptide KASFAFAGL had the strongest inhibitory effect on TNF-α and IL-6 at a low dose, with inhibition rates of 43.59 ± 0.27% and 29.84 ± 0.63%, respectively. However, when its concentration exceeded 25 μM, it did not show inhibitory activity on TNF-α and IL-6 secretion. FGDFNPGGRL only inhibited IL-6 at a concentration of 50 μM. RFR showed the strongest ability to inhibit TNF-α at a concentration of 25 μM, with an inhibition rate of 74.61 ± 1.68%, but this ability gradually weakened as the concentration increased. These phenomena were possibly concerned with cell toleration. Peptides showed an inhibitory effect at a certain dose, but beyond this range, the inhibitory effect weakened or even disappeared. Complex mechanisms of conceivability changes, receptor internalization, and occupancy saturation result in different doses of peptide binding to the target, thereby affecting anti-inflammatory activity. Studies have shown that the peptide

TABLE 2 The energy of molecular docking of anti-inflammatory peptides with iNOS.

Samples	Peptide	Abbreviation	Length	-CDOCKER energy (kcal/mol)	-CDOCKER interaction energy (kcal/mol)
NC & *L. plantarum* A3	GDRW	GW-4	4	92.9559	78.0537
	DGRYW	DW-5	5	110.217	72.6409
	AAMVWPPLGK	AK-10	10	133.552	123.125
L. plantarum A3	QGAGYRW	QW-7	7	121.395	93.4092
	KASFAFAGL	KL-9	9	116.507	97.8707
	FNFH	FH-4	4	95.6975	73.2568
	MHHYW	MW-5	5	106.761	88.6178
	SIWYGPDRP	SP-9	9	81.799	103.996
	HFKQPW	HF-6	6	114.205	103.551
	FGDFNPGGRL	FL-10	10	129.955	99.2752
L. rhamnousus ATCC7469	DPWHNF	DF-6	6	110.896	89.0591
	WKRW	WW-4	4	90.0464	82.2929
NC, *L. plantarum* A3 & *L.rhamnousus* ATCC7469	KWR	KR-3	3	75.5454	66.923
L. plantarum A3 & *L. rhamnousus* ATCC7469	RFR	RR-3	3	71.6026	66.1001
	ADLAHLPF	AF-8	8	124.091	96.4943

The abbreviation is composed of the first amino acid + terminal amino acid + peptide chain length.

KIWHHFF identified from sturgeon protein inhibited LPS-induced IL-6 secretion only at the lowest concentration but did not exhibit TNF-α inhibitory activity (44). Zhao et al. (51) also proved that the peptides identified from antler proteins showed anti-inflammatory activity in a U-shaped dose effect.

Amino acid sequence and position are closely related to peptide function. Previous studies have shown that anti-inflammatory peptides were rich in hydrophobic amino acid residues and positively charged amino acid residues, especially N-terminal or C-terminal (40). Highly hydrophobic peptides can promote the interaction between peptides and cell membranes, thereby regulating downstream pathways and exhibiting anti-inflammatory effects. In addition, one or multiple glutamines, glutamic acid, tyrosine, tryptophan, cysteine, and asparagine acid residues may contribute to the immunoregulatory activity of food protein-derived peptides (52). In addition, peptides containing positively charged amino acid residues (lysine, arginine, and histidine) exert anti-inflammatory effects by binding to LPS released by bacteria. In this study, anti-inflammatory peptides were found to contain one or more hydrophobic amino acids. Such as GDRW, KASFAFAGL, FGDFNPGGRL, and ADLAHLPF were rich in hydrophobic amino acids and aspartic acid, and tryptophan. HFKQPW, RFR, and KWR all had positively charged amino acid residues. To sum up, the constitution and specific location of amino acids might contribute to the anti-inflammatory activity of 17 novel peptides.

3.6. Molecular mechanism based on iNOS of anti-inflammatory peptides

Comprehension of the important active sites of anti-inflammatory peptides was of great significance for understanding the recognition mode of ligands and receptors. Figure 6 reveals the interaction between anti-inflammatory active peptides and iNOS receptor binding sites. There were 43 active sites for non-bonded interaction between 17 anti-inflammatory peptides and iNOS receptors. Among them, Glu371, Asp376, Trp366, Gln257, Arg375, Arg260, and Arg382 are the most active sites for non-bond binding with anti-inflammatory peptides.

The peptide-iNOS interaction in the spatial pattern of binding force has a great impact on anti-inflammatory activity, including hydrogen bonds (salt bridge, conventional hydrogen bond, carbon-hydrogen bond, and pi-donor hydrogen bond)

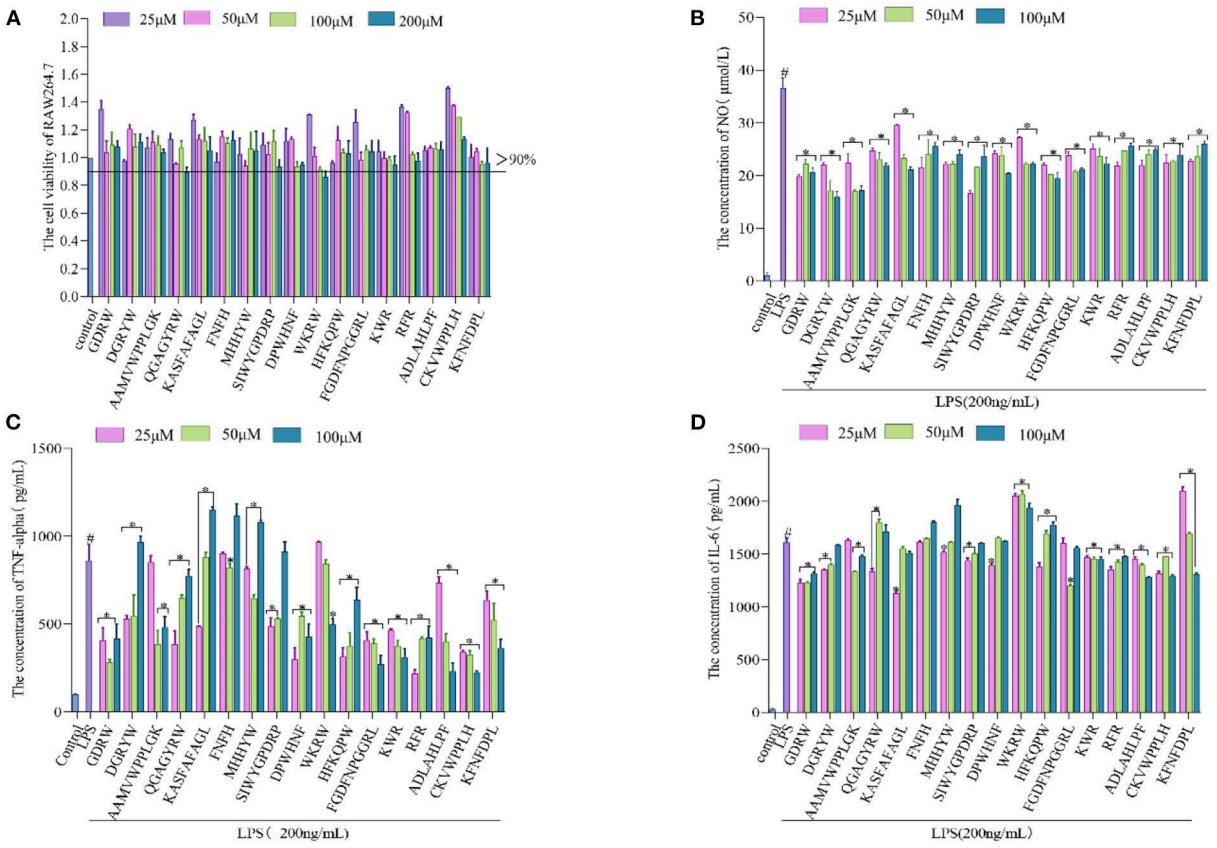

FIGURE 5
Validation of anti-inflammatory activity of the broccoli-derived synthetic peptide. **(A)** Effect of synthetic peptide on RAW264.7 cell viability. **(B)** Effect of synthetic peptide on NO release from inflammatory cells. **(C)** Effect of synthetic peptide on TNF-α release from inflammatory cells. **(D)** Effect of synthetic peptide on IL-6 release from inflammatory cells. #, LPS is significantly different from control; *, The difference between the experimental group and the LPS group was significant ($P < 0.05$).

electrostatic interactions (attractive charge, pi-anion, and pi-cation), hydrophobic interactions (pi-pi T-shaped, pi-sigma, alkyl, and pi-alkyl), and other interactions (37). Figures 7A–D depicts 3D and 2D images of the binding of the anti-inflammatory peptide to the iNOS receptor, showing the most appropriate docking posture. The binding sites of the remaining anti-inflammatory peptides are shown in Supplementary Figure S4. The active sites and forces of 17 anti-inflammatory peptides were analyzed, and it was found that these peptides mainly bind to the iNOS receptor residues through hydrogen bonds and hydrophobic interaction, which was identical to the previous research by Peng et al. (4). The residues in iNOS for the formation of the salt bridge were concentrated on Glu371, Asp376, Arg382, Arg375, and Glu279, while the residues Gln257, Glu371, Trp366, Asp376, Tyr341, Tyr367, Arg260 contributed to the formation of traditional hydrogen bonds. The residues Glu371, Gln257, and Pro344 contributed to the formation of carbon-hydrogen bonds (Supplementary Figure S4 and Figure 7). As described by Cinelli, Do, Miley, and Silverman (53), iNOS has two main domains, C-terminal reductase containing a flavin mononucleotide (FMN) binding subdomain and an N-terminal oxygenase. In the H4B binding pocket of the oxygenase domain, residues Arg375, Trp455, Trp457, and Phe470 are essential for H4B cofactor binding, subsequent dimerization, and enzyme function. When residues Phe831 and Leu832 were metabolized by polar residues (serine and proline), iNOS activity decreased significantly. Anti-inflammatory peptides may bind to amino acid residues (Arg357, Trp457, and Cys194) in the iNOS activity pocket and interact with iNOS and limit iNOS activity (Figure 6).

Peptide AAMVWPPLGK (AK-10) has the lowest docking energy (−133.552 kcal/mol) with iNOS (Table 1). It could be found that Met368, Thr370, Ile195, Glu371, and Arg260 from hydrogen bonds with −C=O, Lys82, Lys82, and Glu279 form hydrogen bonds with −C=O and $-NH^{3+}$ group, respectively, Arg376, Val346, and Met348 formed pi-alkyl bonds (Figure 7A). The peptide SIWYGPDRP with the

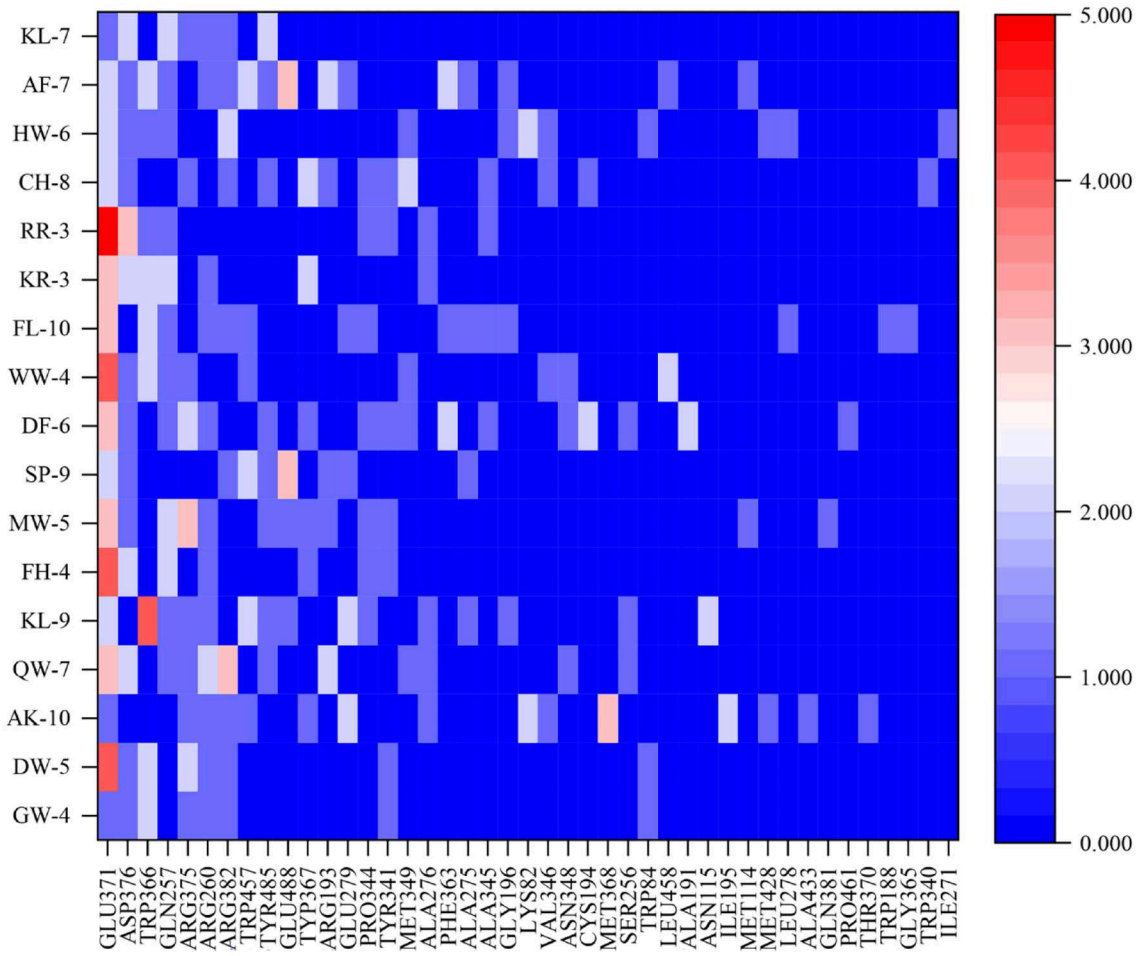

FIGURE 6
The docking sites and interaction forces of 17 anti-inflammatory peptides with iNOS (The abscissa represents the docking site between the peptide and the receptor, and the ordinate value represents the number of forces between the peptide and the receptor).

strongest inhibitory activity on NO release at low concentration has lower docking energy (−88 kcal/mol) with the iNOS receptor (Table 1). As shown in Figure 7B, the interaction between ligand and receptor was mainly hydrogen bond and Alkyl. The N-terminal of SIWYGPDRP interacted with amino acid residues Trp457 and Arg193 through hydrogen bonds and Pi-Pi T-Shaped. In addition, hydrogen bonds were formed with Gly196, Gln257, Trp366, Arg382, and Glu371. In addition to hydrogen bonds, SP-9 also binds to the iNOS receptor cavity through salt bridges, electrostatic interactions, Alkyl, and carbon-hydrogen bonds, thereby inhibiting iNOS enzyme activity. Other anti-inflammatory peptides such as ADLAHLPF and GDRW also demonstrated that they can bind to iNOS receptor, as shown in Figures 7C, D. Hydrogen bond interactions are mainly formed between the oxygen atoms of these anti-inflammatory peptides and the hydrogen atoms of iNOS amino acid residues. Or the hydrogen atom between the amino acid residue and the amino group of the anti-inflammatory peptide forms a hydrogen bond interaction.

4. Conclusion

By peptidomic and virtual screening technology, 17 novel anti-inflammatory peptides were identified from *L. plantarum* A3 and *L. rhamnosus* ATCC7469. These anti-inflammatory peptides were mainly derived from water-soluble proteins dominated by F-box domain-containing proteins. These peptides exert anti-inflammatory activity by inhibiting the secretion of inflammatory factors by inflammatory cells. Combined with the molecular docking results, 17 peptides could produce hydrogen bonds and hydrophobic interactions with multiple receptor residues in the iNOS

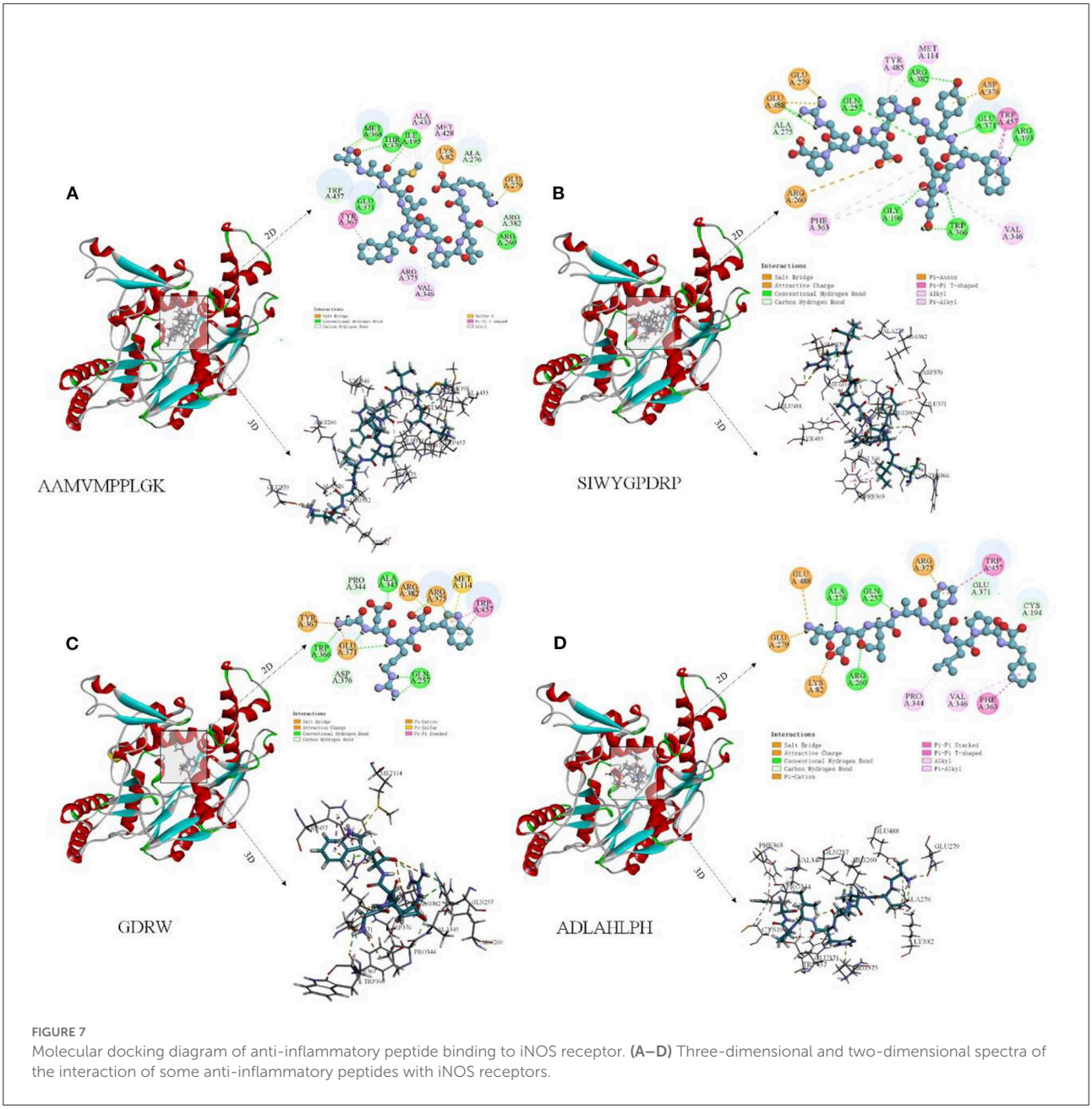

FIGURE 7
Molecular docking diagram of anti-inflammatory peptide binding to iNOS receptor. **(A–D)** Three-dimensional and two-dimensional spectra of the interaction of some anti-inflammatory peptides with iNOS receptors.

binding pocket. Additionally, molecular docking results showed that Glu371, Asp376, Trp366, Gln257, and Arg375 may play an important role in anti-inflammatory activity by molecular docking with iNOS. This study could provide a reference for the research and utilization of food anti-inflammatory peptides. It is estimated that only 10% of drugs have enough data to prove the safety and effectiveness of their use in pregnant women. This study may provide new ideas for anti-infection during pregnancy in terms of safety and effectiveness.

Data availability statement

The original contributions presented in the study are included in the article/Supplementary material, further inquiries can be directed to the corresponding authors.

Author contributions

YL: conceptualization, formal analysis, investigation, methodology, writing–original draft, and visualization.

XG: investigation, software, and supervision. DP: project administration and supervision. ZL: visualization, software, and supervision. CX: data curation, funding acquisition, and project administration. YX: methodology, software, data curation, and investigation. LD: supervision. ZC and WL: methodology, investigation, and validation. YD: methodology, supervision, project administration, funding acquisition, and writing–review and editing. XZ: visualization. All authors contributed to the article and approved the submitted version.

Funding

This work was supported by One Health Interdisciplinary Research Project, Ningbo University (HZ202202), the Science Technology Department of Zhejiang Province (2022C02028 and 2020C02035), Zhejiang Provincial Administration for Market Regulation (CY202234), and the National Natural Science Foundation of China (91856126).

Conflict of interest

The authors declare that the research was conducted in the absence of any commercial or financial relationships that could be construed as a potential conflict of interest.

Publisher's note

All claims expressed in this article are solely those of the authors and do not necessarily represent those of their affiliated organizations, or those of the publisher, the editors and the reviewers. Any product that may be evaluated in this article, or claim that may be made by its manufacturer, is not guaranteed or endorsed by the publisher.

Supplementary material

The Supplementary Material for this article can be found online at: https://www.frontiersin.org/articles/10.3389/fnut.2022.1118900/full#supplementary-material

References

1. Majumder K, Mine Y, Wu J. The potential of food protein-derived anti-inflammatory peptides against various chronic inflammatory diseases. *J Sci Food Agric.* (2016) 96:2303–11. doi: 10.1002/jsfa.7600

2. Franceschi C, Campisi J. Chronic inflammation (inflammaging) and its potential contribution to age-associated diseases. *J Gerontol A Biol Sci Med Sci.* (2014) 69:S4–9. doi: 10.1093/gerona/glu057

3. Huang P, Hong JX, Mi J, Sun BL, Zhang JJ, Li C, et al. Polyphenols extracted from enteromorpha clathrata alleviates inflammation in lipopolysaccharide-induced raw 264.7 cells by inhibiting the Mapks/Nf-κB signaling pathways. *J Ethnopharmacol.* (2022) 286:114897. doi: 10.1016/j.jep.2021.114897

4. Peng Y, Bu L, Zhang X, Ji Z, Xie H, Liang G. Identification and molecular mechanism of a tri-peptide inhibitor targeting inos from duck embryo protein hydrolysates by experimental and bioinformatics studies. *Bioorg Chem.* (2022) 122:105736. doi: 10.1016/j.bioorg.2022.105736

5. Minhas R, Bansal Y, Bansal G. Inducible nitric oxide synthase inhibitors: A comprehensive update. *Med Res Rev.* (2020) 40:823–55. doi: 10.1002/med.21636

6. Yuan D, Li C, Huang Q, Fu X, Dong H. Current advances in the anti-inflammatory effects and mechanisms of natural polysaccharides. *Crit Rev Food Sci Nutr.* (2022) 20:535. doi: 10.1080/10408398.2022.2025535

7. Murray CJL, Ikuta KS, Sharara F, Swetschinski L, Robles Aguilar G, Gray A, et al. Global burden of bacterial antimicrobial resistance in 2019: A systematic analysis. *Lancet.* (2022) 399:629–55.

8. Chilakamarry CR, Sakinah AMM, Zularisam AW, Sirohi R, Khilji IA, Ahmad N, et al. Advances in solid-state fermentation for bioconversion of agricultural wastes to value-added products: opportunities and challenges. *Bioresour Technol.* (2022) 343:126065. doi: 10.1016/j.biortech.2021.126065

9. Tamang JP, Watanabe K, Holzapfel WH. Review: diversity of microorganisms in global fermented foods and beverages. *Front Microbiol.* (2016) 7:377. doi: 10.3389/fmicb.2016.00377

10. Cui L, Yang G, Lu S, Zeng X, He J, Guo Y, et al. Antioxidant peptides derived from hydrolyzed milk proteins by lactobacillus strains: a biopep-uwm database-based analysis. *Food Res Int.* (2022) 156:111339. doi: 10.1016/j.foodres.2022.111339

11. Ashokbhai JK, Basaiawmoit B, Das S, Sakure A, Maurya R, Bishnoi M, et al. Antioxidative, antimicrobial and anti-inflammatory activities and release of ultra-filtered antioxidative and antimicrobial peptides during fermentation of sheep milk: in-vitro, in-silico and molecular interaction studies. *Food Bio.* (2022) 47:101666. doi: 10.1016/j.fbio.2022.101666

12. Qiao YL, Zhang KN, Zhang ZC, Zhang C, Sun Y, Feng Z. Fermented soybean foods: a review of their functional components, mechanism of action and factors influencing their health benefits. *Food Res Int.* (2022) 158:111575. doi: 10.1016/j.foodres.2022.111575

13. Hao LL, Wang XC, Cao YR, Xu J, Xue CH, A. Comprehensive review of oyster peptides: preparation, characterisation and bioactivities. *Rev Aquac.* (2022) 14:120–38. doi: 10.1111/raq.12588

14. Armah CN, Derdemezis C, Traka MH, Dainty JR, Doleman JF, Saha S, et al. Diet rich in high glucoraphanin broccoli reduces plasma ldl cholesterol: evidence from randomised controlled trials. *Mol Nutr Food Res.* (2015) 59:918–26. doi: 10.1002/mnfr.201400863

15. Filannino P, Bai Y, Di Cagno R, Gobbetti M, Ganzle MG. Metabolism of phenolic compounds by *Lactobacillus spp.* during fermentation of cherry juice and broccoli puree. *Food Microbiol.* (2015) 46:272–9. doi: 10.1016/j.fm.2014.08.018

16. Ye J-H, Huang L-Y, Terefe NS, Augustin MA. Fermentation-based biotransformation of glucosinolates, phenolics and sugars in retorted broccoli puree by lactic acid bacteria. *Food Chem.* (2019) 286:616–23. doi: 10.1016/j.foodchem.2019.02.030

17. Das D, Sarkar S, Borsingh Wann S, Kalita J, Manna P. Current perspectives on the anti-inflammatory potential of fermented soy foods. *Food Res Int.* (2022) 152:110922. doi: 10.1016/j.foodres.2021.110922

18. Ulug SK, Jahandideh F, Wu J. Novel technologies for the production of bioactive peptides. *Trends Food Sci Technol.* (2021) 108:27–39. doi: 10.1016/j.tifs.2020.12.002

19. Xu X, Bi S, Lao F, Chen F, Liao X, Wu J. Induced changes in bioactive compounds of broccoli juices after fermented by animal- and plant-derived pediococcus pentosaceus. *Food Chem.* (2021) 357:129767. doi: 10.1016/j.foodchem.2021.129767

20. Zhou T, Liu Z, Pei J, Pan D, Gao X, Dang Y, et al. Novel broccoli-derived peptides hydrolyzed by trypsin with dual-angiotensin i-converting enzymes and dipeptidyl peptidase-iv-inhibitory activities. *J Agric Food Chem.* (2021) 69:10885–92. doi: 10.1021/acs.jafc.1c02985

21. Chen H, Cheng S, Fan F, Tu M, Xu Z, Du M. Identification and molecular mechanism of antithrombotic peptides from oyster proteins released in simulated gastro-intestinal digestion. *Food Funct.* (2019) 10:5426–35. doi: 10.1039/C9FO01433K

22. Zhang T, Hua Y, Zhou C, Xiong Y, Pan D, Liu Z, et al. Umami peptides screened based on peptidomics and virtual screening from ruditapes philippinarum and mactra veneriformis clams. *Food Chem.* (2022) 394:133504. doi: 10.1016/j.foodchem.2022.133504

23. Manguy J, Jehl P, Dillon ET, Davey NE, Shields DC, Holton TA. Peptigram: A web-based application for peptidomics data visualization. *J Proteome Res.* (2017) 16:712–9. doi: 10.1021/acs.jproteome.6b00751

24. Manavalan B, Shin TH, Kim MO, Lee G. Aippred: sequence-based prediction of anti-inflammatory peptides using random forest. *Front Pharmacol.* (2018) 9:276. doi: 10.3389/fphar.2018.00276

25. Gupta S, Sharma AK, Shastri V, Madhu MK, Sharma VK. Prediction of anti-inflammatory proteins/peptides: an insilico approach. *J Transl Med.* (2017) 15:7. doi: 10.1186/s12967-016-1103-6

26. Kumar R, Chaudhary K, Singh Chauhan J, Nagpal G, Kumar R, Sharma M, et al. An in silico platform for predicting, screening and designing of antihypertensive peptides. *Sci Rep.* (2015) 5:12512. doi: 10.1038/srep12512

27. Manavalan B, Basith S, Shin TH, Wei L, Lee G. Mahtpred: a sequence-based meta-predictor for improving the prediction of anti-hypertensive peptides using effective feature representation. *Bioinformatics (Oxford, England).* (2019) 35:2757–65. doi: 10.1093/bioinformatics/bty1047

28. Nagpal G, Chaudhary K, Agrawal P, Raghava GPS. Computer-aided prediction of antigen presenting cell modulators for designing peptide-based vaccine adjuvants. *J Transl Med.* (2018) 16:181. doi: 10.1186/s12967-018-1560-1

29. Agrawal P, Bhagat D, Mahalwal M, Sharma N, Raghava GPS. Anticp 2.0: An updated model for predicting anticancer peptides. *Brief Bioinform.* (2021) 22:bbaa153. doi: 10.1093/bib/bbaa153

30. Aguilar-Toalá JE, Santiago-López L, Peres CM, Peres C, Garcia HS, Vallejo-Cordoba B, et al. Assessment of multifunctional activity of bioactive peptides derived from fermented milk by specific lactobacillus plantarum strains. *J Dairy Sci.* (2017) 100:65–75. doi: 10.3168/jds.2016-11846

31. Wang P, Liu F, Yang X, Liang Y, Li S, Su G, et al. Clerodane diterpenoids from scutellaria formosana with inhibitory effects on no production and interactions with inos protein. *Phytochemistry.* (2017) 144:141–50. doi: 10.1016/j.phytochem.2017.09.005

32. Agyei D, Tsopmo A, Udenigwe CC. Bioinformatics and peptidomics approaches to the discovery and analysis of food-derived bioactive peptides. *Anal Bioanal Chem.* (2018) 410:3463–72. doi: 10.1007/s00216-018-0974-1

33. Guan H, Diao X, Jiang F, Han J, Kong B. The enzymatic hydrolysis of soy protein isolate by corolase pp under high hydrostatic pressure and its effect on bioactivity and characteristics of hydrolysates. *Food Chem.* (2018) 245:89–96. doi: 10.1016/j.foodchem.2017.08.081

34. Kumari R, Sanjukta S, Sahoo D, Rai A. Functional peptides in asian protein rich fermented foods: production and health benefits. *Syst Microbiol Biomanuf.* (2021) 2:1–13. doi: 10.1007/s43393-021-00040-0

35. Chourasia R, Padhi S, Chiring Phukon L, Abedin MM, Singh SP, Rai AK, et al. Potential peptide from soy cheese produced using lactobacillus delbrueckii ws4 for effective inhibition of Sars-CoV-2 main protease and S1 glycoprotein. *Front Mol Biosci.* (2020) 7:601753. doi: 10.3389/fmolb.2020.601753

36. Zhang H, Chen Y, Guo Y, Xu W, Wang W, Wu S, et al. Label-free quantification proteomics reveals the active peptides from protein degradation during anaerobic fermentation of tea. *LWT.* (2021) 150:111950. doi: 10.1016/j.lwt.2021.111950

37. Padhi S, Chourasia R, Kumari M, Singh SP, Rai AK. Production and characterization of bioactive peptides from rice beans using bacillus subtilis. *Bioresour Technol.* (2022) 351:126932. doi: 10.1016/j.biortech.2022.126932

38. Toldrá F, Gallego M, Reig M, Aristoy MC, Mora L. Recent progress in enzymatic release of peptides in foods of animal origin and assessment of bioactivity. *J Agric Food Chem.* (2020) 68:12842–55. doi: 10.1021/acs.jafc.9b08297

39. Wei G, Regenstein JM, Zhou P. The fermentation-time dependent proteolysis profile and peptidomic analysis of fermented soybean curd. *J Food Sci.* (2021) 86:3422–33. doi: 10.1111/1750-3841.15823

40. Vogel HJ, Schibli DJ, Jing W, Lohmeier-Vogel EM, Epand RF, Epand RM. Towards a structure-function analysis of bovine lactoferricin and related tryptophan- and arginine-containing peptides. *Biochem Cell Biol.* (2002) 80:49–63. doi: 10.1139/o01-213

41. Udenigwe CC, Okolie CL, Qian H, Ohanenye IC, Agyei D, Aluko RE. Ribulose-1,5-bisphosphate carboxylase as a sustainable and promising plant source of bioactive peptides for food applications. *Trends Food Sci Technol.* (2017) 69:74–82. doi: 10.1016/j.tifs.2017.09.001

42. Sudhamalla B, Kumar M, Kumar RS, Sashi P, Yasin UM, Ramakrishna D, et al. Enzyme dimension of the ribosomal protein s4 across plant and animal kingdoms. *Biochim Biophys Acta Gen Subj.* (2013) 1830:5335–41. doi: 10.1016/j.bbagen.2013.06.010

43. Ren D, Wang P, Liu C, Wang J, Liu X, Liu J, et al. Hazelnut protein-derived peptide ldapghr shows anti-inflammatory activity on lps-induced raw2647 macrophage. *J Funct Foods.* (2018) 46:449–55. doi: 10.1016/j.jff.2018.04.024

44. Gao R, Shu W, Shen Y, Sun Q, Bai F, Wang J, et al. Sturgeon protein-derived peptides exert anti-inflammatory effects in lps-stimulated raw2647 macrophages via the mapk pathway. *J Funct Foods.* (2020) 72:104044. doi: 10.1016/j.jff.2020.104044

45. Chung J-H, Kong J-N, Choi H-E, Kong K-H. Antioxidant, anti-inflammatory, and anti-allergic activities of the sweet-tasting protein brazzein. *Food Chem.* (2018) 267:163–9. doi: 10.1016/j.foodchem.2017.06.084

46. Sun X, Zhang Y, Li F, Jiao X, Ma D, Zhang L, et al. Effects of lactic acid bacteria fermentation on chemical compounds, antioxidant capacities and hypoglycemic properties of pumpkin juice. *Food Bio.* (2022) 50:102126. doi: 10.1016/j.fbio.2022.102126

47. Zhu W, Luan H, Bu Y, Li X, Li J, Zhang Y. Identification, taste characterization and molecular docking study of novel umami peptides from the Chinese anchovy sauce. *J Sci Food Agric.* (2021) 101:3140–55. doi: 10.1002/jsfa.10943

48. Wen L, Huang L, Li Y, Feng Y, Zhang Z, Xu Z, et al. New peptides with immunomodulatory activity identified from rice proteins through peptidomic and in silico analysis. *Food Chem.* (2021) 364:130357. doi: 10.1016/j.foodchem.2021.130357

49. Qu T, He S, Ni C, Wu Y, Xu Z, Chen M-L, et al. In Vitro Anti-Inflammatory Activity of Three Peptides Derived from the Byproduct of Rice Processing. *Plant Foods Hum Nutr.* (2022) 77:172–80. doi: 10.1007/s11130-022-00963-6

50. Yuan L, Chu Q, Wu X, Yang B, Zhang W, Jin W, et al. Anti-inflammatory and antioxidant activity of peptides from ethanol-soluble hydrolysates of sturgeon (Acipenser Schrenckii) Cartilage. *Front Nutr.* (2021) 8:689648. doi: 10.3389/fnut.2021.689648

51. Zhao L, Wang X, Zhang XL, Xie QF. Purification and identification of anti-inflammatory peptides derived from simulated gastrointestinal digests of velvet antler protein (Cervus Elaphus Linnaeus). *J Food Drug Anal.* (2016) 24:376–84. doi: 10.1016/j.jfda.2015.10.003

52. Guha S, Majumder K. Structural-features of food-derived bioactive peptides with anti-inflammatory activity: a brief review. *J Food Biochem.* (2019) 43:e12531. doi: 10.1111/jfbc.12531

53. Cinelli MA, Do HT, Miley GP, Silverman RB. Inducible nitric oxide synthase: regulation, structure, and inhibition. *Med Res Rev.* (2020) 40:158–89. doi: 10.1002/med.21599

frontiers | Frontiers in Nutrition

TYPE Original Research
PUBLISHED 18 January 2023
DOI 10.3389/fnut.2022.1098954

Check for updates

OPEN ACCESS

EDITED BY
Bin Liang,
Ludong University, China

REVIEWED BY
Bin Li,
Shenyang Agricultural University, China
Lingguang Yang,
Yichun University, China
Caixia Zhang,
Institute of Pomology (CAAS), China

*CORRESPONDENCE
Xiaohong Sun
✉ mingsun9887@163.com
Yugang Zhang
✉ ygzhang@qau.edu.cn

†These authors have contributed equally to this work

SPECIALTY SECTION
This article was submitted to Nutrition and Food Science Technology, a section of the journal Frontiers in Nutrition

RECEIVED 15 November 2022
ACCEPTED 12 December 2022
PUBLISHED 18 January 2023

CITATION
Chen Y, Wang Y, Jiang S, Xu J, Wang B, Sun X and Zhang Y (2023) Red-fleshed apple flavonoid extract alleviates CCl_4-induced liver injury in mice.
Front. Nutr. 9:1098954.
doi: 10.3389/fnut.2022.1098954

COPYRIGHT
© 2023 Chen, Wang, Jiang, Xu, Wang, Sun and Zhang. This is an open-access article distributed under the terms of the Creative Commons Attribution License (CC BY). The use, distribution or reproduction in other forums is permitted, provided the original author(s) and the copyright owner(s) are credited and that the original publication in this journal is cited, in accordance with accepted academic practice. No use, distribution or reproduction is permitted which does not comply with these terms.

Red-fleshed apple flavonoid extract alleviates CCl_4-induced liver injury in mice

Yizhou Chen[1,2†], Yanbo Wang[1†], Shenghui Jiang[1], Jihua Xu[3], Bin Wang[1], Xiaohong Sun[3*] and Yugang Zhang[1,2*]

[1]College of Horticulture, Qingdao Agricultural University, Qingdao, China, [2]Engineering Laboratory of Genetic Improvement of Horticultural Crops of Shandong Province, Qingdao Agricultural University, Qingdao, China, [3]College of Life Sciences, Qingdao Agricultural University, Qingdao, China

In recent years, the global incidence of liver damage has increased. Despite the many known health benefits of red-fleshed apple flavonoids, their potential liver-protective effects have not yet been investigated. In this study, we analyzed the composition of red-fleshed apple flavonoid extract (RAFE) by high-performance liquid chromatography (HPLC). We then induced liver damage in mice with carbon tetrachloride (CCl_4) and performed interventions with RAFE to analyze its effect on liver damage, using bifendate as a positive control. The results showed that catechin was the most abundant flavonoid in 'XJ4' RAFE (49.346 mg/100 g). In liver-injured mice, the liver coefficients converged to normal levels following RAFE intervention. Moreover, RAFE significantly reduced the enzymatic activity levels of glutamic oxaloacetic transaminase (ALT), glutamic alanine transaminase (AST), and alkaline phosphatase (ALP) in mouse serum. Furthermore, RAFE significantly increased the content or enzyme activity level of total glutathione, total antioxidant capacity, and superoxide dismutase, and significantly decreased the content of malondialdehyde in the liver of mice. In parallel, we performed histopathological observations of mouse livers for each group. The results showed that RAFE restored the pathological changes caused by CCl_4 around the central hepatic vein in mice and resulted in tightly bound hepatocytes. The recovery effect of RAFE was dose-dependent in the liver tissue. Regarding intestinal microorganisms, we found that RAFE restored the microbial diversity in liver-injured mice, with a similar microbial composition in the RAFE intervention group and normal group. RAFE reduced the ratio of *Firmicutes* to *Bacteroidetes*, increased the levels of probiotic bacteria, such as *Lactobacillus acidophilus*, and *Clostridium*, and reduced the levels of harmful bacteria, such as *Erysipelothrix Rosenbach.* Therefore, RAFE ameliorated CCl_4-induced liver damage by modulating the abundance and composition of intestinal microorganisms in mice. In conclusion, RAFE alleviated CCl_4-induced liver damage in mice, with H-RAFE (5 mg kg^{-1}) significantly improving liver damage

in mice but M-RAFE (1 mg kg^{-1}) significantly improving the imbalance of intestinal microorganisms in mice. Our research suggests that RAFE could be employed for the adjuvant treatment and prevention of liver damage, and may have important applications in food and medicine.

KEYWORDS

red-fleshed apple, flavonoid, liver injury, intestinal microorganisms, high-performance liquid chromatography

1. Introduction

The liver is the largest digestive gland in the human body, participating in multiple vital functions, such as digestion, synthesis, storage, detoxification, and immunity (1, 2). However, the frequent abuse of alcohol, drugs, chemical additives, and food safety problems has led to annual increases in the incidence of liver injury. Persistent liver injury induces excessive proliferation and deposition of the extracellular matrix and gradually develops into liver fibrosis and cirrhosis, eventually leading to liver failure and even liver cancer (3). Liver injury is classified as acute or chronic according to the severity of the disease. Acute liver injury is a critical condition in humans, characterized by a rapid onset and significant damage, that can cause a large amount of liver tissue necrosis in a short period of time, as well as severe liver failure (4). Chronic liver injury has a complex pathogenesis and is characterized by abnormal proliferation and differentiation of hepatic stellate cells and cellular changes leading to massive deposition of extracellular matrix such as collagen, which ultimately results in abnormal intrahepatic tissue and fibroplasia (5). The main causes of liver injury are exposure to chemical agents (e.g., amoxicillin, ciprofloxacin, and oral contraceptives) and toxic compounds [e.g., alcohol, aflatoxin, and carbon tetrachloride (CCl_4)]. Exposure of the liver to toxic substances leads to oxidative stress by generating large amounts of reactive oxygen species. Excess reactive oxygen species increase lipid peroxidation and cause oxidative injury to hepatocytes, which ultimately leads to fatty liver degeneration, chronic hepatitis, cirrhosis, and hepatocellular carcinoma (6–8). Currently, common treatments for liver injury include the use of specific detoxifying agents (e.g., N-acetylcysteine for acetaminophen toxicity), immunosuppressive therapy (e.g., corticosteroids for drug-induced hypersensitivity reactions or autoimmune injury), general hepatoprotective agents (e.g., ursodiol, silymarin, and glycopyrrolate) and liver transplantation (9). However, currently available treatments have various limitations (10). For example, specific antidotes can only treat specific cases of liver injury, and are virtually ineffective against general liver injury, immunosuppressive therapy is not always effective, and general hepatoprotective agents have little effect in the treatment of acute liver injury. Moreover, the drawbacks of liver transplantation include the limited availability of donor matches and the need for prolonged immunosuppressive therapy after transplantation (11). Therefore, it is crucial to find an effective treatment for liver injury that has a wide range of applications.

A study on CCl_4-induced liver injury found that treatment with high concentrations of imatinib (a protein kinase inhibitor) effectively increased the non-protein sulfhydryl group content and superoxide dismutase (SOD) activity in the liver, but reduced myeloperoxidase activity in the liver to normal control values (12). However, serum levels of glutamic oxaloacetic transaminase (ALT), glutamic alanine transaminase (AST), and total bilirubin, as well as hepatic NADPH oxidase levels, were elevated after treatment with high concentrations of imatinib. These results indicate that treatment with high concentrations of imatinib did not protect the liver, but instead produced liver injury (12). Karimi et al. studied the protective effects of losartan (a receptor type I angiotensin inhibitor) combined with nilotinib (a multi-targeted tyrosine kinase inhibitor) on CCl_4-induced liver fibrosis in rats, and found that this dual treatment had a synergistic effect. The treatment focused on the cytokines that are most important for improving liver fibrosis [transforming growth factor-β (TGF-β) and platelet-derived growth factor], and successfully reduced the expression of both cytokines. Although this treatment achieved the purpose of repairing liver injury, it also includes the side effects of some multi-targeted TK inhibitors, such as fatigue, rash, gastrointestinal symptoms, edema, neurological symptoms, etc., and is further inhibited by relatively high costs (13). Therefore, existing drugs for the treatment of CCl_4-induced liver injury have certain disadvantages. Considering that natural active ingredients have few side effects, it is important to thoroughly explore the alleviation effect of such products on liver injury.

In recent years, several studies have confirmed the positive effects of plants and their natural products on the prevention and treatment of liver injury (14–16). Phenolic substances in plants are the most abundant and structurally diverse plant active substances, whose main role is alleviating oxidative injury, such as cancer, liver injury, and cardiovascular disease (17, 18). Moreover, polyphenols and flavonoids have the potential to protect against CCl_4-induced liver injury in phenolics (19). Adewale and Abiodun reported that hibiscus polyphenol enrichment (HPE) exhibits protective and antioxidant effects

against CCl_4-induced liver injury (20). Specifically, elevated levels of malondialdehyde (MDA) were found in the livers of CCl_4-treated animals, which represented an increase in hepatic lipid peroxidation and therefore hepatic injury; however, treatment with HPE significantly reduced lipid peroxidation levels, suggesting that its ability to protect against CCl_4-induced liver injury may be attributed to its high antioxidant potential. Green tea polyphenols also inhibit oxidative injury and prevent CCl_4-induced liver injury (21). Furthermore, total flavonoids extracted from *Bidens bipinnata* L. can improve acute liver injury in mice and liver fibrosis in rats by inhibiting oxidative stress. These results may be related to the inhibition of nuclear factor kappa B activation by these total flavonoids in hepatic stellate cells (22, 23). However, relatively few studies have investigated the role of polyphenols in apples on CCl_4-induced liver injury, with red-fleshed apple variants being particularly rich in polyphenols, especially flavonoids.

Red-fleshed apples [*Malus sieversii* Roem. *f. niedzwetzkyana* (Dieck) Langenf.] are a variety of Xinjiang wild apples that are native to the Ili region of Xinjiang, China, and Kazakhstan in Central Asia, which have red or dark-red fruits, flowers, and leaves (24, 25). Red-fleshed apples are rich in a variety of active substances such as polysaccharides, polyphenols, anthocyanins, and flavonoids. Notably, the polyphenol content is almost three times that of white-fleshed apples (26). Flavonoids account for a relatively high proportion of the polyphenols in red-fleshed apples, and play a key role in anti-oxidation and maintaining cellular activity (27). Previous studies have investigated anthocyanins, which are a class of flavonoids, in red-fleshed apples. For example, Xu et al. found that red-fleshed apple anthocyanin extract (RAAE) alleviates busulfan-induced dysfunction of the male reproductive system in mice (28) by enhancing sperm motility, increasing the number of mice, and restoring spermatogenesis in male mice. Wang et al. further analyzed the mechanism by which RAAE alleviates busulfan-induced reproductive system dysfunction in mice (29), and found that the total antioxidant capacity (T-AOC), SOD activity, and glutathione catalase activity were significantly increased in the RAAE treatment group, indicating that RAAE can reduce the oxidative injury of busulfan in mice by reducing the content of reactive oxygen species and restoring the reproductive system function of mice. Previous research has also shown that red-fleshed apple flavonoid extract (RAFE) has antioxidant and cell viability maintenance capabilities; however, little research has explored the effects of red-fleshed apple flavonoids on CCl_4-induced liver injury in mice.

Flavonoids are a class of polyphenolic compounds with a structure of 2-phenylchromone, which has the basic structure of C6-C3-C6. Flavonoids are also important secondary metabolites in plants (30–32) that are widely distributed and present at high levels. In plants, flavonoids are often combined with sugars and exist in the form of aglycones or carbon sugars. Multiple categories of flavonoids exist in plants, primarily chalcones, anthocyanins, flavanones, isoflavonoids, flavonoids, and flavonols (33). Chalcones are unique to apples (34). Years of research have shown that flavonoids have important biological activities that play an important role in plant protection and stress resistance, as well as certain antioxidant and antibacterial properties (30, 35, 36). Flavonoids can reduce the level of oxidative stress and have a certain ability to scavenge free radicals. More importantly, flavonoids can scavenge reactive oxygen species, thereby protecting human health (36, 37). For example, Duangjai extracted flavonoids from Pigeon Pea [*Cajanus cajan* (L.) Millsp.] seeds and explored their antioxidant capacity (38). Their results showed that the flavonoid extract can act as an activator and protect the cell membrane of the cell longevity protein (SIR2/SIRT1) from oxidative stress. Therefore, it is important to explore the further effects of flavonoids on hepatic oxidative stress.

In this study, we establish a CCl_4-induced mouse liver injury model to explore the alleviation effect and mechanism of RAFE on CCl_4-induced liver injury in mice. We had previously compared four varieties of red-fleshed apples and found that variety 'XJ4' had the highest total phenol and anthocyanin contents with a strong ability to scavenge free radicals (27). At the same time, we previously treated mice with busulfan-induced reproductive injury with 'XJ4' anthocyanin extract, and the combined analysis of microbiota and plasma metabolites showed that 'XJ4' anthocyanin extract could reduce busulfan-induced reproductive injury (29). So we selected 'XJ4' as the experimental material, and the control was the white-fleshed apple 'Fuji'. The results of this study are expected to provide a theoretical basis for the selection of red-fleshed apples and their nutritional and healthcare functions.

2. Materials and methods

2.1. Flavonoid preparation and purification

Experimental materials were obtained from 'XJ4' apple fruits grown in the Modern Agricultural Science and Technology Demonstration Park of Qingdao Agricultural University, Jiaozhou, China (36°16′49″N, 120°00′36″E).

The preparation method of the RAFE was a slightly modified version of the method of Xiang (39). The apple fruits were cleaned, and 0.1% phosphoric acid/ethanol was added as the extracting solution in liquid nitrogen grinding, with a material-to-liquid ratio of 1:30 (g ml^{-1}). The mixture was then sonicated (Ultrasonic cleaner, Baoding Shengfeng Instrument Technology Co., LTD., HP) for 30 min and macerated for 12 h with protection from light, then finally filtered to obtain a crude extract solution of flavonoids. Concentration was conducted with a rotary evaporator (Rotary evaporators, Shanghai Yarong Biochemical Instrument Factory, RE-6000A)

at 35°C and low speed to remove the organic solvent from the extract until the crude extract became viscous. Finally, the crude extract was diluted by adding an appropriate amount of deionized water (100 ml).

The flavonoid extract was added to NKA-9 macroporous sorbent resin at pH7 and the flow rate of the upper sample was controlled at 1 ml min^{-1}. After reaching equilibrium of resin adsorption, the impurities were eluted with deionized water, the macroporous resin was eluted with 100% (V/V) ethanol eluate at the same flow rate, and all eluates were collected. The eluate was concentrated and dried using a nitrogen blowing machine and vacuum freeze dryer sequentially, and the volume was fixed at a final concentration of 30 mg ml^{-1}. **Figure 1** shows the process flow for the preparation and purification of RAFE.

2.2. Flavonoid HPLC analysis

Protocatechin, catechin, epicatechin, rhizobioside, quercetin, centaureidin-3-O-galactoside, and centaureidin-3-O-glucoside standards were purchased from Sigma-Aldrich (St. Louis, MO, USA). Chromatography-grade methanol was purchased from Tedia (USA). All flavonoid standard stock solutions (1 mg ml^{-1}) were stored at a low temperature and protected from light, and the standard curve was constructed using the external standard method. High-performance liquid chromatography (HPLC, USA, Agilent, 1260) was performed under the following conditions: the chromatographic column was an XDB-C18 column (150 × 4.6 mm, 5 μm); the mobile phase A was 1% aqueous acetic acid solution and the mobile phase B was methanol solution; the elution program was 0–10 min, 5–30%, 10–25 min, 30–50%, 25–35 min, 50–70%, and 35–40 min, 70–5% (all mobile phase B); the flow rate was 0.8 ml/min; the sample volume was 20 μl; the column temperature was 30°C; and the wavelength was 280 nm. Qualitative and quantitative analyses of flavonoids in 'XJ4' RAFE were performed according to the above methods and conditions.

2.3. Animal study

All animal experimental procedures were conducted according to the protocol of the Animal Care and Use Committee of Qingdao Agricultural University (license number: SYXK [SD] 20170005). Specific Pathogen Free (SPF) grade male ICR mice (3 weeks old, 20.0 ± 2.0 g) were housed in an SPF chamber at 22 ± 2°C with a 12 h light/dark cycle and 50–70% humidity, and all mice were fed and watered *ad libitum*. After 3 days of adaptation to the living environment, the mice were randomly divided into the following six groups (10 mice per group): normal control (NC), pathological control (MC), positive control (PC), low RAFE concentration (L-RAFE), medium RAFE concentration (M-RAFE), and high RAFE concentration (H-RAFE). The prepared RAFE was diluted into different concentrations and fed to mice in the RAFE intervention groups by gavage (0.2 mg kg^{-1}, L-RAFE; 1 mg kg^{-1}, M-RAFE; and 5 mg kg^{-1}, H-RAFE). The NC group was administered saline gavage, the MC group was administered saline and CCl_4 as a model (0.1% CCl_4 olive oil solution 10 ml kg^{-1}, intraperitoneal injection, twice a week, 4 weeks in total), and the PC group was treated with bifenthrin drops in aqueous solution (1 mg kg^{-1}, gavage). CCl_4 was injected intraperitoneally at the same time as the gavage in all groups except the NC group, and the injection volume was the same as that of the MC group. The gavage volume was 0.1 ml $mouse^{-1}$, which was administered for 4 weeks. The establishment of the CCL_4 liver injury model was established with reference to Keshavarz et al. and slightly modified (40, 41).

2.4. Sample collection

After 35 days, the mice were deprived of food for 12 h then euthanized by cervical dislocation under ether anesthesia. After euthanasia, heart blood and liver tissues were taken from the mice, weighed, and stored at −80°C for further analysis.

2.5. Biochemical assays of mice plasma and liver tissue

Superoxide dismutase, T-AOC, and MDA diagnostic kits were purchased from Solebro Biotechnology (Beijing, China). AST, ALT, alkaline phosphatase (ALP), and total glutathione (T-GSH) diagnostic kits were purchased from the Nanjing Jiancheng Institute of Biological Engineering, Nanjing, China. Tests were performed according to the manufacturer's instructions.

2.6. Histopathological observation of mice livers

We processed the mice liver tissue samples fixed in 4% paraformaldehyde. The samples were paraffin-embedded and cut into sections 7–8 μm thick, which were stained with hematoxylin-eosin (H&E) dye, then observed and imaged using an optical microscope (Leica fluorescence microscope, Germany Leica Microsystems, DM2500) with a 40× objective to assess pathological changes in the liver tissue.

2.7. Sequencing of microbiota from small intestine digesta samples

The samples used for 16S rRNA gene sequencing were fecal samples from mice fed for 5 weeks. Genomic DNA

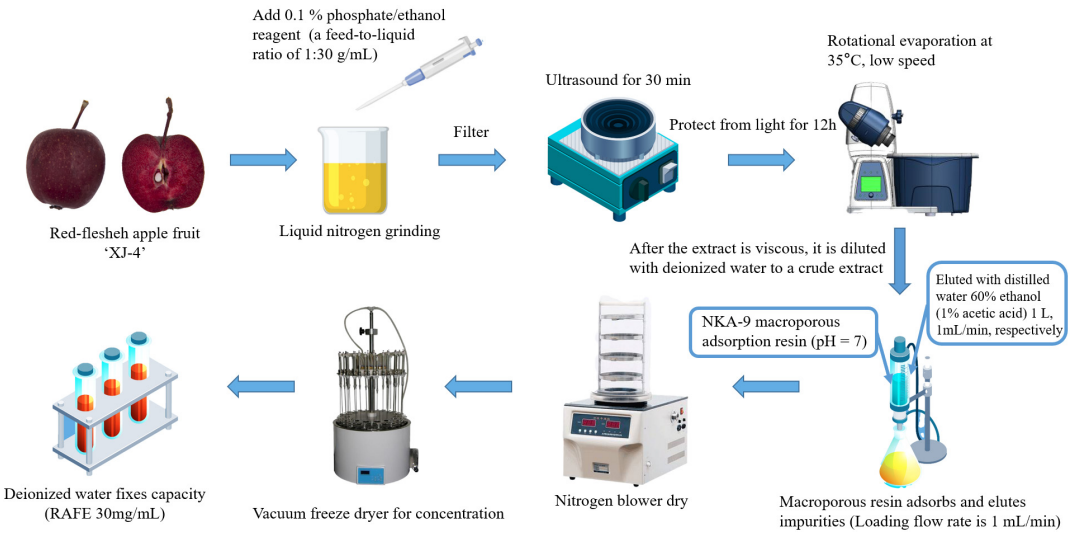

FIGURE 1
Process flow chart of 'XJ4' RAFE preparation and purification.

was extracted using the CTAB method (Nobleryder, China), followed by agarose gel electrophoresis to determine DNA purity and concentration. Finally, the DNA sample was diluted with sterile water to 1 ng μl^{-1}.

The template was diluted genomic DNA, and the variable region V4 of the 16S rRNA gene consisted of forward primers 515 F (5′-GTGCCAGCMGCCGCGGTAA) and 806 R (3′- GGACTACHVGGGTWTCTAAT). PCR uses specific primers with barcodes and a highly efficient High-Fidelity DNA polymerase [Phusion® High-Fidelity DNA polymerase (M0530S, New England Biolabs, USA)] to ensure amplification efficiency and accuracy. The PCR system comprised Phusion Master Mix (2×) 15 μl, PrimerF (1 μM) 1 μl (1 μM), PrimerR (1 μM) 1 μl (1 μM), gDNA (1 ng/μl) 10 μl (5–10 ng), and ddH_2O to make up 30 μl of the system. The PCR reaction program was: 98°C pre-denaturation for 1 min; 30 cycles of 98°C for 10 s, 50°C for 30 s, 72°C for 30 s, and 72°C for 5 min.

PCR products were detected by electrophoresis on 2% agarose gel. The PCR products that passed the test were purified using magnetic beads and quantified using enzyme labeling, then detected by 2% agarose gel electrophoresis after mixing the product in equal amounts according to the concentration of the product. Target bands were recovered using a gel recovery kit (Qiagen). Library construction was performed using a library construction kit (TruSeq DNA PCR-Free Sample Preparation Kit). The constructed libraries were then quantified by Qubit and Q-PCR. If the library qualified, sequencing was performed using NovaSeq6000 (Illumina Novaseq6000, Illumina Corporation, Illumina, San Diego, CA, USA).

2.8. Statistical analysis

Data analysis of the gut microbes was performed using the cloud platform.[1] If there were only two groups of samples, the *t*-test and Wilcoxon test were used; if there were more than two groups of samples, the Tukey test and Kruskal–Wallis test were used. The remaining graphs were produced using GraphPad Prism software (version 8.0.2; GraphPad Software Inc., San Diego, CA, USA). The data were tested for multiple comparisons using Dunnett's method in SPSS (version 24.0; SPSS Inc., Chicago, IL, USA) and ordinary one-way ANOVA. $P < 0.05$ was set as the threshold to indicate a significant difference.

2.9. Data and materials availability

The microbiota raw sequencing data generated in this study have been uploaded to the NCBI SRA database with accession numbers: RJNA901622.[2]

3. Results

3.1. HPLC analysis of RAFE flavonoid composition and contents

To clarify the composition and content of flavonoids in 'XJ4' RAFE, we used HPLC to draw standard curves

1 https://cloud.metware.cn
2 https://www.ncbi.nlm.nih.gov/sra

for eight standards, such as catechins, and delineated the linear range of each standard (Table 1). Flavonoids were identified by comparing the retention times of sample peaks and standard peaks, and the contents of various flavonoids in RAFE were calculated using the standard curves (Figure 2). In the chromatogram of 'XJ4' RAFE (Figure 2), we detected eight flavonoid compounds, including one flavonol, three flavanols, two anthocyanins, and two dihydrochalcone. The data showed that 'XJ4' RAFE had a high content of catechin (49.346 mg·100 g^{-1}), followed by quercetin (23.087 mg·100 g^{-1}), and the least abundant substance was rhizobioside (0.827 mg·100 g^{-1}). Interestingly, the levels of centaureidin-3-O-galactoside and centaureidin-3-O-glucoside reached 13.306 mg·100 g^{-1} and 4.426 mg·100 g^{-1}, respectively (Table 1).

3.2. Effects of RAFE on body weight and liver of mice with CCl_4-induced liver injury

Studies have shown that flavonoids have protective effects against CCl_4-induced liver injury in mice. An elevated liver index is an important indicator of liver injury. During rearing, body weight, fluid consumption, and food consumption were measured every 2 days in each group. Based on the weekly data, we found no significant changes ($P > 0.05$) in the above three basic life indicators (Figures 3A–C). CCl_4-treated mice showed a significant increase in liver size and liver index compared to the normal controls, but RAFE treatment produced a certain recovery effect, especially in the H-RAFE group, where the liver coefficient was significantly lower than that of the MC group ($P < 0.01$) and almost returned to the level of the NC group (Figures 3D, E). The PC group showed a significant effect on the recovery of liver coefficients (Figure 3E). According to the liver images, the livers of the MC group exhibited obvious edema expansion and a yellowish color, as well as many white dotted lesions on the surface of the liver. Conversely, treatment with three different concentrations of RAFE and bifendatatum restored the color and edema of the liver, especially in the M-RAFE, H-RAFE, and PC groups, which were almost restored to normal levels (Figure 3D).

3.3. Effect of RAFE on serum biochemical indexes of mice with CCl_4-induced liver injury

Liver injury adversely affects the transport function and membrane permeability of hepatocytes and causes enzymes to leak out of cells. The most important enzymes that reflect liver injury are ALT, AST, and ALP. In this study, we determined the enzymatic activity levels of ALT, AST, and ALP in mouse plasma (Figure 4). We found that ALT, AST, and ALP enzyme activities increased sharply after CCl_4 intervention in plasma, to 3.86, 12.93, and 82.16 U/L, respectively, whereas the enzyme activity of NC group was only 0.46, 7.38, and 46.56 U/L (Figure 4). This indicated that the liver tissue of mice was severely damaged after CCl_4 treatment. After RAFE intervention, the levels of ALT, AST, and ALP were all significantly reduced, especially in H-RAFE and M-RAFE groups, where the enzymatic activity of AST was restored to almost normal levels ($P < 0.0001$) (Figure 4B). Simultaneously, ALP and ALT levels were significantly decreased in the H-RAFE and M-RAFE groups. Interestingly, RAFE reduced ALT activity in a dose-dependent manner (Figure 4A). Bifendate, a clinical drug used for the treatment of hepatitis, also significantly reduced the plasma levels of ALT, AST, and ALP (Figure 4). These results suggest that RAFE can effectively relieve liver injury caused by CCl_4.

3.4. Effects of RAFE on biochemical indices and liver in CCl_4-liver injury mice

Carbon tetrachloride-induced liver injury is associated with lipid peroxidation in mice, and elevated MDA levels are a key manifestation of liver injury caused by lipid peroxidation. In this study, the level of MDA increased from 17.36 nmol/g quality in the MC group to 27.65 nmol/g quality in the NC group (Figure 5D), which indicated that CCl_4 treatment caused significant peroxidative injury in the mouse liver. However, the level of MDA decreased after RAFE treatment, and the most pronounced effect was in the H-RAFE group, with a reduction of 18.60 nmol/g quality (Figure 5D). This suggests that RAFE alleviates CCl_4-induced liver peroxidation. SOD is the most important antioxidant enzyme in biological systems. T-GSH is the main non-enzymatic antioxidant and regulator of intracellular redox homeostasis. Normally, there is a physiological balance between the production of reactive oxygen species, free radicals, and antioxidant enzymes. Peroxidation of liver tissues usually results in high consumption of antioxidant enzymes/antioxidants, such as SOD and T-GSH. In this study, SOD, T-GSH, and T-AOC decreased to 44.80 U/g quality, 157.59 μmol/L, and 29.76 μmol/g quality, respectively, in the MC group (Figures 5C, E, F). However, RAFE intervention significantly increased the levels of SOD, T-GSH, and T-AOC (Figures 5C, E, F), which followed the same trend as that of enzyme activity in the mouse plasma (Figure 4). Interestingly, the best recovery of T-GSH was observed in the L-RAFE group, which returned to normal levels of 237.67 μmol/L (Figure 5C). The PC group also showed better recovery of biochemical

TABLE 1 Contents of flavonoids identified in RAFE and related HPLC data.

Peak number	Compound	Calibration curves	R^2	Test range (μg/ml)	Retention time (min)	Content (mg/100 g)
1	Cyanidin-3-O-galactoside	$y = 20569x-226.41$	0.9907	6.25–100.0	2.504	13.306
2	Cyanidin 3-O-glucoside	$y = 4343.9x+3.7214$	0.9996	6.25–100.0	2.670	4.426
3	(−)-Catechin hydrate	$y = 5350.1x-16.872$	0.9977	0.25–8.0	7.452	5.148
4	(+)-Catechin	$y = 6171.9x+8.7721$	0.9986	3.75–60.0	12.304	49.346
5	(−)-Epicatechin	$y = 15833x-20.699$	0.9931	3.75–60.0	12.674	19.719
6	Phloridzin	$y = 16967x-1.0121$	0.9995	6.25–100.0	21.610	0.827
7	Quercetin	$y = 32111x-254.54$	0.9981	1.56–50.0	29.048	23.087
8	Phloretin	$y = 121700x+13.2$	0.9982	6.25–100.0	30.370	1.923

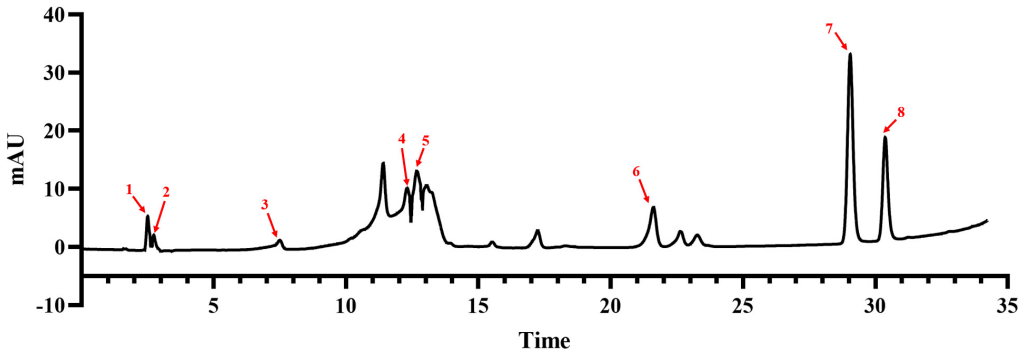

FIGURE 2
Composition and content of flavonoids in RAFE based on HPLC analysis. HPLC plot of RAFE, where the eight peaks labeled in the plot correspond to the flavonoid compounds with the same serial numbers as those in Table 1.

parameters in the liver (Figures 5C–F). Recovery of these liver indices showed that RAFE can improve CCl_4-induced oxidative stress and help reduce oxidative injury in the mouse liver.

Histopathological observations provide visual data on the recovery effect of RAFE in mouse liver injury. H&E staining of liver sections showed that the NC group had well-preserved cytoplasm and typical hepatocytes with clearly visible central veins. The hepatocytes were tightly bound to each other, and the liver porosity was only 2.34% (Figures 5A, B). In contrast, significant pathological changes were observed in the hepatocytes around the central vein of the liver in the MC group, and the cells were loosely bound with a liver porosity of 24.05%. However, after RAFE intervention, hepatic tissue cells normalized, liver porosity significantly decreased, hepatocellular lesions around the central vein were reduced, and the H-RAFE group showed the best recovery, with a 7.89% reduction in porosity, indicating a recovery effect that was second only to that of bifendate. The results of the histological observation analysis were consistent with the trend of serum and liver recovery, which suggested that RAFE intervention significantly ameliorates severe histological lesions in mice with CCl_4-induced liver injury.

3.5. Effect of RAFE on intestinal microorganisms in mice with CCl_4-induced liver injury

It has been shown that there is a bidirectional relationship between the liver and gut microbes, with the portal vein enabling direct transport of gut-derived products to the liver, as well as a hepatic feedback pathway of bile and antibody secretion to the intestine (42). Here, we investigated whether flavonoids extracted from red-fleshed apples can restore liver injury by regulating intestinal microorganisms. We determined the effect of RAFE on the overall structure and abundance of mouse intestinal microorganisms by analyzing the gene sequence of the 16S rRNA (V4 region) in mouse feces. The smoothed dilution curve indicated the reliability of the sequencing results (Figure 6A). The petal diagram showed that CCl_4 reduced the number of operational taxonomic units (OTUs) in the pathological group from that in the normal control group, whereas the bifendate and RAFE intervention groups both restored the number of similar microorganisms to a certain extent, especially in the H-RAFE group. This suggests that RAFE has the potential to restore intestinal microbes (Figure 6B). The

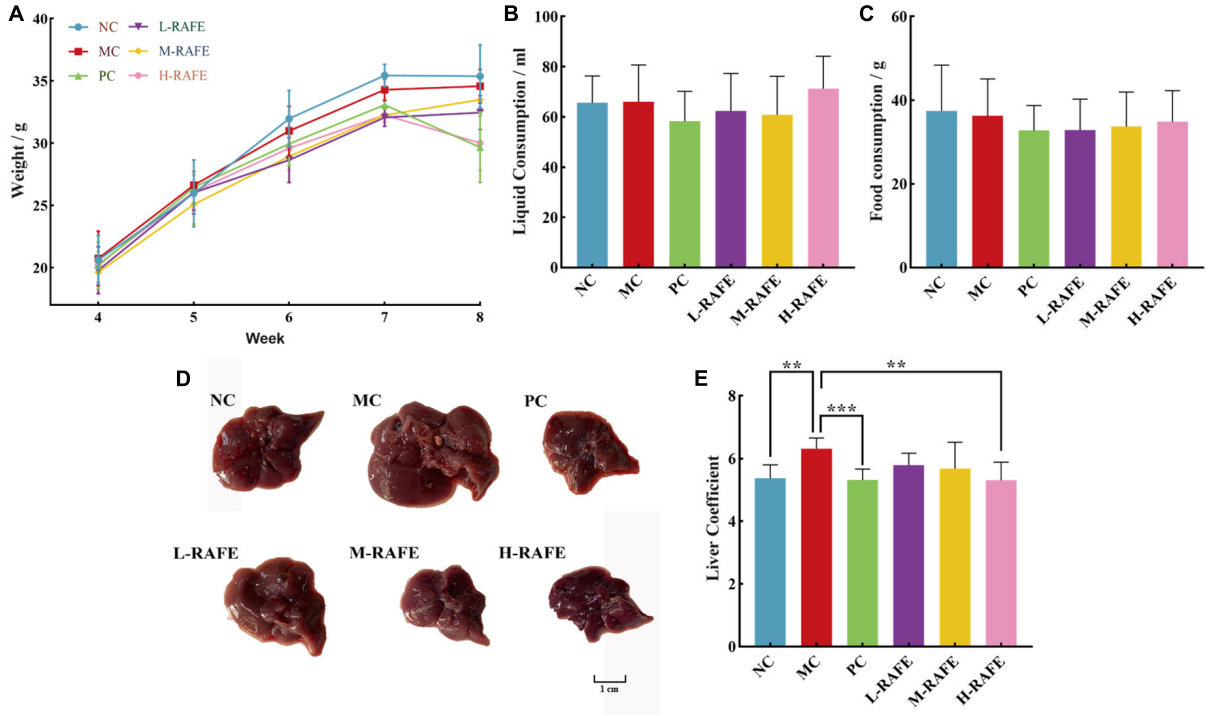

FIGURE 3
Effects of RAFE on basic life indicators and livers of mice. **(A)** Weekly body weight, **(B)** weekly fluid consumption, **(C)** weekly food consumption, **(D)** morphological observation, and **(E)** liver coefficient. Data are expressed as the mean ± SD (n = 4 or 6) $^{**}P < 0.01$, $^{***}P < 0.001$, compared with the pathology group.

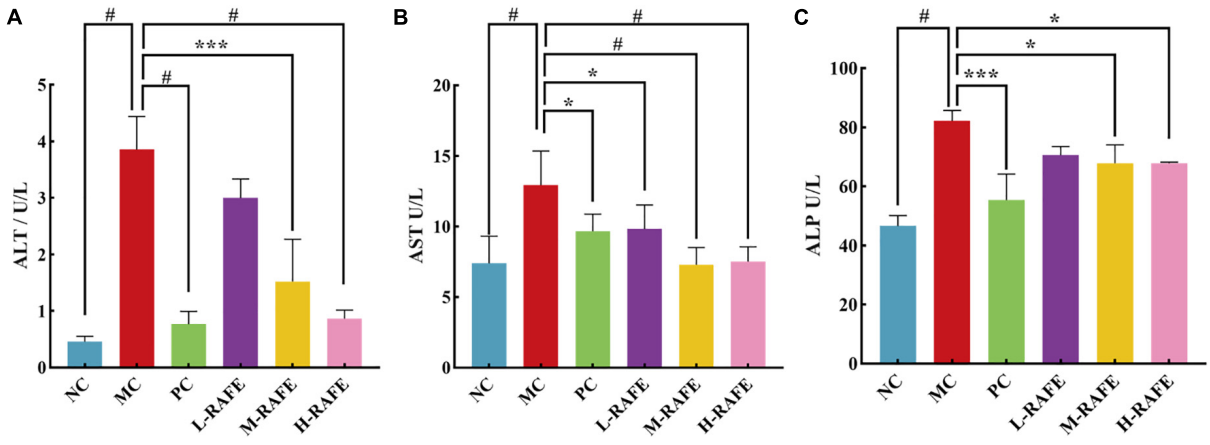

FIGURE 4
Effect of RAFE on serum biochemical parameters in mice. **(A)** ALT, **(B)** AST, and **(C)** ALP. Data are expressed as the mean ± SD (n = 4 or 6) $^{*}P < 0.05$, $^{***}P < 0.001$, $^{\#}P < 0.0001$, compared with the pathological group.

statistical results of the alpha index showed that the diversity of NC and MC groups was negatively correlated, and intervention with RAFE partially restored the diversity of intestinal microbes in mice with CCl_4-induced liver injury. Overall, H-RAFE intervention showed the best effect; however, drug treatment also restored intestinal microbe levels (Figure 6C).

Beta diversity analysis was used to assess the similarity between groups. OTU-based non-metric multidimensional scaling analysis showed that the MC group was clearly distinct from the other treatment groups, whereas all other treatment groups had certain similarities with the NC group, which suggested that RAFE could restore the composition of intestinal

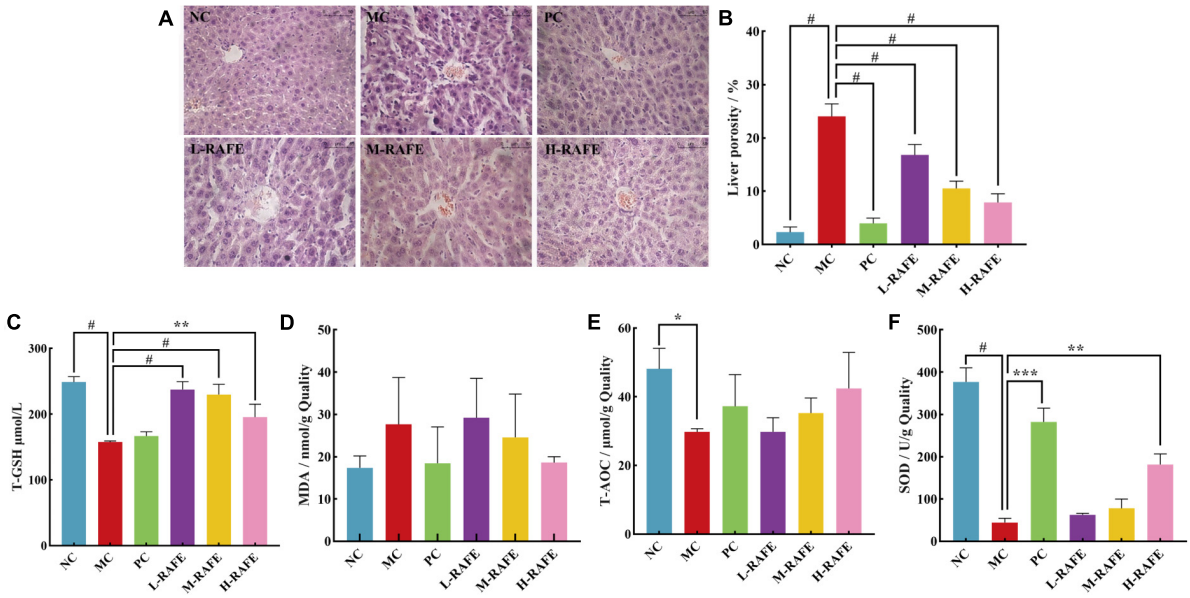

FIGURE 5
Effect of RAFE on biochemical indexes of mouse livers and liver histology. **(A)** Histopathological observations of mouse livers (40× magnification), **(B)** liver porosity, **(C)** T-GSH, **(D)** MDA, **(E)** T-AOC, and **(F)** SOD. Data are expressed as the mean ± SD (n = 4 or 6) $^{*}P < 0.05$, $^{**}P < 0.01$, $^{***}P < 0.001$, $^{\#}P < 0.0001$, compared with the pathological group.

microbes (Figure 7A). We then performed principal coordinates analysis based on the unweighted UniFrac distance. The results showed that the MC group had lower community similarity with the NC group, whereas the distance to the NC group after RAFE treatment was relatively close and the species composition structure was similar, illustrating the success of CCl_4 modeling and the therapeutic effect of RAFE (Figure 7B). The unweighted pair-group method with arithmetic mean dendrogram based on the unweighted UniFrac distance showed that the NC and MC groups had different gut microbial compositions because the two groups were located on different branches, and the microbial composition after RAFE and bifendate intervention was closer to that of the NC group, especially for the M-RAFE group (Figure 7C).

To identify the specific taxa associated with RAFE, the relative abundance of intestinal microbes was determined at the phylum and genus levels (Figures 8A, B). At the phylum level, the microbial community was mainly composed of Firmicutes, Proteobacteria, and Bacteroidetes. The abundance of Firmicutes was higher in the MC group, whereas the abundance of Bacteroidetes was lower, resulting in an increase in the ratio of Firmicutes to Bacteroidetes (F/B) compared to the NC group. RAFE treatment affected the F/B ratio in two ways, increasing the relative abundance of Bacteroidetes and decreasing the relative abundance of Firmicutes, thereby reducing the F/B ratio and returning F/B to normal levels. Interestingly, the interventions of both RAFE and bifendate increased the relative abundance of Proteobacteria and Actinobacteria compared to that in the MC group (Figure 8A). At the genus level, the intervention of RAFE reduced the relative abundance of *Staphylococcus*, increased the relative abundance of probiotics such as Lactobacillus, and restored the intestinal microbial level almost back to normal (Figure 8B). To further validate the differences in intestinal microbes across all groups, the abundance of different species was analyzed at the phylum and genus levels. On the phylum-level abundance heat map, the top 35 dominant bacterial groups in the NC group were similar to those in the bifendate group and RAFE intervention groups (Figure 8A). Interestingly, on the genus-level heatmap, the dominant flora of the NC group was only similar to that of M-RAFE (Figure 8B).

Linear discriminant analysis effect size indicated that the dominant microbes in the MC group were Firmicutes, and intervention with M-RAFE mainly increased nine microbiota induced by CCl_4 in mice, including *Lachnospiraceae*, *Muribaculaceae*, *Clostridia*, and other probiotics (Figure 8C). Taken together, these data suggest that the gut microbiota of mice induced by CCl_4 are imbalanced, and that RAFE can modulate gut disturbance in mice with liver injury by increasing the microbial diversity and relative abundance of probiotics.

4. Discussion

Liver disease is a deadly disease that occurs worldwide. The abuse of alcohol, chemical drugs, and food safety

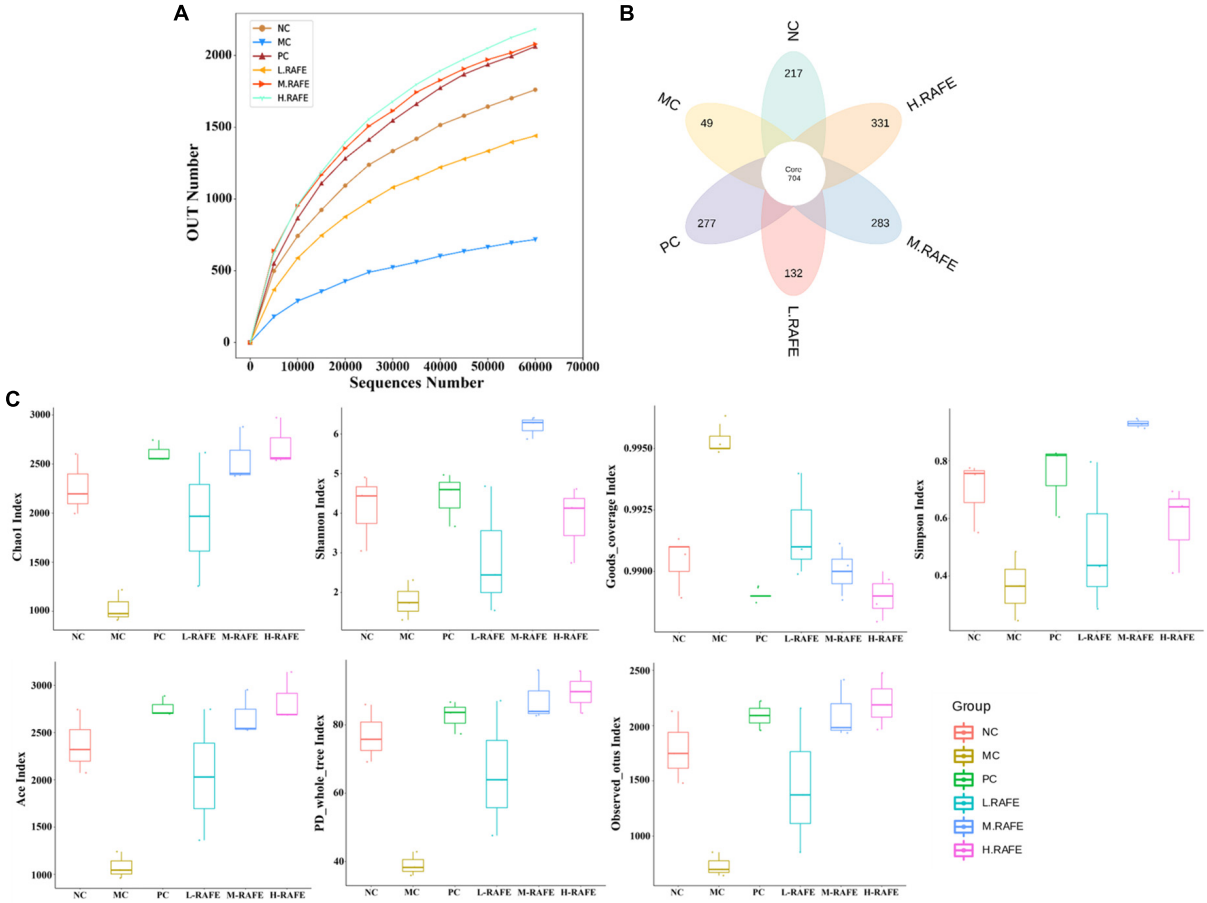

FIGURE 6
Effect of RAFE on OTUs and alpha diversity of mice intestinal microorganisms. **(A)** Grouped dilution curves, where a flatter curve indicates a more uniform species distribution, **(B)** petal plot, and **(C)** alpha diversity analysis (Chao1, Shannon, Goods, Simpson, Ace, PD, and observed). *n* = 3 samples/group.

problems lead to the frequent occurrence of liver injury. According to statistics, more than 75 million people worldwide are at risk of alcoholic liver injury and related diseases. Moreover, approximately 2 billion people are obese and overweight so at risk of non-alcoholic fatty liver disease (43). The current common treatment for liver injury is drug intervention, which can cause undesirable side effects. In recent years, natural plant extracts have received extensive attention because of their safety and ease of preparation. Natural plant extracts are rich in various components, such as flavonoids, which are widely recognized as effective functional components.

Flavonoids have extremely high medicinal value as natural plant extracts, and have been shown to prevent and treat cardiovascular diseases by reducing blood lipids and cholesterol, exhibit anti-oxidation effects, and protect the liver (44, 45). Studies have shown that the bioactive components in blueberries include anthocyanins, polyphenols, and pectin, with the pectin in blueberry powder also including anthocyanin-3-glucoside and anthocyanin. These components can protect vision by reducing vascular endothelial growth factors and activating Akt signaling (46). Ma et al. found that silymarin intervention improved liver steatosis and hepatic lobular inflammation (46). Another study found that black tea extract prevents liver fibrosis in rats by regulating the TGF-β/Smad/ERK signaling pathway (47). Thus, flavonoids have high medicinal value. Nevertheless, few studies have analyzed apple flavonoids, and none have used RAFE to study liver injury and intestinal microbes in CCl_4-induced mice. The flavonoid content varied significantly among apple varieties (48), and the flavonoids in the peel and flesh of common apples on the market varied greatly (49), but the composition of flavonoids in apples did not vary much. Our XJ4, as a red-fleshed apple, is rich in flavonoids in both skin and flesh. Compared with the common apples in the market, the flavonoid content is much richer. In this study, we showed that RAFE contains eight flavonoids, including one flavonol, three flavanols, two anthocyanins, and two dihydrochalcones. Therefore, we speculate that RAFE

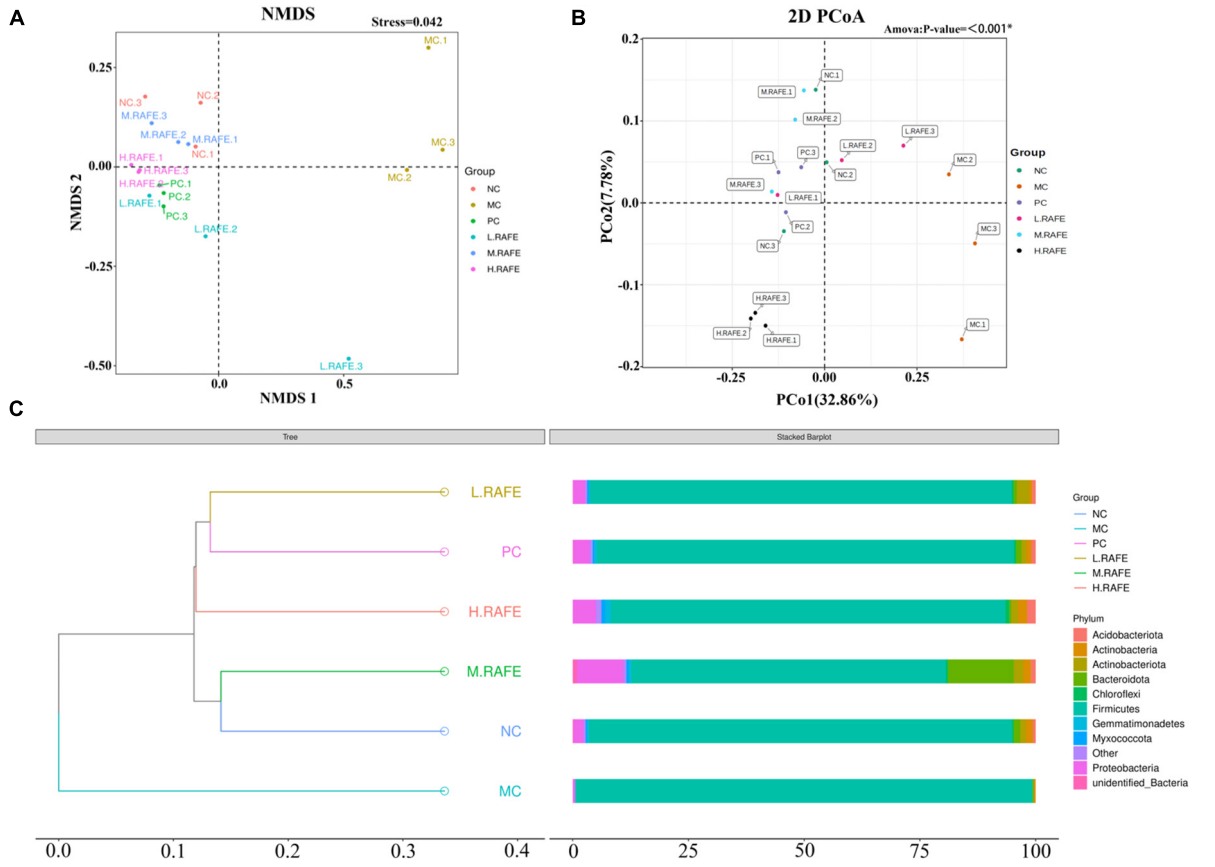

FIGURE 7
Effect of RAFE on beta diversity of mice intestinal microorganisms. **(A)** Non-metric multidimensional scaling analysis based on OTU levels, **(B)** 2D plot of unweighted UniFrac distance-based principal co-ordinates analysis, where closer sample distances indicate more similar species composition structures, and **(C)** unweighted pair-group method with arithmetic mean clustering tree based on unweighted UniFrac distances. *n* = 3 samples/group.

can improve antioxidant capacity and relieve liver injury by regulating intestinal microbes to interfere with biochemical indexes of the plasma and liver.

The CCl_4-induced liver injury model is widely recognized as a common model for screening liver-protective drugs. This model can lead to increased liver weight, an abnormal increase in serum ALT and AST levels, a significant increase in SOD activity, and decreased levels of GSH (50). CCl_4 can also cause lesions in liver tissue, resulting in loose liver tissue, loss of structural integrity, gaps around liver cells, and inflammatory reactions (43). Studies have shown that the flavonoid extract of baicalin can alleviate abnormalities in serum biochemical indicators and heterologous liver injury by reducing inflammation and oxidative injury (51, 52). Another study showed that puerarin alleviates liver injury in rats and zebrafish and attenuates inflammatory infiltration (52, 53). The liver index directly reflects changes in liver weight, and an abnormal liver index is a clear sign of the development of liver disease. Yan et al. found that lychee extract, which is rich in flavonoids, attenuates CCl_4-induced hepatomegaly in rats and has a positive effect on pathological changes in liver tissue (54). Our study found that RAFE has a similar function, not only normalizing the liver index and restoring abnormal enzyme activity and biochemical indices in serum, but also relieving liver tissue injury and reducing liver porosity. In addition, MDA and T-AOC in the liver showed that CCl_4 also caused oxidative stress and oxidative injury to the liver. Interestingly, oxidative injury to the liver was alleviated by different doses of RAFE, where the degree of remission was positively correlated with the dose. This shows that RAFE has antioxidant functions and alleviates liver injury; however, the specific mechanism remains unclear.

The gut has a complex microbial system for nutrient absorption, metabolism, and protection (55). Some of these colonies, such as *Lachnospiraceae*, *Lactobacillus acidophilus*, and *Clostridium*, are considered beneficial, whereas other bacterial groups, such as *Pseudomonas*, *Staphylococcus*, and *Fusobacterium*, are pathogenic bacteria that may produce toxins (56). Poor living and eating habits and the exogenous intake of harmful substances will cause imbalances in the abundance

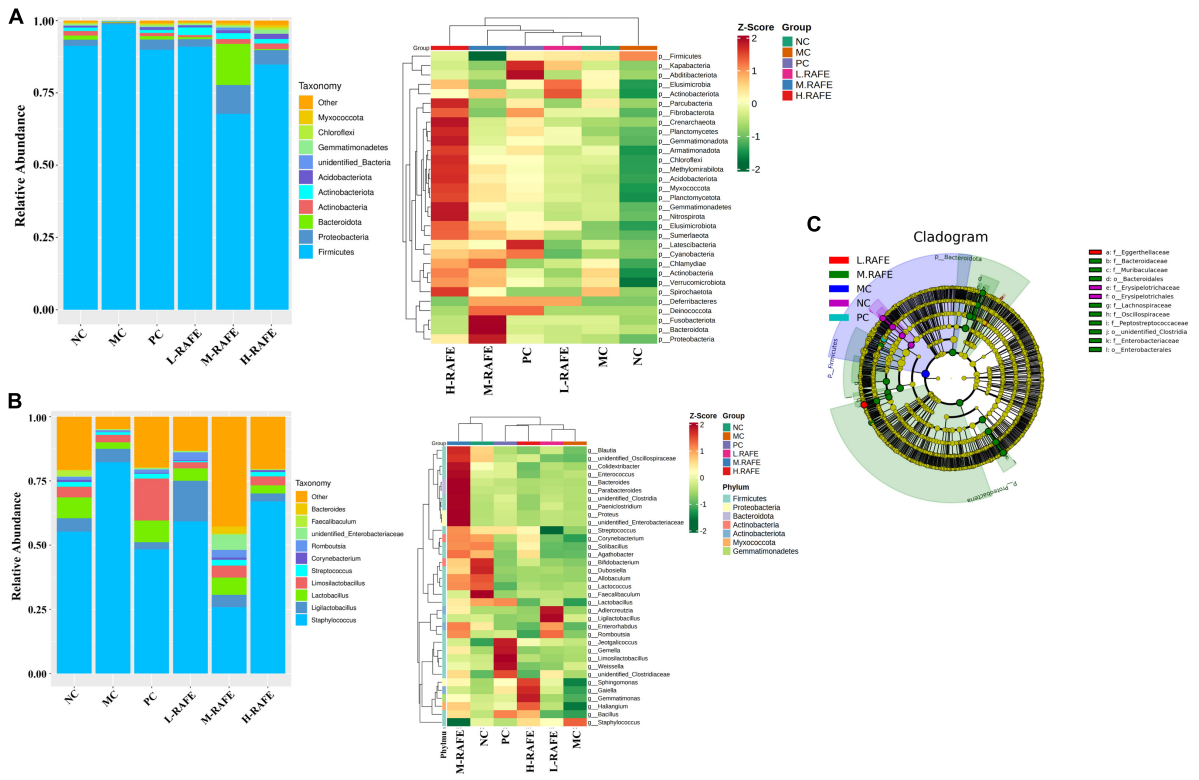

FIGURE 8
Effect of RAFE on species abundance at different taxonomic levels of mice intestinal microorganisms and linear discriminant analysis effect size. **(A)** Abundance chart at the gate level, with a stacked bar diagram of relative species abundance at the gate level on the left and a heat map of species abundance at the gate level for the top 35 microorganisms on the right, **(B)** abundance chart at the genus level, with a stacked bar diagram of relative species abundance at the genus level on the left and a heat map of species abundance at the genus level for the top 35 microorganisms on the right, and **(C)** evolutionary branching diagram, where the circles radiating from interior to exterior represent the taxonomic level from phylum to genus or species. Each small circle at different taxonomic levels represents a taxon at that level, and the diameter of the small circles is proportional to the relative abundance size. Coloring principle: species with no significant differences are uniformly colored yellow, and species with differences follow the group for coloring. *n* = 3 samples/group.

of intestinal microorganisms, as well as structural changes, increase the toxins produced by harmful bacterial colonies, or fail to maintain the corresponding functions of beneficial bacteria, resulting in diarrhea and injury to internal organs. As the largest digestive gland in the human body, the liver is one of the most vulnerable organs (57, 58). It has been shown that there is a bidirectional relationship between the liver and the gut and its microbiota – the gut-liver axis – and that toxic substances can disrupt gut microbes and the intestinal barrier, thereby increasing microbial exposure and the pro-inflammatory environment of the liver (42). In our previous study, we showed that RAAE could improve the abundance and structure of gut microbes. Therefore, we speculate that RAFE may also have beneficial effects on liver injury by improving the diversity and abundance of gut microbial populations. Studies have shown that aronia polyphenols can protect the liver by maintaining the balance of intestinal flora and reducing the translocation of bacteria to enhance intestinal barrier function (57). Changes in the gut microbiota driven by blueberry extract reduce inflammation, protect the integrity of the gut epithelium, and improve gut health, thereby reducing the translocation of bacterial products across the epithelial barrier (59). Li et al. found that treatment of mice on a high-fat diet with sarsaparilla polyphenols increased the ratio of Bacteroidetes to Firmicutes in their gut flora, but decreased the relative abundance of Verrucobacterium, thereby alleviating non-alcoholic liver injury caused by a high-fat diet (60). Our study showed that RAFE can interfere with the gut microbiome of mice, which is consistent with other related studies. However, we found that the regulation of gut microbes by RAFE, especially the regulation of the F/B ratio, not only decreased or increased the relative abundance of a certain phylum but also increased Bacteroidetes and decreased the relative abundance of Firmicutes, resulting in a change in the ratio of the two bacterial groups. Moreover, M-RAFE intervention mainly increased the nine species of microflora induced by CCl_4 in mice, including probiotics such as *Lachnospiraceae*, *Muribaculaceae*, and *Clostridia*. This phenomenon has rarely been reported in previous studies.

5. Conclusion

In conclusion, our study shows that RAFE contains a variety of flavonoids that can restore the disturbance of intestinal microbes by regulating beneficial bacteria and reducing harmful bacteria. RAFE also improves the abnormal biochemical indicators of the plasma and liver caused by CCl_4 poisoning, relieves oxidative injury to liver tissue, and reduces inflammation to protect the liver. According to experiments at different RAFE concentrations, we found that the relieving effect of RAFE on liver injury was not dose-dependent. This suggests that RAFE could be used for the adjuvant therapy and prevention of liver injury. Therefore, this research can promote the use of RAFE in food and medical applications.

Data availability statement

The datasets presented in this study can be found in online repositories. The names of the repository/repositories and accession number(s) can be found in the article/supplementary material.

Ethics statement

This animal study was reviewed and approved by the Animal Care and Use Committee of Qingdao Agricultural University (license number: SYXK [SD] 20170005).

Author contributions

YC and YW designed the research, performed the experiments, and wrote the manuscript. SJ and JX made contributions to perform the experiments and analysis the data. BW provided experiments assistance to YC. XS provided the suggestions and made contributions to design of the experiment. XS and YZ designed this experiment and revised the manuscript. All authors contributed to the article and approved the submitted version.

Funding

This study was supported by the Taishan Scholar Foundation of Shandong Province (ts2022), Agricultural Variety Improvement Project of Shandong Province (2021LZGC024 and 2022LZGC010), China's Agriculture Research System Foundation (CARS-27), and Qingdao Scientific Research Foundation (21-1-4-ny-29-nsh).

Conflict of interest

The authors declare that the research was conducted in the absence of any commercial or financial relationships that could be construed as a potential conflict of interest.

Publisher's note

All claims expressed in this article are solely those of the authors and do not necessarily represent those of their affiliated organizations, or those of the publisher, the editors and the reviewers. Any product that may be evaluated in this article, or claim that may be made by its manufacturer, is not guaranteed or endorsed by the publisher.

References

1. Di Ciaula A, Calamita G, Shanmugam H, Khalil M, Bonfrate L, Wang DQH, et al. Mitochondria matter: systemic aspects of nonalcoholic fatty liver disease (NAFLD) and diagnostic assessment of liver function by stable isotope dynamic breath tests. *Int J Mol Sci.* (2021) 22:7702. doi: 10.3390/ijms22147702

2. Kalra A, Yetiskul E, Wehrle CJ, Tuma F. Physiology, liver. In: Treasure Island (FL) editor. *StatPearls*. Treasure Island, FL: StatPearls Publishing LLC (2022).

3. Andrade RJ, Chalasani N, Björnsson ES, Suzuki A, Kullak-Ublick GA, Watkins PB, et al. Drug-induced liver injury. *Nat Rev Dis Primers.* (2019) 5:58. doi: 10.1038/s41572-019-0105-0

4. Chen T, Li R, Chen P. Gut microbiota and chemical-induced acute liver injury. *Front Physiol.* (2021) 12:688780. doi: 10.3389/fphys.2021.688780

5. Quintal-Novelo C, Rangel-Méndez J, Ortiz-Tello Á, Graniel-Sabido M, Vaca RP-CD, Moo-Puc R. A *Sargassum fluitans* borgesen ethanol extract exhibits a hepatoprotective effect in vivo in acute and chronic liver damage models. *BioMed Res Int.* (2018) 2018:6921845. doi: 10.1155/2018/6921845

6. Kumar SS, Kumar BR, Mohan GK. Hepatoprotective effect of *Trichosanthes cucumerina* var cucumerina L. on carbon tetrachloride induced liver damage in rats. *J Ethnopharmacol.* (2009) 123:347–50. doi: 10.1016/j.jep.2009.02.023

7. Okaiyeto K, Nwodo U, Mabinya L, Okoh A. A review on some medicinal plants with hepatoprotective effects. *Pharmacogn Mag.* (2018) 12:186. doi: 10.4103/phrev.phrev_52_17

8. Subramoniam A, Pushpangadan P. Development of phytomedicine for liver diseases. *Indian J Pharmacol.* (1999) 31:166–75.

9. Stine JG, Lewis JH. Current and future directions in the treatment and prevention of drug-induced liver injury: a systematic review. *Expert Rev Gastroenterol Hepatol.* (2016) 10:517–36. doi: 10.1586/17474124.2016.1127756

10. Kumar N, Surani S, Udeani G, Mathew S, John S, Sajan S, et al. Drug-induced liver injury and prospect of cytokine based therapy; a focus on IL-2 based therapies. *Life Sci.* (2021) 278:119544. doi: 10.1016/j.lfs.2021.119544

11. Reuben A, Koch DG, Lee WM. Drug-induced acute liver failure: results of a U.S. Multicenter, prospective study. *Hepatology.* (2010) 52:2065–76. doi: 10.1002/hep.23937

12. Shaker ME, Zalata KR, Mehal WZ, Shiha GE, Ibrahim TM. Comparison of imatinib, nilotinib and silymarin in the treatment of carbon tetrachloride-induced hepatic oxidative stress, injury and fibrosis. *Toxicol Appl Pharmacol.* (2011) 252:165–75. doi: 10.1016/j.taap.2011.02.004

13. Karimi J, Mohammadalipour A, Sheikh N, Khodadadi I, Hashemnia M, Goudarzi F, et al. Protective effects of combined losartan and nilotinib on carbon tetrachloride (CCl)-induced liver fibrosis in rats. *Drug Chem Toxicol.* (2020) 43:468–78. doi: 10.1080/01480545.2018.1504960

14. Amzar N, Iqbal M. The hepatoprotective effect of clidemia hirta against carbon tetrachloride (CCl4)-induced oxidative stress and hepatic damage in mice. *J Environ Pathol Toxicol Oncol.* (2017) 36:293–307. doi: 10.1615/JEnvironPatholToxicolOncol.2017019824

15. Madrigal-Santillán E, Madrigal-Bujaidar E, Álvarez-González I, Sumaya-Martínez MT, Gutiérrez-Salinas J, Bautista M, et al. Review of natural products with hepatoprotective effects. *World J Gastroenterol.* (2014) 20:14787–804. doi: 10.3748/wjg.v20.i40.14787

16. Shah M, D'Souza U, Iqbal M. The potential protective effect of *Commelina nudiflora* L. against carbon tetrachloride (CCl4)-induced hepatotoxicity in rats, mediated by suppression of oxidative stress and inflammation. *Environ Health Prev Med.* (2017) 22:66. doi: 10.1186/s12199-017-0673-0

17. Adjei IM, Plumton G, Sharma B. Chapter Four - oxidative stress and biomaterials: the inflammatory link. In: Dziubla T, Butterfield DA editors. *Oxidative Stress and Biomaterials*. Amsterdam: Elsevier (2016). p. 89–115. doi: 10.1016/B978-0-12-803269-5.00004-8

18. Venmathi Maran BA, Iqbal M, Gangadaran P, Ahn BC, Rao PV, Shah MD. Hepatoprotective potential of Malaysian medicinal plants: a review on phytochemicals, oxidative stress, and antioxidant mechanisms. *Molecules.* (2022) 27:1533. doi: 10.3390/molecules27051533

19. Ugwu CE, Suru SM. Medicinal plants with hepatoprotective potentials against carbon tetrachloride-induced toxicity: a review. *Egypt Liver J.* (2021) 11:88. doi: 10.1186/s43066-021-00161-0

20. Adewale A, Abiodun OO. Hepatoprotective and antioxidant effect of hibiscus polyphenol rich extract (HPE) against carbon tetrachloride (CCL4) –induced damage in rats. *J Adv Med.* (2010) 3:1574–86. doi: 10.9734/BJMMR/2013/3762

21. Zhen MC, Wang Q, Huang XH, Cao LQ, Chen XL, Liu YJ, et al. Green tea polyphenol epigallocatechin-3-gallate inhibits oxidative damage and preventive effects on carbon tetrachloride–induced hepatic fibrosis. *J Nutr Biochem.* (2007) 18:795–805. doi: 10.1016/j.jnutbio.2006.12.016

22. Li Y, Chen F, Ling L, Bo H, Wu Z. Protective effects of total flavonoids of *Bidens bipinnata* L. against carbon tetrachloride-induced liver fibrosis in rats. *J Pharm Pharmacol.* (2010) 60:1393–402. doi: 10.1211/jpp/60.10.0016

23. Zhong MM, Chen FH, Yuan LP, Wang XH, Cheng W. Protective effect of total flavonoids from *Bidens bipinnata* L. against carbon tetrachloride-induced liver injury in mice. *J Pharm Pharmacol.* (2010) 59:1017–25. doi: 10.1211/jpp.59.7.0015

24. Sekido K, Hayashi Y, Yamada K, Shiratake K, Komatsu H. Efficient breeding system for red-fleshed apple based on linkage with S3-RNase allele in 'pink pearl'. *Hortscience.* (2010) 45:534–7. doi: 10.21273/HORTSCI.45.4.534

25. Yuste S, Ludwig IA. New red-fleshed apple cultivars: a comprehensive review of processing effects, (poly)phenol bioavailability and biological effects. *Food Funct.* (2022) 13:4861–74. doi: 10.1039/d2fo00130f

26. Zhang XY, Chen XS, Yong P, Wang HB, Shi J, Hong Z. Genetic diversity of mineral elements, sugar and acid components in *Malus sieversii*(Ldb.)roem. *Acta Hortic.* (2008) 35:277–80. doi: 10.16420/j.issn.0513-353x.2008.02.009

27. Zhang X, Xu J, Xu Z, Sun X, Zhu J, Zhang Y. Analysis of antioxidant activity and flavonoids metabolites in peel and flesh of red-fleshed apple varieties. *Molecules.* (2020) 25:1968. doi: 10.3390/molecules25081968

28. Xu J, Zhang X, Sun X, Lv Q, Zhang Y. Red-fleshed apple anthocyanin extracts attenuate male reproductive system dysfunction caused by busulfan in mice. *Front Nutr.* (2021) 8:632483. doi: 10.3389/fnut.2021.632483

29. Wang B, Xu J, Jiang S, Wang Y, Zhu J, Zhang Y. Combined analysis of gut microbiota and plasma metabolites reveals the effect of red-fleshed apple anthocyanin extract on dysfunction of mice reproductive system induced by busulfan. *Front Nutr.* (2022) 8:802352. doi: 10.3389/fnut.2021.802352

30. Pupykina K, Farkhutdinov R, Fedorova A, Koroleva E, Akhmadiev P. The study of the quantitative content of flavonoids and biological activity of the herba *Thlaspi arvense* L. In: Kurchenko V, Lodygin A, Machado da Costa RM, Samoylenko I editors. *Intelligent Biotechnologies of Natural and Synthetic Biologically Active Substances*. Cham: Springer (2022). p. 176–83. doi: 10.1007/978-3-030-96641-6_21

31. Sun Z, Li Z, Zhang J, Hou X, Yeh S, Ming X. Recent developments of flavonoids with various activities. *Curr Top Med Chem.* (2022) 22:305–29. doi: 10.2174/1568026622666220117111858

32. Sun Y, Tao W, Huang H, Ye X, Sun P. Flavonoids, phenolic acids, carotenoids and antioxidant activity of fresh eating citrus fruits, using the coupled in vitro digestion and human intestinal HepG2 cells model. *Food Chem.* (2019) 279:321–7. doi: 10.1016/j.foodchem.2018.12.019

33. Sharma B. An analyses of flavonoids present in the inflorescence of sunflower. *Braz J Bot.* (2019) 42:421–9. doi: 10.1007/s40415-019-00552-z

34. Rong T, Yang R, Young JC, Zhu H. Polyphenolic profiles in eight apple cultivars using high-performance liquid chromatography (HPLC). *J Agric Food Chem.* (2003) 51:6347–53. doi: 10.1021/jf0346298

35. Ayele DT, Akele ML, Melese AT. Analysis of total phenolic contents, flavonoids, antioxidant and antibacterial activities of *Croton* macrostachyusroot extracts. *BMC Chem.* (2022) 16:30. doi: 10.1186/s13065-022-00822-0

36. Rice-Evans CA, Miller NJ, Paganga G. Structure-antioxidant activity relationships of flavonoids and phenolic acids. *Free Radic Biol Med.* (1996) 20:933–56. doi: 10.1016/0891-5849(95)02227-9

37. Wang Y, Wang J, Li P, Ma F. Structure-antioxidant capacity relationship of dihydrochalcone compounds in *Malus*. *Food Chem.* (2019) 275:354–60. doi: 10.1016/j.foodchem.2018.09.135

38. Tungmunnithum D, Drouet S, Lorenzo JM, Hano C. Green extraction of antioxidant flavonoids from pigeon pea (*Cajanus cajan* (L.) Millsp.) seeds and its antioxidant potentials using ultrasound-assisted methodology. *Molecules.* (2021) 26:7557. doi: 10.3390/molecules26247557

39. Xiang Y, Zhao R, Lai F, Sun X, Sun X, Dai H. Components of flavonodis and antioxidant activity analysis of exctracts from red-flesh apple peel. *J Plant Physiol.* (2016) 52:8. doi: 10.1007/s11130-015-0497-2

40. Keshavarz Azizi Raftar S, Ashrafian F, Yadegar A, Lari A, Moradi H, Shahriary A, et al. The protective effects of live and pasteurized *Akkermansia muciniphila* and its extracellular vesicles against HFD/CCl4-induced liver injury. *Microbiol Spectr.* (2021) 9:e0048421. doi: 10.1128/Spectrum.00484-21

41. Wu L, Zhang Q, Mo W, Feng J, Li S, Li J, et al. Quercetin prevents hepatic fibrosis by inhibiting hepatic stellate cell activation and reducing autophagy via the TGF-β1/Smads and PI3K/Akt pathways. *Sci Rep.* (2017) 7:9289. doi: 10.1038/s41598-017-09673-5

42. Albillos A, de Gottardi A, Rescigno M. The gut-liver axis in liver disease: pathophysiological basis for therapy. *J Hepatol.* (2020) 72:558–77. doi: 10.1016/j.jhep.2019.10.003

43. Yang JY, Li M, Zhang CL, Liu D. Pharmacological properties of baicalin on liver diseases: a narrative review. *Pharmacol Rep.* (2021) 73:1230–9. doi: 10.1007/s43440-021-00227-1

44. Aguilar-Guadarrama AB, Rios MY. Flavonoids, sterols and lignans from cochlospermum vitifolium and their relationship with its liver activity. *Molecules.* (2018) 23:1925. doi: 10.3390/molecules23081952

45. Wu H, Luo T, Li YM, Gao ZP, Zhang KQ, Song JY, et al. Granny Smith apple procyanidin extract upregulates tight junction protein expression and modulates oxidative stress and inflammation in lipopolysaccharide-induced Caco-2 cells. *Food Funct.* (2018) 9:3321–9. doi: 10.1039/c8fo00525g

46. Ma L, Sun Z, Zeng Y, Luo M, Yang J. Molecular mechanism and health role of functional ingredients in blueberry for chronic disease in human beings. *Int J Mol Sci.* (2018) 19:2785. doi: 10.3390/ijms19092785

47. Zhan J, Cao H, Hu T, Shen J, Wang W, Wu P, et al. Efficient preparation of black tea extract (BTE) with the high content of theaflavin mono- and digallates and the protective effects of BTE on CCl4-induced rat liver and renal injury. *J Agric Food Chem.* (2021) 69:5938–47. doi: 10.1021/acs.jafc.1c01851

48. Geană E, Ciucure C, Ionete R, Ciocârlan A, Aricu A, Ficai A, et al. Profiling of phenolic compounds and triterpene acids of twelve apple (*Malus domestica* Borkh.) cultivars. *Foods.* (2021) 10:267. doi: 10.3390/foods10020267

49. Manzoor M, Anwar F, Saari N, Ashraf M. Variations of antioxidant characteristics and mineral contents in pulp and peel of different apple (*Malus domestica* Borkh.) cultivars from Pakistan. *Molecules.* (2012) 17:390–407. doi: 10.3390/molecules17010390

50. Liang Z, Liang H, Guo Y, Yang D. Cyanidin 3-O-galactoside: a natural compound with multiple health benefits. *Int J Mol Sci.* (2021) 22:2261. doi: 10.3390/ijms22052261

51. Qiao H, Han H, Hong D, Ren Z, Chen Y, Zhou C. Protective effects of baicalin on carbon tetrachloride induced liver injury by activating PPARgamma and inhibiting TGFbeta1. *Pharm Biol.* (2011) 49:38–45. doi: 10.3109/13880209.2010.493179

52. Wen YF, Zhao JQ, Bhadauria M, Nirala SK. Baicalin prevents cadmium induced hepatic cytotoxicity, oxidative stress and histomorphometric alterations. *Exp Toxicol Pathol.* (2013) 65:189–96. doi: 10.1016/j.etp.2011.08.005

53. Liu YS, Yuan MH, Zhang CY, Liu HM, Liu JR, Wei AL, et al. *Puerariae Lobatae* radix flavonoids and puerarin alleviate alcoholic liver injury in zebrafish by

regulating alcohol and lipid metabolism. *Biomed Pharmacother.* (2021) 134:111121. doi: 10.1016/j.biopha.2020.111121

54. Yan J, Feng Y, Fang X, Cui X, Xia X, Li F, et al. Anti-liver fibrosis effects of the total flavonoids of litchi semen on CCl4-induced liver fibrosis in rats associated with the upregulation of retinol metabolism. *Pharm Biol.* (2022) 60:1264–77. doi: 10.1080/13880209.2022.2086584

55. Kong Y, Yan T, Tong Y, Deng H, Tan C, Wan M, et al. Gut microbiota modulation by polyphenols from *Aronia melanocarpa* of LPS-induced liver diseases in rats. *J Agric Food Chem.* (2021) 69:3312–25. doi: 10.1021/acs.jafc.0c06815

56. Xue Y, Huang F, Tang R, Fan Q, Zhang B, Xu Z, et al. Chlorogenic acid attenuates cadmium-induced intestinal injury in Sprague-Dawley rats. *Food Chem Toxicol.* (2019) 133:10751. doi: 10.1016/j.fct.2019.110751

57. Duarte L, Gasaly N, Poblete-Aro C, Uribe D, Echeverria F, Gotteland M, et al. Polyphenols and their anti-obesity role mediated by the gut microbiota: a comprehensive review. *Rev Endocr Metab Disord.* (2021) 22:367–88. doi: 10.1007/s11154-020-09622-0

58. Liang H, Song H, Zhang X, Song G, Wang Y, Ding X, et al. Metformin attenuated sepsis-related liver injury by modulating gut microbiota. *Emerg Microbes Infect.* (2022) 11:815–28. doi: 10.1080/22221751.2022.2045876

59. Lee S, Keirsey KI, Kirkland R, Grunewald ZI, Fischer JG, de La Serre CB. Blueberry supplementation influences the gut microbiota, inflammation, and insulin resistance in high-fat-diet-fed rats. *J Nutr.* (2018) 148:209–19. doi: 10.1093/jn/nxx027

60. Li X, Yang L, Xu M, Qiao G, Li C, Lin L, et al. *Smilax china* L. polyphenols alleviates obesity and inflammation by modulating gut microbiota in high fat/high sucrose diet-fed C57BL/6J mice. *J Funct Foods.* (2021) 77:104332. doi: 10.1016/j.jff.2020.104332

frontiers | Frontiers in Nutrition

TYPE Original Research
PUBLISHED 25 January 2023
DOI 10.3389/fnut.2023.1020328

Check for updates

OPEN ACCESS

EDITED BY
Wenjie Sui,
Tianjin University of Science and Technology, China

REVIEWED BY
Qiang Yu,
Nanchang University, China
Lixin Niu,
Northwest A&F University, China
Ningbo Liao,
Jiangxi Agricultural University, China

*CORRESPONDENCE
Xiaocui Liu
xiaocuiliu777@126.com

†These authors have contributed equally to this work

SPECIALTY SECTION
This article was submitted to Nutrition and Food Science Technology, a section of the journal Frontiers in Nutrition

RECEIVED 16 August 2022
ACCEPTED 09 January 2023
PUBLISHED 25 January 2023

CITATION
Liu X, Tian J, Zhou Z, Pan Y and Li Z (2023) Antioxidant activity and interactions between whey protein and polysaccharides from different parts of *Houttuynia cordata*. *Front. Nutr.* 10:1020328. doi: 10.3389/fnut.2023.1020328

COPYRIGHT
© 2023 Liu, Tian, Zhou, Pan and Li. This is an open-access article distributed under the terms of the Creative Commons Attribution License (CC BY). The use, distribution or reproduction in other forums is permitted, provided the original author(s) and the copyright owner(s) are credited and that the original publication in this journal is cited, in accordance with accepted academic practice. No use, distribution or reproduction is permitted which does not comply with these terms.

Antioxidant activity and interactions between whey protein and polysaccharides from different parts of *Houttuynia cordata*

Xiaocui Liu*†, Jin Tian†, Zhiran Zhou, Yinzhen Pan and Zhongqiao Li

College of Food and Bioengineering, Xihua University, Chengdu, China

Houttuynia cordata polysaccharides (PSY) are known to exhibit a variety of beneficial activities, but these are currently not specifically utilized in food. Hence, using the two edible parts of *Houttuynia cordata*, a herbaceous plant native to Southeast Asia, this study developed polysaccharides of a stem (HCPS)-whey protein concentrate (WPC) complex and a leaf (HCPL)-WPC complex, and studied their stability, structure and antioxidant activity. The results showed that stability differed in complexes with different proportions, exhibiting only relative stability in the two complexes in which the ratio of HCPS-WPC and HCPL-WPC was 1:4, but increased stability in the HCPL-WPC complex (ζ-potential of HCPL-WPC: | -21.87 mv| > ζ-potential of HCPS-WPC: | -21.70 mv|). Structural characterization showed that there was electrostatic interaction between HCPS and WPC and between HCPL and WPC. The HCPL-WPC was found to have better antioxidant activity. The findings of this study, thus, provide a reference for the development of *Houttuynia cordata* polysaccharide applications in food.

KEYWORDS

***Houttuynia cordata*, polysaccharide-whey protein complex, antioxidant activity, interaction, structural characterization**

1. Introduction

Houttuynia cordata is a characteristic, nutritionally rich food in Southwest China, with many Chinese people also utilizing it as a traditional medicine in the treatment of cough, dyspnea, and pneumonia (1). Research has shown that *H. cordata* is rich in phenols, flavonoids, volatile oils, polysaccharides (PSY), and other active substances, *Houttuynia cordata* contains 15.73∼20.29% polysaccharide (2). Shi et al. (3), for example, found that orally administered *H. cordata* PSY could directly regulate the dynamic balance of Th17/Treg cells in the intestines and lung, and reduce lung injury in influenza infected mice. Because of their unique physical and chemical properties and potential biological activity, PSY are often added to food to improve its functional characteristics (4). As yet, few studies have been published on the interaction between *H. cordata* PSY and whey protein (WP), however, there are reports on the interaction between PSY extracted from other plants and WP. Niu et al. (5) studied the interaction mechanism between plantain PSY and WP by preparing a mixture of PSY and WP. At the same time, by comparing the bile acid binding ability of PSY and the PSY-WP mixture, the authors ascertained that the mixture had a threefold greater bile acid binding ability than PSY alone, making it suitable for development into a nutritional additive for the prevention of hyperlipidemia.

Proteins and PSY are two important and abundant biological macromolecules. Commonly, they are separately added to food as functional components (6), to improve the taste, structure, tissue state, stability, apparent characteristics and shelf life of food, while simultaneously increasing its functional characteristics (7). WP is a high-quality natural protein with a high biological titer in milk, in which it accounts for approximately 20% of total protein (8). WP contains β-lactoglobulin, α-lactalbumin, lactoferrin and lysozyme growth factor (9), all trace components that provide a variety of biological activities and health functions. Consequently, WP has the characteristics of high nutritional value, reasonable amino acid composition, easy digestion and absorption by the body, and a high utilization rate of functional activity. It has been found that polysaccharide and WP form complexes through non-covalent and covalent interactions (10). Non-covalent interactions mainly include electrostatic interactions, hydrogen bond actions, hydrophobic interactions and steric exclusion (11); Covalent interactions is mainly the chemical reaction between protein and polysaccharide, such as enzyme cross-linking and non-enzyme cross-linking (12). The interaction between PSY and WP has been widely studied (13) in order to overcome the shortcomings of WP sensitivity to temperature, pH value and ionic strength and, thereby, improve the utilization of WP. For example, WP and PSY were used to prepare covalent complexes through the Maillard reaction, which effectively improved and enhanced the functional properties of WP (14). In addition to the Maillard reaction, the soluble complex formed by the interaction between polysaccharide and WP in an aqueous solution can also be used as a fat substitute, thickener, stabilizer or transport carrier in functional food (15), which not only changes the structure of the food, but also improves its functional characteristics (16).

The edible parts of *H. cordata* include mainly its stems and leaves. In this study, the complex of WPC-HCPS and WPC-HCPL were prepared, the main objective of which was to investigate the effects of proportion on the interaction of the complex.

2. Materials and methods

2.1. Materials and chemicals

Whey protein concentrate (WPC, 80% protein) was obtained from Yuanye Bio-Technology Co., Ltd. (Shanghai, China). *H. cordata* was purchased from Wuxi Xiaogu E-commerce Co., Ltd. (Chongqing, China). Hydrochloric acid, sodium hydroxide and absolute ethanol were provided by Chengdu Kelong Chemical Co., Ltd. (Chengdu, China). All chemicals were of analytical grade.

2.2. Extraction of *H. cordata* stems and leaves (HCPS and HCPL)

The fresh *H. cordata* were dried at 55°C and then the stems (HCPS, 1 kg) and leaves (HCPL, 1 kg) powdered separately and soaked in absolute ethanol overnight at room temperature. Following suction filtration, the HCPS were extracted with deionized water (30 L) at 90°C for 5 h, while the HCPL were extracted with deionized water (50 L) at 90°C for 3 h. The extracts were then concentrated and absolute ethanol was added to the concentrates, whereafter they were left to stand overnight at 4°C, the precipitation then redissolved in deionized water and protein was removed using Sevage reagent. Thereafter, the samples were dialyzed against flowing deionized water for 36 h. The HCPS and HCPL were collected for simple purification by dynamic elution with macroporous resin, then concentrated and vacuum dried. HCPS was mainly composed of Man (4.22%), Rha (24.75%), GlcA (3.67%), GalA (10.42%), Glc (30.42%), and Xyl (20.55%), and HCPL was mainly composed of Man (1.33%), Rha (3.40%), GlcA (1.50%), GalA (2.19%), Glc (8.30%), Xyl (4.12%), Gal (1.50%), and Ara (61.33%) by monosaccharide analysis (17).

2.3. Preparation of complexes

Whey protein concentrate stock solution (10% w/v) and HCPS and HCPL stock solutions (0.25% w/v) were prepared in deionized water and stored at 4°C to ensure both protein dissolution and polysaccharide hydration. The WPC stock solution and HCPS and HCPL stock solutions were mixed separately at volume ratios of 1:0, 4:1, 3:2, 1:1, 2:3, 1:4, and 0:1. The pH value of each mixed solution was adjusted from 6.77 to 7, and the WPC-HCPS and WPC-HCPL solutions were kept overnight at 4°C, then restored to room temperature before use.

2.4. Turbidimetric analysis

The turbidimetry of the mixed solutions at different volume ratios was measured at 600 nm using a Fluostar Omega microplate reader (SpectraMax i3x, Molecular Devices, USAx), using the method described by Aryee and Nickerson (18). The mixed solutions were diluted 1:10. Deionized water was used as the control.

2.5. Particle size and zeta potential measurements

The laser particle size analyzer (Zetasizer Nano ZEN3600, Malvern, UK) was used to determine the particle size and zeta potential of the two mixed solutions (WPC-HCPS and WPC-HCPL) with different proportions. The average particle size was obtained *via* equilibrium for 2 min at 25°C. The zeta (ζ)-potentials of the complexes (WPC-HCPS and WPC-HCPL) were measured and the ζ-potential was estimated according to the Formula 1:

$$U_E = \frac{2\varepsilon \times \zeta \times f(\kappa\alpha)}{3\eta} \quad (1)$$

where U_E is conductivity mobility, ε is the permittivity [F(Farad/m)], η is the solution viscosity (mPa.s), κ is the Debye length (nm^{-1}), α is the particle radius (nm), and f(κα) = 1.5.

2.6. Rheological measurement

A rheometer (MCR302, Anton paar, Austria) was used to measure the mixed solutions in different proportions, and a 50 mm aluminum plate fixture was selected for the measurement. The distance between the fixture and the Peltier plate was 1 mm. Measurements were carried out at 25°C with a shear rate in the range of 0.1–1,000 s^{-1}.

2.7. Differential thermogravimetric measurements

The differential thermogravimetric (DTG) curves of the mixed solutions at different volume ratios were recorded using a DTG-60 analyzer (Shimadzu, Japan). The scanning was determined in the range of 30–800°C, the heating rate was 10°C/min, and the nitrogen flow rate was 30 mL/min.

2.8. Ultraviolet spectrophotometric determination

Each sample was placed in a quartz colorimetric cell for individual ultraviolet (UV) spectrophotometric determination, in which the absorption spectra were scanned in the wavelength range of 230–500 nm.

2.9. Fourier transform infrared spectroscopy

The Fourier transform infrared (FTIR) spectra of lyophilized WPC-HCPS and WPC-HCPL were recorded using an FTIR spectrophotometer (Spectrum Two N, PerkinElmer, USA) within a range of 400–4,000 cm^{-1} *via* 32 scans at a resolution of 4 cm^{-1}. The lyophilized samples were mixed well with potassium bromide and then compressed, after which each milligram of sample was further mixed with 100 milligrams of potassium bromide.

2.10. Scanning electron microscopy

Complex solutions were freeze-dried and then observed *via* a scanning electron microscope (SEM; Gemini 300, ZEISS, Germany), according to the method of Timilsena et al. (19). The lyophilized samples were plated with gold and also then studied *via* SEM with a scanning voltage of 3 kV.

2.11. Antioxidant activity

2.11.1. Scavenging efficiency of DPPH ·

The scavenging efficiency of complexes for DPPH · were determined using the methods of Cheng et al. (20). With vitamin C as the control, 2 mL of each complex was mixed with 0.1 mM DPPH · solution of the same volume and then shaken well. The system was then left to react in a dark place for 30 min, whereafter it was measured at 510 nm. The sample and the DPPH · solution were

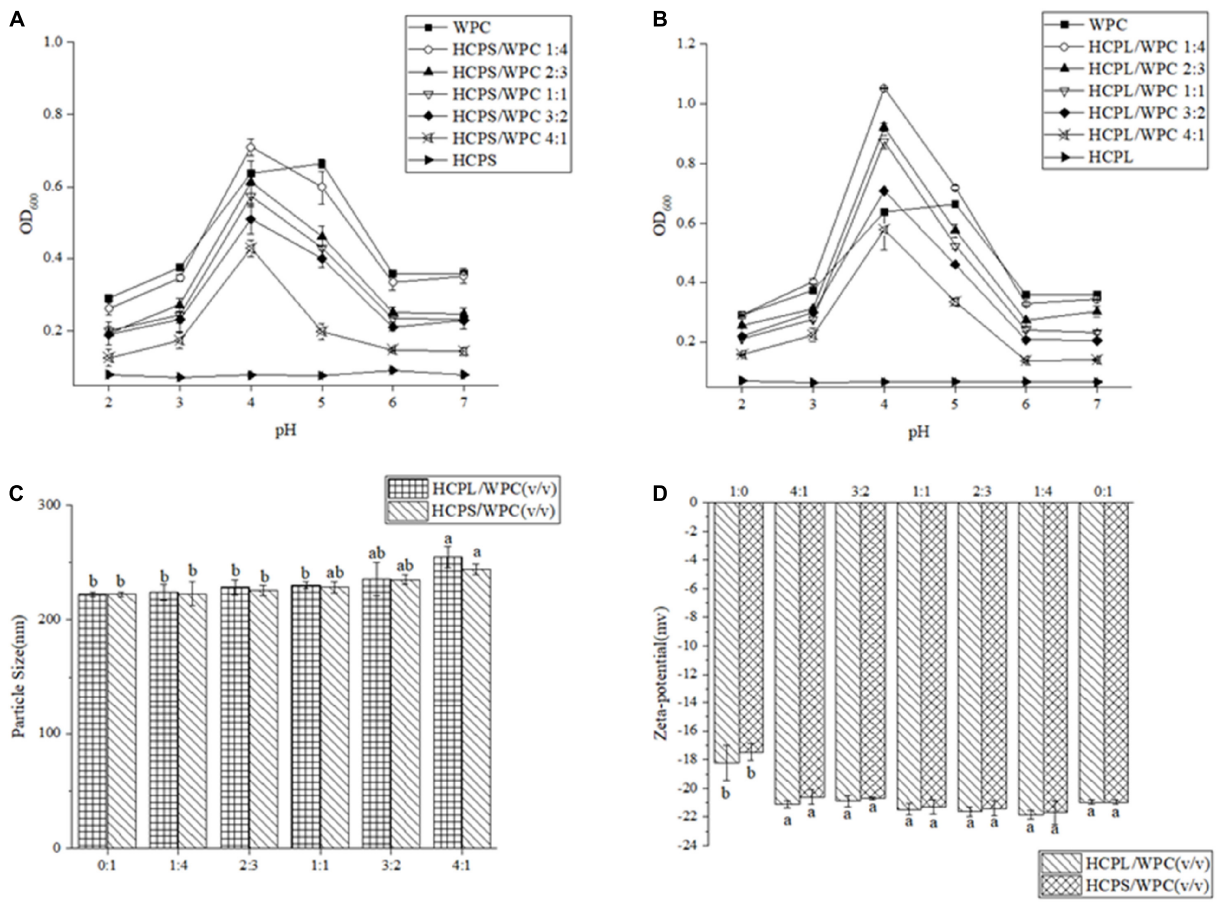

FIGURE 1
Curves of the turbidity of HCPS-WPC **(A)** and HCPL-WPC **(B)** at different volume ratios to the pH. Particle size **(C)** of complexes. The ζ−potential of complexes **(D)**.

then replaced with deionized water and absolute ethanol, respectively. The scavenging efficiency was then calculated using Formula 2:

$$\text{Scavenging efficiency (\%)} = \frac{A_0 - (A_1 - A_2)}{A_0} \times 100 \quad (2)$$

where A_0 is deionized water and DPPH · solution, A_1 is complex and DPPH · solution, A_2 is complex and absolute ethanol.

2.11.2. Scavenging efficiency of ·OH

The scavenging efficiency of ·OH was assessed, with reference to the method described by Tian et al. (21). The two complexes were mixed well with a ferrous sulfate ($FeSO_4$) solution (9 mmol/L) and a hydrogen peroxide (H_2O_2) solution (6 mmol/L) under a constant temperature 37°C for 10 min, whereafter a salicylic acid solution (9 mmol/L) was added to this mixture and then left to react at 37°C in the dark for 30 min. Finally, the mixture was measured at 600 nm. The scavenging efficiency was then calculated using Formula 2:

$$\text{Scavenging efficiency (\%)} = \frac{A_0 - (A_1 - A_2)}{A_0} \times 100 \quad (3)$$

where A_0 is deionized water+ $FeSO_4$+H_2O_2+ salicylic acid solution, A_1 is complex+$FeSO_4$+H_2O_2+salicylic acid solution, and A_2 is complex+ $FeSO_4$+ deionized water+ salicylic acid solution.

2.11.3. Scavenging efficiency of $ABTS^+$·

The scavenging ability of $ABTS^+$· was determined according to the method described by de Falco et al. (22). ABTS and potassium persulfate were mixed and stored at 4°C. The $ABTS^+$· stock solution was then diluted to an OD value of 0.7–0.8 before use. The samples were mixed with the $ABTS^+$· solution, left to react for 3 min and then measured at 734 nm. Deionized water was used as the blank control. The calculation formula was as follows:

$$\text{Scavenging efficiency (\%)} = \frac{OD_{control} - OD_{sample}}{OD_{control}} \times 100 \quad (4)$$

Where, $OD_{control}$ is the blank control and OD_{sample} is the sample.

2.11.4. Reduction capacity of Fe^{3+}

The reduction ability of the sample to Fe^{3+} was determined using the method reported by Yildirim et al. (23). The samples were mixed well with phosphate buffer (0.2 mol/L, pH 6.6) and potassium ferricyanide solution (1%), then left at 50°C for 20 min, and then cooled. Trichloroacetic acid (10%) was added to the above mixture. After being left to stand for 10 min, the absorbance of the mixture was measured at 700 nm. The reduction capacity was expressed in terms of OD value.

2.12. Statistical analysis

All the results were expressed as the mean ± standard error (SE) in the tables. Differences between groups were determined *via* Tukey's test analysis using SPSS 26 statistics software. A probability value of p less than 0.05 was considered significant.

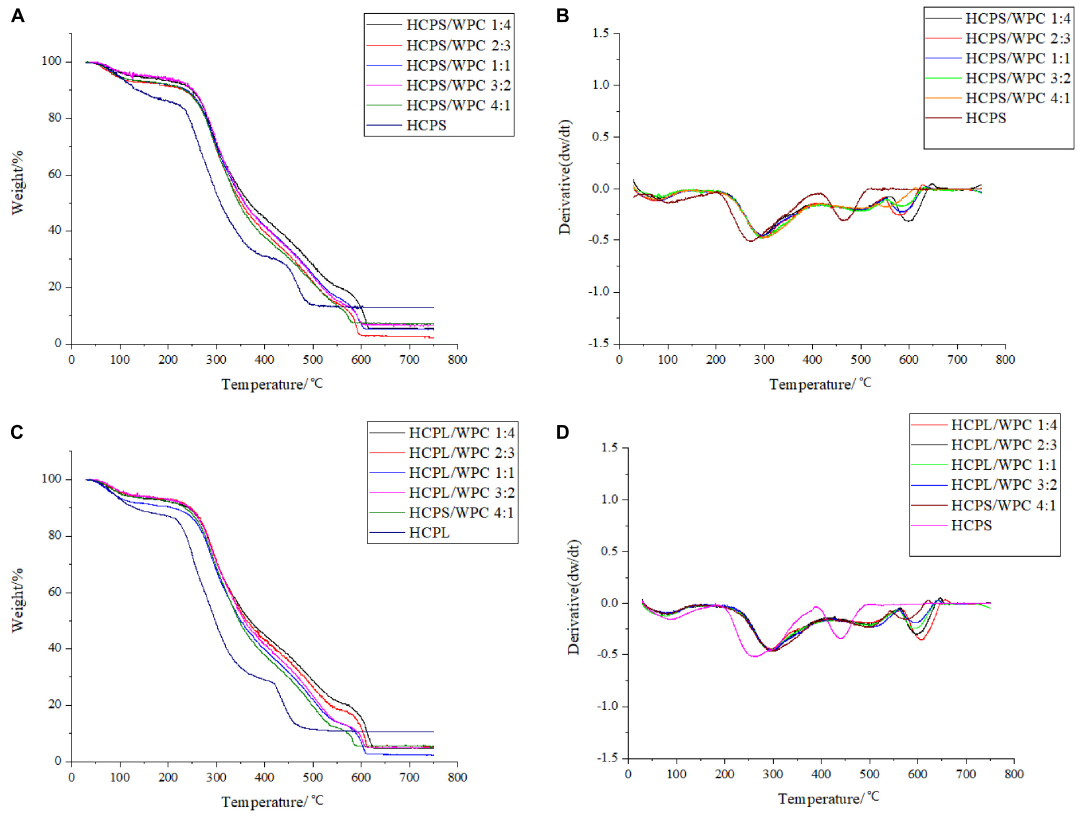

FIGURE 2
Thermogravimetry curve of HCPS-WPC **(A)** and HCPL-WPC **(C)**. The differential thermogravimetric curve of HCPS-WPC **(B)** and HCPL-WPC **(D)**.

3. Results and discussion

3.1. Turbidimetric and particle size analysis

Turbidity value can reportedly show the formation of a complex or condensate during the interaction between polysaccharide and protein (24). In this study, the OD of the HCPS and HCPL changed little, indicating that they were not affected by acidification in Figure 1 (25). Maximum OD was reached at approximately pH 5.0 due to the isoelectric point (pI) of the WPC in the range of pH 5.0–5.2 (Figure 1) (13). The turbidity curve of the WPC first increased and then decreased. The OD of both the HCPS-WPC and HCPL-WPC peaked at pH 4.0 and the curve shapes of the complexes were similar to that of the WPC. The same phenomena were previously observed in WP isolate and a carrageenan system (26). Compared with the WPC, the peak of complexes shifted to a lower pH, thus demonstrating the electrostatic interaction between HCPS or HCPL and WPC, as shown in Figure 1 (27). The HCPS-WPC complexes were observed with the peak of turbidity at a ratio of 1:4 (pH 4.0). At this time, the complexes contained a significantly large amount of coacervates (Figure 1A). The HCPL-WPC complexes were also at the maximum OD at pH 4.0 when the ratio was 1:4 (Figure 1B). However, the OD of HCPL-WPC complexes were higher than that of the HCPS-WPC at the same ratio (pH 3.0–5.0). This phenomenon can be explained by the precipitate yield of the HCPS-WPC complexes, which was less than that of the HCPL-WPC (28). Overall, 1:4 was found to be the optimal ratio for the interaction between HCPS or HCPL, and WPC. Further understanding of the interactions between HCPS and WPC, and HCPL and WPC, under neutral pH conditions could improve the application of HCPS and HCPL in the field of functional food. Therefore, this paper studied the effect of protein-polysaccharide ratio on the type and degree of interaction between HCPS or HCPL and WPC at pH 7.

As shown in Figure 1C, particle sizes were found to increase with the increase in HCPS and HCPL. Furthermore, the particle size of the HPCL-WPC was greater than those of the HPCS-WPC. The maximum difference between the particle size of the WPC and that of the complexes was only 32.6 nm, which could be related to the relatively dispersible structure of complexes (29).

3.2. ζ–potential

The ζ-potential of the HCPS-WPC and HCPL-WPC complexes could reflect the interaction between polysaccharide and WP, as well as their stability. A high absolute value of ζ-potential is indicative of a stable system (30). The ζ-potential of HCPS-WPC and HCPL-WPC

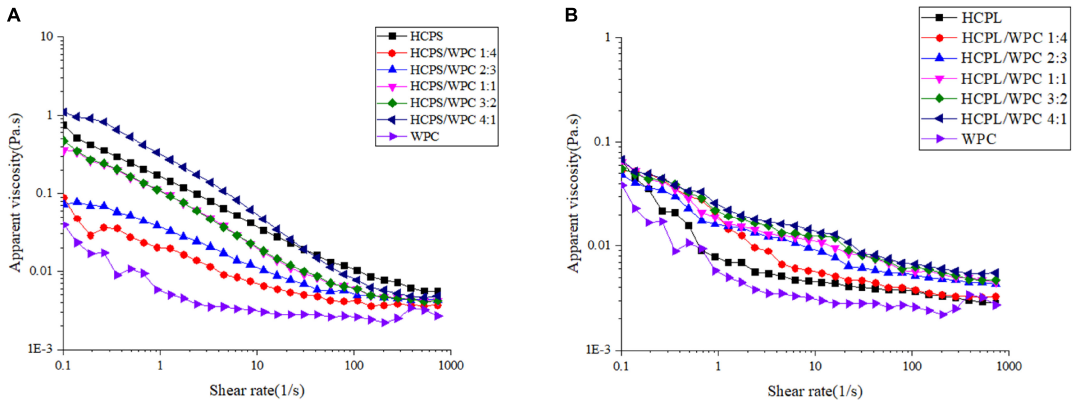

FIGURE 3
The viscosity curve of HCPS-WPC **(A)** and HCPL-WPC **(B)**.

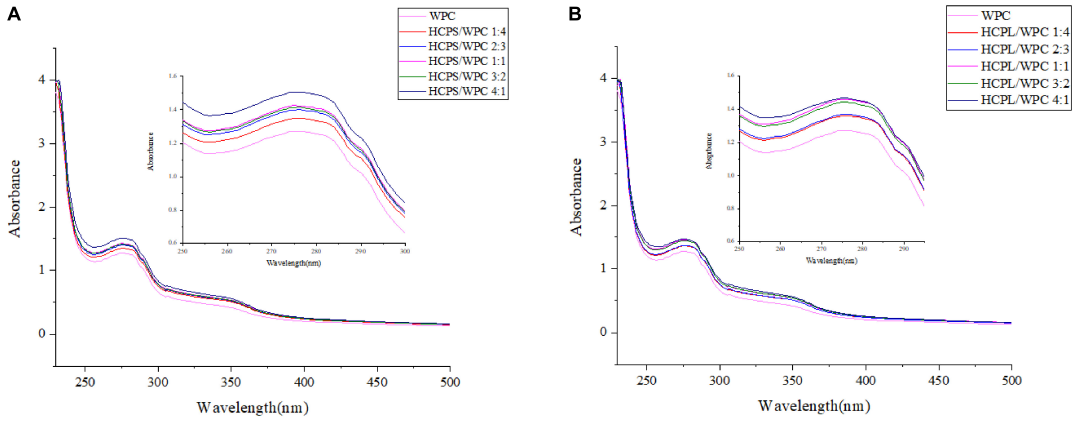

FIGURE 4
The ultraviolet-visible spectroscopy of HCPS-WPC **(A)** and HCPL-WPC **(B)**.

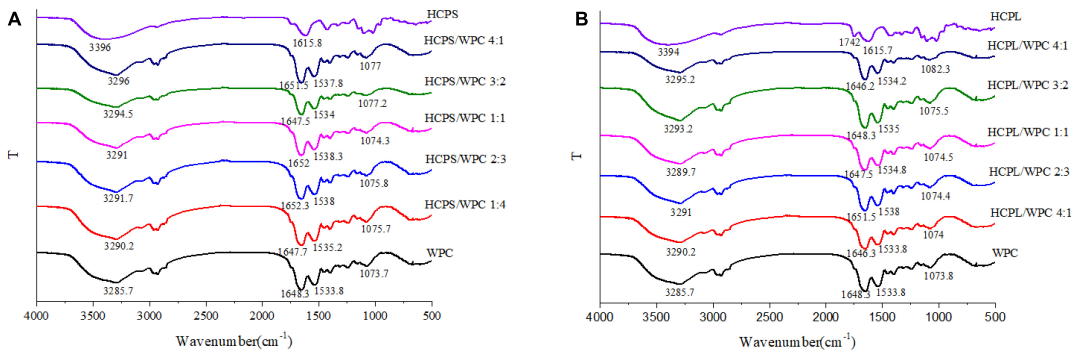

FIGURE 5
Fourier transform infrared spectra of the HCPS-WPC **(A)** and HCPL-WPC **(B)**.

is shown in **Figure 1D**. HCPS, HCPL and WPC were all found to have negative ζ-potential at pH 7.0, and the ζ-potentials of complexes with different volume ratios were insignificant. However, ζ-potential was below that of the WPC when the HCPL-WPC was at a volume ratio of 3:2 and in the HCPS-WPC at ratios of 3:2 and 4:1, indicating that the negative charges of HCPS and HCPL interacted with positive charges of WPC (31). As shown in **Figure 1D**, the highest ζ-potential was observed in both HCPS-WPC (-21.70 ± 0.85 mv) and HCPL-WPC (-21.87 ± 0.29 mv) at ratios of 1:4, because the increase of WPC led to the increase in ζ-potential. Moreover, the potential value of the HCPL-WPC was comparatively higher than that of the HCPS-WPC in the same ratio.

3.3. Thermogravimetric analysis

Thermogravimetric analysis revealed the thermal degradation of both HCPS-WPC and HCPL-WPC, as shown in **Figure 2**. With the gradual increase in program temperature, thermogravimetric change occurred in roughly three stages. For HCPS-WPC, the first stage of weightlessness occurred mainly in the range of 40–120°C (**Figure 2A**), and was due to the water in the sample. Concurrently, the derivative thermogravimetric (DTG) curve appeared to peak at the corresponding temperature (**Figure 2B**). Subsequently, the second stage of weightlessness was seen in the range of 220–400°C (**Figure 2A**). The thermogravimetric loss of approximately 50% in this stage was attributed to structural water and the cleavage of protein and polysaccharide (32). The thermal decomposition rate of the HCPS-WPC shifted to a high temperature and increased by 30°C compared with the HCPS, thus indicating that the HCPS-WPC had better thermal stability (**Figure 2B**). Finally, carbonization occurred in the third stage (530–650°C), in which the average loss rate was 22% (33), and the carbonization temperature of the HCPS-WPC was higher than that of the HCPS.

For the HCPL-WPC, thermogravimetric analysis showed similar results to the thermogravimetric changes occurring in the HCPS-WPC. However, the thermal decomposition temperature of the HCPL-WPC was 40°C higher than that of HCPL in the second weightlessness stage, and the weight loss temperature in the third stage was 540–660°C. In brief, the interaction of WPC with HCPS and HCPL improved the thermal stability of the complexes, which was also previously observed in a mixture of oat β-glucan/soy protein isolates (34).

3.4. Rheological analysis

The apparent viscosity changes in the HCPS-WPC complexes at different volume ratios were selected for study (**Figure 3A**). Shear thinning was observed in all complexes, in which viscosity decreased with the increase of shear rate. The viscosity was dependent on the volume ratio in the HCPS-WPC, with a declining trend of apparent viscosity in line with the increasing WPC. The apparent viscosity of the HCPL-WPC (**Figure 3B**) also decreased with the increase of shear rate, and the viscosity difference between the HCPL-WPC complexes was not significant. These complexes exhibited the characteristics of pseudoplastic fluids (35). However, the viscosity of the HCPS-WPC was higher than that of the HCPL-WPC, possibly due to the higher pectin content of HCPS.

3.5. UV analysis

The interactions between HCPS and WPC, and HCPL and WPC, were further explored *via* UV-vis spectroscopy. An absorption peak of amino acid residues was observed at 260–280 nm. Changes in peak intensity could be used to indicate the strength of an interaction (36). As shown in **Figure 4**, the WPC had a maximum absorption peak at 270–280 nm, corresponding to the vibration of Tyr (277 nm). After WPC was mixed with HCPS and HCPL, respectively, the absorption peak increased significantly, which might have been due to the formation of covalent conjugated complexes (37). More importantly, the peak change in the HCPL-WPC was greater than that of the HCPS-WPC, indicating that the HCPL-WPC interaction was stronger. As is evident in **Figure 4**, the peak positions of the complexes changed and gradually increased with the increase in PSY, possibly due to the microenvironmental change of amino acids. Thus, these results showed that the structure and microenvironment of the amino acid residues in WPC might be affected by changes in the polysaccharide-protein ratio which, in turn, affects the interactions between HCPS or HCPL and WPC.

3.6. FTIR analysis

The FTIR spectroscopy in this study provided more information about the interaction between PSY and WPC, as shown in **Figure 5**. The spectrum of HCPS revealed that the broad band at 3,396 cm^{-1}

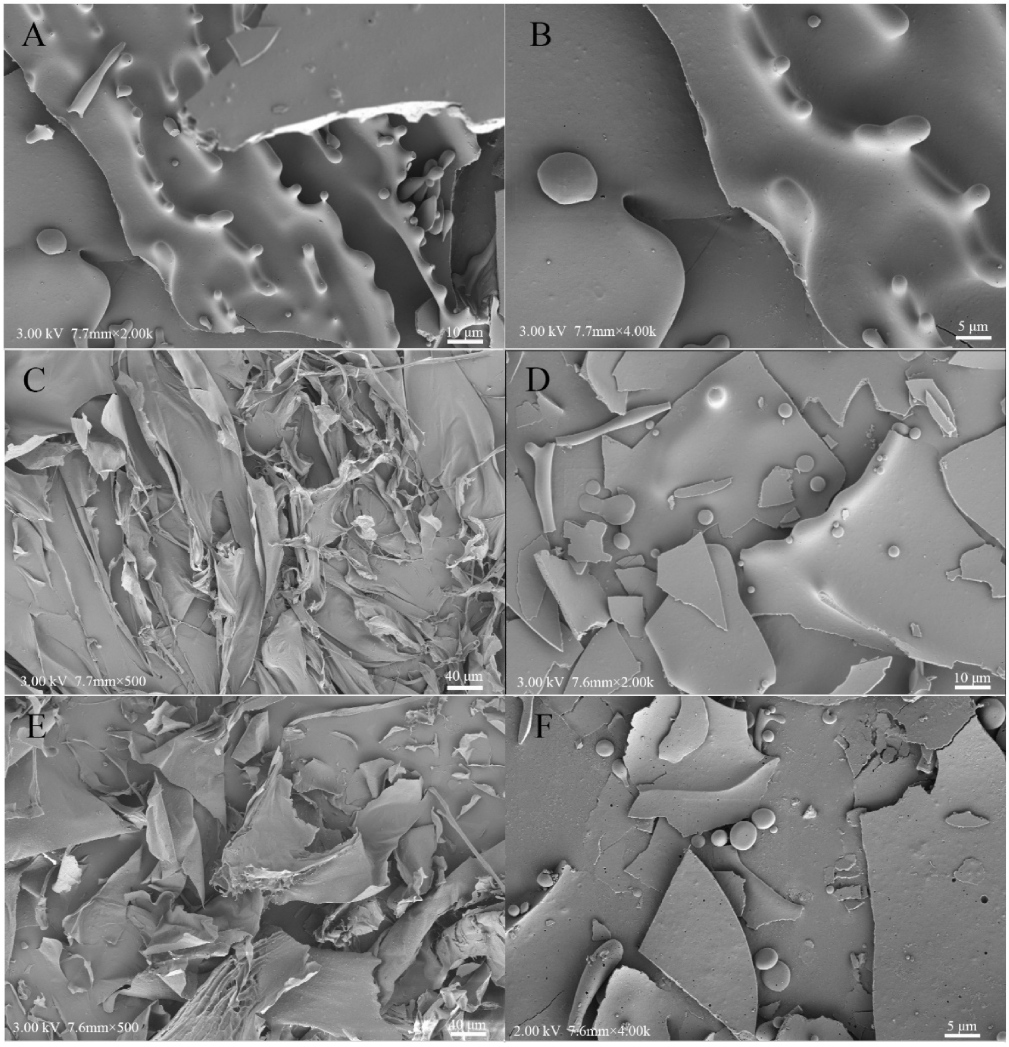

FIGURE 6
Scanning electron microscope observations of WPC **(A,B),** HCPS **(C)**, HCPL **(E)**, HCPS-WPC 1:4 **(D)** and HCPL-WPC 1:4 **(F)**.

was attributed to O–H vibration, while the stretching vibration of C = O on carbonyl groups was observed at 1615.8 cm^{-1} (Figure 5A). For WP, a 1648.3 cm^{-1} band was derived from the C = O stretching of amide I, while the C–N stretching of the amide II peak was observed at 1533.8 cm^{-1}, and the strong band at 3285.7 cm^{-1} was associated with O–H stretching vibration. In the HCPS-WPC complexes, with the increase of WPC and the decrease of HCPS, the O-H absorption peak shifted, it can be inferred the presence of hydrogen bonding and electrostatic interactions between polysaccharide and WP (38). Meanwhile, the amide I peaks of the HCPS-WPC complexes shifted and the peaks related to the amide II were shifted to the higher wavenumber. The shifting of amide characteristic peaks was due to the effect of HCPS-WPC electrostatic interactions on the α -helix structure of the WPC (Figure 5A) (39). Furthermore, compared to the native HCPS, the C = O on carboxyl groups was not observed in the HCPS-WPC complexes, and the bands ranged from 1074.3 to 1077.2 cm^{-1}.

The HCPL and HCPL-WPC complexes are depicted in Figure 5B. In the HCPL, the 3,394 cm^{-1} band was attributed to the O–H stretching vibration, while the distinctive bands at 1,742 and 1,615 cm^{-1} were related to the stretching vibration of C = O on the carboxyl and carbonyl groups, respectively. The spectrum of HCPL-WPC complexes showed two important bands in the ranges of 1646.2–1651.5 cm^{-1} and 1533.8–1,538 cm^{-1}, associated with the shifting of amide I and amide II, respectively. One samples band range from 1074 to 1082.3 cm^{-1} was also observed in the HCPL-WPC complexes (35).

In general, the secondary structure and groups of the WPC were affected by additions of HCPS and HCPL. The contribution of the electrostatic interactions between the carbonyl groups of HCPS or HCPL and the amino groups could explain the shift in amide peaks. Similar interactions have been previously reported in the complex coacervation of pea protein isolate and tragacanth gum (30).

3.7. SEM analysis

The morphological microstructures of the WPC, HCPS, HCPL, HCPS-WPC, and HCPL-WPC complexes at the ratio of 1:4 are presented in Figure 6. The microstructure of pure WPC was found to be orderly and complete, while its internal structure was mainly spherical (Figures 6A, B). The electron microscope image showed

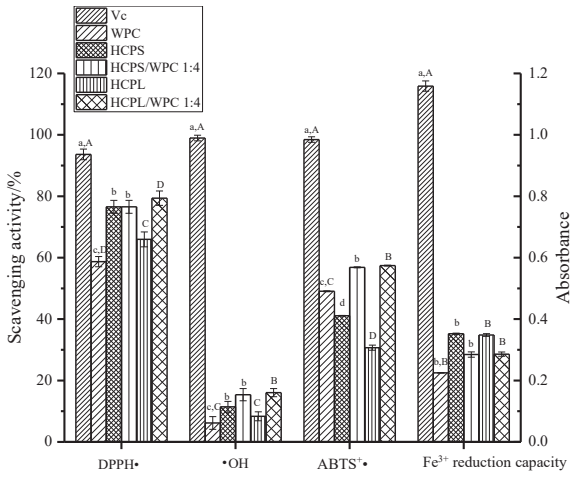

FIGURE 7
The antioxidant capacity analysis. Different lowercase letters indicate significant differences in HCPS-WPC ($p < 0.05$). Different uppercase letters indicate significant differences in HCPL-WPC ($p < 0.05$).

that the surface of HCPS was smooth and intertwined, and the structure was irregular (Figure 6C). HCPL was found to have a more dispersed and flakey structure, indicating it to be mainly amorphous (Figure 6E). In the microstructure of HCPS-WPC (Figure 6D), a smooth and blocky surface was observed, and WPC was adsorbed concurrently by the HCPS. The microstructure of HCPL-WPC was found to be similar to that of the HCPS-WPC, with WPC similarly adsorbed by the HCPL. In brief, the interactions between HCPS or HCPL and WPC were evident. The smooth surface of the complex microstructures could have been due to the use of metal coating (40).

3.8. Antioxidant activity

The antioxidant capacities of the complexes HCPS, HCPL and WPC are shown in Figure 7. The scavenging capacities of the DPPH ·, · OH and $ABTS^{+}$· of the complexes were higher than those of the pure HCPS, HCPL, and WPC, indicating the synergistic effect between HCPS or HCPL and WPC. Among them, the antioxidant capacity of the HCPL-WPC was slightly higher than that of the HCPS-WPC, but the antioxidant capacity of the HCPL was lower than that of the HCPS, which might have been due to the stronger interaction and synergy between HCPL and WPC. These findings concur with the results of the UV analysis in this study. However, the Fe^{3+} reduction capacity of the complexes was lower than those of the HCPS and HCPL, it might be that the interaction between WPC and polysaccharide would inhibit the Fe^{3+} reduction capacity of complexes. In general, the antioxidant activity of the complexes was superior. For better comparison, vitamin C was used as a positive control. Furthermore, in the study of flaxseed gum-WP isolate, the antioxidant capacity of the mixture was also found to be superior to the compounds alone (17).

4. Conclusion

This study explored the interactions between HCPS and WPC, and HCPL and WPC. Turbidity analysis revealed that the interactions of the complexes were greatest when pH was 4 and the mixing ratios of HCPS-WPC and HCPL-WPC were 1:4. The physicochemical properties and structural characterization of the two complexes under neutral conditions were also examined and it was found that there was electrostatic interaction between HCPS/HCPL and WPC under neutral conditions, and that the addition of WPC improved the thermal stability of the complexes. Rheological studies showed that HCPS-WPC and HCPL-WPC were pseudoplastic fluids, and FTIR further confirmed the interaction between HCPS/HCPL and WPC. Comparative analysis of the two complexes showed that the HCPL-WPC system was more stable and also had a higher level of antioxidant activity. This research, thus, provides in-depth information regarding the interactions between HCPL and WPC, which can contribute to the development of functional foods with special nutritional value.

Data availability statement

The raw data supporting the conclusions of this article will be made available by the authors, without undue reservation.

Author contributions

JT: formal analysis and writing—original draft preparation. XL: methodology, formal analysis, validation, project administration, and funding acquisition. ZZ: validation and data curation. YP: validation and writing—review and editing. ZL: writing and review. All authors read the manuscript, critically examined the important intellectual content, and approved the final version.

Funding

This work was financially supported by the Key Scientific Research Fund of Xihua University, China (Grant no. Z17127). This work was supported by the Research and Innovation Fund of Xihua University, China (Grant no. YCJJ2021101).

Conflict of interest

The authors declare that the research was conducted in the absence of any commercial or financial relationships that could be construed as a potential conflict of interest.

Publisher's note

All claims expressed in this article are solely those of the authors and do not necessarily represent those of their affiliated organizations, or those of the publisher, the editors and the reviewers. Any product that may be evaluated in this article, or claim that may be made by its manufacturer, is not guaranteed or endorsed by the publisher.

References

1. Lau K, Lee K, Koon C, Cheung C, Lau C, Ho H, et al. Immunomodulatory and anti-SARS activities of Houttuynia cordata. *J Ethnopharmacol.* (2008) 118:79–85. doi: 10.1016/j.jep.2008.03.018

2. Cheng D, Sun L, Zou S, Chen J, Mao H, Zhang Y, et al. Antiviral effects of houttuynia cordata polysaccharide extract on Murine Norovirus-1 (MNV-1) a human norovirus surrogate. *Molecules.* (2019) 24:1835. doi: 10.3390/molecules24091835

3. Shi C, Zhu H, Li H, Zeng D, Shi X, Zhang Y, et al. Regulating the balance of Th17/Treg cells in gut-lung axis contributed to the therapeutic effect of Houttuynia cordata polysaccharides on H1N1-induced acute lung injury. *Int J Biol Macromol.* (2020) 158:52–66. doi: 10.1016/j.ijbiomac.2020.04.211

4. Spotti M, Perduca M, Piagentini A, Santiago L, Rubiolo A, Carrara C. Does dextran molecular weight affect the mechanical properties of whey protein/dextran conjugate gels? *Food Hydrocoll.* (2013) 32:204–10. doi: 10.1016/j.foodhyd.2012.12.022

5. Niu Y, Xia Q, Jung W, Yu L. Polysaccharides-protein interaction of psyllium and whey protein with their texture and bile acid binding activity. *Int J Biol Macromol.* (2019) 126:215–20. doi: 10.1016/j.ijbiomac.2018.12.221

6. Patino J, Pilosof A. Protein–polysaccharide interactions at fluid interfaces. *Food Hydrocoll.* (2011) 25:1925–37. doi: 10.1016/j.foodhyd.2011.02.023

7. Galazka V, Smith D, Ledward D, Dickinson E. Interactions of ovalbumin with sulphated polysaccharides: effects of pH, ionic strength, heat and high pressure treatment. *Food Hydrocoll.* (1999) 13:81–8. doi: 10.1016/s0268-005x(98)00073-3

8. Du Q, Zhou L, Lyu F, Liu J, Ding Y. The complex of whey protein and pectin: Interactions, functional properties and applications in food colloidal systems-A review. *Colloids Surf B Biointerfaces.* (2022) 210:112253. doi: 10.1016/j.colsurfb.2021.112253

9. Dai Q, Zhu X, Abbas S, Karangwa E, Zhang X, Xia S, et al. Stable nanoparticles prepared by heating electrostatic complexes of whey protein isolate–dextran conjugate and chondroitin sulfate. *J Agric Food Chem.* (2015) 63:4179–89. doi: 10.1021/acs.jafc.5b00794

10. Wagoner TB, Foegeding EA. Whey protein-pectin soluble complexes for beverage applications. *Food Hydrocoll.* (2017) 63:130–8.

11. McClements DJ. Non-covalent interactions between proteins and polysaccharides. *Biotechnol Adv.* (2006) 24:621–5. doi: 10.1016/j.biotechadv.2006.07.003

12. Du Q, Wang S, Lyu F, Liu J, Ding Y. The interfacial covalent bonding of whey protein hydrolysate and pectin under high temperature sterilization: effect on emulsion stability. *Colloids Surf B.* (2021) 206:111936. doi: 10.1016/j.colsurfb.2021.111936

13. Wagoner T, Vardhanabhuti B, Foegeding E. Designing whey protein–polysaccharide particles for colloidal stability. *Annu Rev Food Sci Technol.* (2016) 7:93–116. doi: 10.1146/annurev-food-041715-033315

14. Einhorn S, Ulbrich M, Sever S, Kunzek K. Formation of milk protein–pectin conjugates with improved emulsifying properties by controlled dry heating. *Food Hydrocoll.* (2005) 19:329–40. doi: 10.1016/j.foodhyd.2004.07.005

15. Corredig M, Sharafbafi N, Kristo E. Polysaccharide–protein interactions in dairy matrices, control and design of structures. *Food Hydrocoll.* (2011) 25:1833–41. doi: 10.1016/j.foodhyd.2011.05.014

16. Dong X, Du S, Deng Q, Tang H, Yang C, Wei F, et al. Study on the antioxidant activity and emulsifying properties of flaxseed gum-whey protein isolate conjugates prepared by Maillard reaction. *Int J Biol Macromol.* (2019) 153:1157–64. doi: 10.1016/j.ijbiomac.2019.10.245

17. Liu X, Tian J, Pan Y, Li Z, Zhou Z, Pan Z, et al. Structural characterization and biological activity of polysaccharides from stems of *Houttuynia cordata*. *Foods.* (2022) 11:3622. doi: 10.3390/foods11223622

18. Aryee F, Nickerson M. Effect of pH, biopolymer mixing ratio and salts on the formation and stability of electrostatic complexes formed within mixtures of lentil protein isolate and anionic polysaccharides (kappa-carrageenan and gellan gum). *Int J Food Sci Technol.* (2013) 49:65–71. doi: 10.1111/ijfs.12275

19. Timilsena Y, Wang B, Adhikari R, Adhikari B. Preparation and characterization of chia seed protein isolate-chia seed gum complex coacervates. *Food Hydrocoll.* (2015) 52:554–63. doi: 10.1016/j.foodhyd.2015.07.033

20. Cheng C, Yu X, McClements D, Huang Q, Tang H, Yu K, et al. Effect of flaxseed polyphenols on physical stability and oxidative stability of flaxseed oil-in-water nanoemulsions. *Food Chem.* (2019) 301:125207. doi: 10.1016/j.foodchem.2019.125207

21. Tian L, Zhao Y, Guo C, Yang XB. A comparative study on the antioxidant activities of an acidic polysaccharide and various solvent extracts derived from herbal *Houttuynia cordata*. *Carbohydrate Polym.* (2011) 83:537–44. doi: 10.1016/j.carbpol.2010.08.023

22. de Falco B, Fiore A, Bochicchio R, Amato M, Lanzotti V. Metabolomic analysis by UAE-GC MS and antioxidant activity of *Salvia hispanica (L.)* seeds grown under different irrigation regimes. *Ind Crops Prod.* (2018) 112:584–92. doi: 10.1016/j.indcrop.2017.12.030

23. Yildirim A, Mavi A, Kara AA. Determination of antioxidant and antimicrobial activities of *Rumex crispus L.* extracts. *J Agric Food Chem.* (2001) 49:4083–9. doi: 10.1021/jf0103572

24. Zhong W, Zhang T, Dong C, Li J, Dai J, Wang C. Characterization of interactions between whey protein isolate and hyaluronic acid in aqueous solution: effects of pH and mixing ratio. *Colloids Surf B Biointerfaces.* (2021) 203:111758. doi: 10.1016/j.colsurfb.2021.111758

25. Chen X, Qiu Q, Chen K, Li D, Liang L. Water-soluble myofibrillar protein–pectin complex for enhanced physical stability near the isoelectric point: fabrication, rheology and thermal property. *Int J Biol Macromol.* (2020) 142:615–23. doi: 10.1016/j.ijbiomac.2019.10.003

26. Stone A, Nickerson M. Formation and functionality of whey protein isolate (kappa-, iota-, and lambda-type) carrageenan electrostatic complexes. *Food Hydrocoll.* (2012) 27:271–7.

27. Malay O, Bayraktar O, Batigun A. Complex coacervation of silk fibroin and hyaluronic acid. *Int J Biol Macromol.* (2007) 40:387–93. doi: 10.1016/j.ijbiomac.2006.09.017

28. Huang G, Sun Y, Xiao J, Yang J. Complex coacervation of soybean protein isolate and chitosan. *Food Chem.* (2012) 135:534–9. doi: 10.1016/j.foodchem.2012.04.140

29. Yildiz G, Ding J, Andrade J, Engeseth N, Feng H. Effect of plant protein-polysaccharide complexes produced by mano-thermo-sonication and pH-shifting on the structure and stability of oil-in-water emulsions. *Innov Food Sci Emerg Technol.* (2018) 47:317–25. doi: 10.1016/j.ifset.2018.03.005

30. Carpentier J, Conforto E, Chaigneau C, Vendeville J, Maugard T. Complex coacervation of pea protein isolate and tragacanth gum: comparative study with commercial polysaccharides. *Innov Food Sci Emerg Technol.* (2021) 69:102641. doi: 10.1016/j.ifset.2021.102641

31. Khalesi H, Emadzadeh B, Kadkhodaee R, Fang Y. Whey protein isolate-Persian gum interaction at neutral pH. *Food Hydrocoll.* (2015) 59:45–9. doi: 10.1016/j.foodhyd.2015.10.017

32. Mu C, Guo J, Li X, Lin W, Li D. Preparation and properties of dialdehyde carboxymethyl cellulose crosslinked gelatin edible films. *Food Hydrocoll.* (2012) 27:22–9. doi: 10.1016/j.foodhyd.2011.09.005

33. Wang S, Hu Y, He Z, Wang Q, Xu S. Study of pyrolytic mechanisms of seaweed based on different components (soluble polysaccharides, proteins, and ash). *J Renew Sustain Energy.* (2017) 9:023102. doi: 10.1063/1.4978345

34. Shen R, Liu X, Dong J, Si J, Li H. The gel properties and microstructure of the mixture of oat β-glucan/soy protein isolates. *Food Hydrocoll.* (2015) 47:108–14. doi: 10.1016/j.foodhyd.2015.01.017

35. Hu J, Zhao T, Li S, Wang Z, Wen C, Wang H, et al. Stability, microstructure, and digestibility of whey protein isolate-*Tremella fuciformis* polysaccharide complexes. *Food Hydrocoll.* (2019) 89:379–85. doi: 10.1016/j.foodhyd.2018.11.005

36. Cheng J, Liu J, Prasanna G, Jing P. Spectrofluorimetric and molecular docking studies on the interaction of cyanidin-3-O-glucoside with whey protein, β-lactoglobulin. *Int J Biol Macromol.* (2017) 105:965–72. doi: 10.1016/j.ijbiomac.2017.07.119

37. Kaur J, Katopo L, Hung A, Ashton J, Kasapis S. Combined spectroscopic, molecular docking and quantum mechanics study of β-casein and ferulic acid interactions following UHT-like treatment. *Food Hydrocoll.* (2018) 89:351–9. doi: 10.1016/j.foodhyd.2018.10.055

38. Guerrero P, Kerry JP, de la Caba K. FTIR characterization of protein–polysaccharide interactions in extruded blends. *Carbohydrate Polym.* (2014) 111:598–605. doi: 10.1016/j.carbpol.2014.05.005

39. Mousazadeh M, Mousavi M, Askari G, Kiani H, Adt I, Gharsallaoui A. Thermodynamic and physiochemical insights into chickpea protein-Persian gum interactions and environmental effects. *Int J Biol Macromol.* (2018) 119:1052–8. doi: 10.1016/j.ijbiomac.2018.07.168

40. Conforto E, Joguet N, Buisson P, Vendeville J-E, Chaigneau C, Maugard T. An optimized methodology to analyze biopolymer capsules by environmental scanning electron microscopy. *Mater Sci Eng C.* (2015) 47:357–66. doi: 10.1016/j.msec.2014.11.054

Frontiers in Nutrition

Explores what and how we eat in the context of health, sustainability and 21st century food science

A multidisciplinary journal that integrates research on dietary behavior, agronomy and 21st century food science with a focus on human health.

Discover the latest Research Topics

See more →

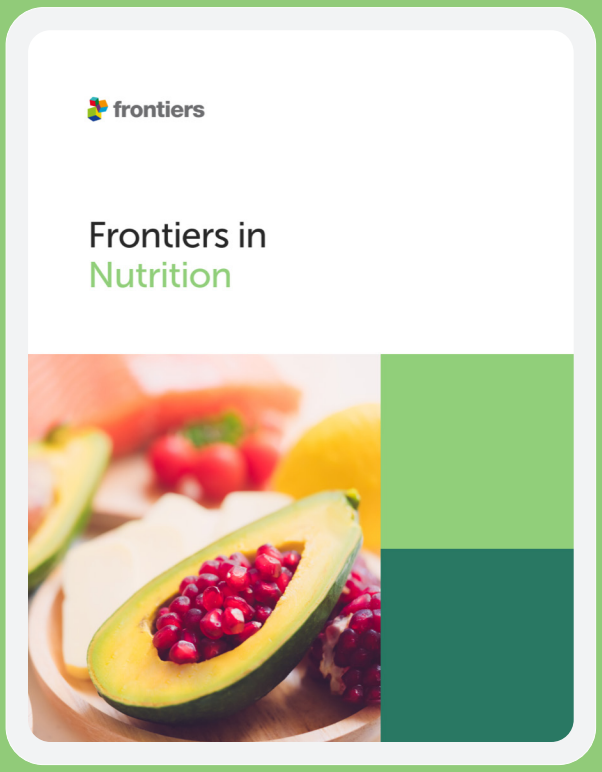

Frontiers

Avenue du Tribunal-Fédéral 34
1005 Lausanne, Switzerland
frontiersin.org

Contact us

+41 (0)21 510 17 00
frontiersin.org/about/contact